2020

Understanding & Exploiting Selectivity in Nickel-catalysed Cross-coupling

DOCTORAL THESIS IN THE DEPARTMENT OF PURE & APPLIED CHEMISTRY UNDER THE SUPERVISION OF DR. DAVID NELSON

ALASDAIR COOPER

Acknowledgements

I would like to thank my PhD supervisor Dr David Nelson for the opportunity to carry out this project and for the invaluable input to both practical work and the writing of this report.

I would also like to thank my industrial supervisor Dr Paul Burton from Syngenta for regular technical discussions about the results and the direction of the project.

Thank you to Craig and John for use of the NMR facilities as well as Pat for use of the GC-FID/GC-MS facilities.

Finally thank you to the Nelson group as a whole (including some past members, as well as the Percy group) for their support.

Abstract

This project was focused on investigating structure & reactivity relationships between nickel(0) species derived from nickel(II) sources and aryl halides with coordinating π systems in Suzuki cross-coupling reactions.

Design of Experiments was used to optimise the cross-coupling conditions to achieve satisfactory conversions and robust reproducibility. Competition couplings were designed in order to compare the conversion of halides with and without coordinating functional groups, as well as between electron rich and poor systems to decouple any selectivity effect from the electronic effects. The selectivity in favour of coordinating substrates was quite prominent with several of the halides.

The selectivity that was observed was quantified and investigated with an analogous palladium(II) complex, where it was found that this effect was less pronounced.

A robustness screen was also carried out to investigate any inhibition to coupling that these coordinating groups might exhibit.

Calorimetry was employed in an attempt to glean kinetic information about the reaction and whether there were significant rate differences in the couplings of these halides.

Finally, the investigation was extended towards heterocyclic aryl chlorides, where novel nickel(II) dimers were characterised by X-ray crystallography and found to inhibit the coupling of ortho-halo heteroarenes.

Table of Contents

1 Introduction

1.1 Palladium Catalysed Cross-Coupling

Cross-coupling reactions have been ubiquitous in modern synthetic chemistry for the past 20 years.[1–4] Prior to the advent of carbon-carbon bond formation between two different centres, metal-mediated homo-coupling was widely used e.g. the Ullmann reaction (**Scheme 1.1**).

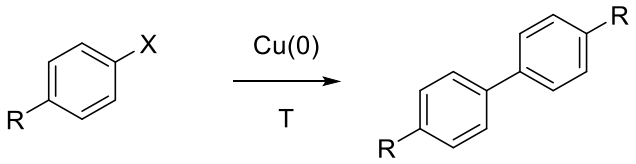

Scheme 1.1 Ullmann homocoupling using copper

While this was a useful transformation, the desire to achieve cross-coupling between distinct centres was apparent. The main advantage of cross-coupling was clear: a huge array of different aryl moieties is available, making the scope quite extensive. However, there were selectivity barriers to consider. For the method to be generally applicable in organic synthesis, possible side reactions (such as homocoupling, β-hydride elimination) had to be controlled or prevented, as well as ensuring that the method was tolerant of various functional groups.

This investigation into a suitable method for metal catalysed cross-coupling hit its stride in the 1970s, where several of the today well-known named reactions were realised, with Suzuki, Miyaura, Heck, Negishi, Stille and Sonogashira amongst the top contributors. The work carried out by these groups showed that carbon atoms in every hybridisation state, though mostly sp^2 (aryl-aryl being the most common, with vinyl groups also possible) could undergo cross-coupling reactions. These reactions were often catalysed by a palladium catalyst bearing some kind of phosphine based ligand(s). A general scheme is shown in **Scheme 1.2**.

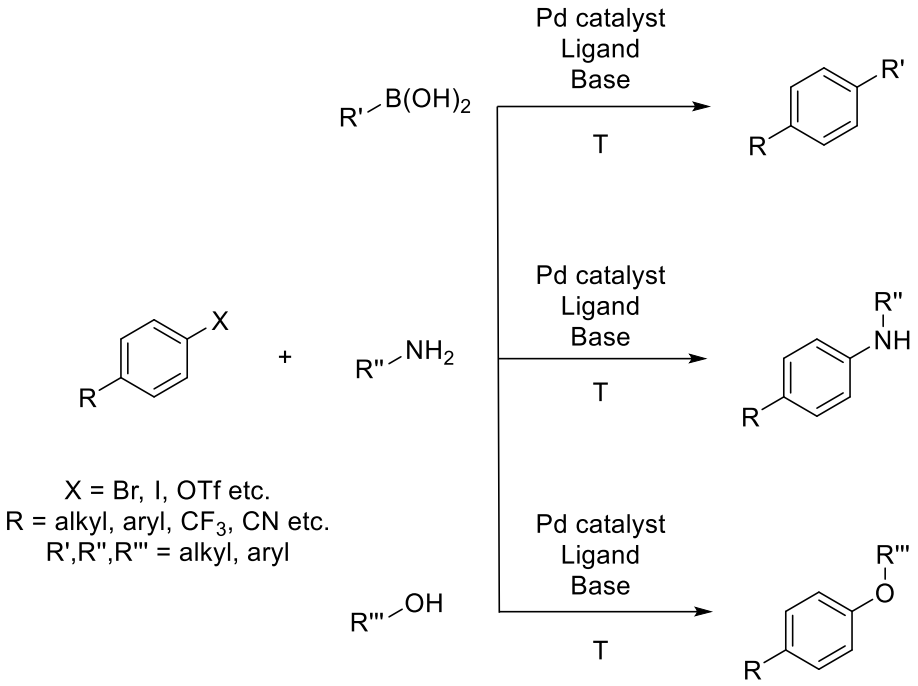

Scheme 1.2 Palladium catalysed cross-coupling

As of 2010, the Suzuki-Miyaura and Heck cross-coupling reactions continue to dominate the modern synthetic chemistry field, with many more papers and patents published using these reactions (**Table 1.1**).[5]

Table 1.1 Carbon-carbon **c**ross-coupling reactions in papers and patents

Reaction	Nucleophile	Total Papers Published (Correct as of 2010)	% Increase from Previous Year	Patents Published
Suzuki	Boronic Acid/Derivative	7900	13.5	101
Heck	Alkene	5900	11.3	92
Sonogashira	Alkyne	2000	14.8	17
Stille	Stannane	2000	9.2	7
Hiyama	Silane	300	11.7	0
Negishi	Organozinc	550	12.5	0
Kumada	Grignard	52	25.0	0

A great deal of investigation has been carried out on the mechanism of these types of cross-coupling reactions. It is now known that there are three fundamental steps that need to take place in order for these reactions to be successful:

i. oxidative addition
ii. transmetalation
iii. reductive elimination

A general catalytic cycle can be drawn, which illustrates these three steps (**Scheme 1.3**).

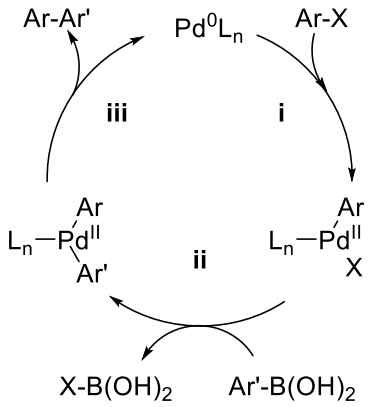

Scheme 1.3 General catalytic cross-coupling cycle

The first step, oxidative addition, is generally rate-determining when using a palladium catalyst, unless iodides are being used. Here, the electrophilic substrate, usually an aryl halide (though now pseudo-halide groups such as tosyl[6] and triflate[7] groups, as well as a range of others including carbamates[8–10] and sulfamates[9–11] are widespread), coordinates to the metal centre, increasing the oxidation state by two, as well as the coordination number i.e. Pd(0) → Pd(II). Due to an increase in coordination number, the active metal species must include a vacant site for oxidative addition. There are a number of factors that can influence the rate of oxidative addition. One of the main influences is the electrophilicity of the carbon bonded to the halide/pseudo-halide. The more electrophilic this carbon is, the faster the rate of oxidative addition will become. In the case of an aryl substrate, this can be altered *via* the nature of other substituents on the aryl ring. For example, an electron-donating substituent in the *para* position would increase the electron density at the site of oxidative addition, reducing electrophilicity and oxidative addition rate. Conversely, an electron-withdrawing substituent would have the opposite effect. This is illustrated in **Figure 1.1** below. The electronic properties of aryl substituents can be quantified using Hammett parameters, derived from the dissociation of benzoic acid from the following equation:

$$\sigma_p = \log K_p - \log K_H$$

H is given a value of 0 and the other factors are stated relevant to this. For $\sigma_p < 0$, the substituent is electron donating, for $\sigma_p > 0$, it is electron withdrawing.

Figure 1.1 Relative oxidative addition rates based on substituent effects

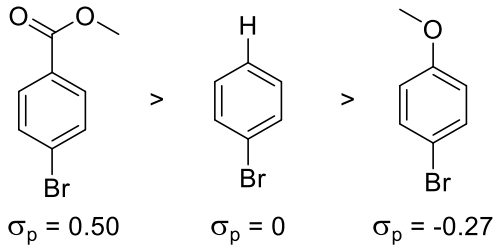

It follows then that catalysts with electron-rich metal centres will also increase the rate of oxidative addition. Many of the catalysts selected for these reactions involve electron-rich phosphine ligands (Buchwald-type ligands such as SPhos or XPhos, or the more electron rich alkyl phosphines such as PCy_3 or P^tBu_3), particularly when aryl chlorides are the chosen substrate.[12,13]

The second fundamental step in cross-coupling reactions is transmetalation. This step is potentially the least well understood of the mechanisms of these reactions. Overall, this step involves the intermediate formed by the oxidative addition and the coupling partner. As Suzuki reactions have been the subject of recent intensive study, the transmetalation step can be considered in terms of the boron species coupling partner. Put simply, the step is the transfer of R' from the boron species to the catalyst, to prime the catalyst for reductive elimination of the final product. There are two competing proposed pathways for the mechanism of this step:

i. The "boronate" pathway

While both pathways rely on the formation of a four-coordinate "ate" complex, they differ on the mechanism by which this complex arises. This first pathway suggests that a four-coordinate boron species is either preformed, or formed *in situ*, then transmetalates to the oxidative addition intermediate (**Scheme 1.4**).[14]

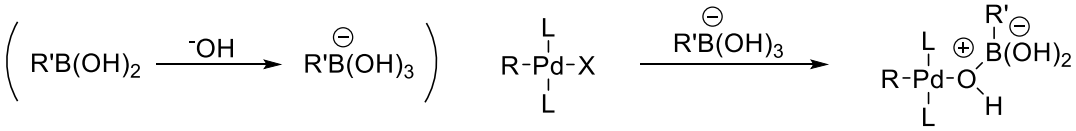

Scheme 1.4 "Boronate" pathway for transmetalation

ii. The "oxo-palladium" pathway

Here, a ligand on the catalyst acts as a Lewis base and associates with the three-coordinate boron species, creating the required four-coordinate species upon association with the catalyst. Specifically, if this ligand is an alkoxy or hydroxy group, then this pathway is referred to as the "oxo-palladium" pathway (**Scheme 1.5**).[15]

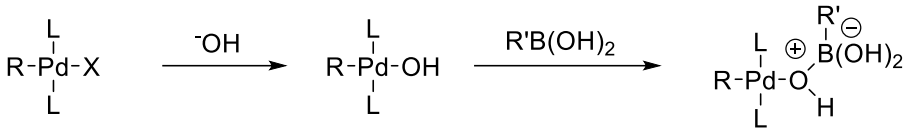

Scheme 1.5 "Oxo-palladium" pathway for transmetalation

A large number of studies have been carried out on this step, which have produced evidence both for and against each pathway. Initially, during the development of the Suzuki-Miyaura coupling itself, it was observed that transmetalation would not occur with a neutral boron species, as this species was not nucleophilic enough.[16] Upon addition of NaOEt or NaOH, the organoboron reagents were converted into the more nucleophilic four-coordinate "ate" complexes, which would undergo transmetalation sufficiently. This would suggest a mechanism *via* the first pathway. A later study on alkenyl-alkenyl coupling[17], however, found that:

i. No coupling was observed when Et_3N was used as a base

ii. The lithium salt of the organoboron reagent used (**Figure 1.2**) yielded 9 % coupled product in the absence of base, while the neutral boron species coupled efficiently (49 – 73 %) in the presence of NaOR/NaOH

Figure 1.2 Lithium salt used for transmetalation elucidation

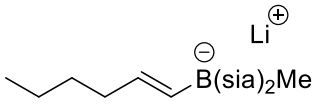

It was concluded in this study that alkoxo-palladium intermediates were formed after oxidative addition, leading to the capture of a neutral three-coordinate boron reagent for transmetalation.

An important factor to take into account when considering the possible mechanisms of transmetalation is the role of the base. Generally, the base is an inorganic base such as K_3PO_4 or Cs_2CO_3. The base can have an impact on the water concentration of the reaction medium (assuming water is present). When a water-immiscible solvent, such as toluene, is used, a biphasic system is apparent with or without base. For solvents that are miscible with water, however, such as THF or 1,4-dioxane, phase splitting can occur with the presence of an inorganic base.[18] The volume of the separate water phase is dependent upon the amount of base added and is usually a very small percentage of the total volume (1 – 5 %). The water concentration affects the speciation of the boron reagent, particularly when the base is present predominantly in this phase (as is generally the case). This causes the water phase to have a considerably higher pH than the organic phase. The result of this is that the boron reagent is weighted much more towards the boronic acid in the organic phase, rather than a charged boronate species. This would suggest that biphasic media facilitate the coupling *via* the second pathway. This pathway is also supported by the idea that an aqueous phase of higher pH value can act as a hydroxide source, which could form the oxo-palladium species. The aqueous phase plays a second role in this mechanism, by sequestering halide and boron salts that remain once the boronic acid has been coupled (X^- and $B(OH)_3$). These species, if left in the bulk organic phase, can negatively influence reaction turnover. For example, $B(OH)_3$ can react with OH^- to form $B(OH)_4^-$, using up crucial OH^-.

Due to the effects that have been studied, it is expected that in a completely homogeneous reaction medium, the coupling would mostly follow the first pathway, while if a biphasic system is established, the reaction would follow the second pathway.

The final fundamental step in a cross-coupling reaction is reductive elimination. This step completes the cycle and is essentially the reverse of oxidative addition, reducing the oxidation state and coordination number of the metal centre by two, regenerating the catalytic species: Pd(II) → Pd(0), and furnishing the coupled product. As mentioned previously, the rate of reductive elimination can be promoted in an analogous manner to oxidative addition. The bulk of the ligand directly around the metal centre affects the rate of reductive elimination, as with oxidative addition, where a bulkier centre promotes reductive elimination.[19] As with oxidative addition, the rate of reductive elimination is faster for less coordinated complexes i.e. [LPd(Ar)R] is faster than [L_2Pd(Ar)R].[20,21] Again, the electronic properties of the catalyst will have an effect on the rate of this step as well, as electron-poor metal centres increase the rate

of reductive elimination. The biaryl phosphine ligands mentioned before (SPhos/XPhos, amongst others) can have their steric properties tuned to enhance this step.

1.2 Nickel vs. Palladium

During the early development of the Suzuki-Miyaura cross-coupling, catalysts and pre-catalysts based on palladium dominated the scene.[19,22–24] It wasn't until 1995 that the first competing nickel-catalysed cross-coupling reaction was reported.[25] It took much longer for nickel-based catalysts to become ubiquitous in cross-coupling since, although nickel is cheaper and "less precious", the higher catalyst loadings (5-10 mol% as opposed to generally <1 mol% for Pd), as well as the more expensive ligands required offset these initially attractive advantages over palladium. The reactions generally required harsher conditions as well, due to generally lower conversions (which in turn made work-up and purification more difficult), employing temperatures of up to 100 °C (**Scheme 1.6**).

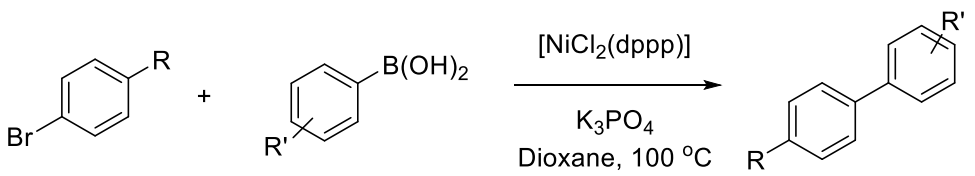

R = NMe_2, OMe, CHO, CO_2Me
R' = OMe, NH_2, CO_2Me, Me

Scheme 1.6 Ni-catalysed Suzuki coupling using higher temperature

Nickel-based catalysts at the time were also much less robust than their palladium counterparts, owing to the sensitivity of Ni(0). The air and moisture sensitivity also often meant the use of equipment such as gloveboxes that were less widely available, reducing its applicability. However, nickel did show promise in converting previously challenging substrates that palladium could not, such as phenols[26], aryl ethers[27] and even aryl fluorides.[28] Since then the area has been investigated more thoroughly by a number of different groups, leading to a wide variety of nickel catalysts and pre-catalysts in use today. Various examples in more recent literature show much lower catalyst loadings, 1 mol% or lower, as well as coupling *via* quite unreactive substituents (sulfamates/carbamates, **Scheme 1.7**).[9]

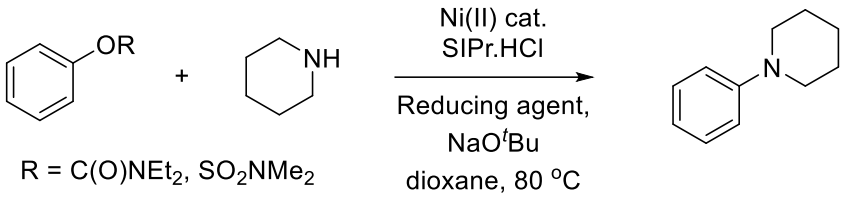

Ph-B(OH)$_2$ as the reducing agent gave the best results

Scheme 1.7 Ni-catalysed cross-coupling of aryl sulfamates

Ligand choice is one of the most important aspects of cross-coupling. Pd-based catalysts are often used in conjunction with phosphine ligands. Perhaps the most notable examples of these ligands are the Buchwald-type ligands, e.g. SPhos and XPhos (**Figure 1.3**).[29,30]

Figure 1.3 SPhos and XPhos ligands

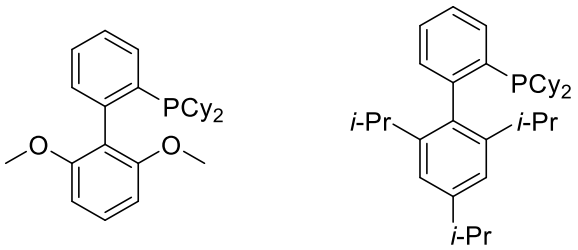

These ligands are bulky, electron-rich, biaryl systems that have been employed across a number of cross-coupling reactions. So wide is the use of these phosphine ligands, that methods of defining the steric bulk (Tolman Cone Angle, TCA) and the electronic properties (Tolman Electronic Parameter, TEP) of the ligands have been developed, to elucidate reaction mechanisms as well as to be able to directly compare different ligands. The TEP is determined by measuring the IR response of carbonyl groups upon addition of a ligand to a metal centre (**Figure 1.4**). If the ligand is electron donating, the electron density on the metal centre will increase, weakening the C-O bond through d-orbital to π^* back-bonding, causing a lowering in IR wavenumber. Conversely, an electron withdrawing ligand will strengthen the C-O bond, increasing the IR wavenumber.

Figure 1.4 Determination of TEP

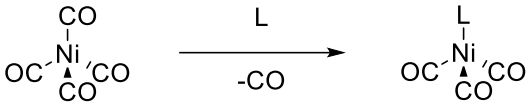

TEP is not the only parameter that has been used to quantify ligand properties. Bite angle is another property which can be measured. This is largely used for bidentate phosphines to determine the angle at which the phosphorus atoms are bound to the metal centre (**Figure 1.5**).

Figure 1.5 Metal complex with bidentate phosphine showing bite angle

This angle will determine how the bulk of the ligand is distributed around the metal. A wider bite angle will push bulk round the sides of the metal towards the opposite face to the ligand. This can reduce the rate of oxidative addition (and conversely increase the rate of reductive elimination) to the opposite metal face. Bite angle will generally increase upon increasing the link length between the two phosphorus atoms (**Figure 1.6**).

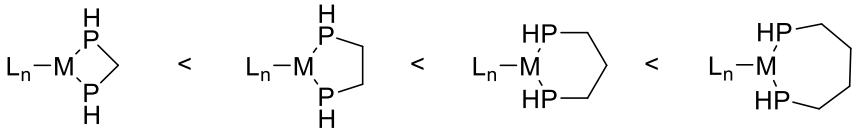

Figure 1.6 Phosphine links increasing in length and increasing bite angle

Due to these differences in rate of certain steps, changing the bite angle of the ligand on the metal centre can sometimes significantly alter the rate of the overall reaction. It is also possible that a ligand with too wide a bite angle will completely inhibit a reaction as oxidative addition will be unfavourable.

Another parameter that is often used is buried volume. This is usually considered when using phosphine and N-heterocyclic carbene ligands. This property is used to describe the space that a ligand occupies around the coordination sphere of the metal centre (**Figure 1.7**).

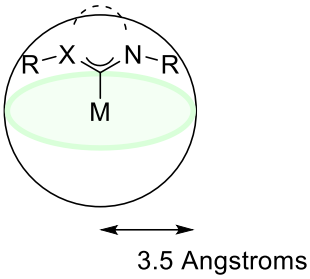

Figure 1.7 Buried volume around a metal centre with defined radius

To determine the buried volume of a ligand, the metal centre, M, must be defined. This is relatively simple in transition metal complexes, as the coordinates of the metal centre can be used. A sphere of radius R, centred on M is then built. The radius can be set at 3.0 - 3.5 Å and the volume of this sphere that the ligand occupies is then calculated. This volume is generally expressed as a percentage, $\%V_{bur}$, of the total coordination sphere which the ligand occupies. The bulkier the ligand, the higher the buried volume.

Together, these parameters can give a great deal of information about ligand bulk, which is one of the most important properties of a ligand in catalysis. Quantifying this property allows one to make informed decisions about ligand choice, as it is possible to rank ligands by relative bulk.

A great deal of these reactions have been towards the applicability of Suzuki-Miyaura reactions.[12] This work has led to the palladium catalysed coupling of aryl chlorides, as well as some heterocyclic substrates (**Scheme 1.8**).

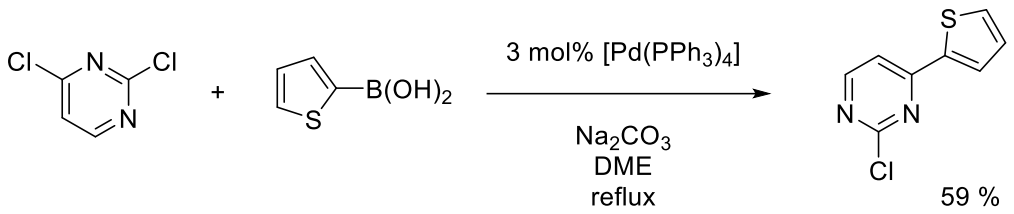

Scheme 1.8 Palladium-catalysed Suzuki cross-coupling using aryl chlorides

The use of aryl chlorides as coupling partners is particularly sought after, due to their higher availability and their presence in an array of already existing products. One ligand in particular, SPhos, has been used in the total synthesis of Biphenomycin B (**Scheme 1.9**).[31]

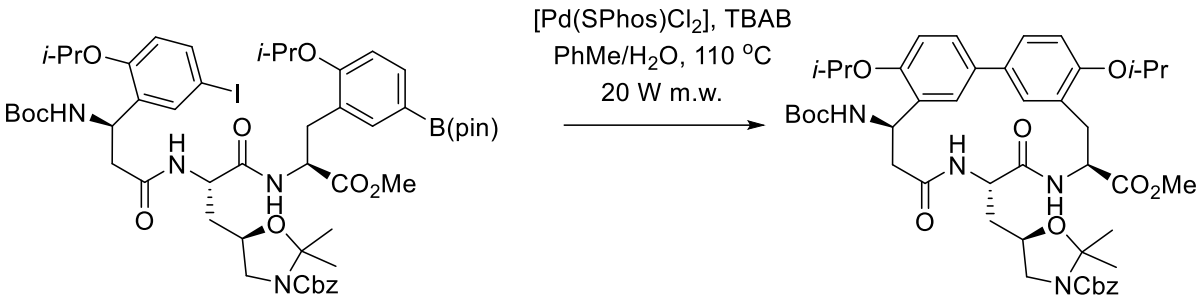

Scheme 1.9 Step of Biphenomycin B total synthesis using palladium-catalysed cross coupling

SPhos has also been shown to be effective at coupling heteroaryl boronic esters with both aryl and heteroaryl halides (**Scheme 1.10**).[12]

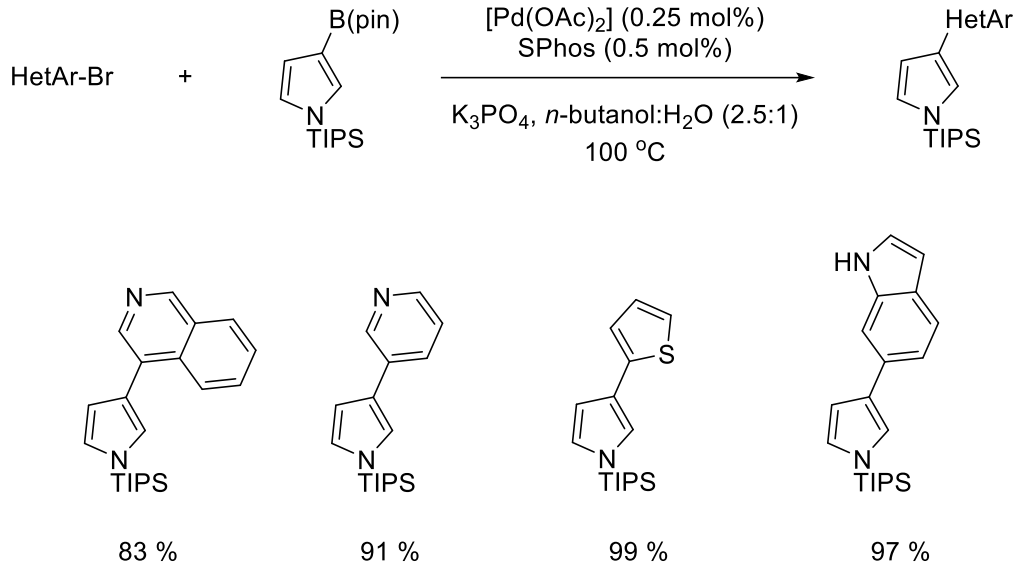

Scheme 1.10 SPhos in the coupling of aryl/heteroaryl boronic acids and halides

A major advantage of these types of ligands is the opportunity to tune the ligands to specific requirements. This is somewhat demonstrated in the examples of reactions that have been given. The variety of substitution available on the biaryl backbone allows for the alteration of several characteristics of the ligand. While some of these can enhance the rate of oxidative addition (e.g. the nature of the alkyl groups on the phosphine can increase the electron density

at this centre), the rate of reductive elimination can also be increased. The size of the alkyl groups attached to the phosphine have potentially the greatest effect on this.

Many of the ligands employed in the nickel catalysis rely on the simple phosphine ligands, rather than the bulkier, more elaborate ligands used for palladium. One of the most popular classes of ligand is the diphenylphosphino-x (dppx, where x can be ferrocene, ethyl, propyl, butyl) class. These are bidentate ligands which provide stability to the metal complex. Complexes made from these ligands are often used as pre-catalysts, such as [$NiCl_2$(dppf)] (**Figure 1.8**).

Figure 1.8 [$NiCl_2$(dppf)]

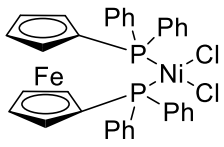

These are sources of Ni(0), believed to be the catalytic species, that are stored as Ni(II), allowing them to be kept in a regular laboratory setting, eliminating the need for a glovebox (though inert conditions *via* Schlenk techniques are still used due to the sensitivity of Ni(0) intermediates). These types of Ni(II) precatalysts do, however, still require an initial reduction to Ni(0) before oxidative addition can occur. One of the earliest examples of this catalyst in use was reported by Percec[32] coupling aryl sulfonates with phenylboronic acid (**Scheme 1.11**).

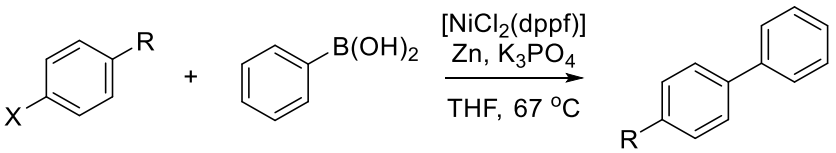

X = CF_3SO_3, *p*-$FC_6H_4SO_3$, *p*-$CH_3C_6H_4SO_3$, $PhSO_3$
R = CH_3O_2C, CH_3CO, CH_3, CH_3O

Scheme 1.11 Coupling of various aryl sulfonates with $PhB(OH)_2$

During this study, some mesylates were also coupled successfully. The work also included a comparison of the analogous palladium complex, [$PdCl_2$(dppf)]. It was shown that for these aryl substrates, the nickel catalysis was superior, owing to an inherently slow oxidative addition step in the case of the palladium catalysis. This was due to the higher nucleophilicity of Ni(0) compared to Pd(0). However, for the Ni(II) to be reduced to Ni(0), a reducing agent

such as Zn is required. In the absence of Zn, no cross-coupling product was observed. Conversely, when using Pd, although the yield was much lower, Zn was not required for turnover, as the Pd(II) was more readily reduced.

In the same class of complexes, [$NiCl_2$(dppp)] (**Figure 1.9**) has also been used to successfully couple various aryl halides (**Scheme 1.12**).[33]

Figure 1.9 [$NiCl_2$(dppp)]

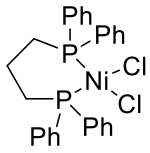

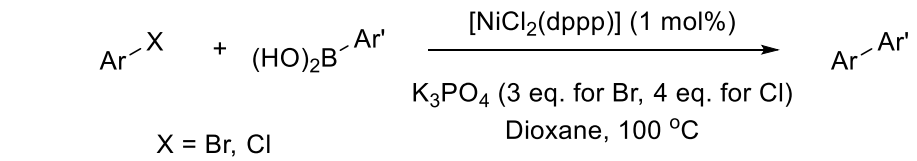

Ar = Ph, napthyl, *p*-$NMe_2C_6H_4$, *p*-$OMeC_6H_4$
Ar' = Ph, *p*-MeC_6H_4, *p*-$OMeC_6H_4$

Scheme 1.12 [$NiCl_2$(dppp)] catalysed coupling of aryl halides

Aryl bromides and aryl chlorides (the latter are usually more problematic, due to their lower reactivity arising from stronger bonds to carbon) were employed using much lower catalyst loadings than with previous Ni-catalyst studies (1 mol% and lower). A large variety of aryl bromides was tested, covering a wide range of aryl substituents, including various heterocyclic systems, giving generally good yields (48 – 98 %). The chloride scope was similarly varied, but with generally better yields (71 – 98 %). One of the most important parts of this investigation was the demonstration of applicability. The group showed that this catalysis was successful in synthesising a key motif of the fungicide Boscalid (**Figure 1.10** & **Scheme 1.13**).[34]

Figure 1.10 Boscalid

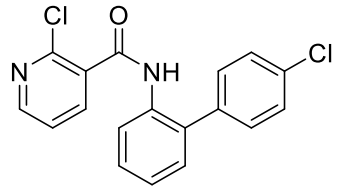

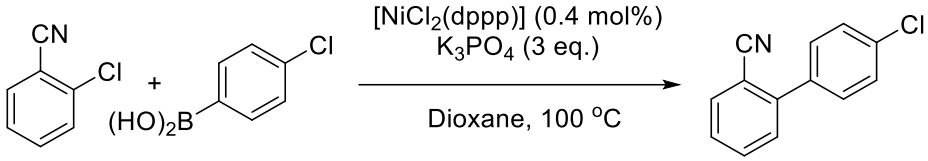

Scheme 1.13 Synthesis of intermediate towards Boscalid using [$NiCl_2$(dppp)]

The catalyst loading for this synthesis was remarkably low at 0.4 mol%, while giving a good isolated yield (69 %) on a gram scale. This methodology was then applied to further biaryl syntheses with industrial importance (**Scheme 1.14**). These biaryl systems are core intermediates for a variety of antihypertensive drugs, including losartan and valsartan (**Figure 1.11**).[35,36]

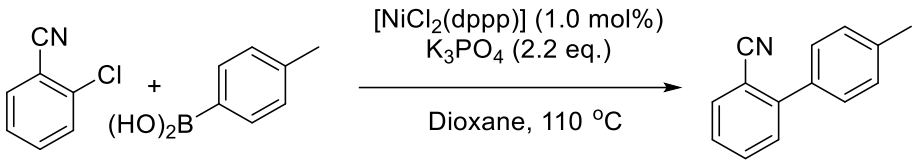

Scheme 1.14 Synthesis of intermediates towards antihypertensive drugs

Figure 1.11 Losartan and valsartan

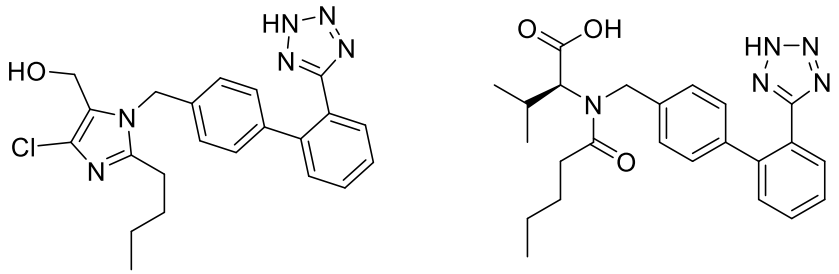

This was of particular significance since the industry standard of production of these compounds was *via* Pd-catalysed cross-coupling.

More recently, an example of Suzuki-Miyaura coupling using a specific aryl amide as a coupling partner in the presence of $Ni(cod)_2$ was reported (**Scheme 1.15**).[37,38]

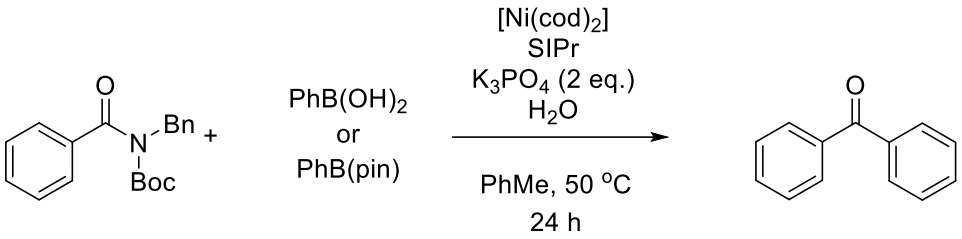

Scheme 1.15 $Ni(cod)_2$ catalysed coupling of aryl amides

This study further exemplified the idea that nickel-based catalysts could cleave unreactive bonds which were a challenge for other transition metals. While the reaction was successful on a number of substrates (51 – 96 %), the catalyst loading required was 5 mol%, as well as 5 mol% of SIPr ligand. Due to the relatively higher cost of $Ni(cod)_2$ and SIPr compared to other catalysts and ligands, this could be a drawback. Furthermore, since $Ni(cod)_2$ is a Ni(0) complex, this means it is much more sensitive to air and moisture than bench-stable Ni(II) sources of Ni(0), as well as having a much higher toxicity. This could potentially limit the industrial applicability of the procedure, as $Ni(cod)_2$ must usually be used in a glovebox. Despite these limitations, the investigation included several examples of syntheses of potentially relevant frameworks. A gram-scale coupling of amide with indolylboronic ester was achieved to deliver an antiproliferative agent (**Scheme 1.16**).

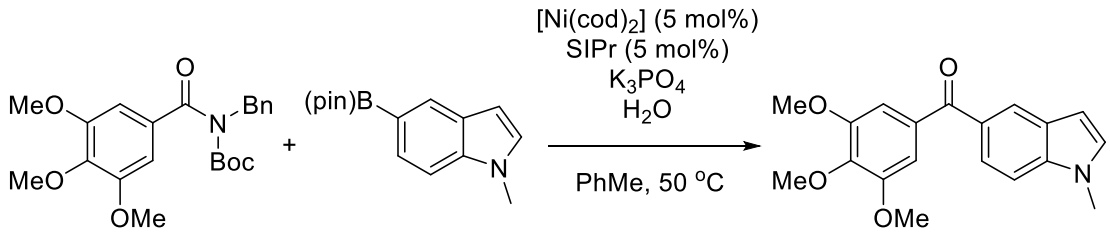

Scheme 1.16 Amide cross coupling *via* Ni catalysis to yield antiproliferative agent

As well as the variety of simple bidentate (dppf, dppe, dppp etc.) and monodentate (PPh_3, PCy_3) phosphine ligands in use, investigation into NHC-type ligands has become more widespread. These ligands have been applied to both Pd and Ni, with one of the most popular systems being a pyridine-enhanced, precatalyst preparation, stabilisation and initiation (PEPPSI) type precatalyst (**Figure 1.12**).[39]

Figure 1.12 Pd-PEPPSI-IPr* precatalyst

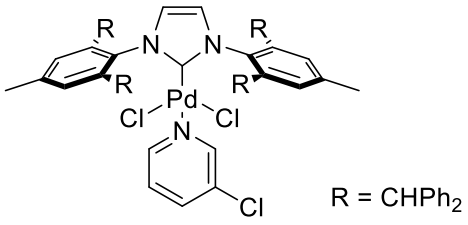

The advantage of this precatalyst was the wide applicability, able to couple a variety of functionalised substrates in excellent yield (70 – 98 %), whilst being relatively facile to prepare on a large scale (35 g).

One of the earliest examples of NHC-type ligands on a Ni complex was the use of a monodentate ligand to obtain complexes $[Ni(tmiy)_2I_2]$ or $[Ni(tmiy)_2(o\text{-tol})Br]$ (where tmiy = 1,3,4,5-tetramethylimidazol-2-ylidine) (**Figure 1.13**).[40]

Figure 1.13 $[Ni(tmiy)_2I_2]$ and $[Ni(tmiy)_2(o\text{-tol})Br]$

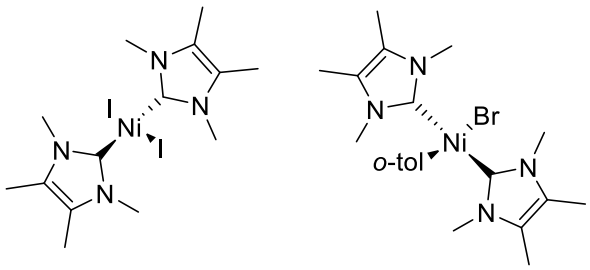

These complexes were used in the coupling of 4-bromoacetophenone with phenylboronic acids. The activity for these catalysts was low, but this result showed that Ni-NHC complexes had potential for these types of cross-coupling reactions. Further research into this area led to the development of Ni-pincer complexes derived from imidazole-NHC ligands (**Figure 1.14**).[41,42]

Figure 1.14 Ni-NHC complex based on imidazole

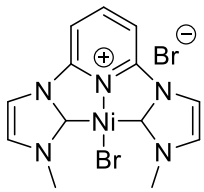

While being initially attractive for cross-coupling catalysts, coupling electron withdrawing and donating aryl bromides with phenylboronic acid at loadings of 1 mol% and electron deficient aryl chlorides at 5 mol%, the high temperatures required (120 °C) and very long reaction times (up to 4 days) limited their use significantly. However, the same group did further develop these catalysts (**Figure 1.15**)[43,44], leading to reaction times of a few hours as well as allowing the coupling of both aryl and alkenyl boronic acids.

Figure 1.15 Modified Ni-NHC imidazole type complexes

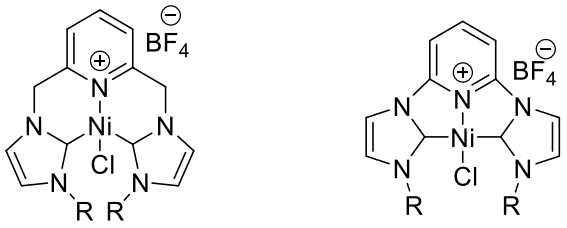

R = Mesityl and diisopropylphenyl (DIPP)

Some of the most well known NHC ligands today are based around the IPr ligand, which was reported in 1999 by Nolan[45], with IPr* first being made in 2010 by Marko (**Figure 1.16**).[46]

Figure 1.16 IPr and IPr* ligands

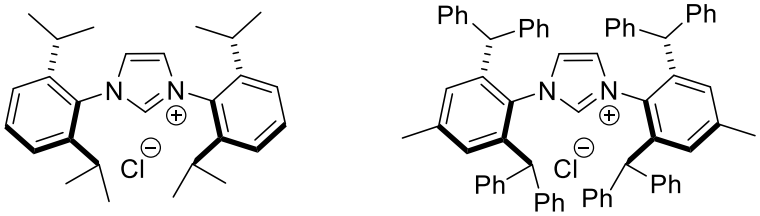

These ligands were developed to introduce controlled steric bulk around the metal centre to which they were bound. Enough steric bulk could potentially reduce the risk of unwanted side reactions during catalysis, such as C-H activation of the *ortho* position on the NHC aryl group, *via* stabilisation of the metal centre, though this has only been reported with 2nd generation Ru catalysts and some Ir catalysts.[4748,49] The bulk introduced must not be too great, however, as too much would potentially prevent oxidative addition to the metal. To this end, there are a variety of IPr-type ligands, ranging in size depending on the substituents on the aryl rings, that have been developed, with IMes and IPr* giving the least and greatest steric bulk respectively. One attractive feature of these ligands is their reasonably facile synthesis. The ligands are generally isolated as an HCl or HBF_4 salt (**Scheme 1.17**).[50,51] The preparation comprises three

straightforward steps: condensation of the starting aniline with benzhydrol (or derivative) to generate the substituted aniline (for IPr* and derivatives), diimine formation with glyoxal and finally cyclisation to the NHC with *p*-formaldehyde under acidic conditions.

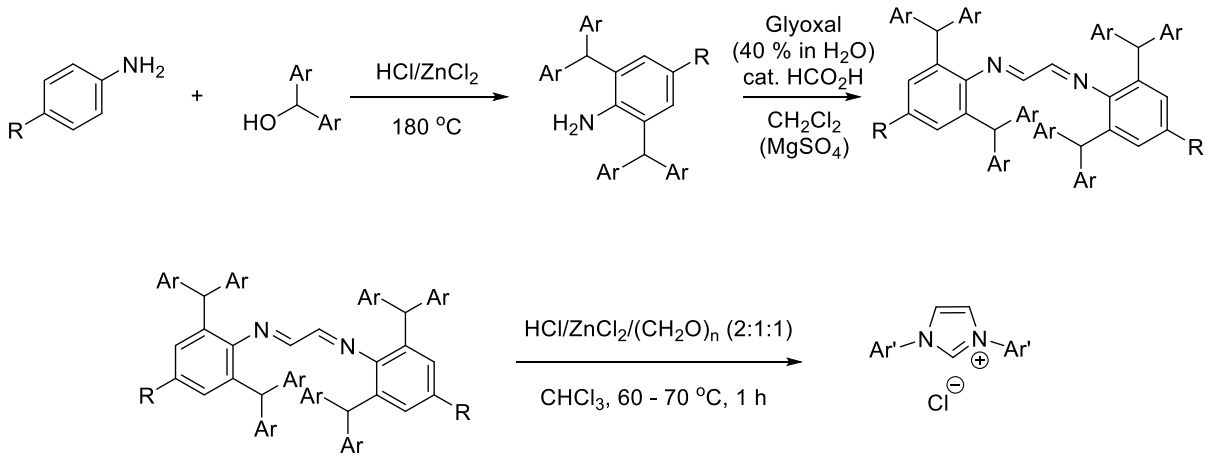

Scheme 1.17 General synthesis of IPr type NHC ligands

IPr* has been used in catalysis on both Ni and Pd centres successfully. Ni-catalysed Buchwald-Hartwig couplings (C-N bond formation, rather than C-C) were carried out effectively using [Ni(IPr)(η^3-allyl)Cl] and [Ni(IPr*^{OMe})(η^3-allyl)Cl] complexes (**Scheme 1.18**).[52,53]

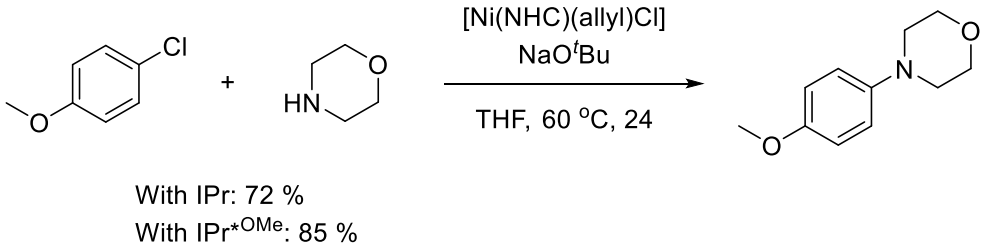

Scheme 1.18 Buchwald-Hartwig amination using Ni-NHC complexes

Loadings as low as 2 mol% were used in the case of the IPr* ligand, with isolated yields of up to 85 % attained. IPr based Pd complexes, [Pd(IPr*)(cin)Cl] for example, have been reported as efficient catalysts for the Suzuki-Miyaura coupling of particularly hindered substrates, leading to tetra-*ortho*-substituted biaryl products in 67 – 99 % yield (**Scheme 1.19**).[54]

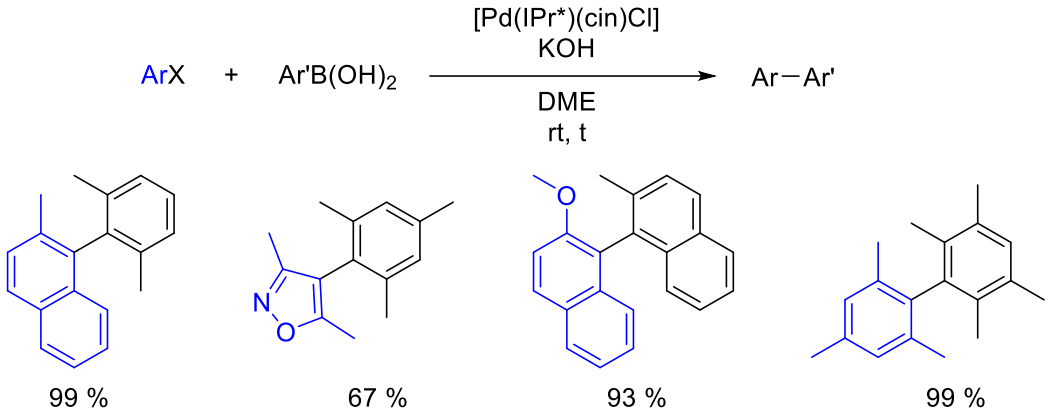

Scheme 1.19 Suzuki coupling using [Pd(IPr*)(cin)Cl]

Mechanistically, the overall cycle for Ni-mediated cross-coupling is thought to be similar to that of Pd, following the same fundamental steps but with variations, particularly in the transmetalation step. There are some studies, however, that have investigated whether some transformations really do proceed *via* a Ni(0) → Ni(II) → Ni(0) pathway. One such study showed that Ni(I) species are also catalytically active for Suzuki cross coupling, in the presence of a suitable organometal reagent.[55] During the study, it was found that the reaction of [Ni(IMes)$_2$] with aryl halides yielded [Ni(IMes)$_2$X], a Ni(I) species, rather than the expected [NiAr(IMes)$_2$X] Ni(II) species. In fact, no Ni(II) species were observed throughout the entire reaction. The group proposed a cycle, similar to that seen for pathways involving a Ni(II) species, but rather undergoing a Ni(I) → Ni(III) → Ni(I) transformation (**Scheme 1.20**).

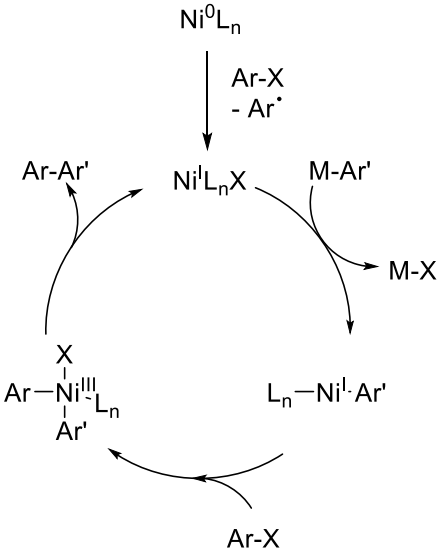

Scheme 1.20 Proposed cycle for Ni(I)-catalysed Suzuki coupling

Oxidative addition to the Ni centre during cross coupling has seen more investigation in recent years, both into the mechanism itself[40,56,57] and into factors that may influence it. Compared to Pd, Ni is more nucleophilic and, therefore, complexes based on Ni are more reactive towards oxidative addition. This can cause selectivity issues when planning syntheses on frameworks with a number of active sites. Ni(0) is also known to form η^2 complexes with carbonyl bearing compounds (**Figure 1.17**).[58] This was investigated in 1979, using [Ni(PEt_3)$_4$] and benzophenone for the initial studies (**Scheme 1.21**).

Figure 1.17 η^2 Ni complex with carbonyl group

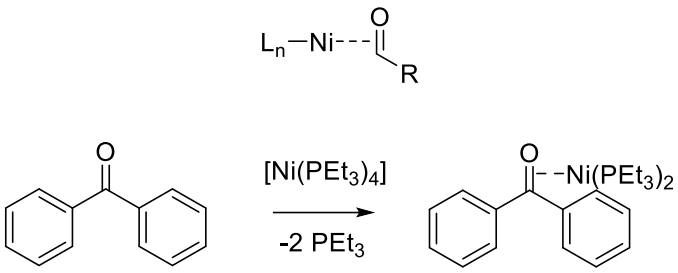

Scheme 1.21 Formation of complex with [Ni(PEt_3)$_4$] and benzophenone

A similar effect was observed when using acetophenone, but not with acetone or methyl benzoate. Similar π systems such as C=C and C=N moieties also exhibited this behaviour. Due

to the *trans* nature of the complexes, it is thought that π back-bonding is an important factor. This is confirmed by the fact that if a C=C moiety has an electron-withdrawing group present, lowering the energy of the antibonding π* orbital, the complex formation is favoured. This mode of bonding can be described by the Dewar-Chatt-Duncanson model. The π-orbital on the C=C donates electron density in a σ-type fashion, while the metal undergoes π-backbonding into the empty π* orbital (**Figure 1.18**).

Figure 1.18 Dewar-Chatt-Duncanson model for alkene-metal complexes

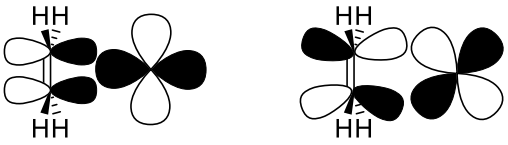

Potential applications of this complex formation have been investigated, with one of the most interesting ideas being that of intramolecular "ring-walking".[13,59,60] This phenomenon is where the metal forms a series of η^2 complexes along a conjugated system, without fully dissociating from the molecule. This essentially means that the metal is locked onto the molecule (assuming the equilibrium constant for complex formation is high enough). It was reported as being possible to use ring-walking as a precursor to oxidative addition *via* a conjugated system (**Scheme 1.22**).

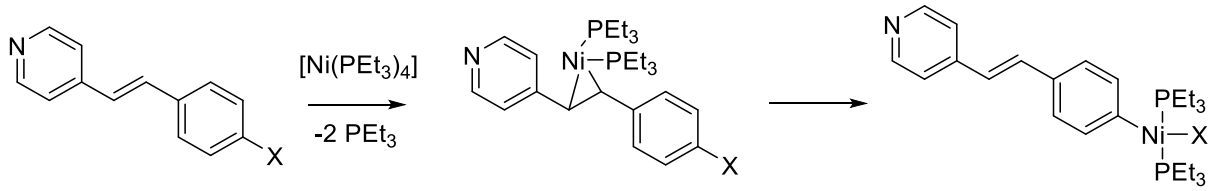

Scheme 1.22 Intramolecular ring-walking with $[Ni(PEt_3)_4]$

It was found during this study, that if the complex was already coordinated to the bromo substrate *via* the double bond, even in the presence of an iodo substrate which would be expected to be more reactive towards oxidative addition, the bromo oxidative addition product was the only product observed (**Scheme 1.23**).

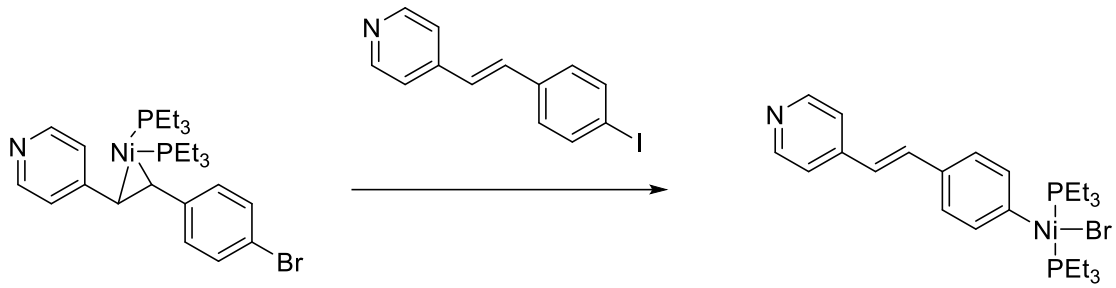

Scheme 1.23 Exclusivity in bromo substrate oxidative addition in presence of iodo substrate

A similar directing effect has been reported with Fe-catalysed alkylation, using aryl alkene groups to facilitate oxidative addition (**Scheme 1.24**).[61] A variety of aryl chlorides were coupled in this way, showing fairly wide applicability.

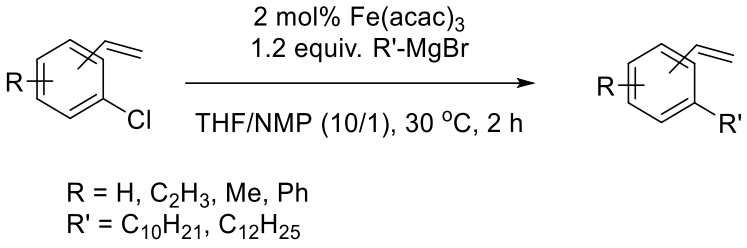

Scheme 1.24 Alkene-directed Fe-catalysed alkylation

It has been shown that [Ni(cod)(dppf)] also forms these η^2 complexes with benzaldehyde, acetophenone and benzophenone.[57] Interestingly, the equilibrium constants measured for the formation of these complexes differ greatly depending on the carbonyl-bearing substrate, with benzaldehyde giving complete conversion ($K_{eq} > 20$). The benzophenone and acetophenone constants were a lot lower at 0.65 and 0.023 respectively.

1.3 References

1 N. Miyaura and A. Suzuki, *Chem. Rev.*, 1995, **95**, 2457–2483.

2 A. Suzuki, *J. Organomet. Chem.*, 1999, **576**, 147–168.

3 F.-S. Han, *Chem. Soc. Rev.*, 2013, **42**, 5270.

4 C. M. Nunes and A. L. Monteiro, *J. Braz. Chem. Soc.*, 2007, **18**, 1443–1447.

5 V. L. Budarin, P. S. Shuttleworth, J. H. Clark and R. Luque, *Curr. Org. Synth.*, 2011, **7**, 614–627.

6 M. R. Netherton and G. C. Fu, *Angew. Chemie Int. Ed.*, 2002, **41**, 3910–3912.

7 A. F. Littke, C. Dai and G. C. Fu, *J. Am. Chem. Soc.*, 2000, **122**, 4020–4028.

8 K. W. Quasdorf, M. Riener, K. V. Petrova and N. K. Garg, *J. Am. Chem. Soc.*, 2009, **131**, 17748–17749.

9 L. Hie, S. D. Ramgren, T. Mesganaw and N. K. Garg, *Org. Lett.*, 2012, **14**, 4182–4185.

10 K. W. Quasdorf, A. Antoft-Finch, P. Liu, A. L. Silberstein, A. Komaromi, T. Blackburn, S. D. Ramgren, K. N. Houk, V. Snieckus and N. K. Garg, *J. Am. Chem. Soc.*, 2011, **133**, 6352–6363.

11 P. R. Melvin, A. Nova, D. Balcells, N. Hazari and M. Tilset, *Organometallics*, 2017, **36**, 3664–3675.

12 R. Martin and S. L. Buchwald, *Acc. Chem. Res.*, 2008, **41**, 1461–1473.

13 M. Orbach, O. V. Zenkina, Y. Diskin-Posner, M. A. Iron and M. E. Van Der Boom, *Organometallics*, 2013, **32**, 3074–3082.

14 A. J. J. Lennox and G. C. Lloyd-Jones, *Angew. Chemie Int. Ed.*, 2013, **52**, 7362–7370.

15 N. Miyaura and A. Suzuki, *J. Chem. Soc. Chem. Commun.*, 1979, 866.

16 N. Miyaura and A. Suzuki, *J. Organomet. Chem.*, 1981, **213**, C53–C56.

17 N. Miyaura, K. Yamada, H. Suginome and A. Suzuki, *J. Am. Chem. Soc.*, 1985, **107**, 972–980.

18 A. J. J. Lennox and G. C. Lloyd-Jones, *J. Am. Chem. Soc.*, 2012, **134**, 7431–7441.

19 U. Christmann and R. Vilar, *Angew. Chemie Int. Ed.*, 2005, **44**, 366–374.

20 T. E. Barder and S. L. Buchwald, *J. Am. Chem. Soc.*, 2007, **129**, 12003–12010.

21 J. F. Hartwig, *Inorg. Chem.*, 2007, **46**, 1936–1947.

22 S. Lou and G. C. Fu, *Adv. Synth. Catal.*, 2010, **352**, 2081–2084.

23 E. A. B. Kantchev, C. J. O'Brien and M. G. Organ, *Angew. Chemie Int. Ed.*, 2007, **46**, 2768–2813.

24 N. Miyaura, K. Yamada and A. Suzuki, *Tetrahedron Lett.*, 1979, **20**, 3437–3440.

25 V. Percec, J.-Y. Bae and D. H. Hill, *J. Org. Chem.*, 1995, **60**, 1060–1065.

26 T. Mesganaw and N. K. Garg, *Org. Process Res. Dev.*, 2013, **17**, 29–39.

27 M. Tobisu, T. Shimasaki and N. Chatani, *Angew. Chemie Int. Ed.*, 2008, **47**, 4866–4869.

28 F. Zhu and Z.-X. Wang, *J. Org. Chem.*, 2014, **79**, 4285–4292.

29 D. W. Old, J. P. Wolfe and S. L. Buchwald, *J. Am. Chem. Soc.*, 1998, **120**, 9722–9723.

30 B. A. Anjali and C. H. Suresh, *ACS Omega*, 2017, **2**, 4196–4206.

31 R. Lépine and J. Zhu, *Org. Lett.*, 2005, **7**, 2981–2984.

32 J. Malineni, R. Jezorek, N. Zhang and V. Percec, *Synthesis (Stuttg).*, 2016, **48**, 2795–2807.

33 H. Gao, Y. Li, Y.-G. Zhou, F.-S. Han and Y.-J. Lin, *Adv. Synth. Catal.*, 2011, **353**, 309–314.

34 F.-X. Felpin, E. Fouquet and C. Zakri, *Adv. Synth. Catal.*, 2009, **351**, 649–655.

35 C. A. Bernhart, P. M. Perreaut, B. P. Ferrari, Y. A. Muneaux, J. L. A. Assens, J. Clement, F. Haudricourt, C. F. Muneaux, J. E. Taillades, M.-A. Vignal, J. Gougat, P. R. Guiraudou, C. A. Lacour, A. Roccon, C. F. Cazaubon, J.-C. Breliere, G. Le Fur and D. Nisato, *J. Med. Chem.*, 1993, **36**, 3371–3380.

36 P. Bühlmayer, P. Furet, L. Criscione, M. de Gasparo, S. Whitebread, T. Schmidlin, R. Lattmann and J. Wood, *Bioorg. Med. Chem. Lett.*, 1994, **4**, 29–34.

37 J. E. Dander and N. K. Garg, *ACS Catal.*, 2017, **7**, 1413–1423.

38 N. A. Weires, E. L. Baker and N. K. Garg, *Nat. Chem.*, 2015, **8**, 75–79.

39 A. Chartoire, X. Frogneux, A. Boreux, A. M. Z. Slawin and S. P. Nolan, *Organometallics*, 2012, **31**, 6947–6951.

40 D. S. McGuinness, K. J. Cavell, B. W. Skelton and A. H. White, *Organometallics*, 1999, **18**, 1596–1605.

41 P. L. Chiu, C.-L. Lai, C.-F. Chang, C.-H. Hu and H. M. Lee, *Organometallics*, 2005, **24**, 6169–6178.

42 C.-C. Lee, W.-C. Ke, K.-T. Chan, C.-L. Lai, C.-H. Hu and H. M. Lee, *Chem. - A Eur. J.*, 2007, **13**, 582–591.

43 T. Tu, H. Mao, C. Herbert, M. Xu and K. H. Dötz, *Chem. Commun.*, 2010, **46**, 7796.

44 K. Inamoto, J. Kuroda, K. Hiroya, Y. Noda, M. Watanabe and T. Sakamoto, *Organo*, 2006, **25**, 3095–3098.

45 F. Izquierdo, S. Manzini and S. P. Nolan, *Chem. Commun.*, 2014, **50**, 14926–14937.

46 G. Berthon-Gelloz, M. A. Siegler, A. L. Spek, B. Tinant, J. N. H. Reek and I. E. Markó, *Dalt. Trans.*, 2010, **39**, 1444–1446.

47 C. Y. Tang, A. L. Thompson and S. Aldridge, *Angew. Chemie Int. Ed.*, 2010, **49**, 921–925.

48 T. Szilvási and T. Veszprémi, *ACS Catal.*, 2013, **3**, 1984–1991.

49 A. Poater, N. Bahri-Laleh and L. Cavallo, *Chem. Commun.*, 2011, **47**, 6674.

50 S. Meiries, K. Speck, D. B. Cordes, A. M. Z. Slawin and S. P. Nolan, *Organometallics*,

2013, **32**, 330–339.

51 A. R. Martin, A. Chartoire, A. M. Z. Slawin and S. P. Nolan, *Beilstein J. Org. Chem.*, 2012, **8**, 1637–1643.

52 M. J. Iglesias, A. Prieto and M. C. Nicasio, *Adv. Synth. Catal.*, 2010, **352**, 1949–1954.

53 A. R. Martin, D. J. Nelson, S. Meiries, A. M. Z. Slawin and S. P. Nolan, *European J. Org. Chem.*, 2014, **2014**, 3127–3131.

54 A. Chartoire, M. Lesieur, L. Falivene, A. M. Z. Slawin, L. Cavallo, C. S. J. Cazin and S. P. Nolan, *Chem. - A Eur. J.*, 2012, **18**, 4517–4521.

55 K. Zhang, M. Conda-Sheridan, S. R. Cooke and J. Louie, *Organometallics*, 2011, **30**, 2546–2552.

56 J. K. Stille and K. S. Y. Lau, *Acc. Chem. Res.*, 1977, **10**, 434–442.

57 S. Bajo, G. Laidlaw, A. R. Kennedy, S. Sproules and D. J. Nelson, *Organometallics*, 2017, **36**, 1662–1672.

58 T. T. Tsou, J. C. Huffman and J. K. Kochi, *Inorg. Chem.*, 1979, **18**, 2311–2317.

59 J. A. Bilbrey, A. N. Bootsma, M. A. Bartlett, J. Locklin, S. E. Wheeler and W. D. Allen, *J. Chem. Theory Comput.*, 2017, **13**, 1706–1711.

60 O. V. Zenkina, A. Karton, D. Freeman, L. J. W. Shimon, J. M. L. Martin and M. E. van der Boom, *Inorg. Chem.*, 2008, **47**, 5114–5121.

61 S. Gülak, T. N. Gieshoff and A. Jacobi von Wangelin, *Adv. Synth. Catal.*, 2013, **355**, 2197–2202.

2 Aims

The aims of this project were to investigate structure/reactivity relationships between nickel catalysts and electrophiles used in Suzuki-Miyaura cross-coupling.

The methods chosen were as follows:

- Attempt the cross-coupling of common simple electrophiles using nickel(II) precatalysts
- Optimise the conditions used in the couplings using DoE in order to obtain conditions that are applicable to many different electrophiles
- Design competition reactions to compare the conversion of substrates which possess π-coordinating groups to those which do not
- Quantify any selectivity that was observed and decouple this effect from electronic properties using Hammett parameters

These aims allowed us to arrive at robust conditions and were a reasonably streamlined process towards observing selectivity effects.

After these initial investigations, the aims then turned towards comparing these effects with palladium(II) catalysts, as well as using a robustness screen approach to determine if the corresponding inhibition would be apparent.

In line with the overall aim of the project, kinetic studies using calorimetry were also designed to ascertain rate information for these couplings.

These initial aims were then extended towards heterocyclic electrophiles as these scaffolds are very common in both pharmaceutical and agrochemical fields.

Chapter 2: Aldehydes and Ketones Influence Reactivity and Selectivity in Nickel Catalysed Suzuki-Miyaura Reactions

2.1 Authors	*Alasdair K. Cooper*[a]	Experimental work, data collection and analysis, article writing and assembly, Supplementary Information assembly
	David K. Leonard[‡]	Experimental work, data collection and analysis
	Sonia Bajo[‡]	Experimental work, data collection and analysis
	Paul M. Burton[b]	Industrial supervisor, experimental discussion and direction
	David J. Nelson[a]	Principal Investigator, project discussion and direction, DFT calculations and analysis, article writing and assembly, Supplementary Information assembly

a WestCHEM Department of Pure and Applied Chemistry, University of Strathclyde, 295 Cathedral Street, Glasgow, G1 1XL, Scotland. david.nelson@strath.ac.uk

b Syngenta, Jealott's Hill International Research Centre, Bracknell, Berkshire, RG42 6EY, UK.

Current address for DKL: Leibniz-Institute for Catalysis, Albert-Einstein-Straße 29a, 18059 Rostock, Germany.

Current address for SB: Institute for Chemical Research (IIQ), CSIC-University of Sevilla, Avda. Américo Vespucio 49, 41092 Sevilla, Spain

2.2 Paper Abstract

The energetically-favourable coordination of aldehydes and ketones – but not esters or amides – to Ni^0 during Suzuki-Miyaura reactions can lead either to exquisite selectivity and enhanced reactivity, or to inhibition of the reaction. Aryl halides where the C-X bond is connected to the same π-system as an aldehyde or ketone undergo unexpectedly rapid oxidative addition to [Ni(COD)(dppf)] (**1**), and are selectively cross-coupled during competition reactions. When aldehydes and ketones are present in the form of exogenous additives, the cross-coupling reaction is inhibited to an extent that depends on the strength of the coordination of the pendant carbonyl group to Ni^0. This work advances our understanding of how common functional groups interact with Ni^0 catalysts and how these interactions affect workhorse catalytic reactions in academia and industry.

2.3 Extended Introduction: Nickel Coordination Complexes of Aldehydes and Ketones

Oxidative addition to the nickel centre during cross coupling has seen more investigation in recent years, both into the mechanism itself[1–3] and into factors that may influence it. Compared to palladium, nickel is more nucleophilic and, therefore, complexes based on nickel are more reactive towards oxidative addition. This can cause selectivity issues when planning syntheses on frameworks with a number of active sites. Nickel(0) is also known to form η^2-complexes with carbonyl bearing compounds (**Figure 2.1**).[4] This was investigated in 1979, using $[Ni(PEt_3)_4]$ and benzophenone for the initial studies (**Scheme 2.1**).

Figure 2.1 η^2 Ni complex with carbonyl group

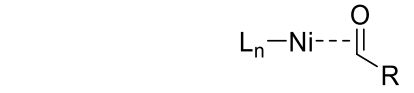

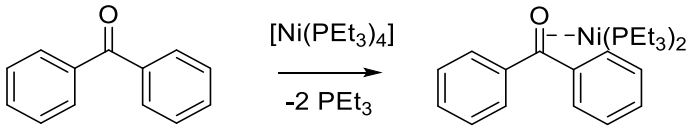

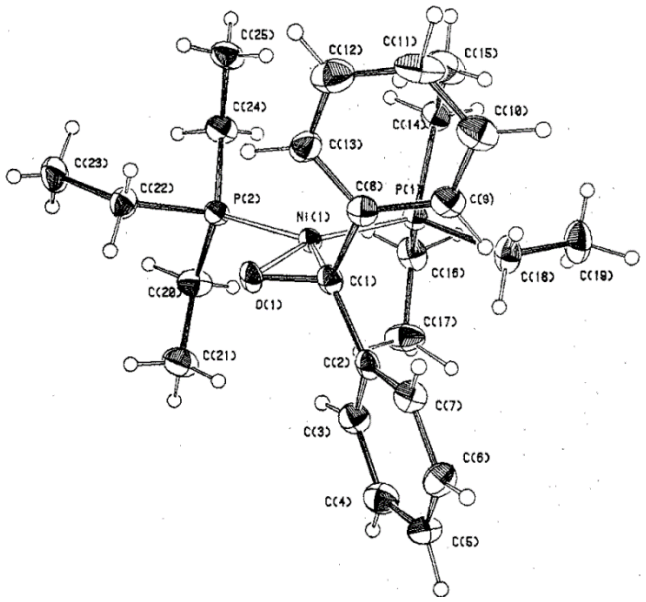

Scheme 2.1 Formation of complex with $[Ni(PEt_3)_4]$ and benzophenone and accompanying crystal structure

A similar effect was observed when using acetophenone, but not with acetone or methyl benzoate. In the case of methyl benzoate, this could be due to resonance stabilisation, where the carbon-oxygen double bond is not able to coordinate to the nickel centre. For acetone, this could be due to the slight increase in steric bulk caused by having two sp^3 carbon centres, rather than two sp^2 or one sp^2 and one sp^3, adjacent to the carbonyl group. Later, in 1989, Yamamoto published a study in which fluorinated ketones (hexafluoroacetone and 2,2,2-trifluoroacetophenone) were reacted with dialkyl nickel complexes (bearing either a bidentate phosphorus or nitrogen based ligand) to give the corresponding η^2 nickel carbonyl complexes *via* displacement of the alkyl ligands through reductive elimination (giving ethane and butane as side products, respectively) **Scheme 2.2**).[5]

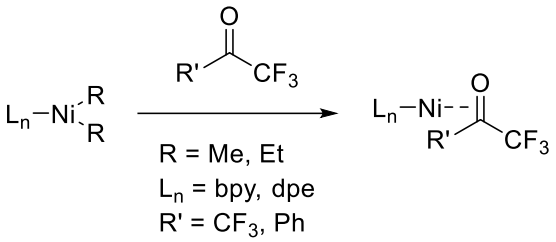

Scheme 2.2 Displacement of alkyl ligands to form η^2 nickel carbonyl complexes

Complexes such as these have been used for a variety of reactions. The partial and full hydrogenation of ketones to the corresponding alcohol and/or alkyl products using $[(dippe)Ni(\mu\text{-}H)]_2$ was reported for a range of carbonyl systems (**Scheme 2.3**).[6]

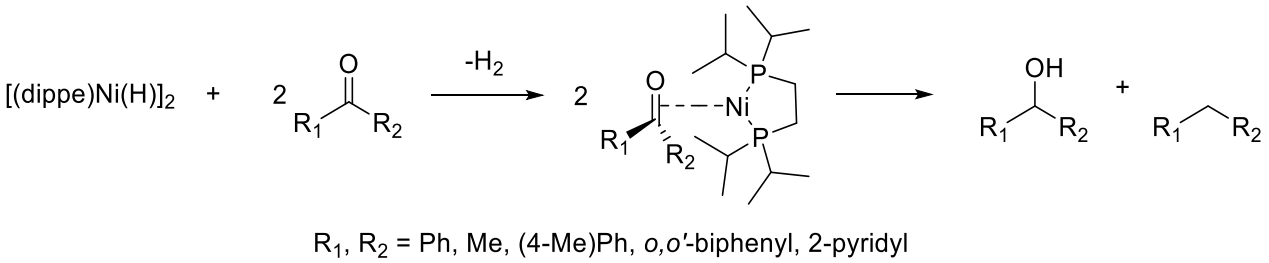

Scheme 2.3 Hydrogenation of ketones involving η^2 nickel carbonyl complexes

These complexes are not limited to ketones, however. It has been found that aldehydes can give rise to these same complexes, as shown in the following example starting from a [Ni(COD)] species (**Scheme 2.4**).[7] This reaction gives several different products, depending

upon the pathway chosen from the η^2 complex, including esters, ketones and silicon protected oxo-species.

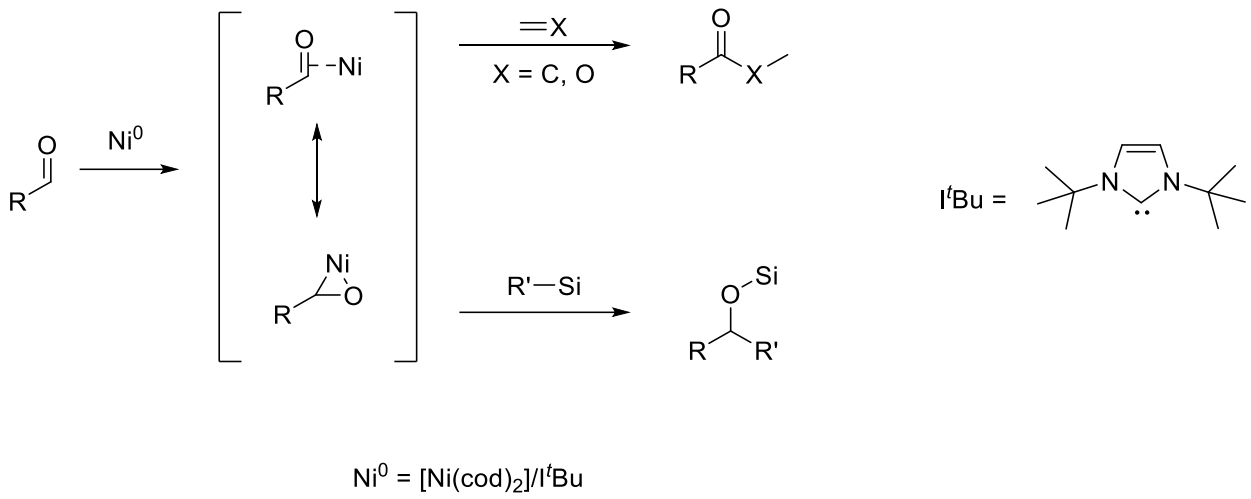

Scheme 2.4 Aldehyde η^2 Ni complexes used for aldehyde functionalisation

The same study reported the use of these functionalisation reactions to perform intramolecular alkene hydroacylations in yields of 70 – 99 % (**Scheme 2.5**).

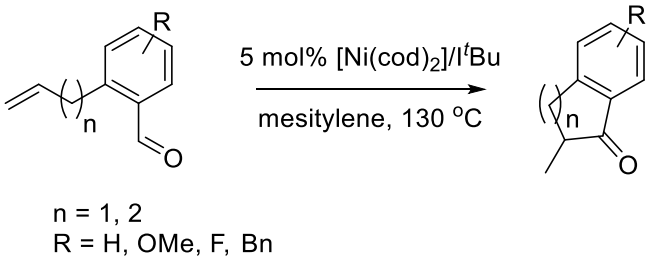

Scheme 2.5 Intramolecular hydroacylation of alkenes *via* η^2 aldehyde Ni complex

As shown in **Scheme 2.4**, the nature of the bonding in these complexes can be expressed in two ways:

i. As a direct interaction between the π-bond and the metal centre through σ-donation, in which the oxidation state of the metal remains unchanged

ii. As a metallacycle, where π-backbonding from the metal centre is sufficient that the π-bond in the ligand is weakened, and the oxidation state of the metal centre is formally increased by 2.

An in depth investigation into the nature of these complexes was conducted and published by Kennepohl and Love in 2019.[8] It was found in this study of [Ni(dtbpe)] complexes (using a combination of spectroscopic and computational techniques) that these systems mainly exist as metallacycles, with minimal σ-donation from the ligands. The π-acidity of the ligand, as well as the ability of the phosphine ligands to induce backbonding, are indicated by the degree of backbonding.

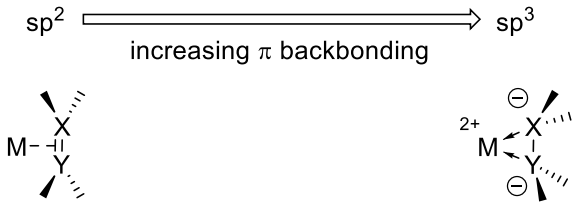

Scheme 2.6 π-adduct to metallacycle comparison

The ligands examined in this study included simple carbonyls (benzaldehyde and cyclohexanone), alkenes (ethene and cyclohexenone; bound through the carbon-carbon double bond), esters (ethyl 2,2,2-trifluoroacetate and *S*-ethyl 2,2,2-trifluoroethanethioate) and benzene. These complexes, it was found (with reference to known square planar Ni(II) complexes), deviated quite strongly from the idealised D_{4h} symmetry. This effect was due to the small bite angle formed from the π-ligand (if it is considered as an η^2 ligand, towards the metallacycle end of the spectrum). As the geometry around the metal centre is square planar, this implies a large degree of π-backbonding and so this is similar to the formation of a Ni(II) d^8 complex or, in this case, a metallacyclic electronic configuration. The report also touched on qualitative methods that have been frequently used such as ligand π-bond elongation and bond angle sum around the π-unit. These methods, however, were quite inconclusive as, for many of the complexes examined, the bond lengths fell between the typical C-O single and double bond lengths (122 and 143 pm respectively) and the bond angle sums fell between the values expected for planar sp^2-hybridised and pyramidal sp^3-hybridised carbon centres.

Introduction

Nickel catalysis has the potential to replace palladium catalysis in some reactions and to enable new reactivity that can be exploited in organic synthesis.[1] These reactions include tandem photocatalysis/cross-coupling,[2, 3] reductive cross-electrophile coupling,[4] and the cross-coupling of phenol derivatives,[5] aryl fluorides,[6, 7] and amides.[8] Several issues remain to be resolved before the full potential and impact of nickel catalysis can be realised. We must understand how nickel interacts with the functional groups that are present in target molecules in the fine chemicals, agrochemicals, and pharmaceutical industries, to understand the scope and limitations of existing methods and the opportunities and challenges to consider when developing new ones. The underlying reaction mechanisms in nickel catalysis, and how these depend on substrate and ligand structure, remain relatively poorly understood compared to palladium catalysis, and so nickel-catalysed reactions are often treated as a 'black box'. Correspondingly, reaction design and optimisation rely heavily on empirical observations.

The mechanisms of nickel-catalysed cross-coupling reactions remain relatively poorly understood and show a complex dependence on ligand and/or substrate. The mechanistic landscape is further complicated by the often-ambiguous role of nickel(I) species in catalysis.[9-12] [Ni(NHC)$_2$] and [Ni(PR$_3$)$_4$] complexes react with aryl halides by oxidative

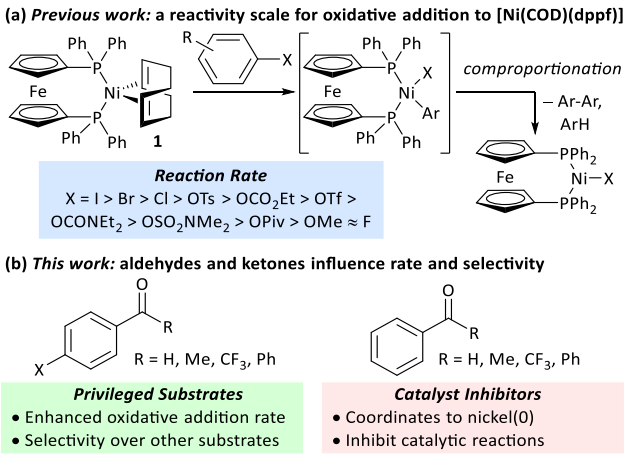

Figure 1. (a) Previous work. (b) This work.

addition or halide abstraction, depending on the ligand and substrate structure.[13-17] [Ni(COD)(dppf)] (**1**)[18] undergoes oxidative addition to aryl halides, followed by rapid comproportionation to form [NiX(dppf)] (Figure 1(a));[19] we have established the order of reactivity of a series of aryl (pseudo) halides. It was noted during our previous studies that aryl halides that had aldehyde or ketone substituents underwent unexpectedly fast oxidative addition. Further investigations have revealed that aldehyde and ketone functional groups can act either as directing groups for selective synthesis or as inhibitors of catalytic reactions (Figure 1(b)). Our initial empirical study showed that various coordinating groups elicit these effects, and that they are considerably more marked for nickel than for palladium.[20] Here, we examine the specific case of aldehydes and ketones in depth using a range of experimental and computational techniques.

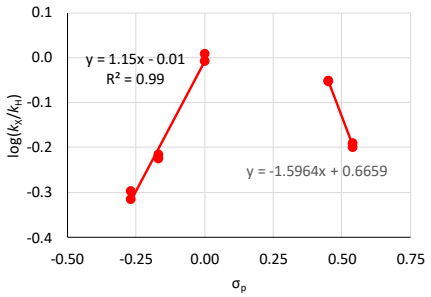

Figure 2. Hammett plot for oxidative addition of aryl chlorides to **1** from reactions at 50 °C in benzene-d_6.[19]

Results and Discussion

Kinetic Studies of Oxidative Addition

Aldehyde and ketone-substituted aryl chlorides undergo surprisingly rapid oxidative addition, compared to the oxidative addition rates for a set of other substrates (Figure 2). The consumption of **1** in the presence of excess aryl halide was monitored using ^{31}P NMR spectroscopy and exhibited pseudo-first order behaviour; rate data are recorded in Table 1. The ultimate nickel-containing products are [NiX(dppf)] complexes, as confirmed by EPR and ^{1}H NMR spectroscopies.[21] In contrast to cross-coupling reactions (*vide infra*) where transmetalation and reductive elimination can take place, the only pathway available to the arylnickel(II) halide intermediates formed during these kinetic experiments is comproportionation with **1** to form Ni^{I} products.

Substrates **2-Cl** to **4-Cl** undergo oxidative addition much more rapidly than electron-deficient aryl chloride **5-Cl** or bromide **5-Br**. These large rate differences cannot be attributed simply to inductive or mesomeric electronic effects; Hammett σ_p is 0.4 – 0.5 for ketones, aldehydes and esters and 0.54 for trifluoromethyl.[22] The Hammett plot for oxidative addition of aryl chlorides to **1** is shown in Figure 2.[19]

Ligand exchange, where COD is replaced with the aryl halide, and the oxidative addition event that follows cannot be deconvoluted; we propose that the favourable coordination of aldehydes and ketones to Ni^0 (*vide infra*) improves the equilibrium position of the ligand exchange (COD *versus* aryl halide), leading to a reaction that is more rapid overall. Consistent with this, signals that are tentatively assigned to an η^2(CO) complex are observed during the oxidative addition reactions of **3-Cl**; various complexes of this type are known,[23-30] and have been implicated in nickel-mediated reactions.[31] The observed signals in the $^{31}P\{^1H\}$ NMR spectrum are consistent with a square planar complex (two doublets with $^2J_{PP}$ of 31 Hz). This geometry is a result of electron donation from the bisphosphine ligand into the $3d(x^2\text{-}y^2)$ orbital, which is also engaged in *d* to π* back-bonding.[32, 33] The measured K_{eq} for the displacement of COD from **1** using benzaldehyde (>20), benzophenone (0.65), and acetophenone (0.02) are sufficiently large that under catalytic conditions – i.e. in the presence of a large excess (*ca.* 10 – 100 equiv.) of each cross-coupling partner – that this coordination would be expected to occur to the extent that between 2 and 100% of the Ni^0 present would be coordinated to a carbonyl group. The lack of a similar effect for esters (e.g. **6-Cl**) is attributed to *n* to π^*_{CO} resonance effects between the oxygen lone pair and the ester carbonyl group.

Table 1. Psuedo-first order and relative rate constants for the reactions between **1** and substrates **2**-**6**. All rate constants are the average of two measurements. [nd] = not determined.

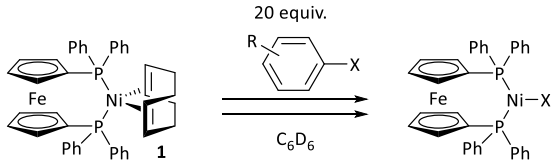

Oxidative Addition Rate Constants

Substrate	k_{obs} (20 °C)	k_{obs} (50 °C)	k_{rel}
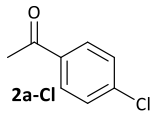 **2a-Cl**	2.5(3) x 10^{-4} s^{-1}	[nd]	0.32
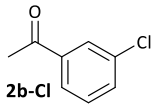 **2b-Cl**	4.2(3) x 10^{-4} s^{-1}	[nd]	0.54
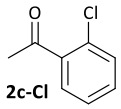 **2c-Cl**	3.0(2) x 10^{-4} s^{-1}	[nd]	0.38
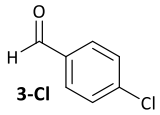 **3-Cl**	1.41(1) x 10^{-4} s^{-1}	[nd]	0.18
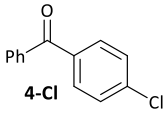 **4-Cl**	9.2(2) x 10^{-5} s^{-1}	[nd]	0.12
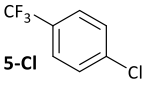 **5-Cl**	[nd]	2.39(3) x 10^{-4} s^{-1}	0.007
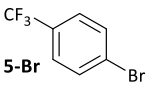 **5-Br**	2.38(4) x 10^{-5} s^{-1}	1.02(1) x 10^{-3} s^{-1}	0.031
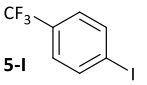 **5-I**	7.8(1) x 10^{-4} s^{-1}	[nd]	1.0
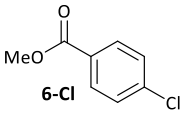 **6-Cl**	[nd]	1.85(4) x 10^{-4} s^{-1}	0.005

Cross-Coupling Selectivity

The coordination of aldehydes and ketones to Ni^0 can be leveraged to achieve selective cross-coupling. Optimised cross-coupling conditions were developed for the prototypical cross-coupling of **2a-Br** with *p*-tolylboronic acid, catalysed by well-defined [NiCl(*o*-tol)(dppf)] pre-catalyst **7**,[34] using factorial experimental design.[‡] To dissect the contributions of electronic and coordination effects, experiments were performed in which bromobenzene and a functionalized aryl bromide competed for a limiting amount of boronic acid (Figure 3 (a)).[§] Data were interpreted by quantifying selectivity using equation (1) (Figure 3 (b)); this has values between -1 and +1 which represent complete selectivity for bromobenzene and functionalised aryl bromide, respectively. The reaction selectivity was plotted versus σ (Figure 3(c)).[35] These data show that selectivity is typically insensitive to the electronic properties of the aryl halide, but significant selectivity is achieved when the aryl halide has a ketone or aldehyde functional group.[36] This selectivity trend is observed for both *meta*- and *para*-substituted aryl bromides. These data confirm that aldehyde and ketone substituents can be used to induce selective cross-coupling at one substrate present within the reaction.

Computational Modelling of Ring Walking and Oxidative Addition

DFT calculations give further insights into these reactions.[§§] [Ni(dppf)(η^2-benzene)] (**8**) was assigned G_{rel} = 0. Consistent with experiment, aldehydes and ketones coordinate [Ni(dppf)] exergonically *via* the carbonyl group (Figure 4 (a)). Free energy profiles were calculated for the oxidative addition reactions of selected aryl bromides (Figure 4 (b));[37] reactions proceed via transition state **B** to irreversibly form Ni^{II} products **C**. The aldehyde substrate can also form the η^2(CO) complex.

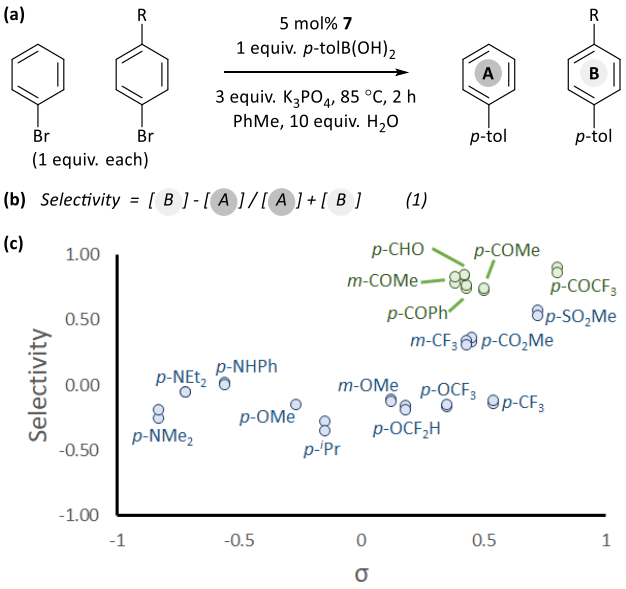

Figure 3. Competition experiments: (a) reaction conditions; (b) quantification of selectivity; and (c) reactions in toluene with 10 equiv. water. Each individual competition experiment is plotted as a separate point

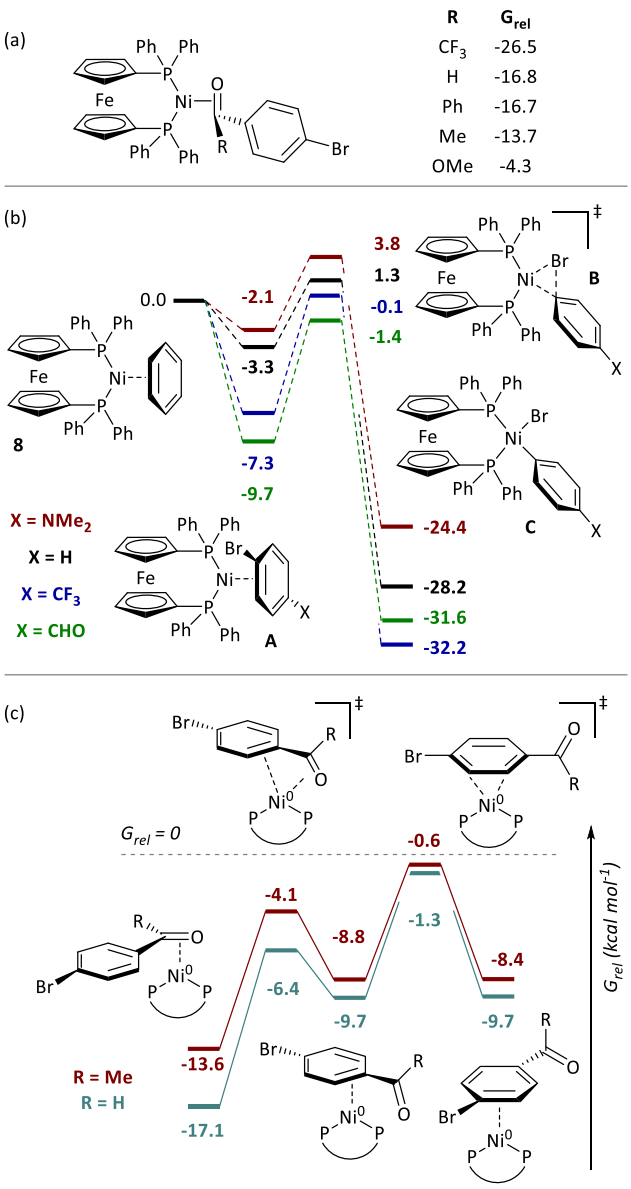

Figure 4. (a) Coordination to aldehydes, ketones, and esters. (b) Free energy profile for oxidative addition. (c) Calculations on the ring-walking process. All energies are free energies in toluene solution and are quoted in kcal mol^{-1}.

Further calculations were undertaken to model the ring-walking[38-42] step, using **2a-Br** and **3-Br** as substrates. In each case, three η^2-complexes are linked by two transition states, leading from the carbonyl group to the halide site (Figure 4 (c)). The transition states for these ring-walking steps are all lower in energy than **8** and so this process is more energetically favourable than the dissociation of the aryl halide and coordination of a new aryl halide; once an aldehyde- or ketone- containing substrate coordinates the nickel centre *via* the carbonyl ligand, it will undergo oxidative addition after ring walking, rather than ligand exchange for an alternative substrate. Substrate **2c-Br**

undergoes a similar ring-walking process, again with no intermediates or transition states that have $G_{rel} > 0$.[‡] These data are consistent with two key experimental observations: (i) the enhanced rate of oxidative

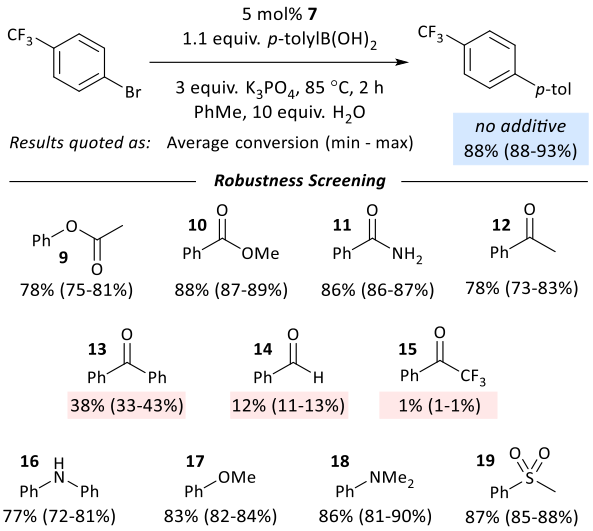

Figure 5. Results from the robustness screen.

addition, because η^2(CO) coordination renders aldehyde- and ketone-containing aryl halides competitive ligands (*versus* COD); and (ii) selective cross-coupling, because aldehyde- and ketone-containing aryl halides are much better ligands for Ni^0 than aryl halides without such strongly coordinating groups.

Catalyst Inhibition by Aldehydes and Ketones

The coordination of ketones and aldehydes to Ni^0 might be expected to have a detrimental effect on the performance of cross-coupling reactions if this behaviour sequesters the active catalyst. A 'robustness screen'[43, 44] was used, in which a model reaction was carried out in the presence of 1 equiv. of each of a series of additives (**9** – **19**).[§] This provides a rapid and quantitative measure of the effect of each additive. A palette of additives was examined (Figure 5).

Most additives had little effect on the reaction conversion. Aldehyde and ketone additives – except for acetophenone (**12**) – had a significant and detrimental effect, with the reaction almost completely ceasing when 1 equiv. of 2,2,2-trifluoroacetophenone (**15**) was present. The degree of inhibition of the reaction is correlated to K_{eq} for the displacement of COD from **1** (*vide supra*); it may be necessary to protect aldehydes and

ketones in some reactions to prevent their coordination to Ni^0. If catalyst decomposition was responsible for the decrease in yield then we would expect that at the end of the reaction ≥5% of the additive would have been consumed;[45] in the case of **13** and **14**, ≤ 2% of the additive is unaccounted for, while **15** hydrates in the presence of water, resulting in the absence of 12 – 15% of **15** at the end of the reaction. There is no correlation between the degree of inhibition and the amount of additive unaccounted for.

Control experiments where one equivalent of benzaldehyde was added to the cross-coupling of **4-Cl** and *p*-tolylboronic acid showed complete conversion to the cross-coupling product. Aldehyde and ketone additives therefore have less of an effect on the cross-coupling reactions of aldehyde- and ketone-

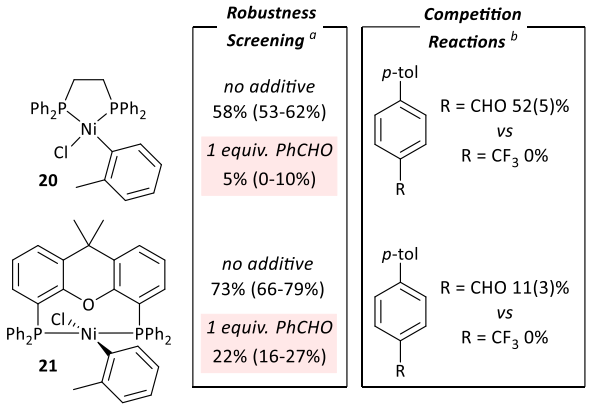

a) 5 mol% catalyst, 1 equiv. **5-Br**, 1.1 equiv. *p*-tolB(OH)$_2$, 3 equiv. K_3PO_4, 10 equiv. H_2O, PhMe, 85 °C, 2 h. b) 5 mol% catalyst, 1 equiv. **3-Br**, 1 equiv. **5-Br**, 1 equiv. *p*-tolB(OH)$_2$, 3 equiv. K_2PO_4, 4:1 *v*/*v* THF/water, 85 °C, 2 h.

Figure 6. Results with dppe and Xantphos catalysts.

containing aryl halides than they do on the cross-coupling of aryl halides that do not contain these functional groups.

The robustness screening data are consistent with coordination of an exogenous additive to the Ni^0 catalyst inhibiting the reaction. No ring-walking is possible from such intermediates to a site for oxidative addition or other exergonic onward reaction.

On the Generality of These Effects

These observations are not limited to dppf-based (pre)catalysts. [NiCl(o-tol)(L)$_n$] (L = dppe (**20**), Xantphos (**21**))[34] were applied in: (i) competition reactions between **5-Br** and **3-Br**, in which **3-Br** reacts exclusively; and (ii) robustness screening reactions

using **5-Br** as the substrate and benzaldehyde as the additive, showing significant reaction inhibition (Figure 6).[§] Complexes **20** and **21** perform significantly less well than **7** but may yield better results if further reaction optimisation was carried out. The results in Figure 6 illustrate that the effect is general to nickel phosphine complexes, and not limited to dppf-based catalysts. Palladium, specifically [$PdCl_2$(dppf)], shows a far reduced propensity to undergo selective cross-coupling reactions, but has far better functional group tolerance. [20]

Opportunities for Exploitation

The carbonyl coordination effect was leveraged to achieve site selectivity in cross-coupling reactions, both intermolecularly and intramolecularly (Figure 7). The aldehyde/ketone effect allows the normal reactivity order of aryl halides (I > Br > Cl)[19] to be entirely overridden, to the extent that an aryl chloride (2a-Cl) undergoes selective coupling in the presence of an electron- deficient aryl bromide (5-Br) and even in the presence of an aryl iodide (5-I) (Figure 7 (a)). Reactions are selective for aldehydes over ketones, as judged from further competition experiments.[‡] Ketones that are not in conjugation with the aryl halide π-system are not selectively coupled (e.g. 22-Br) (Figure 7 (b)). Intramolecular competition experiments were carried out using 23-Cl, which has two aryl chloride sites that are available for cross-coupling but only one is in conjugation with a ketone (Figure 7 (c)); reactions with **23-Cl** establish that selective cross-coupling occurs at the site that is in conjugation with the ketone. Intrinsic differences in the reactivities of aryl chlorides, bromides, and iodides have been leveraged in the past for selective cross-coupling reactions,[46] but this work shows that the substitution pattern of the aryl halide can significantly change the order of reactivity, opening new avenues for creative organic synthesis using nickel-catalysed cross-coupling.

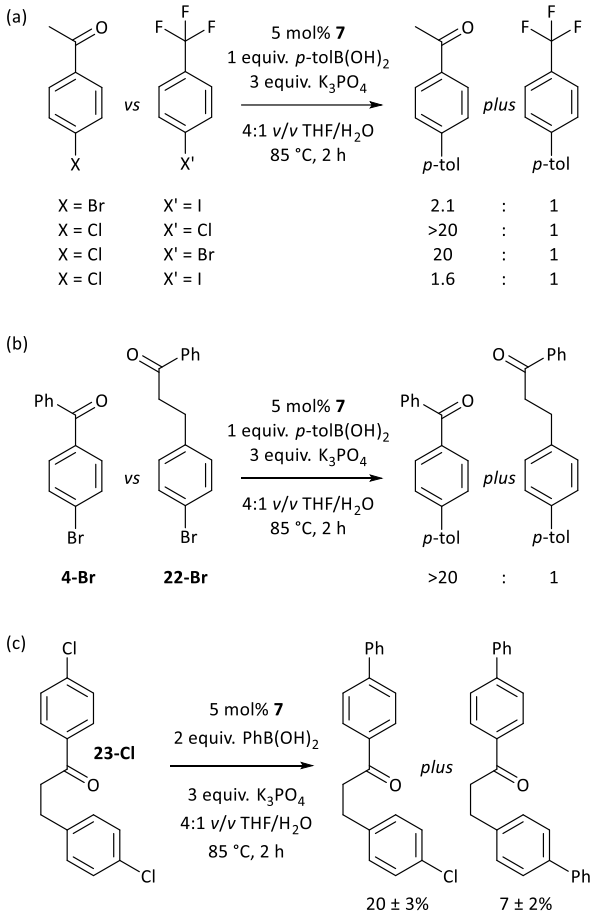

Figure 7. (a) Overriding the intrinsic reactivity differences between aryl halides. (b) Selectivity between different carbonyl-containing substrates. (c) Site-selectivity within a molecule, enforced by carbonyl coordination.

Conclusions

This work establishes how aldehydes and ketones can have positive or negative effects on nickel-catalysed reactions, depending on their location. The formation of η^2-complexes has been implicated in some nickel-catalysed reactions 30, 31, 39, 47, 48 but this work shows that coordination effects can influence even simple and ubiquitous Suzuki-Miyaura reactions.

- Aryl halides with aldehyde and ketone functional groups undergo rapid oxidative addition because of favourable ligand exchange and ring-walking processes.
- Selectivity is achieved for aldehyde- or ketone-containing aryl halides over other aryl halide substrates because of this favourable coordination.

• Aldehydes and ketones that are present in cross-coupling reactions but are not in conjugation with the aryl halide act as inhibitors of catalysis.

• Aldehydes and ketone-containing aryl halides undergo successful cross-coupling.

Figure 8 summarises the conclusions of this study using Ni^0/Ni^{II} cycles based on literature evidence from studies of nickel/dppf-catalysed reactions.18, 19, 49-53 Figure 8 (a) shows a cycle for a reaction in which an aldehyde or ketone is present as an additive; a low energy η^2(CO) complex sequesters the active catalyst and slows the reaction because the η^2-complex with the aryl halide is higher in energy. Figure 8 (b) shows a cycle for an aryl halide with an aldehyde or ketone substituent.

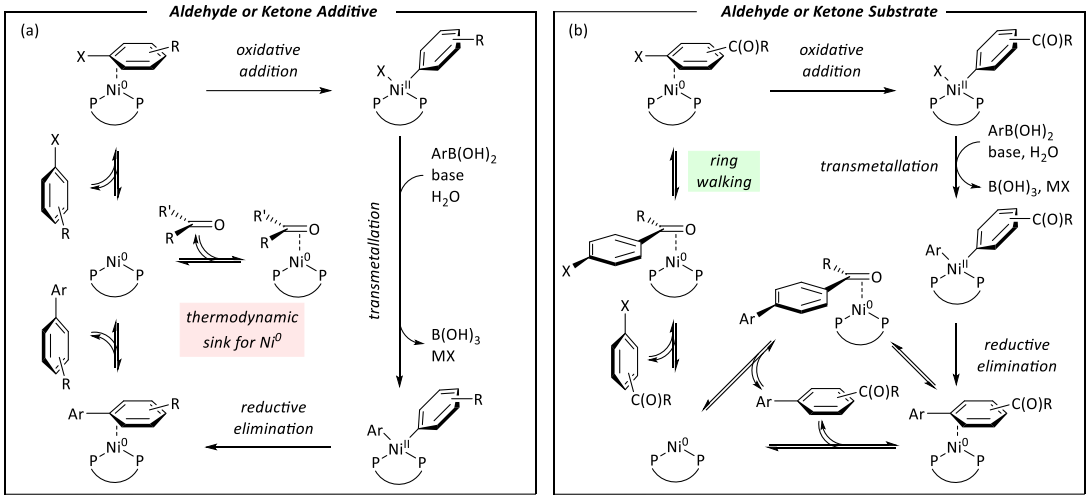

Figure 8. (a) Catalytic cycle for nickel-catalysed Suzuki-Miyaura reactions in the presence of exogenous aldehyde or ketone. (b) Catalytic cycle for nickel-catalysed Suzuki-Miyaura reactions of aldehyde- and ketone-containing aryl halides.

We are currently pursuing further work within our laboratories to understand the effects of a wider range of functional groups on nickel-catalysed reactions and their fundamental steps using kinetic and mechanistic studies.

Conflicts of interest

There are no conflicts to declare.

Acknowledgements

We are grateful for funding from: a Syngenta/Engineering and Physical Sciences Research Council (EPSRC) Industrial CASE Studentship for AKC (EP/P51066X/1); the EPSRC (EP/M027678/1); the University of Strathclyde for a Chancellor's Fellowship for DJN (2014-2018); and the Carnegie Trust for the Universities of Scotland for a Research Incentive Grant

(RIG008165). We thank the Department of Pure and Applied Chemistry at the University of Strathclyde for consumables and facilities funding for DKL. We thank Mr G. Bain, Mr C. Irving, Ms P. Keating, and Dr J. Parkinson for assistance with technical and analytical facilities. We thank Dr J. Sanderson (University of Newcastle) for assistance with initial factorial experimental design studies. Some of the results reported here were obtained using the EPSRC-funded ARCHIE-WeSt high-performance computer (archie-west.ac.uk) (EP/K000586/1); we are grateful to Mr J. Buzzard, Dr K. Kubiak-Ossowska, and Dr R. Martin for their assistance with this facility. We thank Dr S. Sproules for EPR analyses and Dr A. Watson (University of St Andrews) for helpful discussions.

Notes and references

‡ See the supporting information for further details.

§ Reaction outcomes were analysed using calibrated GC-FID analyses. In some competition experiments, total yield sometimes slightly exceeded 100% which is likely to be due to errors in weighing out exactly one equivalent of boronic acid.

§§ Calculations were carried out using Gaussian09 Rev. D01.[54] Geometry optimisations were carried out without symmetry constraints using the B3LYP functional with Grimme's D3 dispersion corrections, the LANL2DZ(dp) basis set on Br and I, the LANL2TZ(f) basis set on Ni and Fe, and the 6-31G(d) basis set on all other atoms. The nature of stationary points was confirmed using frequency calculations. Energies were refined using single point calculations in which the 6-31G(d) basis set was exchanged for 6-311+G(d,p). All calculations were carried out in toluene solvent using the SMD solvent model.

1. S. Z. Tasker, E. A. Standley and T. F. Jamison, *Nature*, 2014, **509**, 299-309.
2. J. Twilton, P. Zhang, M. H. Shaw, R. W. Evans and D. W. MacMillan, *Nature Reviews Chemistry*, 2017, **1**, 0052.
3. J. C. Tellis, C. B. Kelly, D. N. Primer, M. Jouffroy, N. R. Patel and G. A. Molander, *Acc. Chem. Res.*, 2016, **49**, 1429-1439.
4. D. J. Weix, *Acc. Chem. Res.*, 2015, **48**, 1767-1775.
5. T. Mesganaw and N. K. Garg, *Org. Proc. Res. Dev.*, 2012, **17**, 29-39.
6. T. Schaub, M. Backes and U. Radius, *J. Am. Chem. Soc.*, 2006, **128**, 15964-15965.
7. M. Tobisu, T. Xu, T. Shimasaki and N. Chatani, *J. Am. Chem. Soc.*, 2011, **133**, 19505-19511.

8. J. E. Dander and N. K. Garg, *ACS Catal*, 2017, **7**, 1413-1423.
9. C. Y. Lin and P. P. Power, *Chem Soc Rev*, 2017, **46**, 5347-5399.
10. J. Jover, *Catal. Sci. Technol.*, 2019, DOI: 10.1039/C9CY01365B.
11. T. Inatomi, Y. Fukahori, Y. Yamada, R. Ishikawa, S. Kanegawa, Y. Koga and K. Matsubara, *Catal. Sci. Technol.*, 2019, **9**, 1784-1793.
12. G. D. Jones, J. L. Martin, C. McFarland, O. R. Allen, R. E. Hall, A. D. Haley, R. J. Brandon, T. Konovalova, P. J. Desrochers, P. Pulay and D. A. Vicic, *J. Am. Chem. Soc.*, 2006, **128**, 13175-13183.
13. I. Funes-Ardoiz, D. J. Nelson and F. Maseras, *Chem. Eur. J.*, 2017, **23**, 16728-16733.
14. D. J. Nelson and F. Maseras, *Chem. Commun.*, 2018, **54**, 10646-10649.
15. K. Zhang, M. Conda-Sheridan, S. R. Cooke and J. Louie, *Organometallics*, 2011, **30**, 2546-2552.
16. D. S. McGuinness, K. J. Cavell, B. W. Skelton and A. H. White, *Organometallics*, 1999, **18**, 1596-1605.
17. A. Manzoor, P. Wienefeld, M. C. Baird and P. H. M. Budzelaar, *Organometallics*, 2017, **36**, 3508-3519.
18. G. Yin, I. Kalvet, U. Englert and F. Schoenebeck, *J. Am. Chem. Soc.*, 2015, **137**, 4164-4172.
19. S. Bajo, G. Laidlaw, A. R. Kennedy, S. Sproules and D. J. Nelson, *Organometallics*, 2017, **36**, 1662-1672.
20. A. K. Cooper, P. M. Burton and D. J. Nelson, *Synthesis*, 2020, DOI: 10.1055/s-0039-1690045.
21. We have established the mechanism of this reaction, and showed that this proceeds via oxidative addition to form Ni(II) intermediates - which are only observable when the aryl halide has ortho-substituents - which then undergo comproportionation to Ni(0). Please see reference 15 for details.
22. C. Hansch, A. Leo and R. W. Taft, *Chem. Rev.*, 1991, **91**, 165-195.
23. D. Walther, *Z. Anorg. Allg. Chem.*, 1977, **431**, 17-30.
24. D. Walther, *J. Organomet. Chem.*, 1980, **190**, 393-401.
25. J. Kaiser, J. Sieler, D. Walther, E. Dinjus and L. Golic, *Acta Crystallographica Section B*, 1982, **38**, 1584-1586.
26. R. Countryman and B. R. Penfold, *Journal of Crystal and Molecular Structure*, 1972, **2**, 281-290.
27. T. T. Tsou, J. C. Huffman and J. K. Kochi, *Inorg. Chem.*, 1979, **18**, 2311-2317.

28. A. Flores-Gaspar, P. Pinedo-González, M. G. Crestani, M. Muñoz-Hernández, D. Morales-Morales, B. A. Warsop, W. D. Jones and J. J. García, *J. Mol. Cat. A., Chem.*, 2009, **309**, 1-11.
29. R. Doi, K. Kikushima, M. Ohashi and S. Ogoshi, *J. Am. Chem. Soc.*, 2015, **137**, 3276-3282.
30. C. Lei, Y. J. Yip and J. S. Zhou, *J Am Chem Soc*, 2017, **139**, 6086-6089.
31. Y. Hoshimoto, M. Ohashi and S. Ogoshi, *Acc. Chem. Res.*, 2015, **48**, 1746-1755.
32. A. N. Desnoyer, W. He, S. Behyan, W. Chiu, J. A. Love and P. Kennepohl, *Chemistry*, 2019, **25**, 5259-5268.
33. W. He and P. Kennepohl, *Faraday Discussions*, 2019, DOI: 10.1039/C9FD00041K.
34. E. A. Standley, S. J. Smith, P. Müller and T. F. Jamison, *Organometallics*, 2014, **33**, 2012-2018.
35. Equivalent data are obtained in a THF/water solvent mixture; please see reference 16.
36. Control experiments with ketone-functionalised boronic acids did not lead to selective cross-coupling of these species (see the Supporting Information). Coordination occurs to Ni(0) only, and not to the more sterically-crowded and less electron-rich Ni(II) intermediates.
37. Free energy profiles for the corresponding reactions of a wider range of aryl halides can be found in the Supporting Information.
38. N. Yoshikai, H. Matsuda and E. Nakamura, *J. Am. Chem. Soc.*, 2008, **130**, 15258-15259.
39. L. Guo, S. Dai, X. Sui and C. Chen, *ACS Catal.*, 2016, **6**, 428-441.
40. O. V. Zenkina, A. Karton, D. Freeman, L. J. W. Shimon, J. M. L. Martin and M. E. van der Boom, *Inorg. Chem.*, 2008, **47**, 5114-5121.
41. J. A. Bilbrey, A. N. Bootsma, M. A. Bartlett, J. Locklin, S. E. Wheeler and W. D. Allen, *J. Chem. Theor. Comput.*, 2017, **13**, 1706-1711.
42. S. K. Sontag, J. A. Bilbrey, N. E. Huddleston, G. R. Sheppard, W. D. Allen and J. Locklin, *J. Org. Chem.*, 2014, **79**, 1836-1841.
43. K. D. Collins and F. Glorius, *Acc. Chem. Res.*, 2015, **48**, 619-627.
44. K. D. Collins and F. Glorius, *Nat Chem*, 2013, **5**, 597-601.
45. This assumes a >1:1 additive:nickel stoichiometry in such a decomposition reaction, based on the low concentrations of nickel in the reactions and the high concentrations of additive (20 equiv. with respect to nickel).

46. C. P. Seath, J. W. B. Fyfe, J. J. Molloy and A. J. B. Watson, *Angew. Chem. Int. Ed.*, 2015, **54**, 9976-9979.
47. E. L. Lanni and A. J. McNeil, *J. Am. Chem. Soc.*, 2009, **131**, 16573-16579.
48. W. He, B. O. Patrick and P. Kennepohl, *Nature Communications*, 2018, **9**, 3866.
49. L. M. Guard, M. Mohadjer Beromi, G. W. Brudvig, N. Hazari and D. J. Vinyard, *Angew. Chem. Int. Ed.*, 2015, **54**, 13352-13356.
50. I. Kalvet, Q. Guo, G. J. Tizzard and F. Schoenebeck, *ACS Catal.*, 2017, **7**, 2126-2132.
51. M. Mohadjer Beromi, A. Nova, D. Balcells, A. M. Brasacchio, G. W. Brudvig, L. M. Guard, N. Hazari and D. J. Vinyard, *J Am Chem Soc*, 2017, **139**, 922-936.
52. M. Mohadjer Beromi, G. Banerjee, G. W. Brudvig, N. Hazari and B. Q. Mercado, *ACS Catal.*, 2018, **8**, 2526-2533.
53. M. Mohadjer Beromi, G. Banerjee, G. W. Brudvig, D. J. Charboneau, N. Hazari, H. M. C. Lant and B. Q. Mercado, *Organometallics*, 2018, DOI: 10.1021/acs.organomet.8b00589.
54. M. J. Frisch, G. W. Trucks, H. B. Schlegel, G. E. Scuseria, M. A. Robb, J. R. Cheeseman, G. Scalmani, V. Barone, B. Mennucci, G. A. Petersson, H. Nakatsuji, M. Caricato, X. Li, H. P. Hratchian, A. F. Izmaylov, J. Bloino, J. Zheng, L. Sonnenberg, M. Hada, M. Ehara, K. Toyota, R. Fukuda, J. Hasegawa, M. Ishida, T. Nakajima, Y. Honda, O. Kitao, T. Nakai, T. Vreven, J. A. Montgomery, J. E. Peralta, F. Ogliaro, M. Bearpark, J. J. Heyd, E. Brothers, K. N. Kudin, V. N. Staroverov, R. Kobayashi, J. Normand, K. Raghavachari, A. Rendell, J. C. Burant, S. S. Iyengar, J. Tomasi, M. Cossi, N. Rega, J. M. Millam, M. Klene, J. E. Knox, J. B. Cross, V. Bakken, C. Adamo, J. Jaramillo, R. Gomperts, R. E. Stratmann, O. Yazyev, A. J. Austin, C. Cammi, C. Pomelli, J. W. Ochterski, R. L. Martin, K. Morokuma, V. G. Zakrzewski, G. A. Voth, P. Salvador, J. J. Dannenberg, S. Dapprich, A. D. Daniels, O. Farkas, J. B. Foresman, J. V. Ortiz, J. Cioslowski and D. J. Fox, *Journal*, 2009.

2.4 Extended Discussion

2.4.1 Design of Experiments Theory

In order to fully investigate the effect of different functional groups on the Ni-catalysed Suzuki couplings, a set of optimised and generally applicable reaction conditions had to be obtained.

A Design of Experiments (DoE) method was deemed the most suitable method. DoE is an attractive method of optimisation, as it allows multiple variables to be investigated simultaneously. This is superior to a linear style of optimisation, where one variable is altered at a time. The disadvantages of linear styles, apart from being far more time consuming, are that they do not allow potential interactions between variables to be observed. Moreover, linear approaches may lead to what appears to be a favourable, optimised result, but what actually may be a "local" maximum, rather than the global maximum. This is depicted graphically (**Figure 2.2**).

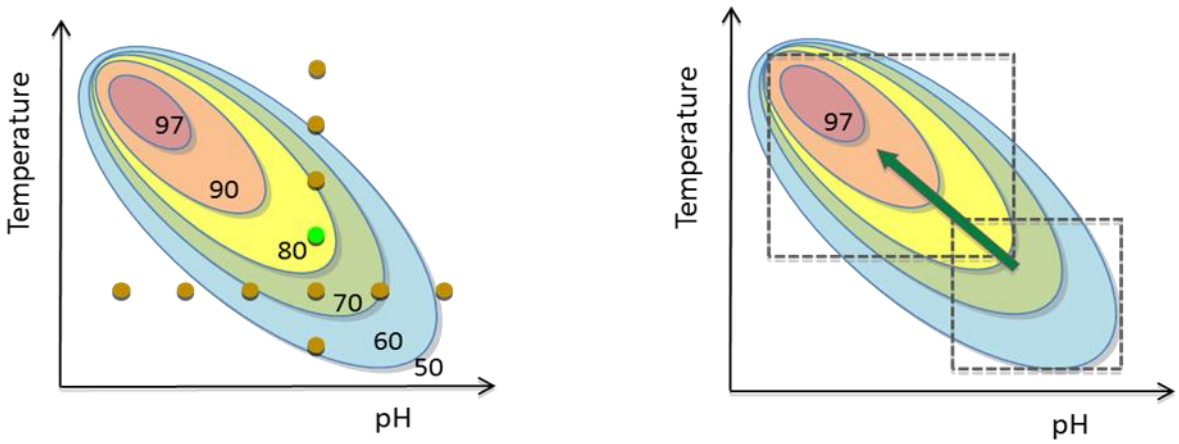

Figure 2.2 Linear optimisation vs. multivariate optimisation

The DoE approach incorporates both the variables themselves and their respective levels. The levels are the values for the variables tested. For example, a two level design would use the highest and lowest values for each variable. To ensure reproducibility and to establish any errors in the reaction design, control experiments are added to the method. These are known as centre points and use the middle level values for each factor. The number of reactions to be carried out, *N*, is determined using the equation:

$$N = l^n$$

Where *l* is the number of levels and *n* is the number of factors. So a 3 factor, 2 level design would require 8 reactions, plus any centre points, to be carried out. It is possible to modify this, to decrease the number of experiments required, by using a half-fractional design. This simply halves the number of experiments to be performed, while still covering as much of the design area as possible (**Figure 2.3**).

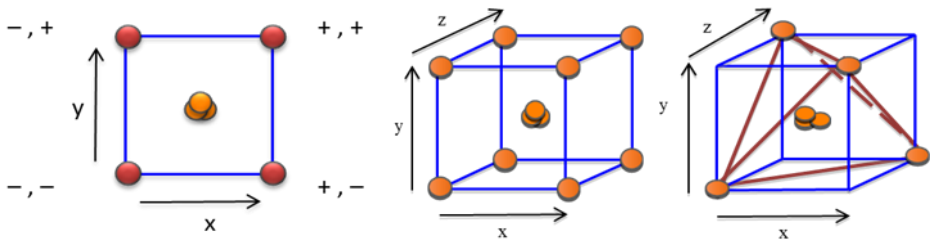

Figure 2.3 Design areas and half-fractional design area

The factors to be investigated and their minimum and maximum levels are entered into a piece of DoE software (Design Expert v10®, initially accessed by James Sanderson at GSK) and this generates the reactions to be performed. Once all the required reactions have been completed, the conversions obtained can be entered into this software and the results processed. Various representations can be generated, such as a 3D response surface or a half-normal plot (**Figure 2.4**).

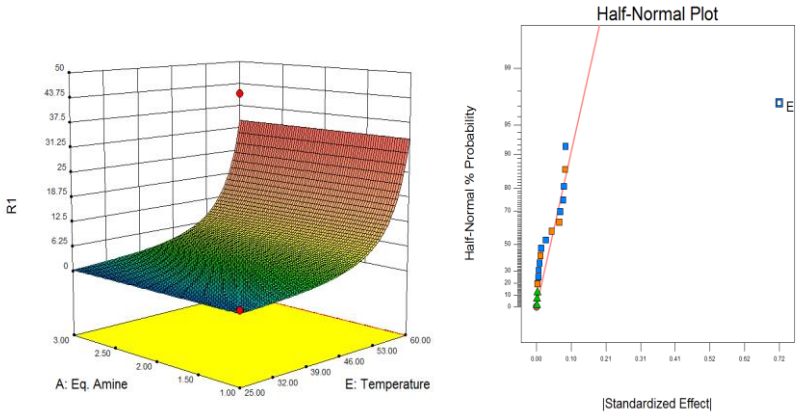

Figure 2.4 3D response surface and half-normal plot

The half-normal plot can be used to determine which factors, if any, have the greatest effect on the conversion. The 3D surface can be used to determine whether a combination of factors affects the response.

2.4.2 Initial Screen

The first DoE screen to be adopted was a 5 factor, 2 level, half fractional-design. This gave 16 reactions to be carried out, with an additional 4 centre points. At this time, the reaction time was fixed at 24 hours, while the factors to be tested, including their respective levels, were:

- Temperature 30 – 110 °C (centre at 70 °C)
- Catalyst loading 1 – 10 mol % (centre at 5.5 mol %)
- Equivalents of boronic acid 1 – 2 eq. (centre at 1.5 eq.)
- Equivalents of base 1 – 5 eq. (centre at 3 eq.)
- Equivalents of water 0 – 20 eq. (centre at 10 eq.)

The substrate chosen to be optimised for was 4'-chloroacetophenone, while the catalyst was the dppe based catalyst, as this had performed slightly better in previous screens. The method of conversion analysis was also altered. Rather than using the consumption of starting material to calculate the conversion, the presence of product was used. This helps to improve the accuracy of the results, as consumption of starting material does not always mean conversion to product. The results of this initial screen are shown in **Table 2.1**.

Table 2.1 Results of initial DoE screen

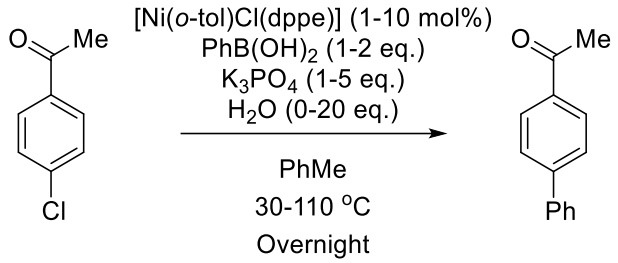

RUN	T (°C)	CAT. LOADING (MOL%)	BORONIC ACID EQ.	BASE EQ.	WATER EQ.	CONVERSION (%)
1	30	10	1	1	0	0
2	110	1	1	1	0	62
3	110	10	2	1	0	96
4	110	1	2	1	20	0
5	30	1	1	5	0	2
6	110	10	1	5	0	69
7	110	1	2	5	0	80
8	110	10	1	1	20	75
9	30	1	2	5	20	20
10	70	5.5	1.5	3	10	99*

11	30	10	1	5	20	0
12	110	1	1	5	20	78
13	70	5.5	1.5	3	10	99*
14	30	1	1	1	20	5
15	30	10	2	5	0	18
16	30	1	2	1	0	0
17	70	5.5	1.5	3	10	99*
18	30	10	2	1	20	15
19	70	5.5	1.5	3	10	99*
20	110	10	2	5	20	97

*denotes full conversion

The centre points of the design (10, 13, 17, 19) were carried out first, in order to ensure that the results were reproducible, before committing to performing the entire design. Since these were satisfactory, the rest of the reactions were carried out. They were not carried out in the random order dictated by the software, as it was more practical to perform reactions that were at the same temperature together. Runs 3, 7, 10, 13, 17, 19 and 20 all gave conversions of 80% and above, which was encouraging. From the table of results, it is not immediately apparent if any one of the factors in particular was having an effect on the conversion. The half normal plot was generated by the software and this indicated that the temperature was having the greatest effect on the conversion as shown by being the furthest point to the right (**Figure 2.5**).

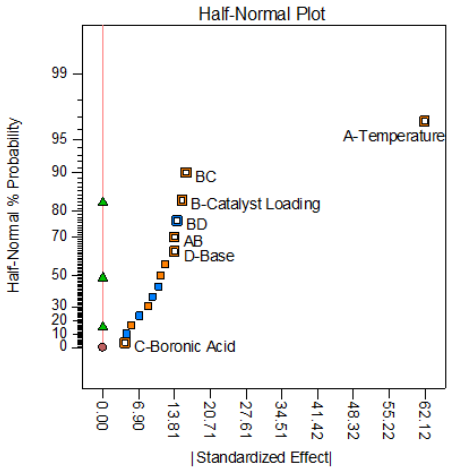

Figure 2.5 Half-normal plot

A straight line is drawn through the factor points, and any factor that lies off this line is deemed as having an effect on conversion. A 3D response surface was also generated from these results (**Figure 2.6**).

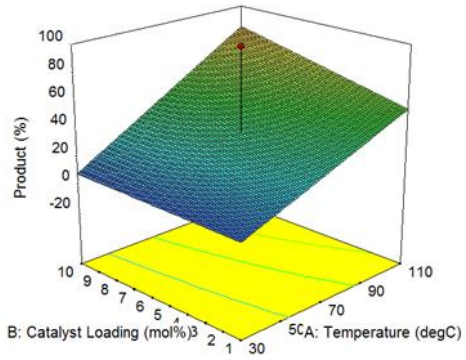

Figure 2.6 3D response surface

From this, it was deduced that the catalyst loading had a positive effect on conversion, though it was not as significant as the temperature effect. Overall, this initial screen gave positive results, since the centre points appeared to proceed to full conversion. In order to further probe the reaction conditions, and potentially reduce factors such as catalyst loading, the experiment design was augmented to narrow in on optimised conditions.

2.4.3 Second Screen

The results of the initial screen were given to the software, which then generated another 10 reactions, with 2 further centre points added. These reactions were performed in the same manner as previously, carrying out the centre points first, followed by groups of reactions at the same temperature. The results of these reactions are shown in **Table 2.2**.

Table 2.2 Results of the second DoE screen

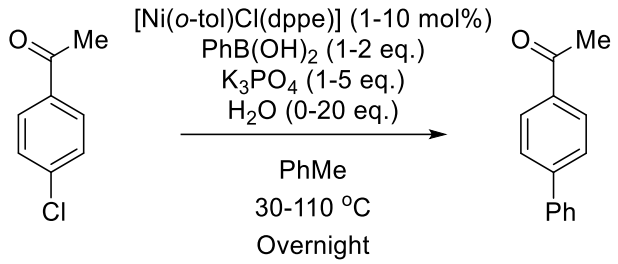

RUN	T (°C)	CAT. LOADING (MOL%)	BORONIC ACID EQ.	BASE EQ.	WATER EQ.	CONVERSION (%)
21	70	1	1.5	3	10	0
22	70	5.5	1.5	5	10	91
23	70	5.5	1.5	3	0	90
24	70	5.5	1.5	1	10	21
25	110	5.5	1.5	3	10	97
26	70	5.5	1	3	10	81
27	70	5.5	1.5	3	10	98
28	70	5.5	1.5	3	10	97
29	70	5.5	1.5	3	20	58
30	30	5.5	1.5	3	10	0
31	70	5.5	2	3	10	70
32	70	10	1.5	3	10	91

Again, it was the centre points (runs 27 and 28) that gave the best conversion. The results were entered into the software, but this time the prediction tools were used to give conditions which would give the same full conversion, while keeping the equivalents of base and catalyst loading to a minimum.

This led to a set of conditions as follows:

- 5 mol % catalyst loading
- 1.1 equivalents of boronic acid
- Temperature of 85 ^{o}C
- 3 equivalents of base
- 10 equivalents of water

These conditions were carried out on the model substrate three times and also on a separate substrate to ensure reproducibility (**Table 2.3**).

Table 2.3 Predicted conditions on model substrate and extra substrate

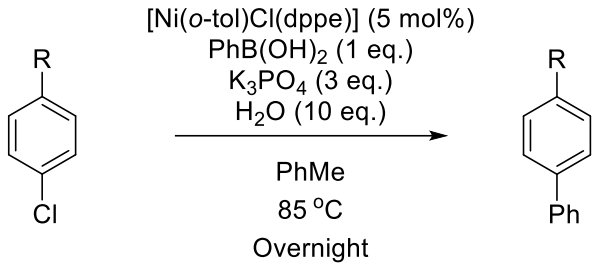

R = COMe, CF_3

SUBSTRATE	CONVERSION (%)
4’-CHLOROACETOPHENONE	92
4’-CHLOROACETOPHENONE	95
4’-CHLOROACETOPHENONE	99*
4-CHLOROBENZOTRIFLUORIDE	91

*denotes full conversion

As shown, the results were very consistent, even when using a different substrate (without a carbonyl group).

At this point, the reactions were still carried out overnight. A small time study was conducted, using these optimised conditions, in an effort to reduce the reaction time. Reactions were set up and left to stir for 2, 4, 6 and 8 hours and the conversions recorded from the GC-FID (**Table 2.4**).

Table 2.4 Results of time study

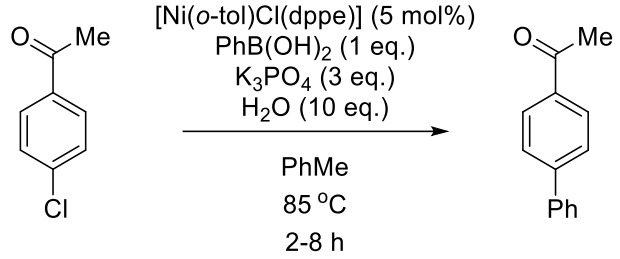

SUBSTRATE	REACTION TIME (H)	CONVERSION (%)
4'-CHLOROACETOPHENONE	2	99*
4'CHLOROACETOPHENONE	4	99*
4'CHLOROACETOPHENONE	6	99*
4'CHLOROACETOPHENONE	8	99*

Surprisingly, the reaction was complete after 2 hours with 5 mol % nickel catalyst. A replicate of this reaction was carried out with the dppf catalyst to probe general applicability, and the result was the same.

2.4.4 Further Work

In this body of work we were able to thoroughly explore coordination to nickel(0) centres with carbonyl groups. We were able to not only observe this selectivity effect, but also decouple the origin of the effect from electronic properties as functional groups with very similar σ_p values behaved very differently (e.g. *p*-CO_2Me *vs* *p*-COMe). While we were able to collect qualitative data to show that aryl electrophiles that possess these groups reach higher conversions than those that do not, there was no indication of whether the overall rate of reaction was affected. It could be that these privileged substrates simply react faster, or that the ability to form complexes allows the catalyst to be sequestered onto these substrates and

prevented from reacting with non-coordinating substrates. The next steps, then, were to investigate this effect with a variety of different functional groups which could form these same kinds of complexes (nitriles, alkenes, alkynes etc.) and deduce whether these would have a similar beneficial effect during cross-coupling competitions and also if they exhibited the same inhibitory effect when used as additives. Moreover, it would be prudent to elucidate whether this same coordination effect was exhibited at all (and, if so, to what degree) with analogous palladium(0) complexes.

2.5 References

1 J. K. Stille and K. S. Y. Lau, *Acc. Chem. Res.*, 1977, **10**, 434–442.

2 S. Bajo, G. Laidlaw, A. R. Kennedy, S. Sproules and D. J. Nelson, *Organometallics*, 2017, **36**, 1662–1672.

3 D. S. McGuinness, K. J. Cavell, B. W. Skelton and A. H. White, *Organometallics*, 1999, **18**, 1596–1605.

4 T. T. Tsou, J. C. Huffman and J. K. Kochi, *Inorg. Chem.*, 1979, **18**, 2311–2317.

5 Y.-J. Kim, K. Osakada and A. Yamamoto, *Bull. Chem. Soc. Jpn.*, 1989, **62**, 964–966.

6 A. Flores-Gaspar, P. Pinedo-González, M. G. Crestani, M. Muñoz-Hernández, D. Morales-Morales, B. A. Warsop, W. D. Jones and J. J. García, *J. Mol. Catal. A Chem.*, 2009, **309**, 1–11.

7 Y. Hoshimoto, M. Ohashi and S. Ogoshi, *Acc. Chem. Res.*, 2015, **48**, 1746–1755.

8 A. N. Desnoyer, W. He, S. Behyan, W. Chiu, J. A. Love and P. Kennepohl, *Chem. – A Eur. J.*, 2019, **25**, 5259–5268.

Chapter 3: Nickel *versus* Palladium in Cross-Coupling Catalysis: On the Role of Substrate Coordination to Zerovalent Metal Complexes

3.1 Authors		
	Alasdair K. Cooper[a]	Experimental work, data collection and analysis, article writing and assembly, Supplementary Information assembly
	Paul M. Burton[b]	Industrial supervisor, experimental discussion and direction
	David J. Nelson[a]	Principal Investigator, project discussion and direction, DFT calculations and analysis, article writing and assembly, Supplementary Information assembly

a WestCHEM Department of Pure and Applied Chemistry, University of Strathclyde, 295 Cathedral Street, Glasgow, G1 1XL, Scotland. david.nelson@strath.ac.uk

b Syngenta, Jealott's Hill International Research Centre, Bracknell, Berkshire, RG42 6EY, UK.

3.2 Paper Abstract

We report a detailed comparison of the effect of coordinating functional groups on the performance of Suzuki-Miyaura reactions catalysed by nickel and palladium, using competition experiments, robustness screening, and density functional theory calculations. Nickel can interact with a variety of functional groups, which manifests as selectivity in competitive cross-coupling reactions. The presence of these functional groups on exogenous additives has a range of effects on cross-coupling reactions that range from a slight improvement in yield to the complete cessation of the reaction. In contrast, palladium does not interact sufficiently strongly with these functional groups to induce selectivity in cross-coupling reactions; the selectivity of palladium-catalysed cross-coupling reactions is predominantly governed by aryl halide electronic properties.

3.3 Extended Introduction

3.3.1 Further Functional Group Coordination

As shown in the previous chapter, it is evident that carbonyl-based coordinating groups present on the aryl halide coupling partner exhibit an apparently positive effect on the conversion of these reactions. As might be expected, carbonyl systems are not the only π-acceptors capable of coordinating in an η^2 fashion to the nickel centre. Van der Boom has shown that alkenes can also form these complexes. A much more recent article has discussed the synthesis of a *tris*-alkene Ni complex, using three stilbene molecules as the ligands, all coordinated *via* an η^2 interaction (**Scheme 3.1**).[1]

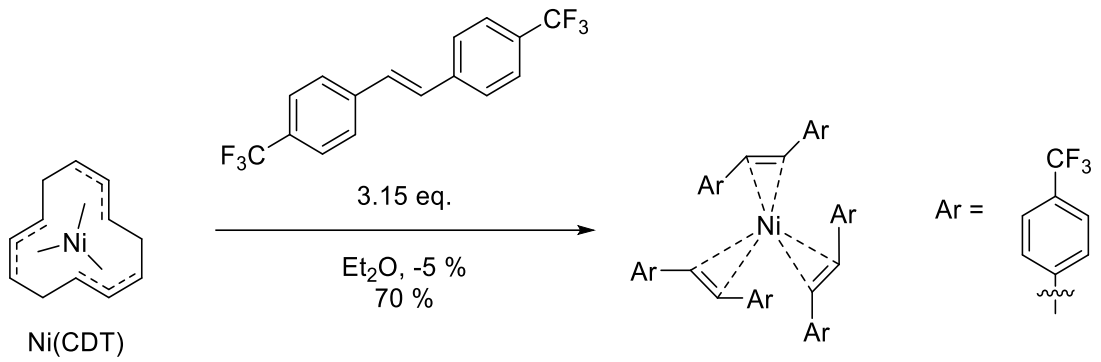

Scheme 3.1 Synthesis of *tris*-stilbene nickel(0) complex

While ring-walking is not employed in this example, it serves as further evidence of the ability of Ni to form very stable complexes of this type, this particular example being air stable. This complex was synthesised either from Ni(CDT) or $Ni(acac)_2$ and the stilbene on a gram scale. A series of ligand exchange reactions were carried out on this complex to replace the stilbene ligands with common ligands used in catalysis, successfully yielding [(dppf)Ni(stb)], [(bipy)Ni(stb)], [(thf(?))$Ni(stb)_2$] and [$(PPh_3)_2$Ni(stb)], which were all characterised by X-ray crystallography. The catalytic properties of this complex were also explored to probe its efficacy as a reliable source of nickel(0). The complex was a competent pre-catalyst, successfully performing Suzuki cross-coupling, C-H activation, C-N formation, oxidative cycloaddition to form pyridines, Negishi cross-coupling and Heck reactions, in moderate to high conversions.

There are several examples of nitrile-based complexes of this kind reported in the literature. Hartwig et al. showed the use of a (±)-BINAP nickel-nitrile complex as a competent pre-catalyst for heterocyclic aminations (**Scheme 3.2**).[2]

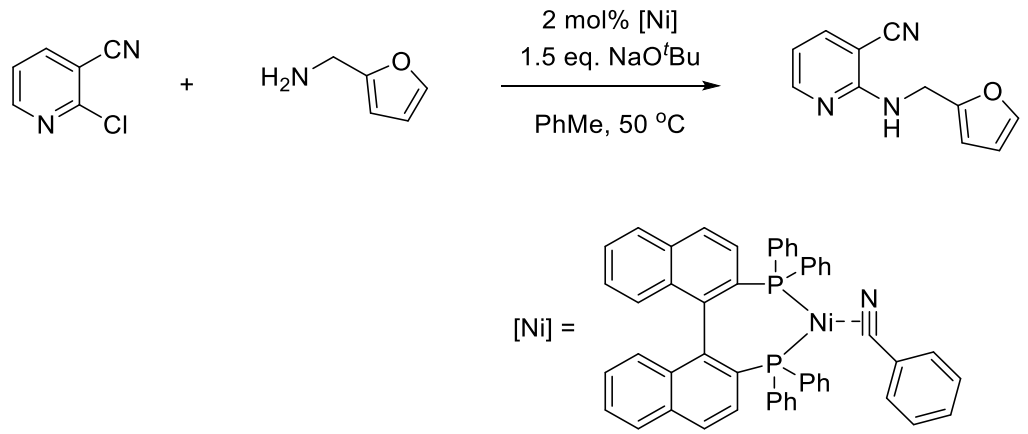

Scheme 3.2 Heterocyclic amination using [(BINAP)Ni(η^2-NC-Ph)]

While the heteroaryl chloride scope was mainly limited to pyridine systems (with a range of steric and electronic properties), the amine scope included several different functional groups. The yields ranged from 57 – 96 %, which, at this relatively low temperature, is impressive. Due to the use of a well-defined nickel catalyst, detrimental side reactions such as the formation of inactive [(BINAP)$_2$Ni] and the nickel(I) species [(BINAP)Ni(μ-Cl)]$_2$ were avoided.

Another report by Louie showed nickel-nitrile complexes with bidentate phosphine ligands being used as cycloaddition catalysts for the formation of pyridines (although interestingly, this report showed that the nitrile acted simultaneously as both an $\eta^1$and an η^2 ligand) (**Scheme 3.3**).[3]

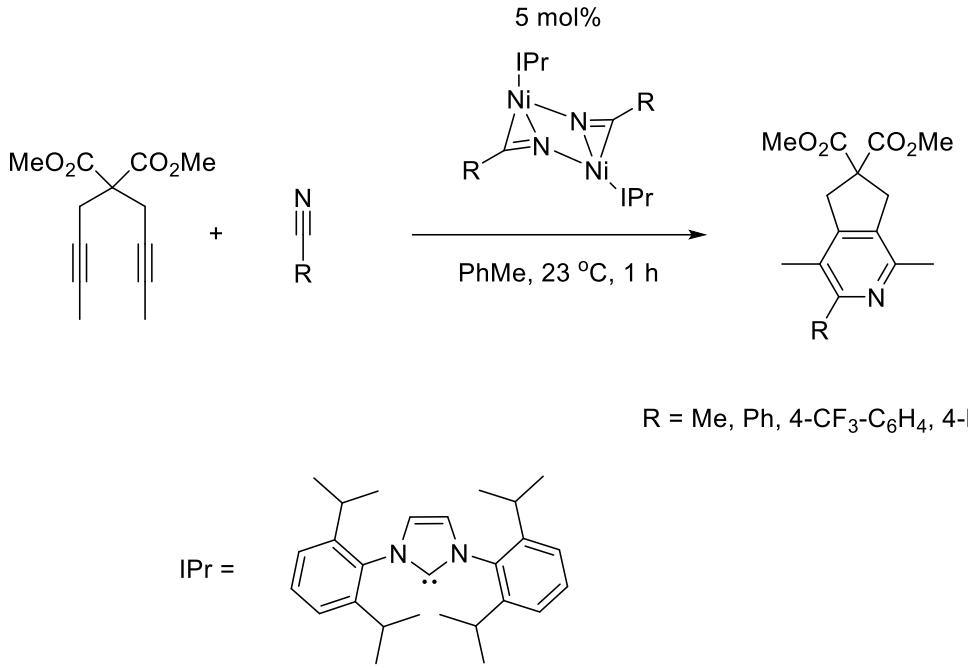

Scheme 3.3 Nickel-nitrile dimer as a catalyst for cycloaddition to form pyridines

Jones et al showed that a zerovalent nickel species $[Ni(dippe)H]_2$ could activate the C – CN bond in acetonitrile *via* coordination to the carbon nitrogen triple bond (**Scheme 3.4**).[4]

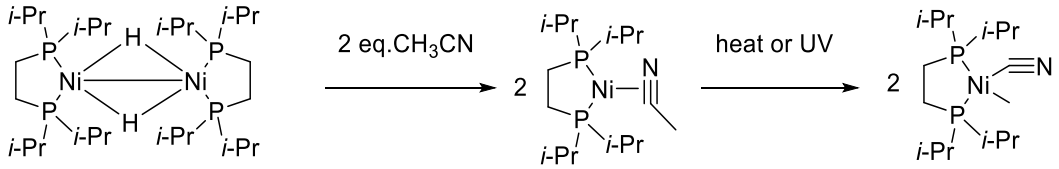

Scheme 3.4 C-CN bond activation with a zerovalent nickel complex

During this study, it was also shown that if BEt_3 was added, the reaction stopped at the η^2 complex, with the BEt_3 group attached to the nitrogen. After heating at 100 °C for 2 days, no C – CN bond cleavage occurred. Under UV light, however, after 2 hours, the cleavage was able to take place in a 50 % yield. Attempts to preferentially achieve C – H bond activation over C – CN activation were unsuccessful, with the former product not observed from heat or photochemical reactions as it is unstable above - 40 °C. A competition reaction was carried out where a mixture of the nickel complex and CH_3CN was irradiated with UV light at – 65 °C. Only the C – CN bond activation product was observed, suggesting that this pathway is more kinetically favourable (potentially due to the η^2 complex formed this way).

The Schoenebeck group have also reported an η^2 complex formed with MeCN that led to an increase in conversion in nickel catalysed trifluoromethylation of aryl chlorides.[5] It was found that when the original pre-catalyst, $[Ni(cod)_2]$, was used, the equivalent of cod that was generated, *via* coordination of dppf ligand to form the active catalytic species, would hinder the reaction. The solution was to find an additive that had a weaker binding ability to nickel(0) than cod, which would generate a more reactive catalytic species. Computational modelling showed that the acetonitrile nickel(0) complex was indeed higher in energy than the [(dppf)Ni(cod)] complex, leading to a lower energetic barrier to oxidative addition when using this η^2 complex. The use of acetonitrile led to increased yields of up to 61% and even promoted some heterocyclic couplings.

There are also examples of imine-nickel η^2 complexes which are catalytically active. One such complex was used as a catalyst in the [2 + 2 + 2] cycloaddition of alkynes and an imine to form 6-membered heterocycles.[6] The complex in question is formed quantitatively *via* reaction of $[Ni(cod)_2]$ with tricyclohexyl phosphine and a phenyl sulfonimine equipped with an electron withdrawing group (**Scheme 3.5**).

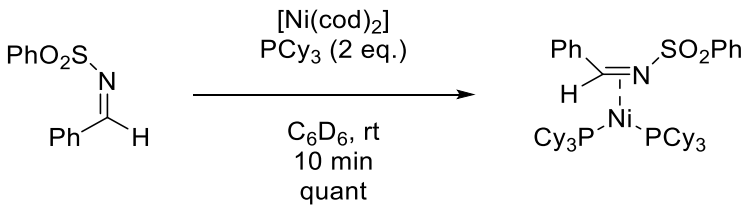

Scheme 3.5 Formation of η^2-imine nickel complex

The resulting species could then form a 5-membered ring with the first alkyne, followed by insertion of the second alkyne to form a 7-membered ring which could then reductively eliminate the desired product. In this study, the proposed mechanism also includes the first alkyne coordinating to the nickel centre in an η^2 fashion simultaneously to the imine, though no evidence or discussion of this step is presented (**Scheme 3.6**).

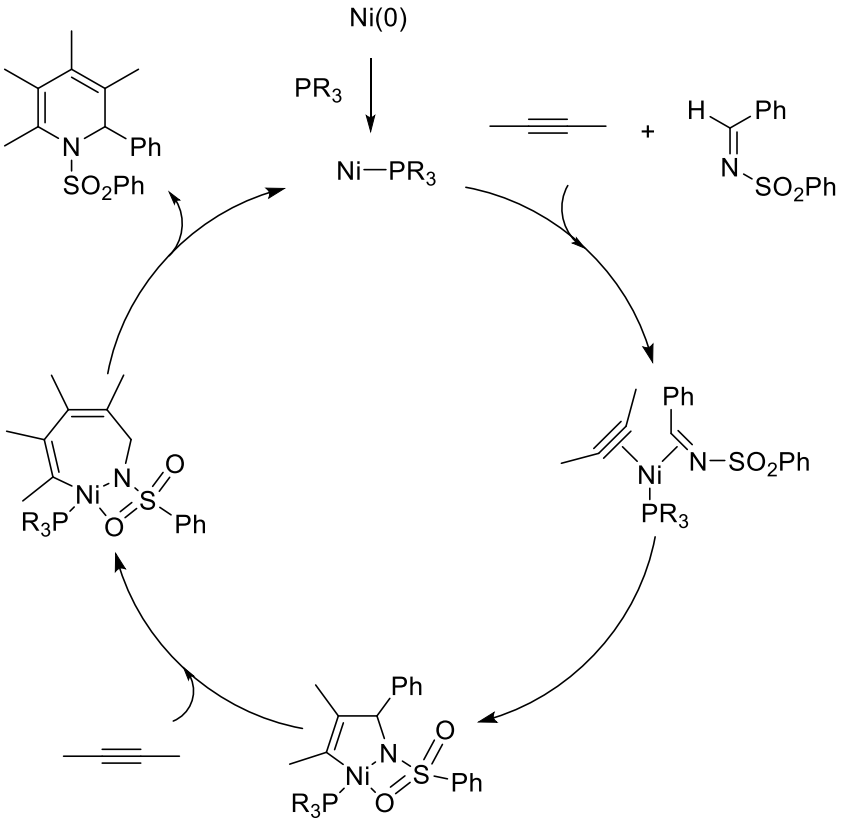

Scheme 3.6 Catalytic cycle for cycloaddition using sulfonimine and alkynes

Previous work in the Nelson group yielded equilibrium constants for the formation of η^2 Ni complexes *via* the displacement of COD with the ligand in question (**Scheme 3.7**).

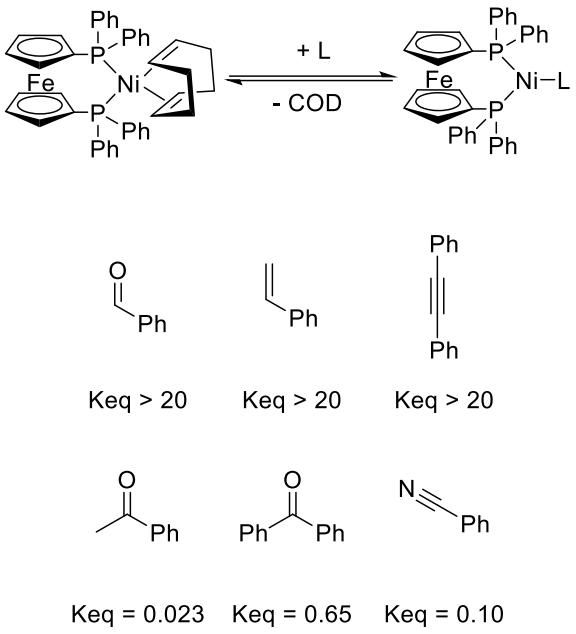

Scheme 3.7 Binding equilibrium constants for different π-systems

These constants were obtained using [Ni(COD)(dppf)] with an excess of ligand and following the reaction by ^{31}P NMR. Here it can be seen that alkynes are also able to form these complexes, with a binding strength comparable to alkenes and aldehydes. The low equilibrium constant for the nitrile group suggests that this is a labile ligand, as also discussed in the Schoenebeck study.

Introduction

Palladium-catalysed cross-coupling reactions are amongst the most widely deployed tools in the synthesis of fine chemicals, pharmaceuticals, and agrochemicals, due to their robustness, functional group tolerance, and their ability to use reagents such as boronic acids and boronic esters; these reagents are typically straightforward to prepare on scale and are usually stable under ambient conditions.[1-4] The development of nickel-catalysed reactions of this type is a subject of much recent research, with a variety of new reactions taking advantage of the different properties of nickel versus palladium.[5] A full and detailed evaluation of the reactivity differences between these two metals is important to understand their capabilities, and to underpin the development of new synthetic chemistry methodology.[6] It is known that nickel will react with a wide range of substrates[7] and that nickel(I) intermediates can arise through comproportionation[7, 8] or halide abstraction[9-12] during catalytic reactions. West and Watson have recently conducted a comparative study of nickel- and palladium-dppf complexes in

Suzuki-Miyaura reactions.[13] However, the functional group tolerance of nickel versus palladium catalysis, and the underlying reasons behind why these can differ so much, has not yet been fully and satisfactorily understood.

We have recently disclosed that aldehydes and ketones have a significant influence on the outcomes of nickel-catalysed Suzuki-Miyaura reactions (Scheme 1 (a)).[4] When these groups are substituents on the aryl halide, they lead to a significantly enhanced rate of oxidative addition and can be used to enable site-selective catalysis; when these groups are substituents on exogenous additives as part of a robustness screen[14] they inhibit the catalytic reaction. A series of competition reactions established that aryl halides with aldehyde or ketone (but not ester) substituents will undergo cross-coupling in the presence of other aryl halides that do not have these substituents, to the point that the normal order of reactivity of different organohalides (I > Br > Cl) is overridden.

Here, we report our studies of the analogous palladium-catalysed reactions, applying our methodology to measure reaction selectivity, and utilising a robustness screen to understand the effects, if any, of a wider range of functional groups on the outcomes of nickel- and palladium-catalysed Suzuki Miyaura reactions (Scheme 1(b)).

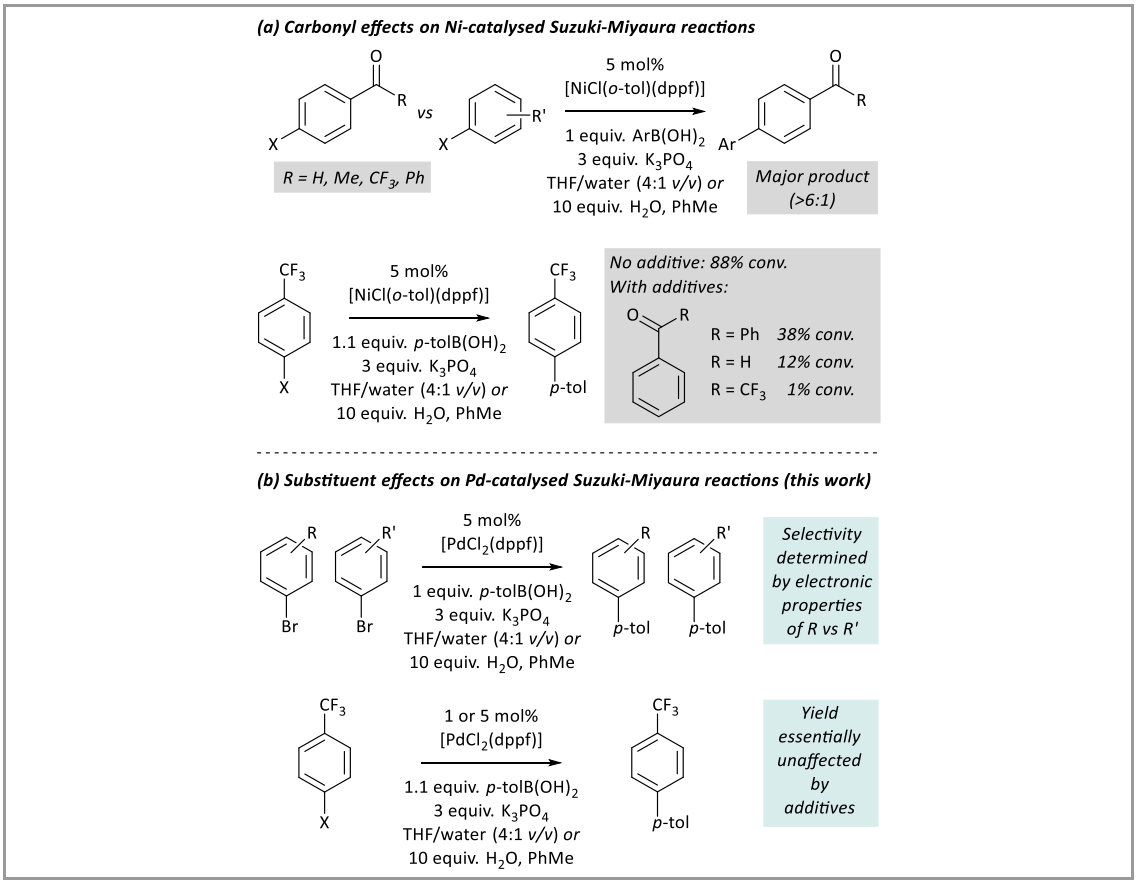

Results & Discussion

All reactions were carried out under the conditions that were used for our previous study (Scheme 2 (a)).[4] [$PdCl_2$(dppf)] (**1**) was used in place of [NiCl(o-tol)(dppf)] (**2**) for the palladium-catalysed reactions (dppf = 1,1'-bis(diphenylphosphino) ferrocene); complexes **1** and **2** often offer comparable reactivity in Suzuki-Miyaura reactions.[13] Our reaction conditions require only a slight excess of boronic acid in order to activate the M^{II} pre-catalyst *via* transmetalation and reductive elimination.[8] The outcomes of the reactions described here were determined using GC-FID analysis with *n*-dodecane as an internal standard; the apparatus was calibrated using authentic samples of each substrate and product, which were used to prepare solutions containing known ratios of substrate to internal standard.

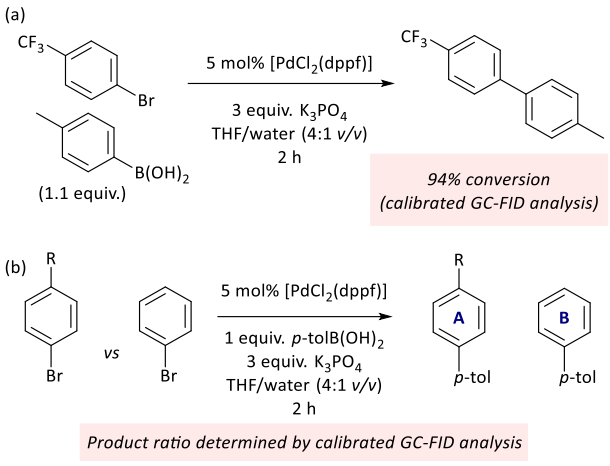

R = NMe_2 (**S1**), NEt_2 (**S2**), NHPh (**S3**), OMe (**S4**), *i*-Pr (**S5**), C(H)=C(H)Ph (**S6**), SMe (**S7**), CCPh (**S8**), OCF_2H (**S9**), OCF_3 (**S10**), CHO (**S11**), C(H)=NPh (**S12**), COPh (**S13**), CO_2Me (**S14**), SOMe (**S15**), COMe (**S16**), CF_3 (**S17**), CN (**S18**), SO_2Me (**S19**)

In our earlier study,[4] competition reactions were conducted in both a THF/water (4:1 v/v) mixture and in toluene with 10 equivalents of water and gave comparable results, while robustness screening reactions were performed in toluene; here, all reactions were performed in the THF/water solvent system as this avoids issues with clumping of the base and instead forms a homogeneous biphasic mixture.

Reactions were performed in which 1 equiv. of a substituted aryl bromide (*p*-YC_6H_4Br, **S1** – **S19**) and 1 equiv. of bromobenzene competed for 1 equiv. of boronic acid (Scheme 2(b)). The conversion to each of the two possible products (**P1** to **P19** or 4-methylbiphenyl) was quantified by GC-FID analysis, and the resulting data were interpreted using equation 1, which defines the selectivity for the cross-coupling of the substituted aryl bromide. A value of 1 represents a reaction that is entirely selective for the cross-coupling of *p*-YC_6H_4Br, and a value of -1 represents a reaction that is entirely selective for the cross-coupling of bromobenzene.

Selectivity = ([A] – [B]) / ([A] + [B])

Equation 1 Measurement of selectivity in competition reactions between an aryl bromide and bromobenzene, yielding products A and B, respectively.

For each competition reaction, the selectivity number was plotted versus σ_p, which quantifies the net electron donating or withdrawing property of substituent Y (Figure 1);[15] some of the data have been reported previously,[4] but this study adds several additional data points. Data points are colour coded according to whether they feature a coordinating π-system (nitrile, ketone, aldehyde, imine, alkene, alkyne; green points) or not (blue points).

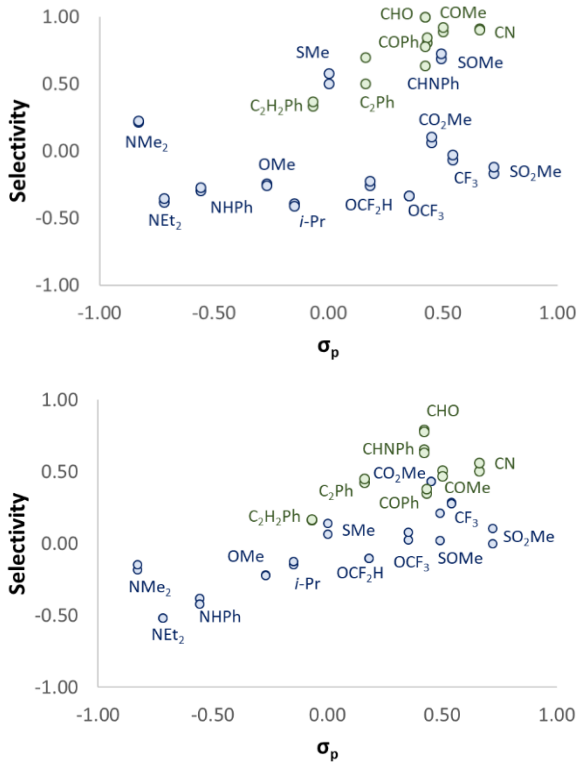

The plot for nickel (Figure 1 (a)) shows a relatively flat profile for the blue points (except **S7** (R = SMe) and **S15** (R = SOMe), showing that selectivity in these reactions is relatively insensitive to the electronic properties of the aryl halide. Species with known coordinating groups such as ketones, aldehydes, nitrile, alkene, and alkynes show enhanced selectivity in these Suzuki-Miyaura reactions. Future work will further investigate the effect of the sulfide and sulfoxide groups on reaction selectivity, as these can potentially coordinate transition metals *via* the lone pair(s) on the relatively soft sulfur.

The plot for the palladium-catalysed reactions (using **1**) is consistent with the accepted trend that electron-poor aryl bromides undergo more rapid oxidative addition than electron-rich aryl bromides (Figure 1 (b)).[16] The results here are significantly different from those obtained with nickel catalyst **2**. The trend is dominated by electronic effects but some selectivity is seen for the functional groups that might coordinate metal centres *via* a π-system. These reactions are far less selective than the corresponding nickel-catalysed competition reactions.

These data establish that coordinating functional groups have much less of an effect in palladium catalysis than they do in nickel catalysis, and so a robustness screen[14] was carried out with additives **A1** to **A18** to understand whether additives with coordinating functional groups affect the outcomes of prototypical Suzuki-Miyaura reactions (Scheme 3). In these reactions, 1 equiv. of each additive was added to the reaction of *p*-

(trifluoromethyl)bromobenzene with *p*-tolylboronic acid. GC-FID analysis was used to quantify the conversion of the reaction; this technique therefore allows us to rapidly assess whether the additive interferes with the reaction. Reactions were initially carried out with 5 mol% of **1** or **2**. The results of this robustness screen show little or no inhibition of the palladium-catalysed reactions by most of these additives; in the majority of cases, high (>90%) conversions are observed. This is in stark contrast to the results with nickel catalysis, where many functional groups inhibit an otherwise productive cross-coupling reaction. Imines and phenylacetylene also had a significant impact on the outcomes of nickel-catalysed reactions, but stilbene and benzonitrile had only a modest effect. Only phenylacetylene had an impact on the yields of palladium-catalysed reactions. The robustness screen was repeated with only 1 mol% of **1** to understand whether this would make the reaction more susceptible to poisoning by additives; this had little impact on the yields of the reactions, generally decreasing them by only a few percent. For the nickel-catalysed reactions, attempts were made to correlate reaction inhibition to selectivity data from Figure 1, but there is no clear correlation here.

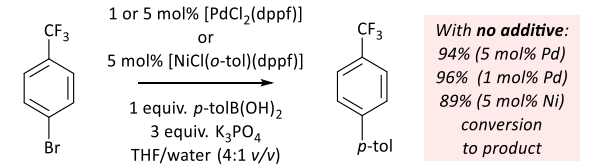

*Conversions to product, in the presence of **additives**:*

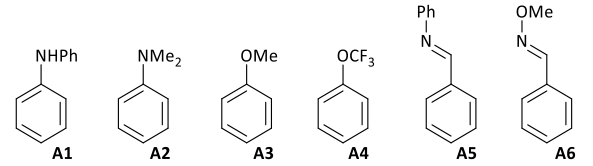

A1	A2	A3	A4	A5	A6
95% (5Pd)	93% (5Pd)	94% (5Pd)	88% (5Pd)	94% (5Pd)	97% (5Pd)
94% (1Pd)	88% (1Pd)	93% (1Pd)	83% (1Pd)	91% (1Pd)	94% (1Pd)
48% (5Ni)	68% (5Ni)	51% (5Ni)	54% (5Ni)	10% (5Ni)	1% (5Ni)

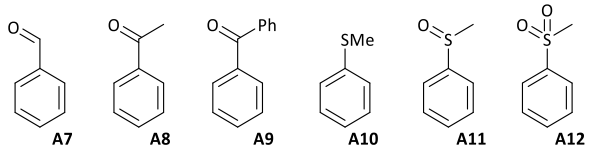

A7	A8	A9	A10	A11	A12
89% (5Pd)	95% (5Pd)	92% (5Pd)	82% (5Pd)	97% (5Pd)	93% (5Pd)
93% (1Pd)	97% (1Pd)	94% (1Pd)	91% (1Pd)	93% (1Pd)	93% (1Pd)
18% (5Ni)	42% (5Ni)	17% (5Ni)	15% (5Ni)	8% (5Ni)	44% (5Ni)

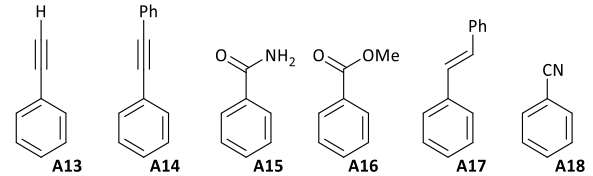

A13	A14	A15	A16	A17	A18
62% (5Pd)	93% (5Pd)	87% (5Pd)	96% (5Pd)	96% (5Pd)	84% (5Pd)
56% (1Pd)	89% (1Pd)	93% (1Pd)	90% (1Pd)	90% (1Pd)	88% (1Pd)
12% (5Ni)	48% (5Ni)	50% (5Ni)	55% (5Ni)	77% (5Ni)	77% (5Ni)

These experimental observations were probed further using density functional theory (DFT) calculations. We have previously reported the free energy surfaces for oxidative addition of a number of these substrates to Ni^0, in toluene solution, considering [Ni(η^2-benzene)(dppf)] to have G_{rel} = 0. All computational data in this manuscript are reported in THF solution, consistent with experimental work. Complexes **3** (Ni) and **4** (Pd) were considered to have G_{rel} = 0, as these are the M^0 complexes that will arise from the activation of **2** or **1**, respectively, by transmetalation with *p*-tolylboronic acid (Scheme 4). These arene ligands can be replaced by aryl halide substrates; these can co-ordinate to the metal centre to form an η^2-complex (**A**), which then undergoes oxidative addition (**TS-AB**) to form [M(Ar)Br(dppf)] (**B**). Alternatively, some substrates can coordinate to M^0 through their functional groups (**A'**). The values of interest are (i) the relative energies of **A** and **A'**, and (ii) the barrier from **A** to **TS-AB** for oxidative addition. If **A'** is much lower in energy than **A** then this might decrease the rate of oxidative addition. The results of these calculations are recorded in Table 1 for both the palladium and the nickel complexes. We did not directly compare the turnover numbers for nickel and palladium; the transmetalation step is not modelled here, as there are multiple possible mechanisms for boronic acid transmetalation.[17, 18] Instead, we have used DFT data to reveal the nature of the competition between the reversible coordination of M^0 to functional groups and the (irreversible) oxidative addition step. These data show that the oxidative addition reactions of dppf-Ni^0 present much lower barriers and are much more exergonic than those for dppf-Pd^0, consistent with established reactivity trends.[6] Oxidative addition is unlikely to be the rate-determining step in these nickel-catalysed reactions. For nickel, complexes of the form **A'** are typically much lower in energy than the corresponding complexes of type **A**, and it is this effect, and a facile 'ring-walking' process that is proposed to lead to the observed selectivity for substrates with coordinating functional groups.[4, 19-22] For those substrates with amide and ester functional groups the pre-oxidative addition complex **A** is lower in energy than **A'**. There are unfortunately no clear correlations between the energy of **A'** and the selectivity of cross-coupling reactions or the degree of reaction inhibition.

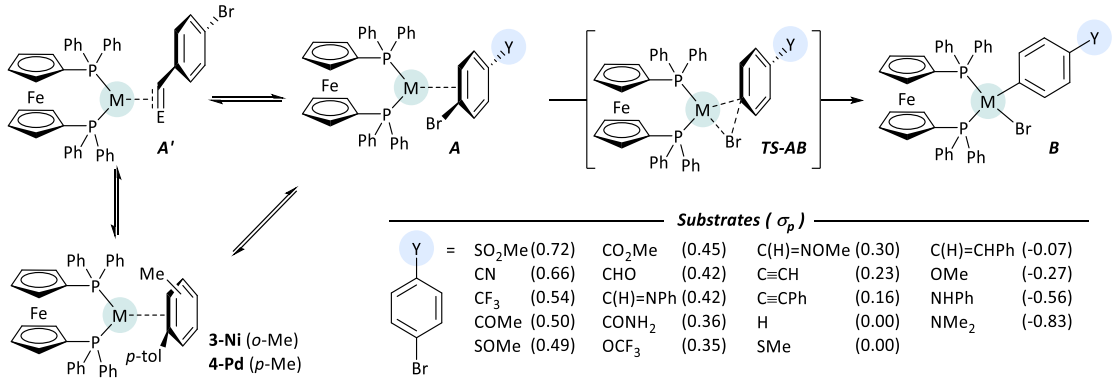

Y	Nickel (3)						Palladium (4)					
	A	A'	TS-AB	B	A *vs* A' [a]	TS-AB *vs* A	A	A'	TS-AB	B	A *vs* A' [a]	TS-AB *vs* A
SO_2Me	-9.5		-2.8	-35.0		6.7	-3.3		6.9	-27.9		10.2
CN	-9.5	-11.1	-3.6	-34.9	1.5	5.9	-3.0	0.9	7.9	-27.4	-3.9	10.9
CF_3	-7.9		-1.2	-33.3		6.7	-0.3		8.5	-25.9		8.8
COMe	-9.3	-12.6	-2.0	-33.1	3.3	7.3	-2.1	-0.2	8.3	-26.0	-1.9	10.4
SOMe	-7.4		0.9	-32.9		8.3	-0.8		9.1	-25.8		9.9
CO_2Me	-7.5	-3.5	-1.6	-32.1	-4.0	5.9	-1.7	4.5	8.9	-25.0	-6.2	10.6
CHO	-10.3	-16.0	-2.6	-33.5	5.7	7.7	-3.0	-2.5	7.9	-26.0	-0.5	11.0
C(H)=NHPh	-8.7	-17.7	-2.0	-32.9	9.0	6.7	-0.4	-6.8	8.3	-24.4	6.4	8.7
$CONH_2$	-6.6	0.4	-1.9	-32.2	-7.0	4.7	-1.1	6.6	9.2	-25.7	-7.6	10.3
OCF_3	-6.3		-0.8	-33.1		5.5	-0.4		9.9	-26.2		10.3
C(H)=NOMe	-7.7	-13.1	-1.3	-31.9	5.4	6.4	1.0	-2.5	10.1	-24.4	3.5	9.1
C≡CH	-7.0	-22.4	-1.6	-32.3	15.4	5.4	0.1	-8.9	9.7	-24.8	9.0	9.6
C≡CPh	-6.5	-23.9	-1.2	-31.8	17.3	5.4	-0.1	-9.7	9.8	-24.0	9.5	9.9
H	-3.8		1.5	-30.1		5.2	2.4		11.4	-22.9		9.0
SMe	-5.4		0.7	-30.6		6.1	1.1		10.2	-22.8		9.1
C(H)=CHPh	-5.1	-20.1	1.0	-31.6	15.0	6.2	-0.2	-10.0	10.4	-22.8	9.7	10.6
OMe	-1.5		2.6	-28.3		4.2	3.3		11.9	-22.8		8.6
NHPh	-4.7		2.1	-27.8		6.8	1.7		12.5	-22.4		10.9
NMe_2	-2.0		3.3	-25.3		5.3	3.7		14.0	-19.9		10.2

For palladium, none of the **A'** complexes for carbonyl-containing aryl halides were found to be lower in energy than the corresponding pre-oxidative addition η^2-complexes. The coordination of various other functional groups to the Pd^0 complex (forming **A'**) is often exergonic, but far less so than for nickel.[20, 23] This goes some way to explaining the lack of selectivity in competition experiments and the lack of any significant inhibition by any of these additives in the robustness screening studies. A search of the Cambridge Structural Database reveals only one palladium-ketone complex, but this is in the form of a benzophenone-derived bisphosphine ligand in which the coordination of two phosphines forces the ketone to interact with the Pd^0 centre also.[24] There is one example of a structurally-characterised imine complex of Pd^0.[25]

The coordination of aldehydes and ketones to Ni^0 has been studied in depth by Love and Kennepohl, using a variety of experimental and computational techniques.[26, 27] All of the η^2-complexes **A'** in this work are square planar; attempts to locate tetrahedral complexes were unsuccessful, with the structure optimising to the square planar geometry in each case. While the strength of coordination of palladium to functional groups is evidently much lower than in the case of nickel, the reasons behind the observed square planar geometry – donation from a bidentate phosphine into the same *d* orbital used for $d \rightarrow \pi^*$ back-bonding – are likely to be the same. Several plots were constructed to visualise these differences in behaviour between palladium and nickel. Plots of G_{rel}(**TS-AB**) *versus* σ_p give reasonably good linear correlations that have very similar slopes for Pd and Ni (-4.1 *versus* -4.2) (Figure 2(a)). However, when $\Delta G^{\ddagger}$(**A**→**TS-AB**) is plotted versus σ_p the plot is almost flat, although there is significant scatter

(Figure 2 (b)); each substituent influences the free energies (G_{rel}) of the pre-oxidative addition η^2-complex **A** and oxidative addition transition state **TS-AB** almost equally. These data, combined with the experimental data in Figure 1, suggest that for palladium catalysis the oxidative addition event may be rate-determining, and **TS-AB** may be the turnover-determining transition state.[28] In contrast, coordination effects clearly dominate in nickel catalysis, with more subtle differences in the electronic properties of the substituents having little effect.

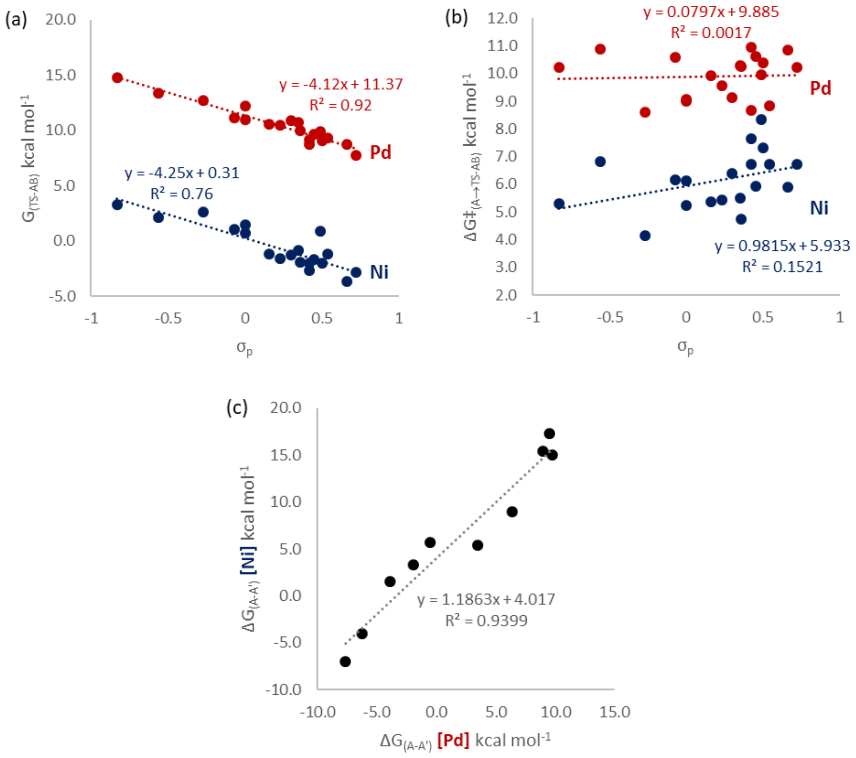

The relative energies of **A** versus **A'** were compared for palladium *versus* nickel (Figure 2(c)). A good linear correlation was obtained, albeit with nickel favouring **A'** over **A** in most cases. This is further evidence of the same interactions at work for both palladium and nickel; these simply manifest less strongly in the case of palladium, leading to the lack of significant engagement of these functional groups with the Pd^0 catalyst, and therefore the lack of leverageable selectivity or observable inhibition in catalysis.

While we present a significant experimental and computational dataset that interrogates functional group effects in cross-coupling catalysis, particularly with nickel, a quantitative link and a robust quantitatively predictive model remain to be established. Semi-quantitatively, where complex **A'** is lower in energy than **A** for nickel catalysis then we would expect selective cross-coupling of the corresponding aryl halide and the inhibition of cross-coupling

reactions by an additive featuring this functional group. The same does not hold for palladium: imines, alkynes, and alkenes should show interesting behaviour based on the difference between the energies of **A** and **A'**, but experimental observations are limited to some inhibition of catalysis by phenylacetylene. A limitation of our approach here is that we have no time-resolved studies, and so the difference in behaviour may be due to differences in rates or relative rates of key steps.

Conclusion

In conclusion, a detailed and systematic comparison of palladium and nickel and their interactions with potentially coordinating functional groups is reported, and key differences between these two metals are highlighted. Data comprise: measured selectivities from competition experiments; the measurement of the (lack of) inhibition of reactions in which functionalised additives are present; and DFT calculations of the coordination of these functional groups and the oxidative addition pathways of the corresponding aryl bromides. Together, these data show that nickel and palladium interact with functional groups in a considerably different manner. Nickel will strongly interact with many functional groups, resulting in selective cross-coupling reactions, but at the cost of reduced functional group tolerance. Palladium derives no selectivity benefits from these functionalised aryl halides, but therefore shows much better functional group tolerance. This work contributes towards our understanding of cross-coupling catalysis by highlighting differences in the behaviour of palladium and nickel catalysis, and its implications for the application of cross-coupling chemistry in organic synthesis.

Experimental

Complex **1** was obtained from commercial sources and used as supplied. Complex **2** was prepared according to a literature method.[29] Most aryl halides (**S1 – S5**, **S7** – **S11**, **S13**, **S14**, **S16**- **S19**) and additives (**A1 – A5, A7 - A10, A12 - A16, A18**) were obtained from commercial sources and used as supplied; synthetic methods and characterisation data for those that were prepared can be found below or in our previous manuscripts.[4, 30] Samples of most products (**P1** – **P5**, **P9** – **P11**, **P13**, **P14**, **P16**, **P17**, **P19**) were prepared by cross-coupling catalysis, and the data for these are reported below or in our previous study.[4] Anhydrous, oxygen-free THF was obtained from an Innovative Technologies PureSolv apparatus. Distilled water was degassed

by sparging with nitrogen or argon before use. Potassium phosphate was obtained from commercial sources, dried overnight in a vacuum oven (50 °C) before use, and stored in a desiccator.

NMR spectra were obtained using a Bruker AV3-400 instrument with a liquid nitrogen Prodigy cryoprobe. ^{1}H NMR spectra are referenced to residual protonated solvent,[31] ^{13}C NMR spectra are referenced to solvent signals,[31] and ^{19}F spectra are externally referenced to $CFCl_3$. GC-MS analyses were performed using an Agilent 7890A gas chromatograph fitted with a RESTEK RXi-5Sil column (30 m x 0.32 mm I.D. x 0.25 μm) and an Agilent 5975C MSD running in EI mode. GC-FID analyses were carried out using an Agilent 7890A gas chromatograph fitted with an Agilent HP5 column (30 m x 0.25 mm I.D. x 0.25 μm).

DFT calculations were carried out in Gaussian 09 (Rev. D.01)[32] at the B3LYP level of theory, with Grimme D3 dispersive corrections.[33] Geometry optimisations were carried out without symmetry constraints, using the 6-31G(d) basis set for H, C N, O, P, and S, the LANL2DZ(dp) basis set and pseudopotential for Br, and the LANL2TZ(f) basis set and pseudopotential for Fe, Ni, and Pd. Energies were refined using single point calculations in which 6-311+G(d,p) was used for all atoms except Br, Fe, Ni, and Pd. Solvation (THF) was applied throughout, using the SMD implicit solvent model. The nature of each stationary point was confirmed using frequency calculations.

Procedures

General Procedure for Synthetic Cross-Coupling Reactions. A microwave vial equipped with a stir bar was charged with 4-tolylboronic acid (1.1 equiv.), [$PdCl_2$(dppf)] (**2**), and K_3PO_4 (3 equiv.). If the aryl halide was a solid, this was charged at this time also (1 equiv.). The vial was sealed with a crimp cap and evacuated and backfilled three times with nitrogen or argon. The vial was then charged with anhydrous, oxygen-free toluene or THF and the aryl halide if liquid (1 equiv.). Degassed water was also added at this stage, if used. The reaction was stirred for 2 h at 85 °C then cooled to room temperature and quenched by piercing the septum. The reaction mixture was filtered through celite, evaporated to dryness, and purified by column chromatography on silica gel.

General Procedure for Cross-Coupling Competition Reactions. A microwave vial equipped with a stir bar was charged with 4-tolylboronic acid (0.25 mmol, 1 equiv.), [$PdCl_2$(dppf)] or [NiCl(*o*-tol)(dppf)] (5 mol%), and K_3PO_4 (0.75 mmol, 3 equiv.). If the substituted aryl halide was a solid, this was charged at this time also (0.25 mmol, 1 equiv.). The vial was sealed with a crimp cap and evacuated and backfilled three times with nitrogen or argon. The vial was then charged with anhydrous, oxygen-free THF (0.8 mL),

bromobenzene (0.25 mmol, 1 equiv.), and the substituted aryl halide if liquid (0.25 mmol, 1 equiv.). Degassed water (0.2 mL) was also added. The reaction was stirred for 2 h at 85 °C then cooled to room temperature and quenched by piercing the septum. An accurately-known mass of *n*-dodecane was added, the reaction was mixed, and a sample was taken, filtered, and diluted in chloroform for GC analysis.

General Procedure for Robustness Screening. A microwave vial equipped with a stir bar was charged with 4-tolylboronic acid (0.275 mmol, 1.1 equiv.), [$PdCl_2$(dppf)] or [NiCl(*o*-tol)(dppf)] (1 or 5 mol%), and K_3PO_4 (0.75 mmol, 3 equiv.). If the additive was a solid, this was charged at this time also (0.25 mmol, 1 equiv.). The vial was sealed with a crimp cap and evacuated and backfilled three times with nitrogen or argon. The vial was then charged with anhydrous, oxygen-free THF (0.8 mL), bromobenzene (0.25 mmol, 1 equiv.), and the additive if liquid (0.25 mmol, 1 equiv.). Degassed water (0.2 mL) was also added. The reaction was stirred for 2 h at 85 °C then cooled to room temperature and quenched by piercing the septum. An accurately-known mass of *n*-dodecane was added, the reaction was mixed, and a sample was taken, filtered, and diluted in chloroform for GC analysis.

(*E*)-1-bromo-4-styrylbenzene (S6)

Benzyltriphenylphosphonium chloride (2.547 g, 6.6 mmol) was added to a 100 mL round bottom flask equipped with a stirrer bar. A suspension of LiOH.H_2O (0.370g, 8.7 mmol) in *i*-PrOH (50 mL) was added and the mixture was stirred at room temperature for 20 min. 4-Bromobenzaldehyde (1.003 g, 6.2 mmol) was added and the reaction was stirred at reflux for 16 h. Once cooled to room temperature, the reaction mixture was extracted with EtOAc (75 mL) and washed with brine (75 mL). The organic phase was dried over $MgSO_4$, filtered, and evaporated under reduced pressure. The product was recrystallised from EtOH to give a white powder (1.103 g, 67 %).

IR (ATR, neat): 3014, 1999, 1493 cm^{-1}.

^{1}H NMR ($CDCl_3$, 400 MHz): δ_H = 7.70 – 7.54 (m, 4H, Ar CH), 7.41 – 7.37 (m, 4H, Ar CH), 7.31 (d, *J* = 7.0 Hz, 1H, Ar CH), 7.13 (d, *J* = 16.7 Hz, 1H, CH=CH), 7.06 (d, *J* = 16.7 Hz, 1H, CH=CH).

^{13}C{^{1}H} NMR ($CDCl_3$, 101 MHz): δ_C = 136.5, 135.8, 131.3, 128.9, 128.3, 127.5, 127.4, 126.9, 126.1, 120.8.

MS (GC-MS, EI): *m*/z (%) = 258 $[M]^+$.

M.P.: 138 – 140 °C.

(*E*)-1-(4-bromophenyl)-*N*-phenylmethanimine (S12)

4-Bromobenzaldehyde (501.2 mg, 2.7 mmol) was added to a microwave vial equipped with a stirrer bar and molecular sieves. The vial was closed using a septum-fitted crimp cap and purged and backfilled with nitrogen. Aniline (0.246 mL, 2.7 mmol, 1 eq.) and anhydrous toluene (2.5 mL) were added and the mixture was heated using microwave irradiation at 200 °C for 4 h. Once cooled to room temperature, the reaction mixture was extracted with water (150 ml) and Et_2O (3 x 50 mL). The organic layers were combined, dried over $MgSO_4$, and filtered. The solvent was removed under reduced pressure and the product was recrystallised from DCM/pentane to give a yellow amorphous solid (100.3 mg, 14 %).

IR (ATR, neat): 3040, 2880, 1904, 1622, 1584, 1564, 1501, 1485 cm^{-1}.

^1H NMR (CD_3CN, 400 MHz): δ_H = 8.55 (s, 1H, CHN), 7.88 – 7.84 (m, 2H, Ar CH), 7.72 – 7.70 (m, 2H, Ar CH), 7.47 – 7.43 (m, 2H, Ar CH), 7.29 – 7.26 (m, 2 H, Ar CH), 7.23 (d, *J* = 6.1 Hz, 1H, Ar CH) .

$^{13}C\{^1H\}$ NMR (CD_3CN, 101 MHz): δ_C = 158.8, 131.5, 129.7, 129.5, 128.8, 125.7, 124.7, 120.6, 120.4.

MS (GC-MS, EI): *m*/z (%) = 259.0 $[M]^+$.

1-bromo-4-(methylsulfinyl)benzene (S15)

4-Bromothioanisole (998.6 mg, 4.9 mmol) was added to a 100 mL round bottom flask equipped with a stirrer bar and dissolved in DCM (20 mL). A solution of *m*CPBA (1.593 g, 1.2 eq.) in DCM (10 mL) was added to the solution at 0 °C over 5 min, and the reaction was stirred at room temperature for 12 h. The reaction mixture was diluted with saturated aq. $NaHCO_3$ (100 mL) and extracted with DCM (2 x 50 mL). The organic layers were combined, dried over $MgSO_4$, and filtered. The solvent was removed under reduced pressure and the product was recrystallised from DCM/hexane to give a white solid (472.0 mg, 47 %).

IR (ATR, neat): 2990, 2911, 1570, 1470 cm^{-1}.

^1H NMR ($CDCl_3$, 400 MHz): δ_H = 7.70 (d, J = 8.1 Hz, 2H, Ar CH), 7.5 (d, J = 8.4 Hz, 2H, Ar CH), 2.74 (s, 3H, CH_3).

$^{13}C\{^1H\}$ NMR ($CDCl_3$, 101 MHz): δ_C = 144.4, 132.1 , 125.0, 124.7, 43.5.

M.P.: 80 – 82 °C.

Analytical data are consistent with the literature.[34]

(*E*)-4-methyl-4'-styryl-1,1-biphenyl (P6)

Synthesised according to the general procedure for synthetic cross-coupling reactions using (*E*)-1-bromo-4-styrylbenzene (259.5 mg, 1 mmol), 4-tolylboronic acid (149.2 mg, 1.1 mmol), **2** (6.8 mg, 1 mol%), and K_3PO_4 (635.7 mg, 3 mmol) in 2 mL of a 4:1 *v*/*v* THF/water mixture.

The desired product was purified by recrystallisation from hexane/DCM to yield a white solid (251.9 mg, 93%).

IR (ATR, neat): 3021, 2914, 2046, 1755, 1578, 1493 cm^{-1}.

^{1}H NMR ($CDCl_3$, 400 MHz): δ_H = 7.61 (s, 4H, Ar CH), 7.56 – 7.54 (m, 4H, Ar CH), 7.41 – 7.38 (m, 2H, Ar CH), 7.27 (s, 1H, Ar CH), 7.17 (s, 2H, CH), 2.43 (CH_3).

MS (GC-MS, EI): *m*/z (%) = 270.1 $[M]^+$.

M.P.: 226 – 228 °C.

Analytical data are consistent with the literature.[35]

methyl(4'-methyl-[1,1'-biphenyl]-4-yl]sulfane (P7)

Synthesised according to the general procedure for synthetic cross-coupling reactions using 4-bromothioanisole (203.8 mg, 1 mmol), 4-tolylboronic acid (148.5 mg, 1.1 mmol), **2** (7.1 mg, 1 mol%), and K_3PO_4 (636.9 mg, 3 mmol) in 2 mL of a 4/1 *v*/*v* THF/water mixture. The desired product was purified by recrystallisation from hexane/DCM to yield a white solid (171.2 mg, 80%).

^{1}H NMR ($CDCl_3$, 400 MHz): δ_H = 7.55 – 7.49 (m, 4H, Ar CH), 7.35 (d, *J* = 9.1 Hz, 2H, Ar CH), 7.27 (d, *J* = 9.1 Hz, 2H, Ar CH), 2.55 (s, 3H, SCH_3), 2.42 (s, 3H, $ArCH_3$).

$^{13}C\{^{1}H\}$ NMR ($CDCl_3$, 101 MHz): δ_C = 137.6 (Ar C), 137.2 (Ar C), 136.7 (Ar C), 136.5 (Ar C), 129.0 (Ar CH), 126.8 (Ar CH), 126.6 (Ar CH), 126.2 (Ar CH), 20.6 (SCH_3), 15.5 ($ArCH_3$).

MS (GC-MS, EI): *m*/z (%) = 214.1 $[M]^+$.

M.P.: 120 – 122 °C.

4-methyl-4'-(phenylethynyl)-1,1'-biphenyl (P8)

Synthesised according to the general procedure for synthetic cross-coupling reactions using 1-bromo-4-(phenylethynyl)benzene (257.4 mg, 1 mmol), 4-tolylboronic acid (149.3 mg, 1.1 mmol), **2** (7.4 mg, 1 mol%), and K_3PO_4 (638.1 mg, 3 mmol) in 2 mL anhydrous toluene. The desired product was purified by passing the reaction mixture through a pad of silica and evaporating the solvent under reduced pressure to yield a white solid (141.2 mg, 53%).

IR (ATR, neat): 3021, 1578, 1493 cm^{-1}.

^{1}H NMR ($CDCl_3$, 400 MHz): δ_H = 7.65 – 7.58 (m, 6H, Ar CH), 7.56 (d, *J* = 8.1 Hz, 2H, Ar CH), 7.42 – 7.37 (m, 3H, Ar CH), 7.30 (d, *J* = 7.8 Hz, 2H, Ar CH), 2.44 (s, 3H, CH_3).

$^{13}C\{^{1}H\}$ NMR ($CDCl_3$, 101 MHz): δ_C = 140.4 (Ar C), 137.02 (Ar C), 136.99 (Ar C), 131.5 (Ar CH), 131.1 (Ar CH), 129.1 (Ar CH), 127.9 (Ar CH), 127.7 (A r C), 126.4 (Ar CH), 126.3 (Ar CH), 122.9 (Ar C), 121.4 (Ar C), 89.5 (CC), 88.9 (CC), 20.6 (CH_3).

MS (GC-MS, EI): *m*/z (%) = 268.1 $[M]^+$.

M.P.: 160 – 162 °C.

Analytical data are consistent with the literature.[36]

(*E*)-1-(4'-methyl-(1,1'-biphenyl)-4-yl)-*N*-phenylmethanimine (P12)

Synthesised according to the general procedure for synthetic cross-coupling reactions using (*E*)-1-(4-bromophenyl)-*N*-phenylmethanimine (261.0 mg, 1 mmol), 4-tolylboronic acid (149.4 mg, 1.1 mmol), **2** (7.2 mg, 1 mol%), and K_3PO_4 (637.1 mg, 3 mmol) in 2 mL of a 4:1 *v*/*v* THF/water mixture. The desired product was purified by recrystallisation from hexane/DCM to yield a pale orange/brown solid (225.1 mg, 83%).

IR (ATR, neat): 3048, 2976, 2355, 1531 cm^{-1}.

^1H NMR (CD_3CN, 400 MHz): δ_H = 8.61 (s, 1H, CHN), 8.00 (d, *J* = 8.1 Hz, 2H, Ar CH), 7.79 (d, *J* = 8.1 Hz, 2 H, Ar CH), 7.64 (d, *J* = 8.1 Hz, 2H, Ar CH), 7.46 (t, *J* = 8.6 Hz, 2H, Ar CH), 7.34 (d, *J* = 8.6 Hz, 2H, Ar CH), 7.29 – 7.27 (m, 3H, Ar CH), 2.42 (s, 3H, CH_3).

$^{13}C\{^1H\}$ NMR (CD_3CN, 101 MHz): δ_C = 159.6, 151.6, 143.1, 137.6, 136.5, 134.8, 129.2, 128.8, 128.7, 126.6, 126.4, 125.5, 120.4, 19.7.

MS (GC-MS, EI): *m*/z (%) = 268.1 $[M]^+$.

M.P.: 134 – 136 °C.

4-methyl-4'-(methylsulfinyl)-1,1'-biphenyl (P15)

Synthesised according to the general procedure for synthetic cross-coupling reactions using 1-bromo-4-(methylsulfinyl)benzene (218.4 mg, 1 mmol), 4-tolylboronic acid (147.1 mg, 1.1 mmol), **2** (7.5 mg, 1 mol%), and K_3PO_4 (633.1 mg, 3 mmol) in 2 mL of a 4:1 *v*/*v* THF/water mixture. The desired product was purified by passing through a silica plug and eluting with hexane, then EtOAc, then MeOH to yield a white solid (105.3 mg, 46%).

^1H NMR ($CDCl_3$, 400 MHz): δ_H = 7.74 (d, *J* = 8.3 Hz, 4 H, Ar CH), 7.53 (d, *J* = 7.5 Hz, 2H, Ar CH), 7.30 (d, *J* = 8.3 Hz, 2H, Ar CH), 2.79 (s, 3H, CH_3), 2.44 (s, 3H, CH_3).

$^{13}C\{^1H\}$ NMR ($CDCl_3$, 101 MHz): δ_C = 143.7, 143.6, 137.6, 136.4, 129.2, 127.4, 126.6, 123.6, 43.6, 20.6.

MS (GC-MS, EI): *m*/z (%) = 230.1 $[M]^+$.

M.P.: 140 – 142 °C.

4'-methyl-[1,1'-biphenyl]-4-carbonitrile (P18)

Synthesised according to the general procedure for synthetic cross-coupling reactions using 4-bromobenzonitrile (182.0 mg, 1 mmol), 4-tolylboronic acid (148.4 mg, 1.1 mmol), **2** (7.2 mg, 1 mol%), and K_3PO_4 (634.2 mg, 3 mmol) in 2 mL anhydrous toluene. The desired product was

purified by flash column chromatography on silica gel using 5% EtOAc/hexane (R_f = 0.32) to yield a white solid (148.5 mg, 77%).

IR (ATR, neat): 3464, 3055, 2995, 1709, 1582, 1476 cm^{-1}

^1H NMR ($CDCl_3$, 400 MHz): δ_H = 7.73 (d, J = 8.3 Hz, 2H, Ar CH), 7.69 (d, J = 8.3 Hz, 2H, Ar CH), 7.52 (d, J = 8.0 Hz, 2H Ar CH), 7.32 (d, J = 8.2 Hz, 2H, Ar CH), 2.45 (s, 3H, CH_3).

$^{13}C\{^1H\}$ NMR ($CDCl_3$, 101 MHz): δ_C = 145.1, 138.3, 135.8, 132.1 (2C), 129.4 (2C), 127.0 (2C), 126.6 (2C), 118.5, 110.1, 20.7.

MS (GC-MS, EI): *m*/z (%) = 193.1 $[M]^+$.

M.P.: 110 – 112 °C.

Analytical data are consistent with the literature.[37]

(*E*)-benzaldehyde *O*-methyl oxime (A6)

Methoxyamine hydrochloride (231.4 mg, 2.7 mmol) was added to a microwave vial equipped with a stirrer bar and molecular sieves. The vial was closed using a septum-fitted crimp cap and purged and backfilled with nitrogen. Benzaldehyde (0.276 mL, 2.7 mmol, 1 eq.), pyridine (0.220 mL, 2.7 mmol, 1 equiv.), and anhydrous toluene (2.5 mL) were added and the mixture was heated using microwave irradiation at 200 °C for 4 h. Once cooled to room temperature, the reaction mixture was extracted with water (150 ml) and Et_2O (3 x 50 mL). The organic layers were combined, dried over $MgSO_4$, and filtered. The solvent was removed under reduced pressure and the product was recrystallised from DCM/pentane to give a pale straw-coloured amorphous solid (241.3 mg, 65 %).

IR (ATR, neat): 3069, 2936, 2816, 1690, 1603, 1452 cm^{-1}.

^1H NMR (CD_3CN, 400 MHz): δ_H = 8.14 (s, 1H, C*H*NOMe), 7.64 – 7.61 (m, 2H, Ar CH), 7.44 – 7.43 (m, 3H, Ar CH), 3.95 (s, 3H, CH_3).

$^{13}C\{^1H\}$ NMR (CD_3CN, 101 MHz): δ_C = 148.0, 129.4, 129.1, 128.3, 126.3, 60.9.

MS (GC-MS, EI): *m*/z (%) = 135.1 $[M]^+$.

Analytical data are consistent with the literature.[38]

(methylsulfinyl)benzene (A11)

Thioanisole (0.950 mL, 8.1 mmol) was added to a 100 mL round bottom flask equipped with a stirrer bar and dissolved in DCM (20 mL). A solution of *m*CPBA (2.084 g, 12.2 mmol, 1.5 equiv.) in DCM (10 mL) was added to the solution at 0 °C over 5 min, and the reaction was stirred at room temperature for 12 h. The reaction mixture was diluted with saturated aq. $NaHCO_3$ (100 mL) and extracted with DCM (2 x 50 mL). The organic layers were combined, dried over $MgSO_4$, and filtered. The solvent was removed under reduced pressure and the

product was recrystallised from DCM/hexane to give a viscous colourless liquid (411.2 mg, 36 %).

IR (ATR, neat): 3464, 3055, 2995, 2913, 1709, 1582, 1476 cm^{-1}.

^{1}H NMR ($CDCl_3$, 400 MHz): δ_H = 7.52 – 7.50 (m, 2H, Ar CH), 7.39 – 7.34 (m, 3H, Ar CH), 2.57 (s, 3H, CH_3).

$^{13}C\{^{1}H\}$ NMR ($CDCl_3$, 101 MHz): δ_C = 145.0, 130.5, 128.8, 122.9, 43.2.

MS (GC-MS, EI): *m*/z (%) = 140.0 $[M]^+$.

Analytical data are consistent with the literature.[34]

(*E*)-1,2-diphenylethene (A17)

Benzyltriphenylphosphonium chloride (3.842 g, 9.9 mmol) was added to a 100 mL round bottom flask equipped with a stirrer bar. A suspension of $LiOH.H_2O$ (0.557 g, 13.2 mmol) in *i*-PrOH (50 mL) was added and the mixture was stirred at room temperature for 20 min. Benzaldehyde (0.960 mL, 9.4 mmol) was added and the reaction was stirred at reflux for 16 h. Once cooled to room temperature, the reaction mixture was extracted with EtOAc (75 mL) and washed with brine (75 mL). The organic phase was dried over $MgSO_4$, filtered, and evaporated under reduced pressure. The product was recrystallised from EtOH to give a white powder (1.412 g, 83 %).

IR (ATR, neat): 3059, 3021, 1597, 1576, 1495 cm^{-1}.

^{1}H NMR ($CDCl_3$, 400 MHz): δ_H = 7.56 (d, *J* = 7.8 Hz, 4H, Ar CH), 7.40 (t, *J* = 7.5 Hz, 4H, Ar CH), 7.30 (t, *J* = 7.0 Hz, 2H, Ar CH), 7.16 (s, 2H, CH=CH).

$^{13}C\{^{1}H\}$ NMR ($CDCl_3$, 101 MHz): δ_C = 136.9, 128.23, 128.20, 127.1, 126.0.

MS (GC-MS, EI): *m*/z (%) = 180.1 $[M]^+$.

M.P.: 124 – 126 °C.

Analytical data are consistent with the literature.[39]

Funding Information

We thank Syngenta and the Engineering and Physical Sciences Research Council for an Industrial CASE Studentship for AKC (EP/P51066X/1), and the University of Strathclyde for a Chancellor's Fellowship for DJN (2014-18). We are grateful to the Carnegie Trust for the Universities of Scotland for a Research Incentive Grant (RIG008165).

Acknowledgment

We thank Mr Gavin Bain, Mr Craig Irving, Ms Patricia Keating, and Dr John Parkinson for assistance with technical and analytical facilities. We thank Dr Michael Rogers for providing the benzyltriphenylphosphonium chloride used in this study. Some of the calculations in this manuscript were performed using the Archie-WEST high-performance computer based at the University of Strathclyde, and we are grateful to Mr Jonathan Buzzard, Dr Karina Kubiak-Ossowska, and Dr Richard Martin for assistance with this facility.

Supporting Information

YES (this text will be updated with links prior to publication)

Primary Data

YES (this text will be updated with links prior to publication)

References

1. Negishi, E.-i. *Angew. Chem. Int. Ed.* **2011,** 50, (30), 6738-6764.
2. Suzuki, A. *Angew. Chem. Int. Ed.* **2011,** 50, (30), 6722-6737.
3. Johansson Seechurn, C. C. C.; Kitching, M. O.; Colacot, T. J.; Snieckus, V. *Angew. Chem. Int. Ed.* **2012,** 51, (21), 5062-5085.
4. Cooper, A.; Leonard, D.; Bajo, S.; Burton, P.; Nelson, D. *ChemRxiv* **2019**.
5. Tasker, S. Z.; Standley, E. A.; Jamison, T. F. *Nature* **2014,** 509, (7500), 299-309.
6. Ananikov, V. P. *ACS Catal.* **2015,** 5, (3), 1964-1971.
7. Bajo, S.; Laidlaw, G.; Kennedy, A. R.; Sproules, S.; Nelson, D. J. *Organometallics* **2017,** 36, 1662-1672.
8. Guard, L. M.; Mohadjer Beromi, M.; Brudvig, G. W.; Hazari, N.; Vinyard, D. J. *Angew. Chem. Int. Ed.* **2015,** 54, (45), 13352-13356.
9. Zhang, K.; Conda-Sheridan, M.; R. Cooke, S.; Louie, J. *Organometallics* **2011,** 30, (9), 2546-2552.
10. Tsou, T. T.; Kochi, J. K. *J. Am. Chem. Soc.* **1979,** 101, (21), 6319-6332.
11. Nelson, D. J.; Maseras, F. *Chem. Commun.* **2018,** 54, (75), 10646-10649.
12. Funes-Ardoiz, I.; Nelson, D. J.; Maseras, F. *Chem. Eur. J.* **2017,** 23, (66), 16728-16733.
13. West, M. J.; Watson, A. J. B. *Org Biomol Chem* **2019,** 17, (20), 5055-5059.
14. Collins, K. D.; Glorius, F. *Nat Chem* **2013,** 5, (7), 597-601.

15. Hansch, C.; Leo, A.; Taft, R. W. *Chem. Rev.* **1991,** 91, (2), 165-195.

16. Portnoy, M.; Milstein, D. *Organometallics* **1993,** 12, (5), 1665-1673.

17. Christian, A. H.; Müller, P.; Monfette, S. *Organometallics* **2014,** 33, (9), 2134-2137.

18. Payard, P. A.; Perego, L. A.; Ciofini, I.; Grimaud, L. *ACS Catal.* **2018,** 8, (6), 4812-4823.

19. Strawser, D.; Karton, A.; Zenkina, O. V.; Iron, M. A.; Shimon, L. J. W.; Martin, J. M. L.; van der Boom, M. E. *J. Am. Chem. Soc.* **2005,** 127, (26), 9322-9323.

20. Zenkina, O. V.; Karton, A.; Freeman, D.; Shimon, L. J. W.; Martin, J. M. L.; van der Boom, M. E. *Inorg. Chem.* **2008,** 47, (12), 5114-5121.

21. Zenkina, O. V.; Gidron, O.; Shimon, L. J. W.; Iron, M. A.; van der Boom, M. E. *Chem. Eur. J.* **2015,** 21, (45), 16113-16125.

22. Orbach, M.; Shankar, S.; Zenkina, O. V.; Milko, P.; Diskin-Posner, Y.; van der Boom, M. E. *Organometallics* **2015,** 34, (6), 1098-1106.

23. He, W.; Patrick, B. O.; Kennepohl, P. *Nature Communications* **2018,** 9, (1), 3866.

24. Rothstein, P. E.; Comanescu, C. C.; Iluc, V. M. *Chem. Eur. J.* **2017,** 23, (67), 16948-16952.

25. Tejel, C.; Asensio, L.; del Río, M. P.; de Bruin, B.; López, J. A.; Ciriano, M. A. *Angew. Chem. Int. Ed.* **2011,** 50, (38), 8839-8843.

26. Desnoyer, A. N.; He, W.; Behyan, S.; Chiu, W.; Love, J. A.; Kennepohl, P. *Chemistry* **2019,** 25, (20), 5259-5268.

27. He, W.; Kennepohl, P. *Faraday Discussions* **2019**.

28. Kozuch, S.; Shaik, S. *Acc. Chem. Res.* **2011,** 44, (2), 101-110.

29. Standley, E. A.; Smith, S. J.; Müller, P.; Jamison, T. F. *Organometallics* **2014,** 33, (8), 2012-2018.

30. McIntyre, J.; Mayoral-Soler, I.; Salvador, P.; Poater, A.; Nelson, D. J. *Catal. Sci. Technol.* **2018,** 8, (12), 3174-3182.

31. Fulmer, G. R.; Miller, A. J. M.; Sherden, N. H.; Gottlieb, H. E.; Nudelman, A.; Stoltz, B. M.; Bercaw, J. E.; Goldberg, K. I. *Organometallics* **2010,** 29, (9), 2176-2179.

32. Frisch, M. J.; Trucks, G. W.; Schlegel, H. B.; Scuseria, G. E.; Robb, M. A.; Cheeseman, J. R.; Scalmani, G.; Barone, V.; Mennucci, B.; Petersson, G. A.; Nakatsuji, H.; Caricato, M.; Li, X.; Hratchian, H. P.; Izmaylov, A. F.; Bloino, J.; Zheng, J.; Sonnenberg, L.; Hada, M.; Ehara, M.; Toyota, K.; Fukuda, R.; Hasegawa, J.; Ishida, M.; Nakajima, T.; Honda, Y.; Kitao, O.; Nakai, T.; Vreven, T.; Montgomery, J. A.; Peralta, J. E.; Ogliaro, F.; Bearpark, M.; Heyd, J. J.; Brothers, E.; Kudin, K. N.; Staroverov, V. N.; Kobayashi, R.; Normand, J.;

Raghavachari, K.; Rendell, A.; Burant, J. C.; Iyengar, S. S.; Tomasi, J.; Cossi, M.; Rega, N.; Millam, J. M.; Klene, M.; Knox, J. E.; Cross, J. B.; Bakken, V.; Adamo, C.; Jaramillo, J.; Gomperts, R.; Stratmann, R. E.; Yazyev, O.; Austin, A. J.; Cammi, C.; Pomelli, C.; Ochterski, J. W.; Martin, R. L.; Morokuma, K.; Zakrzewski, V. G.; Voth, G. A.; Salvador, P.; Dannenberg, J. J.; Dapprich, S.; Daniels, A. D.; Farkas, O.; Foresman, J. B.; Ortiz, J. V.; Cioslowski, J.; Fox, D. J. *Gaussian 09. Revision D.01*, Gaussian, Inc.: Wallingford CT, 2009.

33. Fey, N.; Ridgway, B. M.; Jover, J.; McMullin, C. L.; Harvey, J. N. *Dalton Trans.* **2011,** 40, (42), 11184-11191.

34. Yuan, Y.; Shi, X.; Liu, W. *Synlett* **2011,** 2011, (04), 559-564.

35. Tobisu, M.; Xu, T.; Shimasaki, T.; Chatani, N. *J. Am. Chem. Soc.* **2011,** 133, (48), 19505-19511.

36. Kim, D.-S.; Ham, J. *Org. Lett.* **2010,** 12, (5), 1092-1095.

37. Yu, D.-G.; Yu, M.; Guan, B.-T.; Li, B.-J.; Zheng, Y.; Wu, Z.-H.; Shi, Z.-J. *Org. Lett.* **2009,** 11, (15), 3374-3377.

38. Dubost, E.; Fossey, C.; Cailly, T.; Rault, S.; Fabis, F. *J. Org. Chem.* **2011,** 76, (15), 6414-6420.

39. Bandari, R.; Höche, T.; Prager, A.; Dirnberger, K.; Buchmeiser, M. R. *Chem. Eur. J.* **2010,** 16, (15), 4650-4658.

3.4 Extended Discussion

In this chapter, we were able to elucidate some of the differences between palladium and nickel complexes as catalysts. Whilst the results gleaned from this kind of direct comparison may come as no surprise, they are nevertheless a key step in understanding the mechanistic differences in these metals. As palladium has long been considered to be the gold standard for cross-coupling reactions, its robust functional group tolerance and therefore non-coordinating nature (only seemingly affected by the strongest coordinating groups), is to be expected. Our palladium catalyst of choice was mildly affected by the strongest groups when these groups were attached to an electrophile, as shown in Figure 1b, where the difference in selectivity between coordinating and non-coordinating groups is not as stark as with nickel. However, when using the nickel catalyst in our robustness screen, there is evidence to suggest a trend with inhibitory strength (and hence, conversion) relating to binding strength (based upon K_{eq} for complex formation) (**Figure 3.1**).

Figure 3.1 Binding strength relating to reaction conversion trend

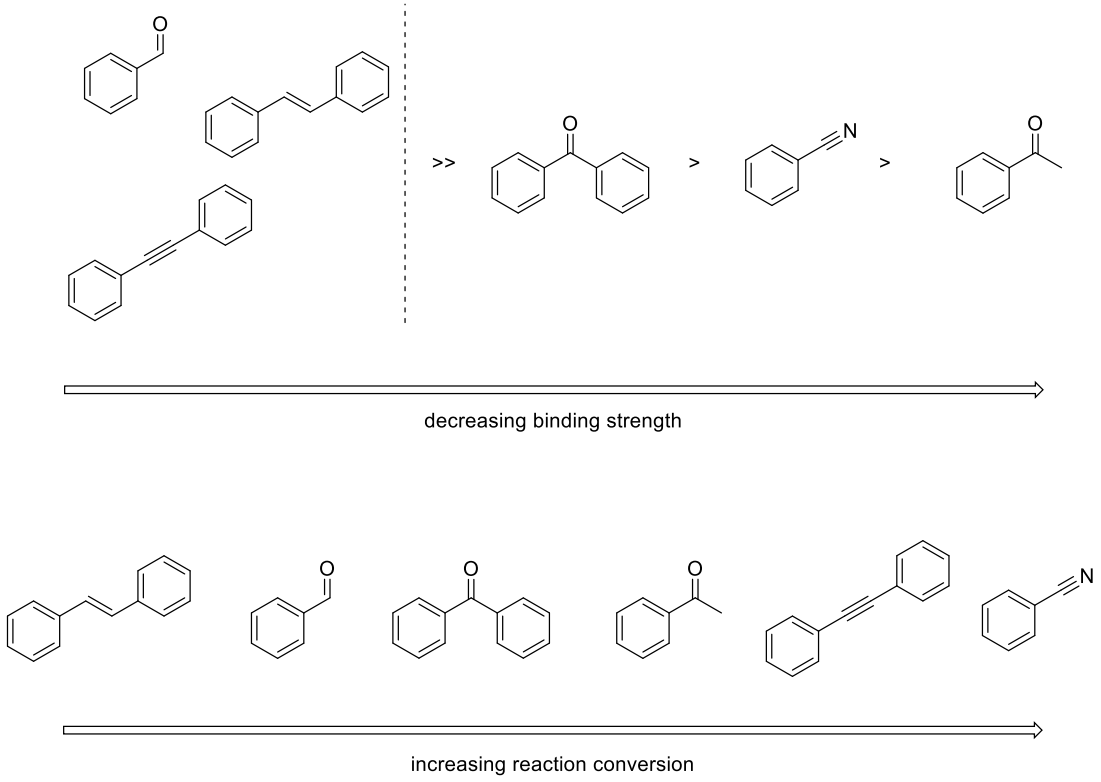

The trend holds true for the carbonyl compounds alone, as their relative binding strengths decrease along with an increase in the reaction conversion. The stilbene also exhibits low conversion with high binding strength. Diphenylacetylene however remains an outlier and we have no explanation for this. Benzonitrile also behaves as an outlier in this scale as the total conversion is actually increased above the conversion with no additive. Palladium remained unaffected in this robustness screen, owing to its high functional group tolerance, one of its attractive advantages over nickel catalysts. Since publication of this work and the work shown in the previous chapter, it has been cited by groups investigating nickel mechanisms and palladium robustness.[7] The Amgoune group reports no coordination of nickel(0) complexes to acetone, which is a result we also observed. Due to this, they were able to arylate acetone in the α-position, even in the presence of excess acetone which did not inhibit oxidative addition.

This does however pose a niche where nickel may start to become more widely used, as the selectivity exhibited during competition cross-couplings is remarkable. With more work towards a fuller understanding of this coordination effect, it may become possible for intramolecular selectivity (without the need for protecting groups) to be achieved, leading to sequential cross-couplings on a single starting molecule to build complex frameworks simply by changing the catalyst used.

Up until now, our findings have focussed purely on end point conversion analysis. We can see that during our competition reactions, one substrate reacts preferentially to the other, provided it has a coordinating functional group present. However, the exact mechanistic implications of this have not been investigated. It could be possible that the coordination enhances the rate of oxidative addition, or that initial coordination prevents oxidative addition to the other substrate. To answer these questions, full kinetic studies of the mechanisms of these cross-couplings would need to be carried out.

3.5 References

1 L. Nattmann, R. Saeb, N. Nöthling and J. Cornella, *Nat. Catal.*, 2020, **3**, 6–13.

2 S. Ge, R. A. Green and J. F. Hartwig, *J. Am. Chem. Soc.*, 2014, **136**, 1617–1627.

3 R. M. Stolley, H. A. Duong, D. R. Thomas and J. Louie, *J. Am. Chem. Soc.*, 2012, **134**, 15154–15162.

4 T. A. Ateşin, T. Li, S. Lachaize, W. W. Brennessel, J. J. García and W. D. Jones, *J. Am. Chem. Soc.*, 2007, **129**, 7562–7569.

5 G. Yin, I. Kalvet, U. Englert and F. Schoenebeck, *J. Am. Chem. Soc.*, 2015, **137**, 4164–4172.

6 S. Ogoshi, H. Ikeda and H. Kurosawa, *Pure Appl. Chem.*, 2008, **80**, 1115–1125.

7 S. A. Derhamine, T. Krachko, N. Monteiro, G. Pilet, J. Schranck, A. Tlili and A. Amgoune, *Angew. Chemie Int. Ed.*, 2020, **59**, 18948–18953.

Chapter 4: Understanding Selectivity-Based Mechanistic Aspects of Nickel-Catalysed Cross Coupling

4.1 Authors	*Alasdair K. Cooper*[a]	Experimental work, data collection and analysis, article writing and assembly, Supplementary Information assembly
	Paul M. Burton[b]	Industrial supervisor, experimental discussion and direction
	David Sale[b]	Assistance with use of calorimetry equipment and data interpretation
	Tom Corrie[b]	Assistance with use of calorimetry equipment and data interpretation
	David J. Nelson[a]	Principal Investigator, project discussion and direction, DFT calculations and analysis, article writing and assembly, Supplementary Information assembly

a WestCHEM Department of Pure and Applied Chemistry, University of Strathclyde, 295 Cathedral Street, Glasgow, G1 1XL, Scotland. david.nelson@strath.ac.uk

b Syngenta, Jealott's Hill International Research Centre, Bracknell, Berkshire, RG42 6EY, UK.

4.2 Abstract

Insights into the mechanism for Ni-catalysed Suzuki cross-coupling reactions have been discovered through the use of reaction calorimetry, as well as valuable observations on the effects of η^2 π-complexes upon selectivity in these couplings. The marked rate difference between coordinating and non-coordinating aryl halides is shown in detail, as well as the resulting 9:1 or greater selectivity that this rate difference leads to in the context of competition couplings between such aryl halides. This effect allows the successful prediction of cross coupling selectivity(?) in the presence of multiple functional groups.

4.3 Extended Introduction

Until this point in our investigation, all of our results have been based upon end point analysis. Whilst useful for being able to qualitatively define the observed effects, this does not give us any information about what is happening *during* the reaction. This is important as it can help to determine conditions beneficial to the most efficient conversion of the reaction. A reaction that achieves 90 % conversion in a 12 hour timeframe could exhibit a variety of different reaction profiles (zero order or first order in starting material, it could include a long initiation phase followed by rapid reaction, or the reaction could even be completed in the first 10 minutes, followed by catalyst death). To be able to monitor the reaction as it proceeds and identify reactive intermediates, transition states and the rates of each step would be a huge step forwards in understanding not only the specific processes we have studied, but also in the area of nickel catalysis as a whole. There are a variety of *in situ* monitoring methods available for studies such as this, each with associated advantages and disadvantages. As explained by Donna Blackmond, these methods can fall into one of two categories.[1,2]

i. *Integral Measurements* – These methods use a measurable parameter, such as absorbance, which can be related to the concentration of a species in the reaction. The integral of the reaction rate is then proportional to the concentration. An example of this is FTIR reaction monitoring. where absorbance is measured and related to concentration through the Beer-Lambert Law:

$$A = \varepsilon bc$$

where A is absorbance, ε is extinction coefficient, b is path length and c is concentration. Differentiating the concentration versus time gives the rate of reaction. For these methods, then, rate of reaction is a processed parameter, whilst the primary parameter is concentration (or conversion).

ii. *Differential Measurements* – These methods measure reaction rate directly and can also be called derivative measurements. One such method is reaction calorimetry, which measures the instantaneous heat flow of a reaction at rapid intervals (typically several times every minute). The reaction rate can be related to the heat flow through the heat of the reaction:

$$\dot{q} = \Delta H_{rxn}\ x\ V\ x\ rate$$

where $\dot{q}$ is the heat flow, ΔH_{rxn} is the heat of the reaction and V is volume. For differential methods, the parameters are reversed, so the rate is the primary parameter, whilst concentration or conversion (proportional now to rate versus time) are the processed parameters.

Both of these categories of measurements are used extensively in academic research and industrial process chemistry. Godala et al used isothermal reaction calorimetry to study the decomposition of formic acid in the heterogeneous Fenton reaction.[3] Traditionally, the Fenton process is used to generate OH· radicals *via* the reaction of hydrogen peroxide with ferrous ions (Fe^{2+}). These radicals are potent and non-selective oxidants and can react with organic pollutants in wastewater resulting in the formation of carbon dioxide and water. Naturally, understanding this process is attractive as and improvements made would lead to significant environmental impact. During their study, iron oxyhydroxide was used as the catalyst due to its already widespread use in large-scale applications. One such organic pollutant which can be oxidised is formic acid, as it is used widely in the textiles industry as a result of the dyeing and finishing processes. As both the decomposition of hydrogen peroxide and the accompanying oxidation of formic acid are both exothermic reactions, reaction calorimetry is a suitable technique to evaluate the mechanisms. According to a mechanism modelled by Cassano et al, the decomposition of hydrogen peroxide is actually independent of the oxidation of the organic substance in question and can compete with the desired process, reducing the overall efficiency.[4] By measuring the rates of each of these reactions using calorimetry, Godala et al were able to discover several key points about each process, as well as to evaluate the use of calorimetry and its associated advantages and disadvantages. The main drawback that was illustrated by this study is that this technique can only be used to effectively monitor single reactions. Moreover (as is shown in our own studies further into this chapter), studying reactions with multiple steps becomes increasingly difficult. To supplement the data obtained through calorimetry, the Godala group used additional techniques, including monitoring measuring the gas production rates of each reaction to give a significant improvement on the kinetic analysis. It was also found that, in order to avoid experimental errors, the kinetic runs could not last for more than two hours. A reaction with too low a rate will lead to difficulties in determining the baseline, which would significantly negatively impact the signal to noise ratio. During this study, however, the group was able to make several significant observations:

i. As long as the catalyst and hydrogen peroxide are present in sufficient amounts, formic acid can indeed be decomposed by the Fenton reaction

ii. If the catalyst concentration is increased, the rates of both reactions are also increased, though the rate of decomposition of hydrogen peroxide is increased much more

iii. At neutral pH (i.e. with no formic acid present), the decomposition of hydrogen peroxide occurred much more readily

This study highlights the advantages and limitations of calorimetry as a reaction kinetics analysis technique. Another group used *in situ* ReactIR to monitor a selected Diels-Alder reaction catalysed by various ferrocene-stabilised silicon cations (**Scheme 4.1**).[5]

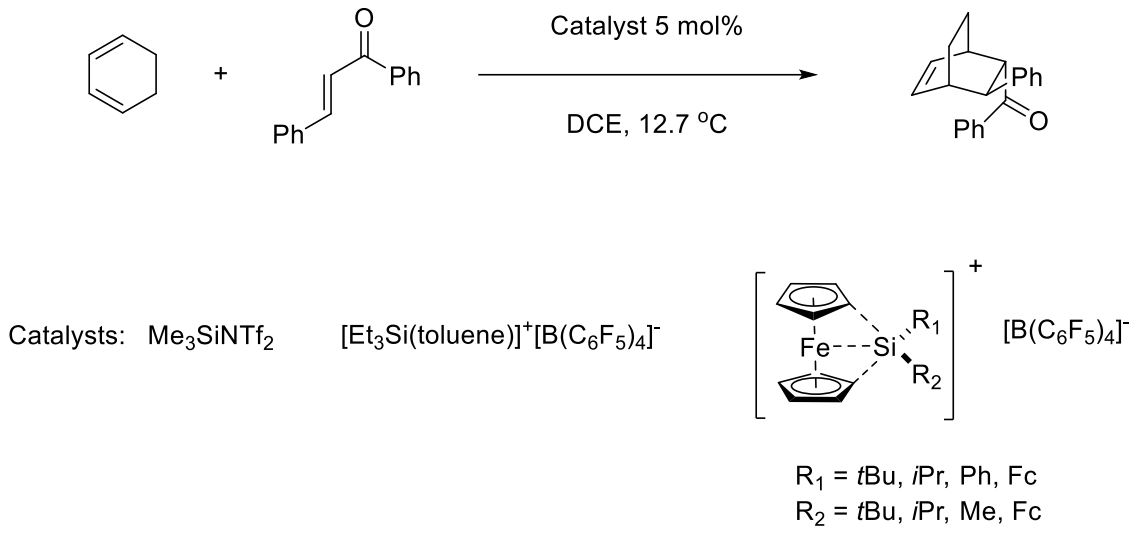

Scheme 4.1 Diels-Alder catalysed by silicon cations

In order to be a suitable reaction candidate for this technique, the selected process must include groups that are distinguishable in an IR spectrum (compared to calorimetry, where there must be a significant, measurable heat change over the course of the reaction). Here, the group chose a dienophile with a carbonyl group which can be readily monitored spectroscopically. Additionally, the corresponding ketone on the product has a stretching band which is sufficiently removed from the starting material that no overlap and resulting errors would occur. It was found that the reaction was complete by the time the sample was first analysed when using the non-stabilised catalysts, whilst the reaction time to full conversion (where this

was achieved) was usually closer to half an hour. Since the reaction temperature could not be significantly lowered to extend the reaction time (DCE freezes at – 18 °C and the ferrocene complexes are unstable above – 40 °C in DCM), the analysis was focused on the ferrocene complexes (**Figure 4.1**).

Figure 4.1 Reaction profiles of the selected Diels-Alder reaction using different catalysts

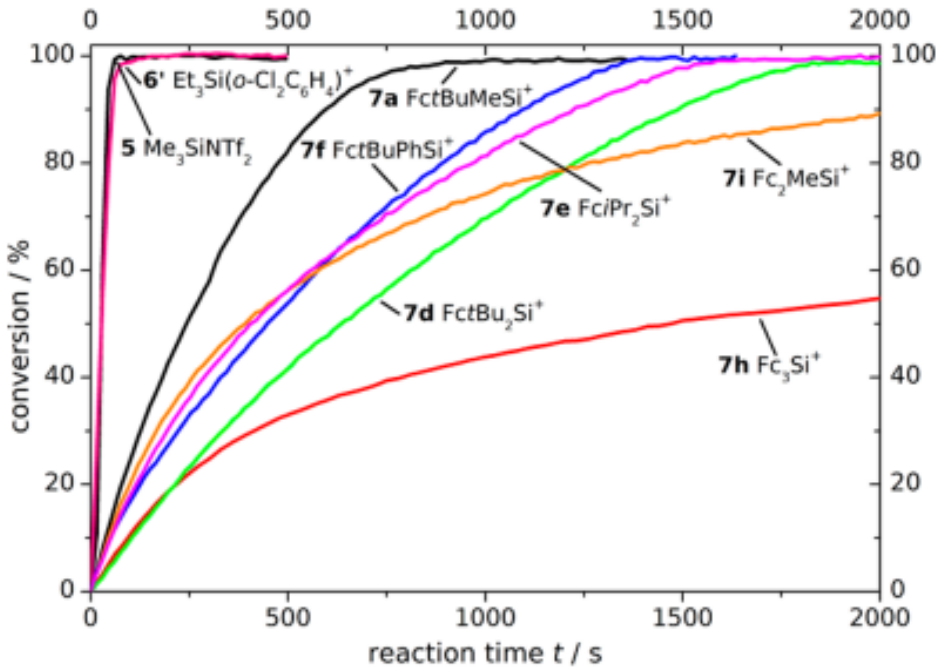

From these profiles, it is not possible to obtain an overall reaction order, but some observations can be made. Within the group containing one ferrocene ligand (**7a**, **7d**, **7e** and **7f**), the best catalyst has the least steric bulk (R_1 = Me, R_2 = Fc). The difference in curve between the catalysts containing one ferrocene and the species with two or three could be explained by the stabilising effect of the ferrocene ligands, reducing the Lewis acidity of the species and, therefore, its competency as a catalyst. Another finding that was made during this research was that the Diels-Alder reaction in question is diastereoconvergent, as both *E* and *Z* dienophiles lead to *trans*-product with a d.r. of 99:1.

As shown by these two studies, there is a vast amount of reaction data that can be collected by running the reaction (often with no changes or minor changes to the conditions) using an *in situ* monitoring method. These methods do have limitations, also shown in these studies, and

so careful consideration is required when choosing which method of monitoring to employ and how best to supplement the obtained data:

- The method must have a good enough signal:noise ratio to observe significant results
- The method must be rapid enough to measure all aspects of the reaction, particularly if the reaction has a quick initial step
- It may be necessary to characterise the components of the reaction, so the method must be able to do this (i.e. *via* following a diagnostic NMR signal)

Introduction

Transition metal catalysed cross coupling reactions have been ubiquitous in areas of academic and industrial research since the 1970s, with the Suzuki-Miyaura coupling being one of the most widely used reactions in fine chemical synthesis.[1–4] It has been common practice in these reactions to use a palladium-based catalyst equipped with either phosphine or NHC-type ligands.[5–8] Palladium catalysts have seen such widespread use due to their robustness, both physically (inert conditions are still required for the reactions, but the pre-catalysts are typically bench-stable long term) and in terms of reproducibility. However, the higher cost and lower abundance of palladium means it is important to find cheaper and more abundant catalysts for these transformations. More recently, nickel-based catalysts have seen increased use in academic examples as a viable alternative. While nickel has shown promise in academic settings, it has not been used extensively in industry, due to its much higher air sensitivity and need for higher catalyst loadings (often 1-5 mol%, compared to <1 mol% for palladium). One significant advantage of nickel over palladium is its higher nucleophilicity, which allows oxidative addition into much more inert groups (phenol derivatives, aryl ethers and aryl fluorides) to be possible.[9–11] This would allow a much wider range of electrophiles to be coupled, increasing the applicability of these cross coupling reactions.

We have also previously shown that this inherent reactivity can be exploited to selectively cross-couple electrophiles in the presence of potentially more reactive sites. This selectivity arises from the tendency for nickel to form η^2-type complexes with π systems, such as carbonyls or alkenes.[12] Once the complex has formed, the Ni centre is able to "ring walk" across a conjugated system (if such a system exists on the molecule in question) towards a potential site for oxidative addition (**Figure 1**).[13–15]

Figure 1 Dewar-Chatt-Duncanson metal-pi bonding and ring-walking

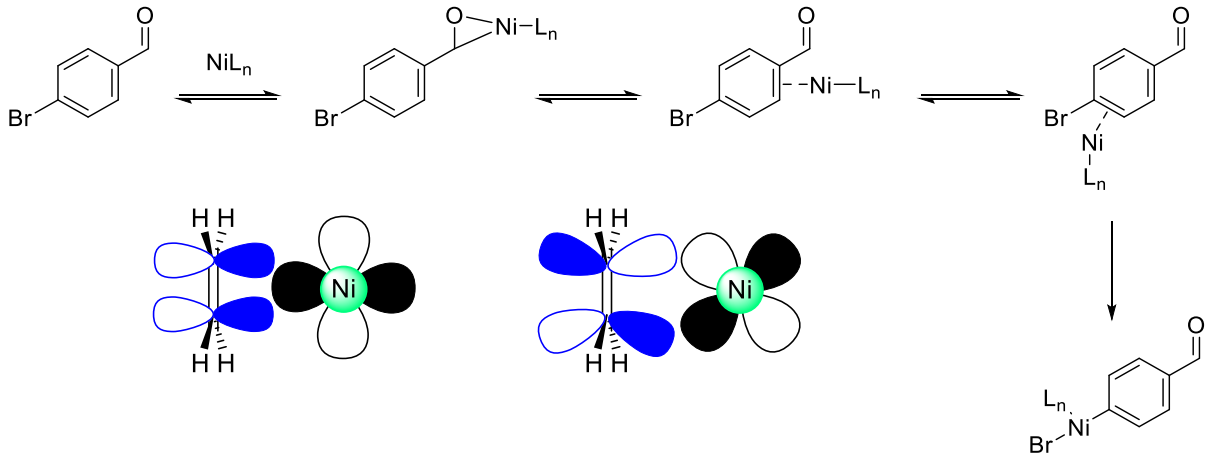

We have shown that this effect overrides the expected rates of reaction based on relative oxidative addition rates (**Figure 2**).

Figure 2 Relative oxidative addition rates for selected aryl halides with conflicting observed selectivity

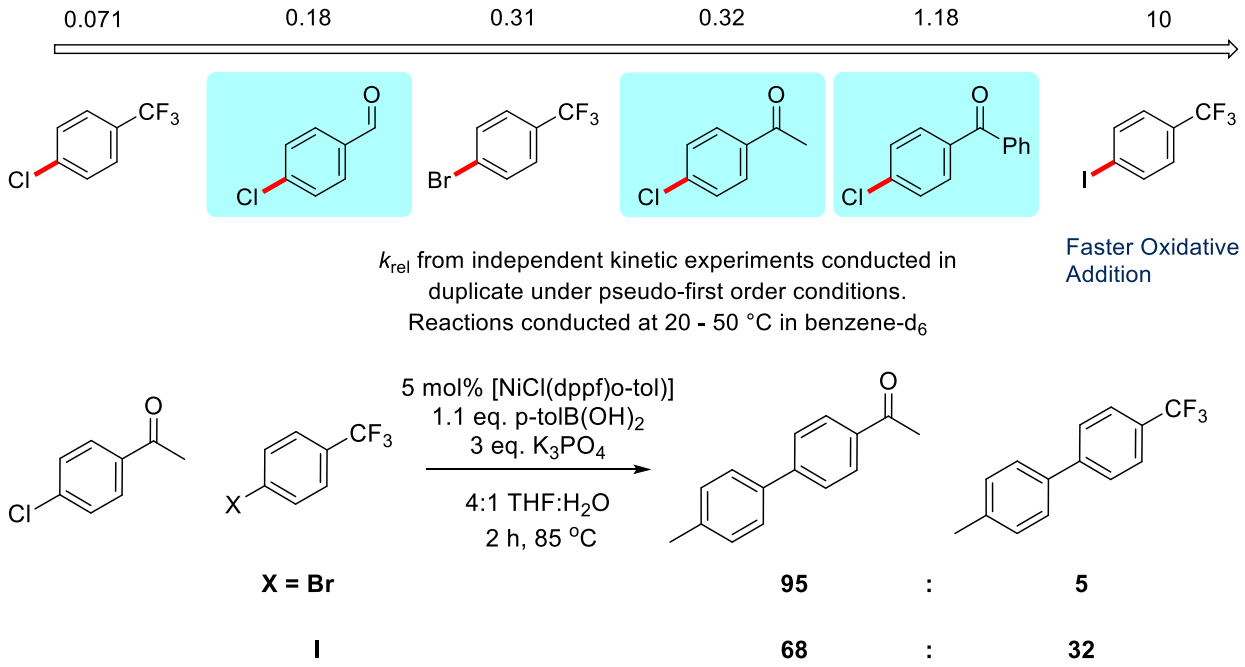

Furthermore, we were able to quantify this selectivity by relating the Hammett parameters of aryl halides, σ_p, (both coordinating and non-coordinating) to the observed selectivity. Competition reactions between bromobenzene (R1) and an aryl halide bearing a *para* substituent (R2) were carried out (**Figure 3**), with selectivity defined as in equation (1).

$$\text{Selectivity} = \frac{[P_1 - P_2]}{[P_1 + P_2]} \quad (1)$$

The results of this were plotted as selectivity vs. σ_p, showing a stark contrast between coordinating and non-coordinating aryl halide substituents. The coordinating groups gave almost total selectivity in each case (often a 95:5 ratio) for the coordinating substrate, while other groups across a range of σ_p values did not exhibit any effect (graph in **Figure 4**).

Figure 3 Hammett competition selectivity study

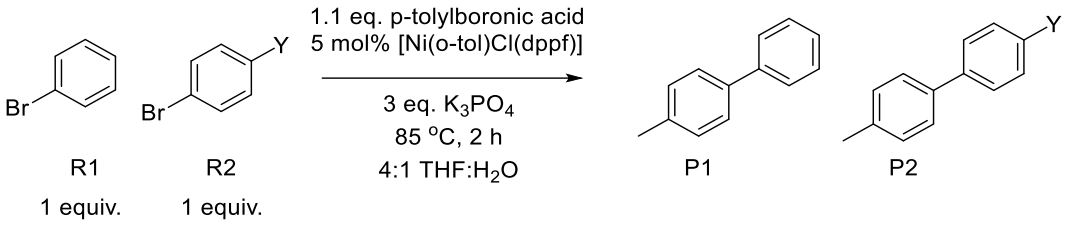

Y = CHO, COMe, COPh, NMe_2, NHPh, $CH(CH_3)_2$, CF_3, OMe, CO_2Me, NEt_2, SO_2Me, OCF_2H, OCF_3

In spite of these advantages and remarkable reactivity traits, much less is known about the mechanism of the nickel-catalysed Suzuki cross coupling. Proposed mechanisms range from Ni(0)/Ni(II) cycles (analogous to palladium), to pathways involving single electron transfer and reactive Ni(I) species.[16,17] It is widely accepted that oxidative addition is rate-limiting for many palladium-catalysed cross-coupling reactions (except with particularly reactive electrophiles such as aryl iodides), but the same cannot be said for nickel, due to its higher reactivity. There is speculation that transmetalation may be rate-limiting, but this is the subject of much debate.[18–22]

Our aims in this study were:

- To develop an understanding of the effects of coordinating functional groups on the selectivity of cross-coupling and to probe the limits of these effects
- To investigate whether these coordinating groups have an effect on the reaction rate (as our previous studies were based upon final conversions)

These aims would be achieved by using high throughput analysis techniques such as reaction calorimetry, which allow heterogeneous reaction monitoring (which is otherwise challenging).

Results & Discussion

Prior Work

Following on from our previous study, we elected to extend the scope to include potential non-carbonyl coordinating substituents (such as nitriles, alkynes, alkenes). There is precedent in the literature for Ni to form similar complexes with nitriles[23] and alkenes (Van der Boom)[15] and it would greatly enhance the applicability of this effect if the selectivity was still apparent with other π-systems that are able to engage in back-bonding with electron rich Ni(0) centres. Several new substrates were tested in competition reactions *versus* bromobenzene, and the selectivities of the reactions were quantified as in our previous work (equation 1). These data were then added to an updated plot (**Figure 4**).

In addition to this study showing the benefits of this coordination effect, we have investigated the potential for a detrimental effect if the coordinating substituents are present on a separate molecule used as an additive, using a 'Robustness Screening' approach (**Figure 5**). The general trend that was observed followed previously reported results of equilibrium constants for the formation of Ni η^2 complexes. The coordinating substrates did generally lower the conversion. Benzaldehyde greatly inhibited the reaction, lowering conversion to <15 %, while benzonitrile actually improved conversion to >95 %.

Figure 4 Selectivity vs. Hammett parameter with added coordinating (orange) and non-coordinating (blue) aryl substituents (Y)

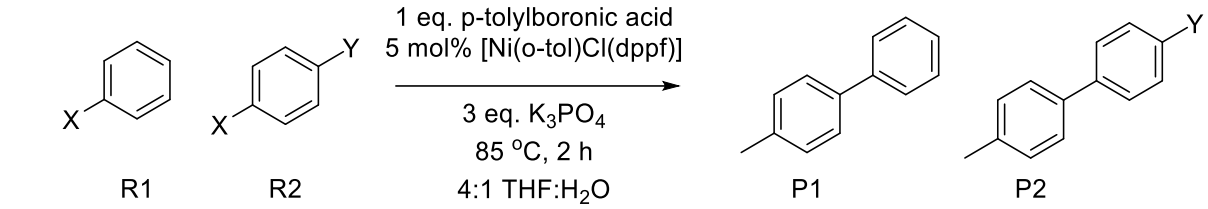

Y = as above plus CN, $(CH)_2Ph$, C_2Ph

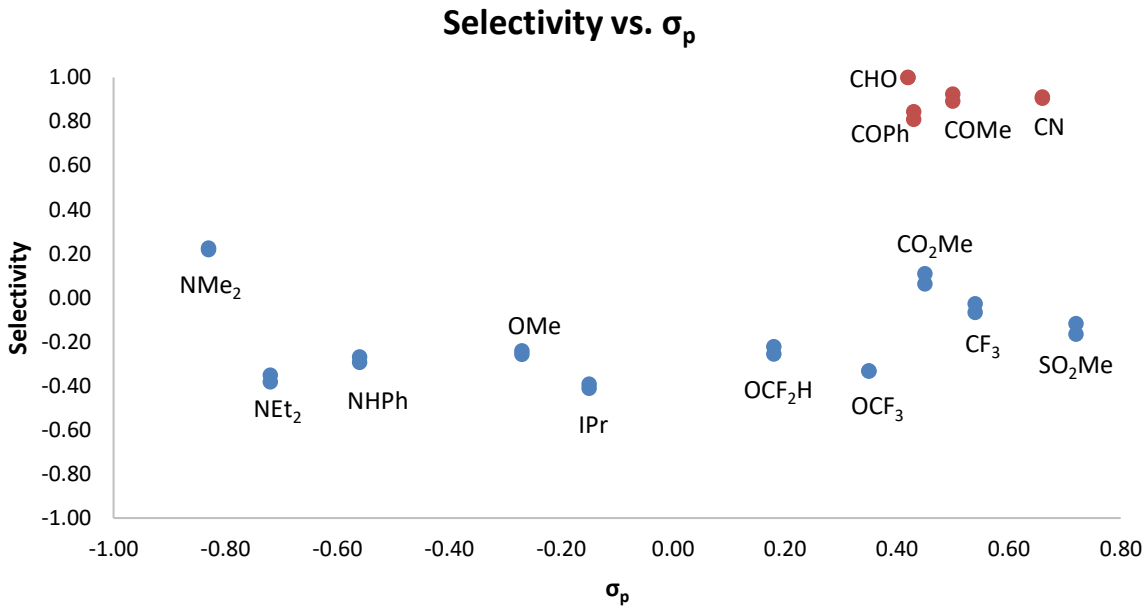

Figure 5 Inhibition study and equilibrium constants for complex formation

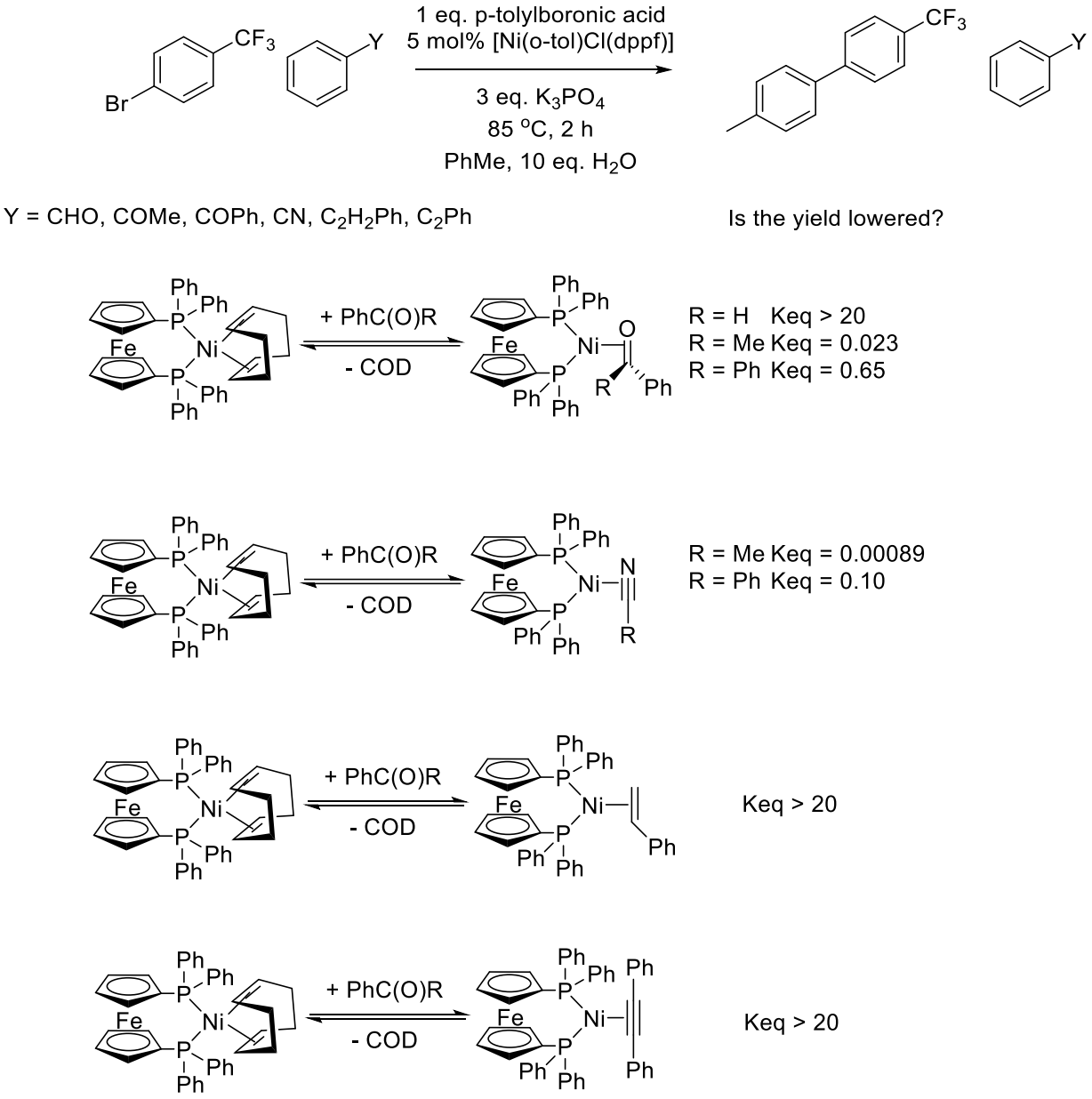

Additive	Conversion/% (Average of 2 replicates)
None	88
Benzaldehyde (Y = CHO)	12
Acetophenone (Y = COMe)	78
Benzophenone (Y = COPh)	38
Benzonitrile (Y = CN)	98
Stilbene (Y = C_2H_2Ph)	2
Diphenylacetylene (Y = C_2Ph)	82

While this study was successful, proving our initial hypothesis that coordinating substrates were privileged in cross-coupling (if attached to the electrophile), these results *do not elucidate any information about the rates of any of these reactions*. It was also observed that, in the case of an alkyne as a coordinating group, the reaction is much slower, suggesting that coordination is potentially very strong and actually might hinder the reaction. This data would be invaluable in understanding how to fine-tune Suzuki cross coupling conditions for nickel catalysts to achieve the best possible results. To complement this existing data and to gain further insight into the mechanism of nickel-catalysed cross-coupling as a whole, it was decided that a method of *in situ* reaction monitoring would be beneficial. Two popular methods of on-line monitoring were considered, both of which avoid the need for manual sampling:

i. ReactIR

This technique provides information on the speciation of the reactants involved in the reaction as well as rate data after processing, though it is not suitable for biphasic reactions due to the limited path length.

ii. Reaction Calorimetry

This is a powerful monitoring technique, which monitors heat flow (watts) in the reaction and gives immediate information on the rate, provided there is a significant heat change and that background heat (such as heat of mixing of solvents) can be accounted for and subtracted. This can also be used for multiphase reactions as the heat is measured throughout the entire system.

The instrument must be allowed to reach a stable heat flow prior to monitoring, which can take several hours.

While both methods were attractive for our purposes, ReactIR did not seem suitable as the solvent mixture is 20 % water, which could potentially dominate the IR spectrum and obscure relevant information. Reaction calorimetry was chosen since there were examples in the literature of groups using this technique to monitor cross-coupling reactions (such as Buchwald Hartwig aminations) and the throughput was much higher (the instrument to be used could monitor eight reactions simultaneously).
Through the use of this technique, the aims were:

- To glean information on the rate-determining step of the reaction. For palladium cross-coupling reactions, this is generally oxidative addition (except for faster substrates such as aryl iodides), but oxidative addition to nickel is generally more facile.

- To determine if there is a significant difference in rate between substrates that coordinate and substrates that do not i.e. do the graphs reported previously reflect rate after all?

- To determine if there is a significant difference in rate between electron deficient aryl halides and electron rich aryl halides.

Initial Monitoring

Some initial cross-coupling reactions were monitored using calibrated GC-FID, taking samples every 5 minutes for the first part of the reaction. This was to ensure that the reaction rate was appropriate for accurate monitoring by calorimetry, as rapid reactions can often give poor resolution with this technique. The use of our previously optimised conditions gave a profile that showed an initial rate that was too high (**Figure 6)**.
Furthermore, due to the nature of the reaction vessels to be used for the calorimetry studies, it is not possible to carry out this procedure if the reaction mixture is heated at (or close to) reflux. To combat these issues, THF was substituted with 2-MeTHF. This allowed the reaction to reach the desired temperature while remaining below the boiling point of the solvent (THF b.p. = 66 ^{o}C; 2-MeTHF b.p. = 80 ^{o}C). The reaction temperature was lowered to 60 ^{o}C and the

Figure 6 Initial GC-FID monitoring showing optimal calorimetry conditions for both substrates (red lines)

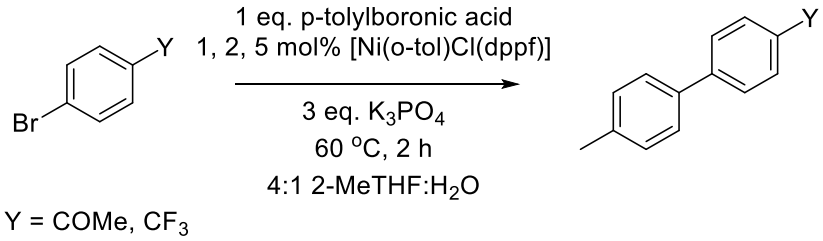

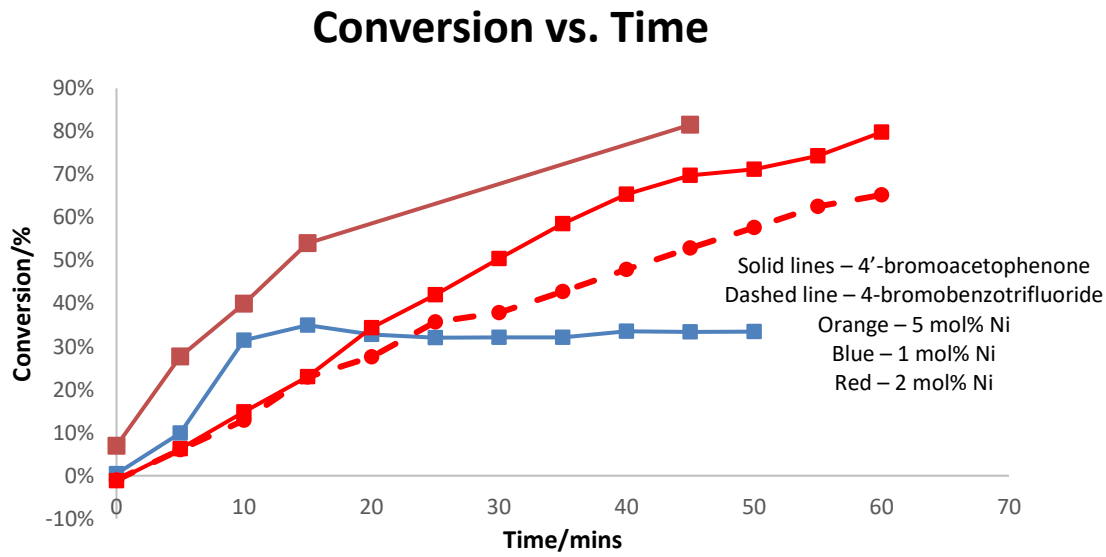

catalyst loading was lowered to 1 mol%, which resulted in significant turnover loss, presumably due to catalyst deactivation, as turnover ceased completely after *ca.* 10 minutes. Increasing the catalyst loading to 2 mol% gave reaction rates that were deemed suitable for monitoring *via* calorimetry for both coordinating (4'-bromoacetophenone) and non-coordinating (4-bromobenzotrifluoride) model substrates. Even from these initial results, it could be suggested that oxidative addition is not rate-determining, since the rates of reaction of these two substrates are very similar. Following this, reactions where either the aryl halide or the boronic acid were in excess were monitored over time, to give more information on oxidative addition and transmetalation. Reactions were monitored with both model substrates using a 3:1 ratio of aryl halide:boronic acid and a 3:1 ratio of boronic acid:aryl halide (**Figure 7**). For these reactions, it was expected that these excess equivalents would increase the rate, achieving higher conversions in shorter times. This might indicate that oxidative addition (3:1 aryl halide:boronic acid) or transmetalation (3:1 boronic acid:aryl halide) was rate-limiting.

Figure 7 Excess aryl halide/boronic acid monitored reactions

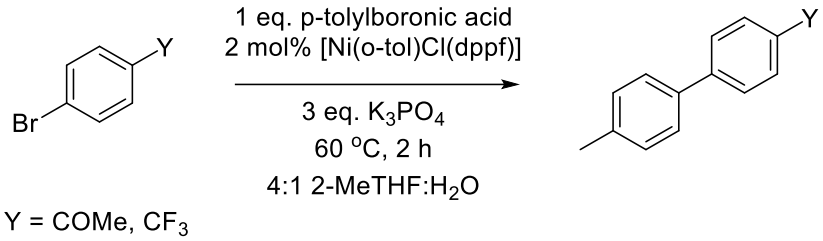

Y = COMe, CF_3

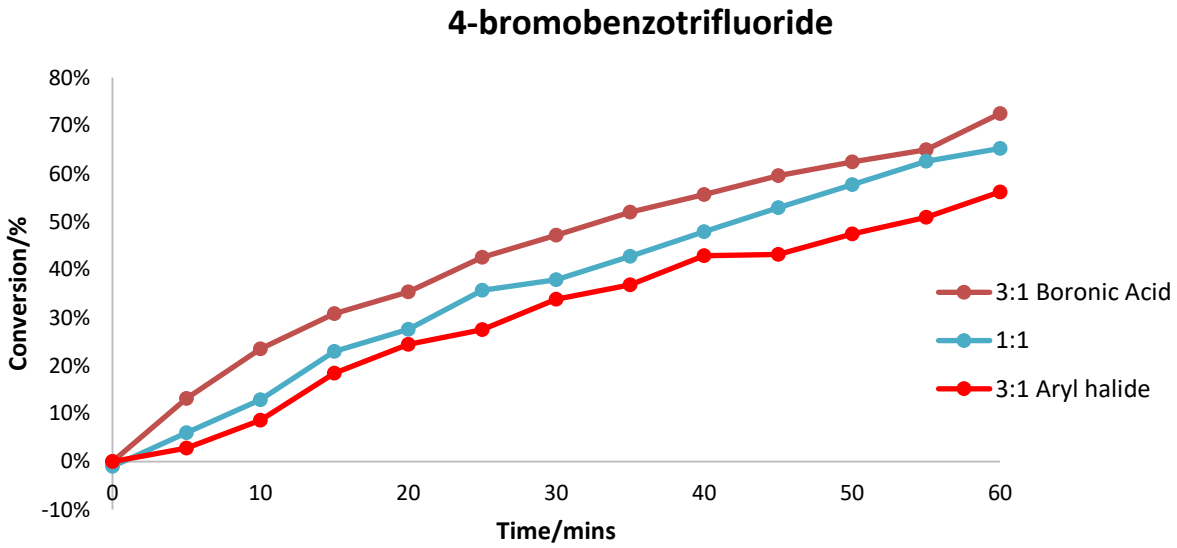

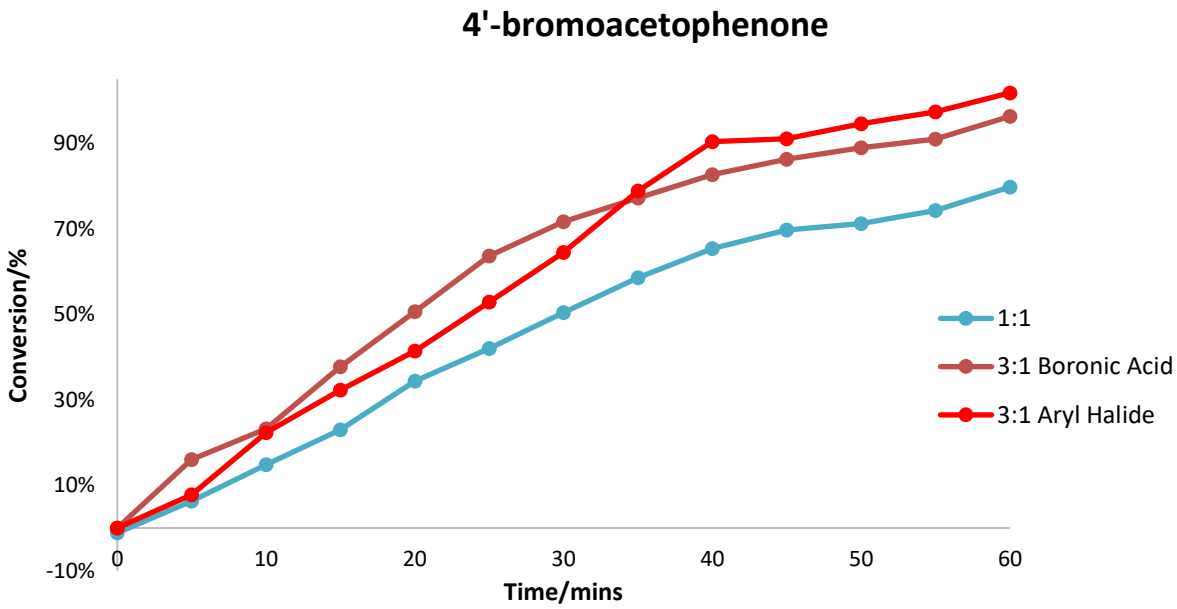

The results of these excess reactions infer that oxidative addition is not rate-limiting, since using an excess of aryl halide does not appear to alter the reaction rate significantly. However, the same can be said of transmetalation from these graphs, as the boronic acid excess reactions also do not differ greatly. From this, it could be inferred that reductive elimination is potentially rate-limiting, or that there are physical rate-limiting processes that could be taking place (such as mass transfer between the two phases of the reaction or formation of a NiOH species for transmetalation). With these initial observations in hand, a series of reactions were then monitored using calorimetry, which gives far greater data density and precludes the need for tedious, low-throughput manual sampling.

Reaction Calorimetry

A selection of substrates was chosen for this study which covered as much experimental space as possible, while also allowing a focus on coordinating substrates. Initial reactions that were studied using calorimetry were simple Suzuki-Miyaura cross-coupling reactions using the conditions from the work described above, with six substrates (**Figure 8**). From these results, it can be seen that 4-bromobenzaldehyde and 4-bromobenzonitrile react much more quickly than the other substrates tested here. The heat flow is directly correlated to the rate of reaction, and so these plots represent rate *versus* time. The other coordinating substrates do exhibit a larger heat spike than bromobenzene, which suggests faster reaction, though not as fast as the 4-bromobenzaldehyde or 4-bromobenzonitrile. The magnitude of the heat flow is also in line with expected results based on previously determined equilibrium constants for the formation of η^2-Ni complexes with these carbonyls. From the conversion *versus* time plot, the aldehyde and nitrile substrates reach full conversion in 70 – 80 minutes, exhibiting a slight s-shaped curvature compared to the non-coordinating substrates. This suggests that the mechanism for coordinating substrates involves some slightly more complex finer points than for substrates which do not coordinate.

Figure 8 Initial calorimetry results

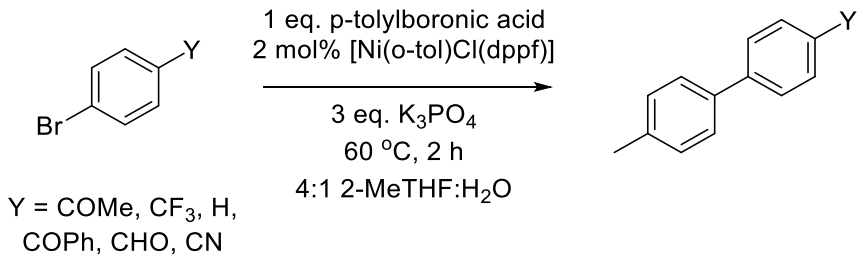

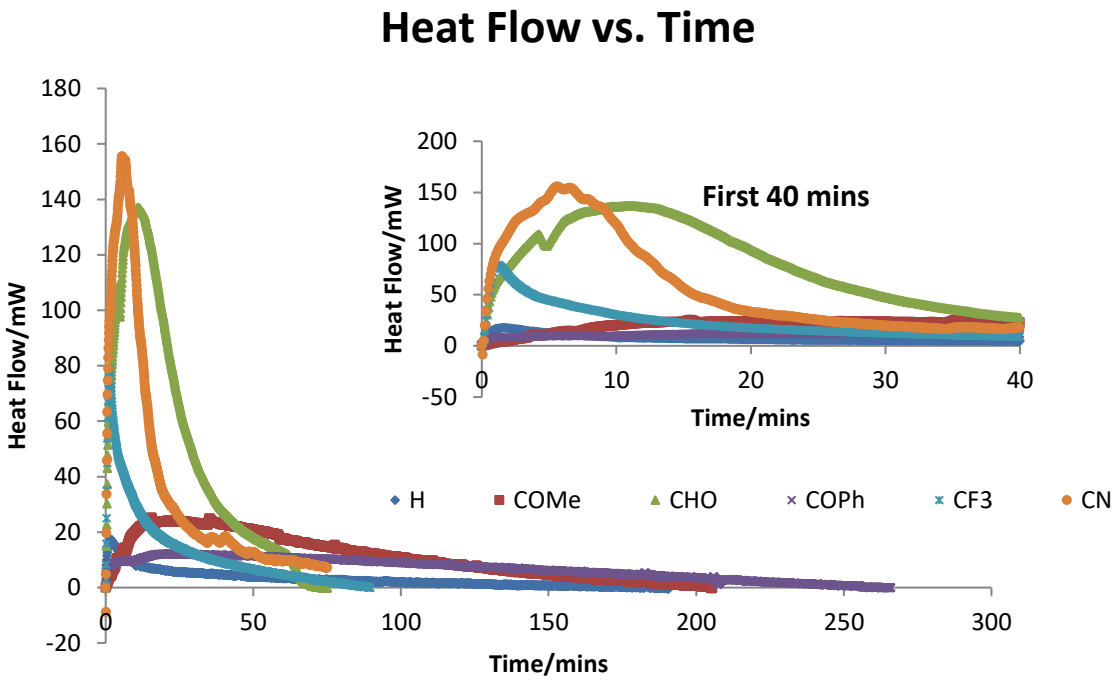
Heat Flow vs. Time
Heat Flow/mW
Time/mins
First 40 mins
H
COMe
CHO
COPh
CF3
CN

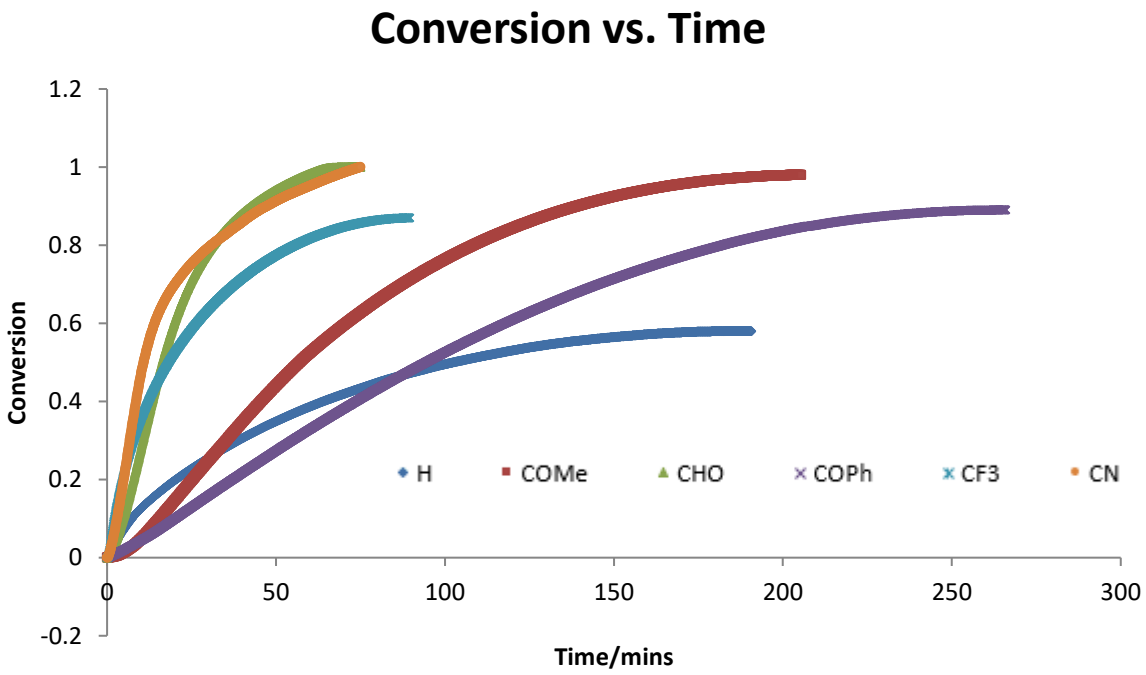
Conversion vs. Time
Conversion
Time/mins
H
COMe
CHO
COPh
CF3
CN

Following these initial results, particular attention was paid to 4-bromobenzaldehyde, since the equilibrium constant for the formation of an η^2 complex with Ni is known, and further reactions were monitored.

In order to tentatively investigate the effect of catalyst decomposition on the reaction rate, a cross-coupling reaction was monitored where 0.25 mmol aliquots of 4-bromobenzaldehyde were added over time. This, theoretically, should produce heat spikes of equal magnitude each time an addition was made, assuming slow catalyst decomposition and negligible product inhibition. What was actually observed were two initial spikes that were almost identical, followed by two smaller spikes (**Figure 9**).

Figure 9 Monitored coupling with sequential addition of aryl halide

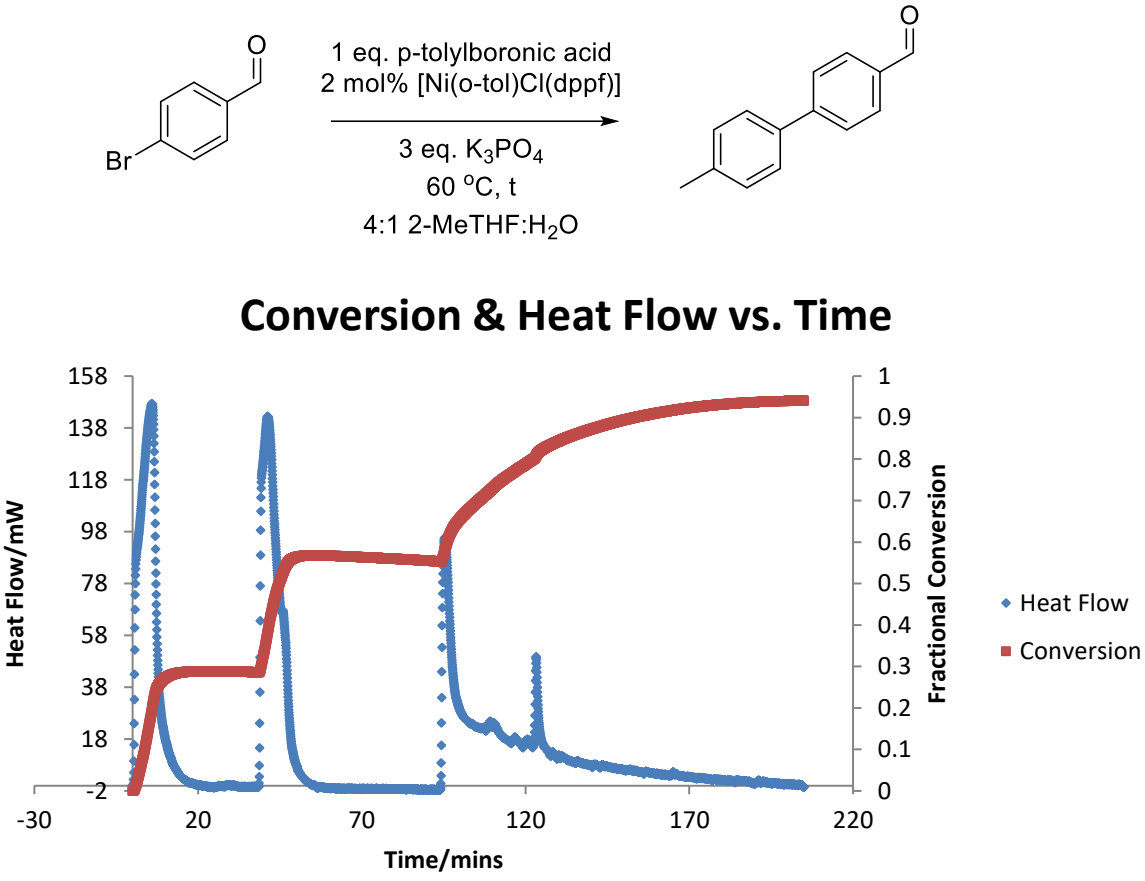

This pattern could be attributed to some degree of catalyst decomposition, although not of all the catalyst undergoes decomposition as the reaction still proceeded to full conversion.

Determination of Reaction Order

To further investigate the reaction and potentially determine the order of reaction in catalyst, further analysis was carried out using techniques pioneered by Bures (**Figure 10**).

Figure 10 Catalyst Order Determination Graphs

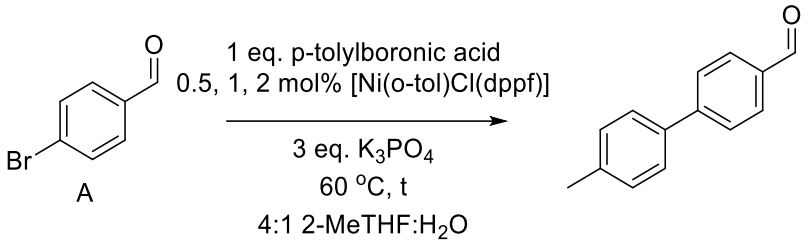

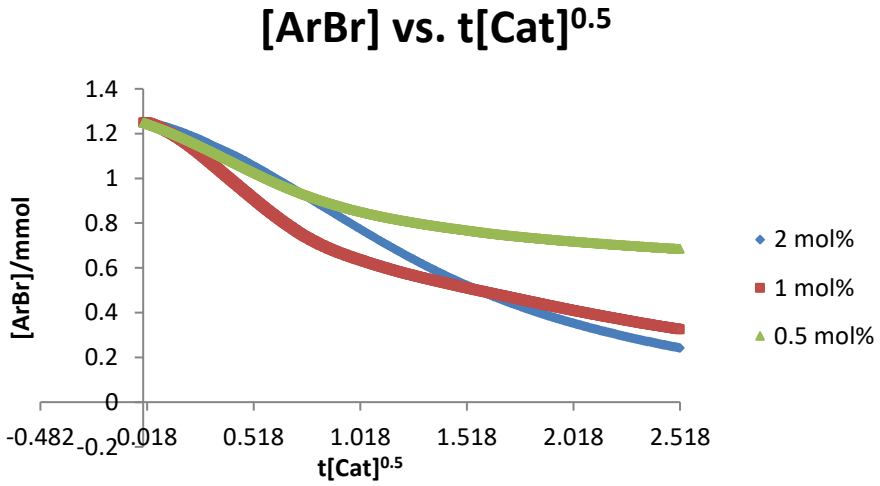

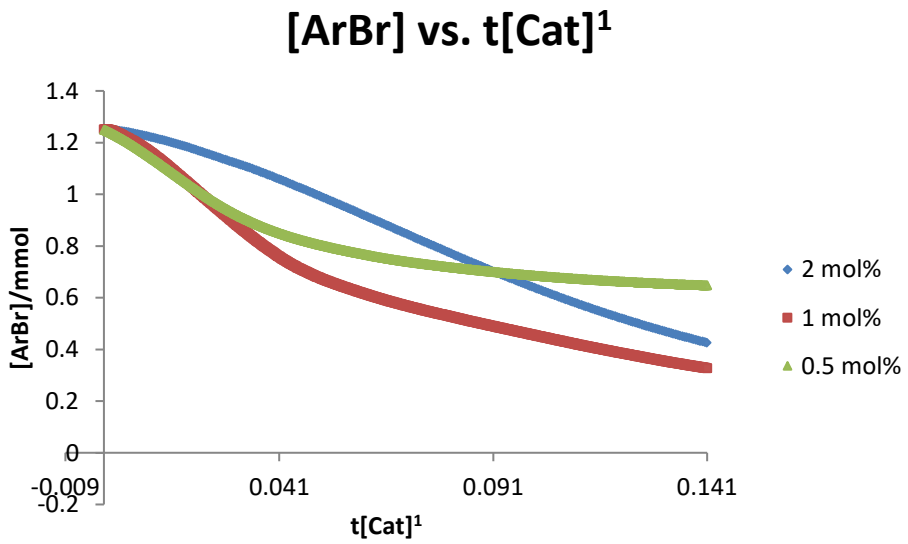

The cross-coupling reaction of 4-bromobenzaldehyde and 4-tolylboronic acid was performed using three different catalyst loadings and the concentration of aryl halide, [ArBr] (determined *via* calorimetry and end point analysis by GC-FID), was plotted *versus* t[catalyst]$^{0.5}$ and t[catalyst]^{1} respectively. If the plotted lines overlay, then the order in catalyst is determined as 0.5 or 1 respectively (plots using t and t[catalyst]^{2} to give orders 0 & 2 were drawn, though there was little correlation, see Supporting Information). The lines do not significantly overlay in either plot, but it may be that a fractional order between 0 & 1 might fit. This analysis also assumes that the catalyst concentration remains constant throughout the reaction, which has been shown is not always the case. Further experimentation is required, utilising some higher catalyst loadings (up to 10 mol%) to attain higher data density and to mitigate the effects of catalyst decomposition during the reaction.

Some more traditional kinetic models for determination of the order of reaction in aryl halide were used for each substrate. **Figure 11** shows plots of ln[ArBr] *vs* time; plots of [ArBr] *vs* time and 1/[ArBr] *vs* time for zero and second order analysis can be found in the Supporting Information. Again, these plots highlight the difference in behaviour between substrates that coordinate to the Ni centre (4-bromobenzonitrile and 4-bromobenzaldehyde) and those that do not (bromobenzene). The rate of reaction for the coupling of bromobenzene is significantly lower, with the plot having a much shallower gradient. In each case, there seems to be a potentially linear relationship, which is slightly more pronounced and easier to observe with the 4-bromobenzaldehyde and 4-bromobenzonitrile. This suggests a degree of first order behaviour in aryl halide for substrates that do coordinate. Again, further analysis is required in order to gain a fuller understanding of the mechanism of these couplings.

Figure 11 Plots of ln[ArBr] vs time

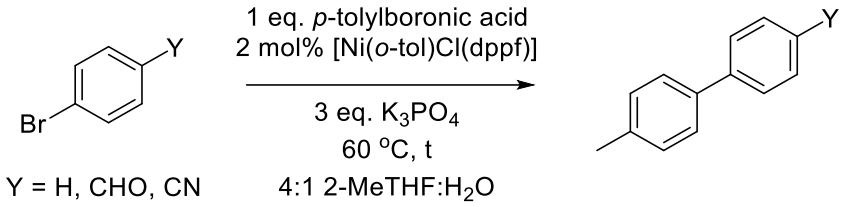

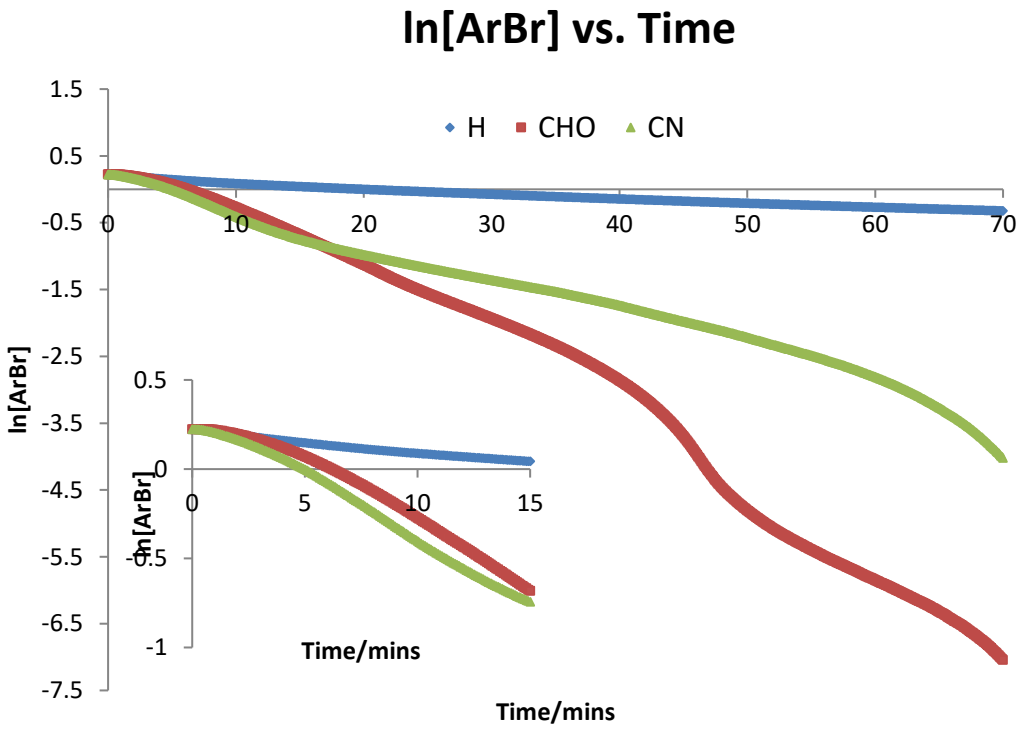

Conclusions

In summary, these initial analyses raise some further questions about the nature of these couplings.

We have shown that the high degree of selectivity in Ni-catalysed cross couplings achieved by using carbonyl-bearing substrates can also be attained when other π systems such as nitriles, alkynes and alkenes are used, enhancing the applicability of this effect. Conversely, we have shown that these types of systems actually inhibit the reaction if they are present in the system as an additive and if they are strongly coordinating enough.

We have shown that there is indeed a large difference in rate between aryl halides that are able to coordinate the Ni centre and those that do not coordinate. There is not yet a clear indication of which step may be rate-limiting for these couplings. Reaction calorimetry has proven to be a powerful technique for the monitoring of these reactions, allowing us to attain high data density. Further insights would be gained from carrying out excess reactions such as "same" and "different" excess reactions (see Donna Blackmond group)[24,25] in order to observe behaviour changes in rate for each substrate.

References

1 N. Miyaura and A. Suzuki, *Chem. Rev.*, 1995, **95**, 2457–2483.

2 A. Suzuki, *J. Organomet. Chem.*, 1999, **576**, 147–168.

3 F.-S. Han, *Chem. Soc. Rev.*, 2013, **42**, 5270.

4 C. M. Nunes and A. L. Monteiro, *J. Braz. Chem. Soc.*, 2007, **18**, 1443–1447.

5 U. Christmann and R. Vilar, *Angew. Chemie Int. Ed.*, 2005, **44**, 366–374.

6 S. Lou and G. C. Fu, *Adv. Synth. Catal.*, 2010, **352**, 2081–2084.

7 E. A. B. Kantchev, C. J. O'Brien and M. G. Organ, *Angew. Chemie Int. Ed.*, 2007, **46**, 2768–2813.

8 N. Miyaura, K. Yamada and A. Suzuki, *Tetrahedron Lett.*, 1979, **20**, 3437–3440.

9 T. Mesganaw and N. K. Garg, *Org. Process Res. Dev.*, 2013, **17**, 29–39.

10 M. Tobisu, T. Shimasaki and N. Chatani, *Angew. Chemie Int. Ed.*, 2008, **47**, 4866–4869.

11 F. Zhu and Z.-X. Wang, *J. Org. Chem.*, 2014, **79**, 4285–4292.

12 T. T. Tsou, J. C. Huffman and J. K. Kochi, *Inorg. Chem.*, 1979, **18**, 2311–2317.

13 M. Orbach, O. V. Zenkina, Y. Diskin-Posner, M. A. Iron and M. E. van der Boom, *Organometallics*, 2013, **32**, 3074–3082.

14 J. A. Bilbrey, A. N. Bootsma, M. A. Bartlett, J. Locklin, S. E. Wheeler and W. D. Allen, *J. Chem. Theory Comput.*, 2017, **13**, 1706–1711.

15 O. V. Zenkina, A. Karton, D. Freeman, L. J. W. Shimon, J. M. L. Martin and M. E. van der Boom, *Inorg. Chem.*, 2008, **47**, 5114–5121.

16 K. Zhang, M. Conda-Sheridan, S. R. Cooke and J. Louie, *Organometallics*, 2011, **30**, 2546–2552.

17 R. A. Jagtap, C. P. Vinod and B. Punji, , DOI:10.1021/acscatal.8b04267.

18 A. J. J. Lennox and G. C. Lloyd-Jones, *Angew. Chemie Int. Ed.*, 2013, **52**, 7362–

7370.

19 N. Miyaura and A. Suzuki, *J. Chem. Soc. Chem. Commun.*, 1979, 866.

20 N. Miyaura and A. Suzuki, *J. Organomet. Chem.*, 1981, **213**, C53–C56.

21 N. Miyaura, K. Yamada, H. Suginome and A. Suzuki, *J. Am. Chem. Soc.*, 1985, **107**, 972–980.

22 A. J. J. Lennox and G. C. Lloyd-Jones, *J. Am. Chem. Soc.*, 2012, **134**, 7431–7441.

23 J. J. Garcia, N. M. Brunkan and W. D. Jones, *J. Am. Chem. Soc.*, 2002, **124**, 9547–9555.

24 D. G. Blackmond, *J. Am. Chem. Soc.*, 2015, **137**, 10852–10866.

25 D. G. Blackmond, *Angew. Chemie Int. Ed.*, 2005, **44**, 4302–4320.

4.4 Extended Discussion

Over the course of the work presented in this chapter, we were able to make some progress toward understanding the selectivity apparent in the Suzuki couplings. However, due to issues with reproducibility, particularly in the case of the calorimetry, there is still a lot of information that is not yet known. During calorimetry, the vials used were not the microwave vials that have been used previously, but were instead a variety of screwcap vials. This could mean that there were inconsistencies in the seals of these vials, potentially allowing air into the reaction system, causing catalyst decomposition. As shown by the graph presented in Figure 9, catalyst decomposition is a viable pathway to low rate of reaction and potentially lower conversion in our system. However, the other potential cause to this shape of graph could be product inhibition from the catalyst binding to the carbonyl group of the final product (**Scheme 4.2**).

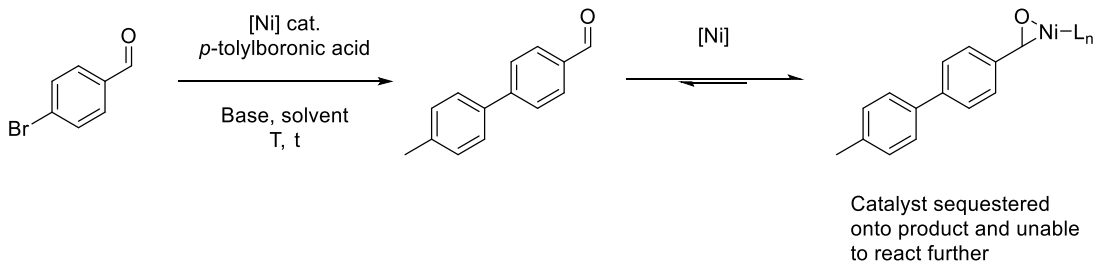

Scheme 4.2 Potential route to catalyst deactivation through product inhibition

This would be in line with our findings shown in the previous chapter through our inhibition studies. In that work, however, we used one equivalent of inhibitor, whilst in the situation presented above this would not be the case until the reaction would finish. We know that the relative equilibrium constant for complex formation for benzaldehyde is very high ($K_{eq} > 20$ versus $K_{eq} = 0.023$ for acetophenone) so it would not be unreasonable to assume that any product after 10 % conversion might hinder the reaction. Given more time, further investigation into this could have been carried out. One method would be simply to use an equivalent of the product as an additive and observe whether the final conversion was altered. A method that would give more kinetic information would be to run the coupling as normal and, simultaneously, run the coupling with 0.5 equivalents of product and boronic acid present. Sampling these reactions as before and building a reaction profile for each using GC-FID would give two different plots. The plot of the reaction where product is already present should overlay directly onto the second half of the other plot, if no inhibition is occurring (**Scheme 4.3**).

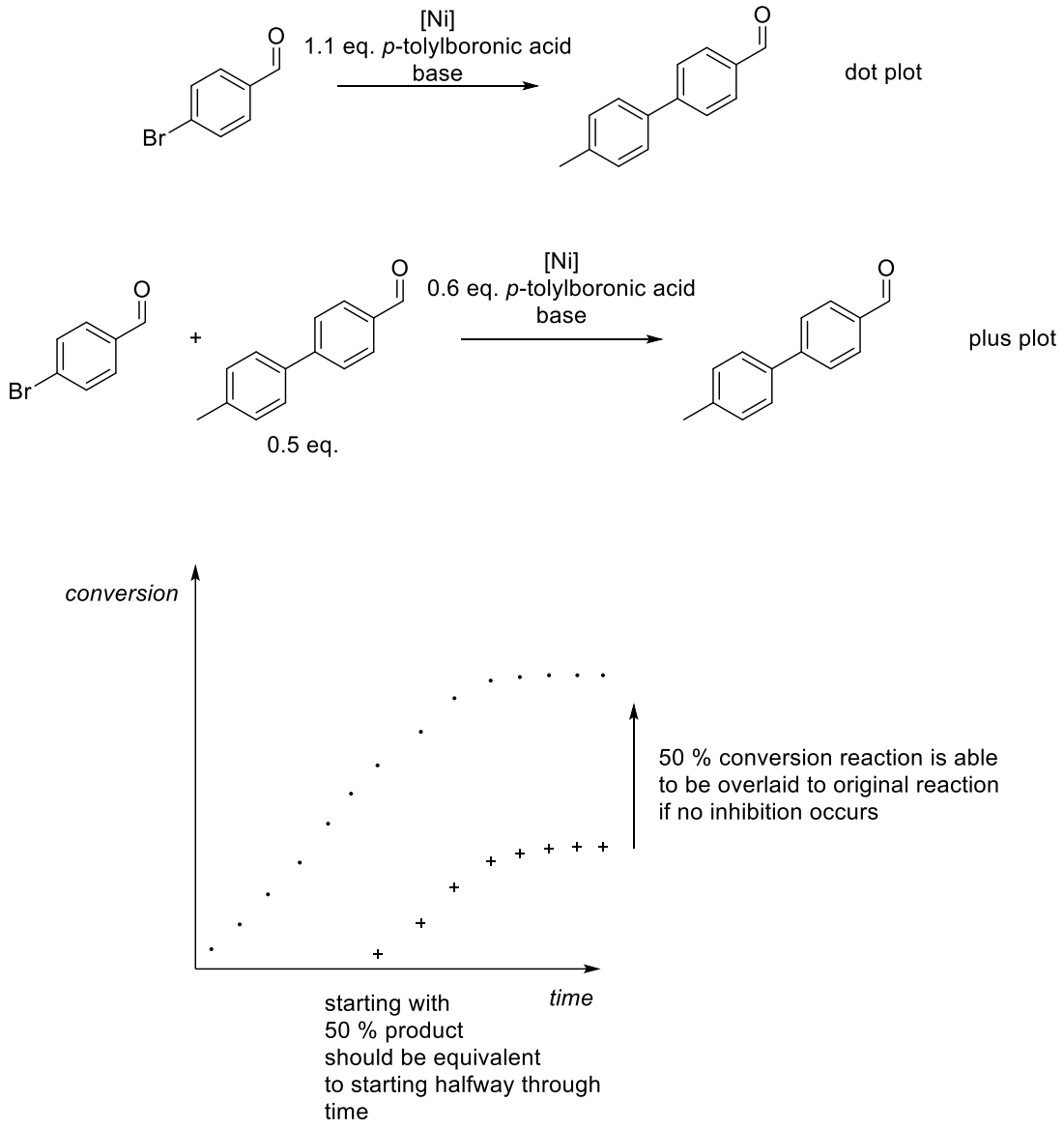

Scheme 4.3 Product inhibition probing reactions

Another area of this work which requires a lot more progress is the determination of order of reaction in various reactants. As shown, we did attempt to determine the order in catalyst using a simplified method from Burés. The results of this were inconclusive as there are certain limitations associated with using this technique. The largest factor is that, when using this method, it is assumed that catalyst concentration remains constant throughout the course of the reaction. For our reactions, this is unlikely to be true, as the catalyst has several potential resting states in which it could exist, such as coordination to either the starting substrate or final product. If air is allowed into the reaction, this will also reduce the concentration of the

catalyst, making this method inaccurate for our purposes. Using higher catalyst loadings would alleviate this issue somewhat, as the effects of decomposition or sequestration would be mitigated, perhaps giving results that overlay more satisfactorily. A further limitation, noted in the reporting of this technique itself, is that due to this analysis being purely visual (based on degree of overlay), there is no mathematical function which could be used to describe the error in order determination.

To combat issues arising from non-constant catalyst concentration, the "same [xs]" method (similar to the method described above, starting a reaction at "50 % conversion" but without adding the product to the second reaction) can be used. If the two plots do not overlay, there are two key differences in the reaction conditions that may help to explain the results:

- The reaction under normal conditions has already undergone a number of catalytic turnovers by the time it reaches 50 % conversions, whilst the reaction which starts at 50 % uses fresh catalyst
- The reaction under normal conditions will already contain 50 % product whilst the reaction starting at 50 % does not contain any

The first point would point towards catalyst decomposition, whilst the second would indicate product inhibition. Thus, introducing the experiment described above (where product is present from the 50 % conversion point), would help to distinguish these two possibilities. Using the same [xs] method allows us to monitor the stability of the catalyst throughout the reaction, a point crucial in multi-step syntheses (such as Suzuki coupling) or in syntheses with off-cycle equilibria (such as catalyst initiation or pre-coordination).

As can be seen, further work is needed in this area in order to progress the knowledge of these mechanisms. Whilst, generally, catalytic reactions are generally first order in [catalyst], our results (with the limitations suggested) do not reflect this. Lower orders than one are generally due to higher order off-cycle species[2], which could indicate an important coordination step between catalyst and substrate (in the cases where coordination is apparent).

As the placement at Syngenta came to an end and we no longer had access to the high-grade equipment to monitor reactions, we felt an important continuation of the project was to attempt to apply our findings from the aryl halide work to heterocyclic substrates.

4.5 References

1 D. G. Blackmond, *Angew. Chemie Int. Ed.*, 2005, **44**, 4302–4320.

2 D. G. Blackmond, *J. Am. Chem. Soc.*, 2015, **137**, 10852–10866.

3 L. Nowicki, D. Siuta and M. Godala, *Thermochim. Acta*, 2017, **653**, 62–70.

4 G. B. Ortiz de la Plata, O. M. Alfano and A. E. Cassano, *Appl. Catal. B Environ.*, 2010, **95**, 1–13.

5 A. R. Nödling, K. Müther, V. H. G. Rohde, G. Hilt and M. Oestreich, *Organometallics*, 2014, **33**, 302–308.

Chapter 5: Investigating Oxidative Addition of *Ortho*-Heteroaryl Chlorides to Nickel(II) Centres

5.1 Authors	*Alasdair K. Cooper*[a]	Experimental work, data collection and analysis, article writing and assembly, Supplementary Information assembly
	Paul M. Burton[b]	Industrial supervisor, experimental discussion and direction
	David J. Nelson[a]	Principal Investigator, project discussion and direction, DFT calculations and analysis, article writing and assembly, Supplementary Information assembly

a WestCHEM Department of Pure and Applied Chemistry, University of Strathclyde, 295 Cathedral Street, Glasgow, G1 1XL, Scotland. david.nelson@strath.ac.uk
b Syngenta, Jealott's Hill International Research Centre, Bracknell, Berkshire, RG42 6EY, UK.

5.2 Paper Abstract

Several nickel(II) dimers that arise as a result of attempting to cross-couple *ortho*-haloheteroarenes in Suzuki-Miyaura coupling have been separately synthesised, characterised and observed during the coupling reactions. These dimers have been found to be completely catalytically inert in Suzuki-Miyaura conditions. However, the use of stronger transmetalating reagents (Grignard reagents to perform Kumada couplings) causes the dimers to either be prevented from forming, or allows the dimer to react directly with these, resulting in the formation of cross-coupled product.

5.3 Extended Introduction

So far, the work presented has focused on relatively simple aryl-aryl cross-coupling. Whilst this has been useful for elucidating the various differences in nickel and palladium cross-coupling and showcasing the remarkable reactivity and selectivity which nickel catalysts can exhibit, the nature of heterocyclic coupling has remained untouched.

5.3.1 Heterocycles in Modern Synthetic Chemistry

Heterocycles can be found in a wide variety of pharmaceuticals, agrochemicals and fine chemicals, typically introduced through cyclisation chemistry. As of 2013, it was estimated that 70 % of all agrochemicals that had been introduced to market in the previous 20 years bore at least one heterocyclic ring.[1] It is quite common during lead-finding stages of route design to fine tune physicochemical properties of a specific active ingredient with choices of heterocycle (**Figure 5.1**).[2]

Figure 5.1 Fine-tuning physicochemical properties using heterocycles

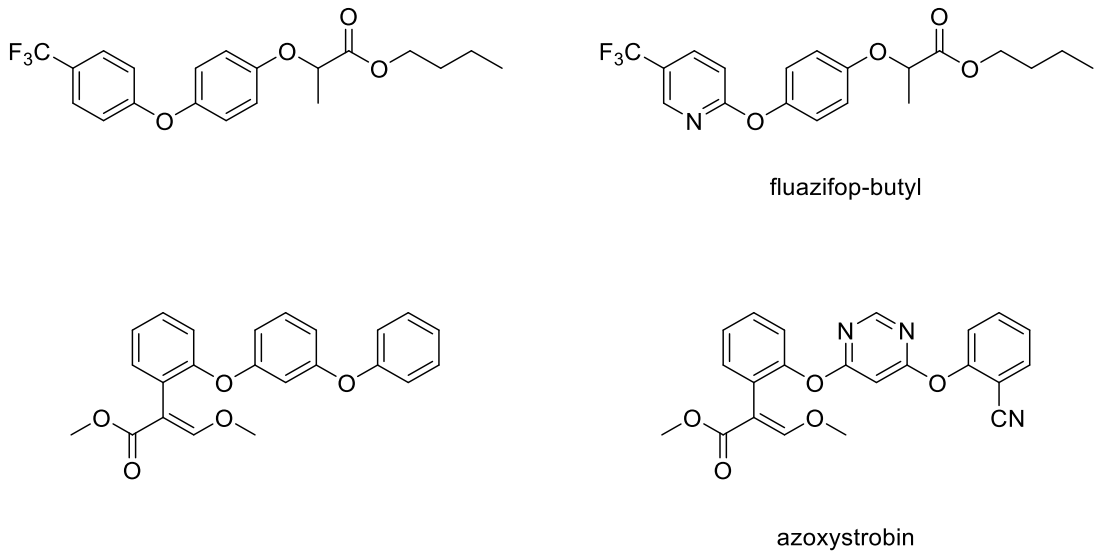

One advantage of using heterocycles over phenyl analogues is the synthetic accessibility, as the heterocycles can be furnished within a lower number of steps than the equivalent substituted phenyl system. Heterocycles can also act as propesticides in certain molecules,

where the compound does not exhibit herbicidal activity, but exposure to certain enzymes or to UV light facilitates the breakdown of the heterocyclic component to an active herbicide (**Figure 5.2**).[3]

Figure 5.2 Heterocyclic propesticides

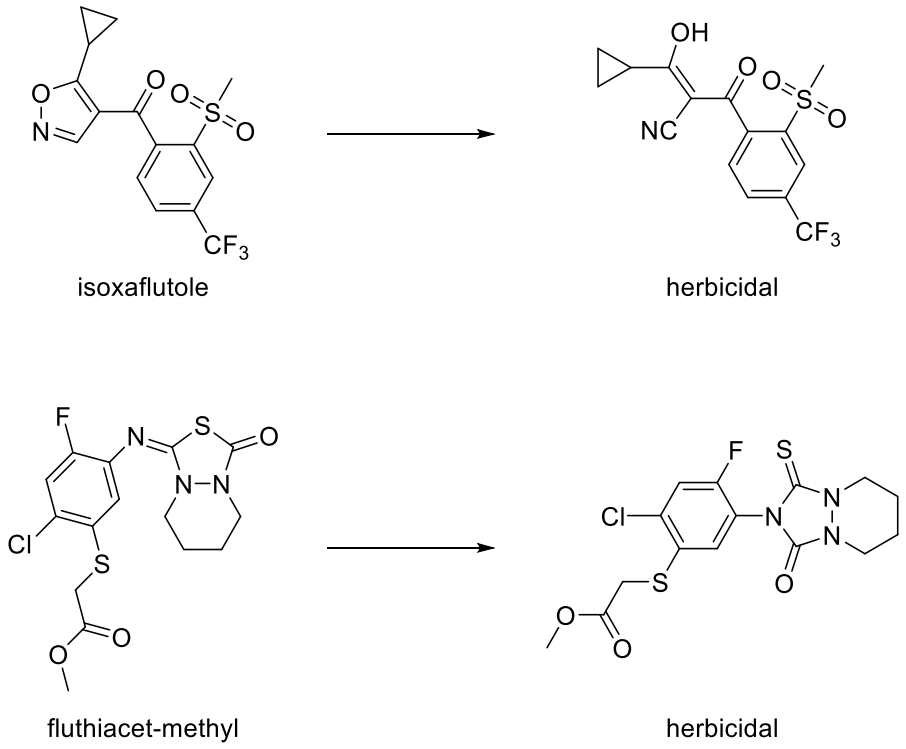

As can be seen from the above figures and the literature, the majority of heterocycles present in agrochemicals that have been brought to market contain nitrogen. There are very few products which contain purely sulfur or oxygen heterocycles and, if these heteroatoms are present, they are more often than not accompanied by a nitrogen in the ring. This means that many agrochemical syntheses begin with the condensation of a nitrogen functional group (such as amines or hydrazines) with another carbonyl group (**Scheme 5.1**).

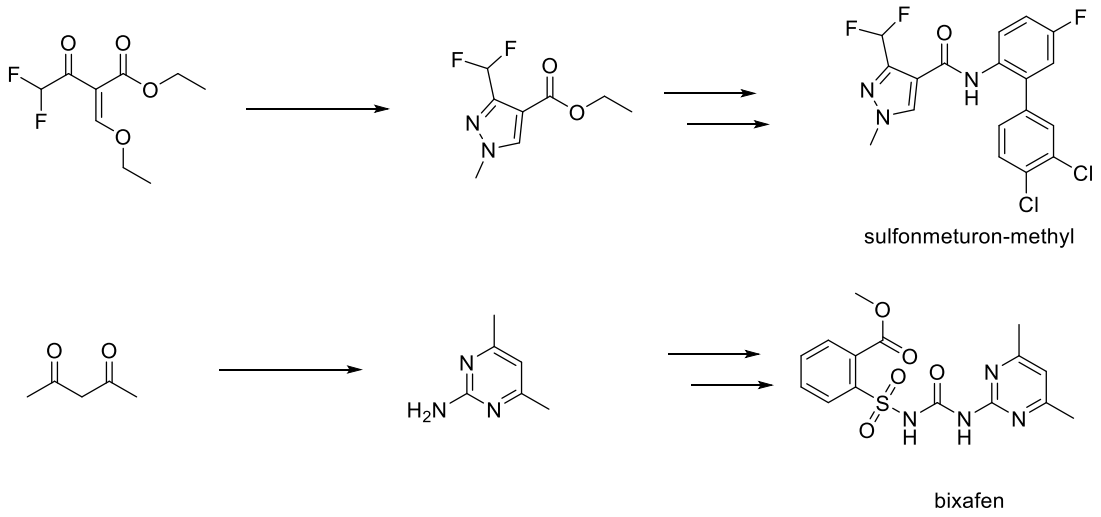

Scheme 5.1 Condensation of amino compounds with carbonyl compounds to produce heterocyclic cores

Due to these various positive aspects of heterocyclic core-structures, it is important to develop methods for their production and efficient synthesis. Many of the structures shown contain free N-H groups, which can cause the standard methods of C-C bond formation to fail when using palladium catalysts (**Scheme 5.2**).[4]

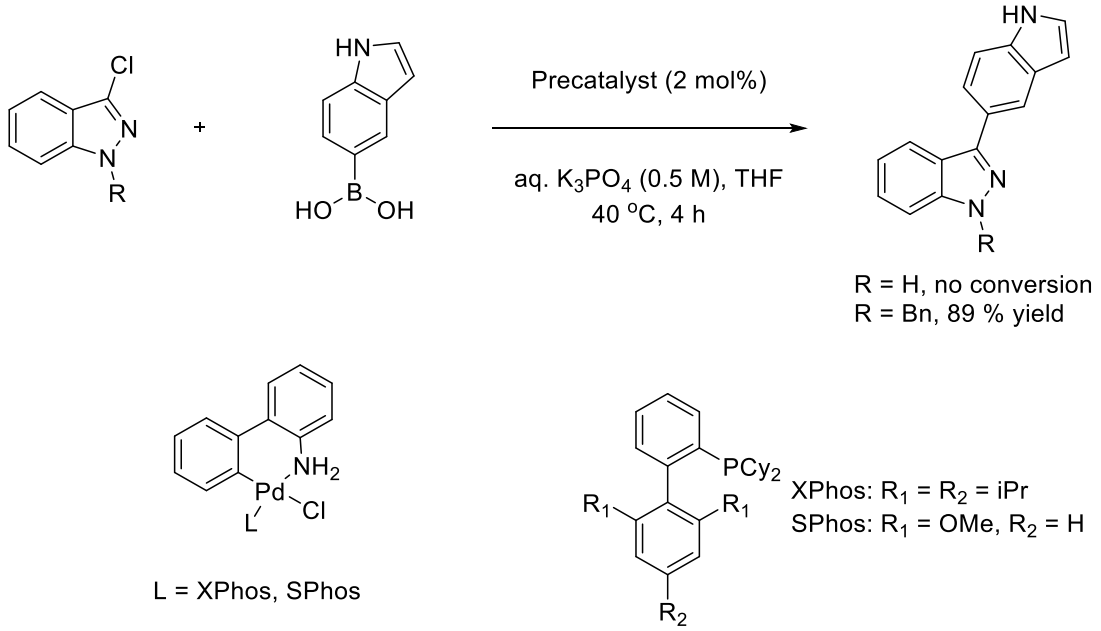

Scheme 5.2 Palladium catalysed heterocyclic cross-coupling where unprotected N-H gives no product, while protected N gives high yield

Increasing the temperature and equivalents of boronic acid allowed the unprotected heteroaryl chlorides to be coupled. The difficulties with this coupling appear to arise from the acidity of the substrates. The same group who reported the improvement on this coupling developed a reactivity scale based on the relative acidities of electrophile coupling partners (**Figure 5.3**).

Figure 5.3 Acidity-based reactivity scale with relative pK_a values

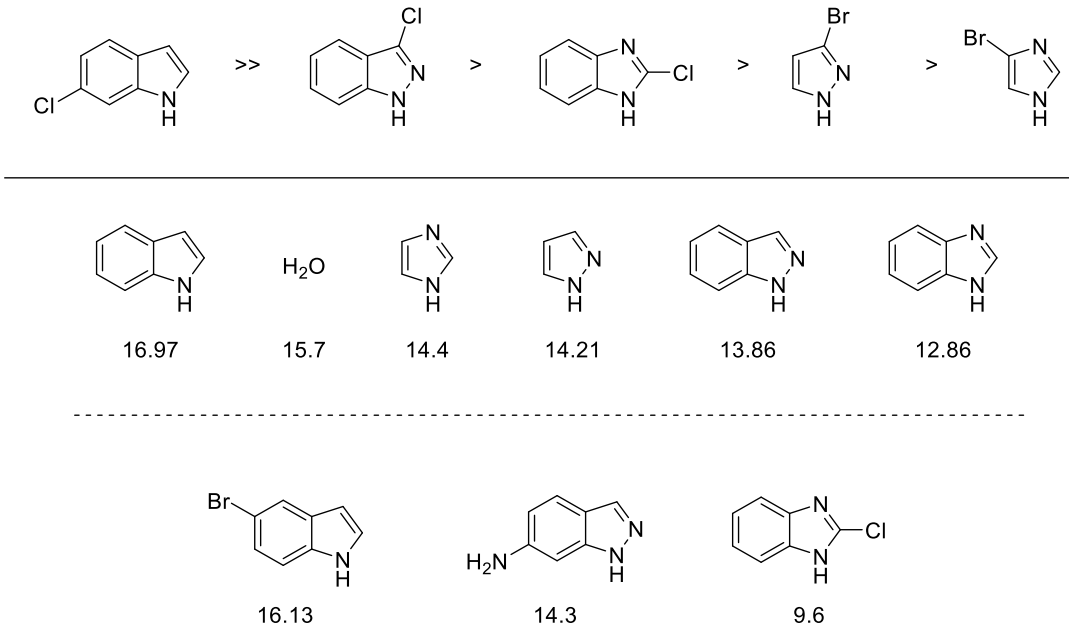

Due to the basicity of Suzuki-Miyaura conditions (K_3PO_4 is a common reagent), many of the more acidic compounds would exist mainly in their deprotonated form. The decrease in reaction rate from indole electrophiles to azaindole and benzimidazole substrates could be attributed to the pK_a values of each substrate. The more acidic substrates will exist with a higher ratio of azole-anion to azole-H, which would promote the formation of *N*-azoyl palladium complexes, inhibiting catalysis. However, for the pyrazole and imidazole substrates this theory does not apply, as the pK_a for these substrates is higher, but they exhibit lower reactivity. There could be some minor influence on reaction rate arising from complexation of the basic imine-type nitrogens, although this would require further investigation. A similar situation can occur when using nickel catalysts for heterocyclic coupling.[5] Stereospecific Suzuki coupling of esters with inversion or retention of stereochemistry was reported by Jarvo *et al* (**Scheme 5.3**).

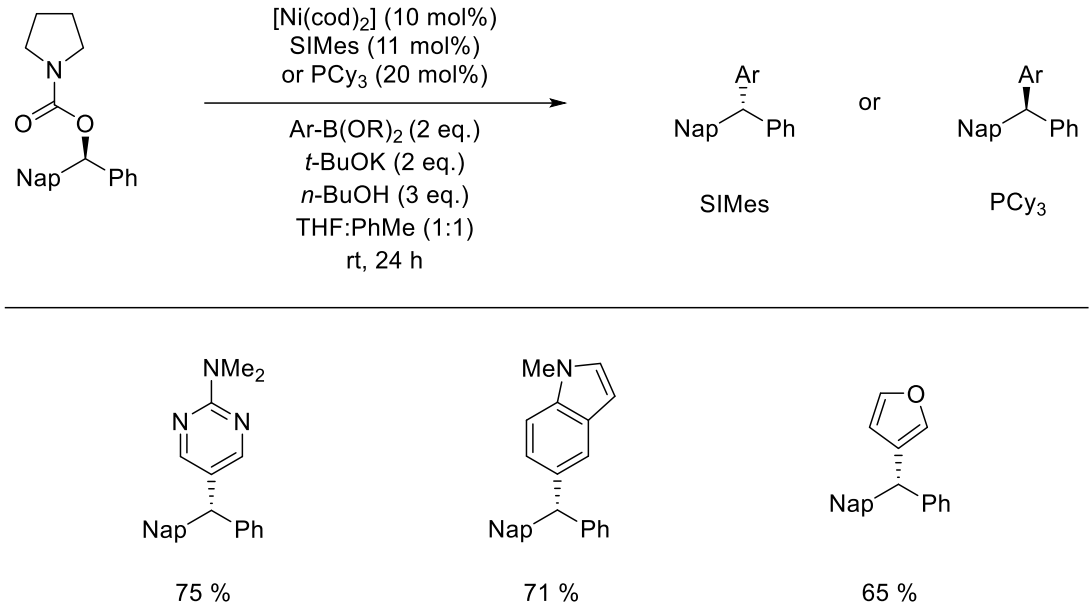

Scheme 5.3 Suzuki cross-coupling of heterocyclic boronic derivatives with esters

Here, in the cases with amino groups, the nitrogen atoms are blocked with methyl groups. The study makes no mention of attempts with free -NH groups. Although these couplings were successful, the nickel catalyst used was [Ni(cod)$_2$], which is very air-sensitive and expensive. In order to facilitate these couplings, very electron rich ligands are required, as well as a reasonably bulky NHC ligand in the cases where stereochemistry is retained. Stradiotto *et al* reported successful nickel-catalysed C-N bond formation of primary heteroarylamines and heteroaryl chlorides (**Scheme 5.4**).[6]

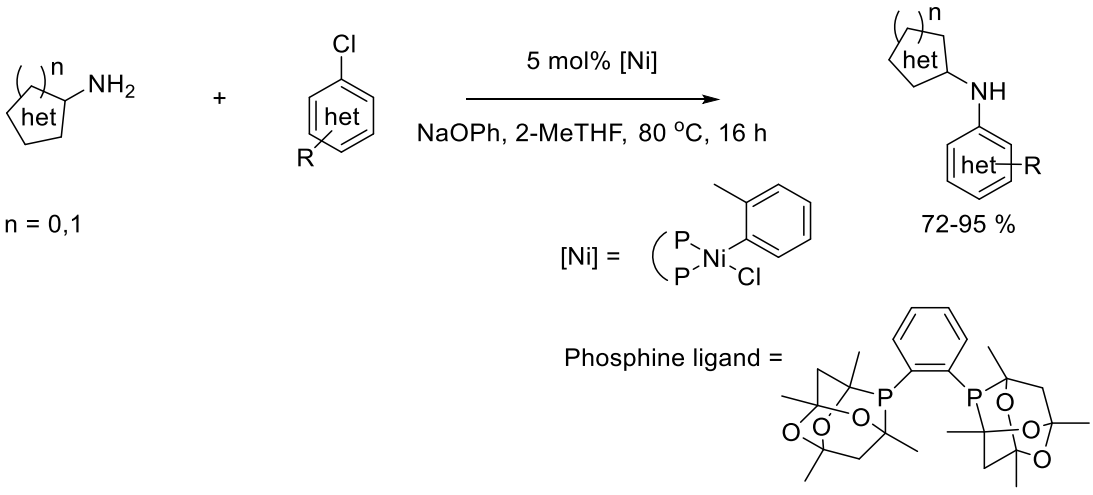

Scheme 5.4 Amination of heterocyclic amines and chlorides using nickel catalyst

The amino heterocycles coupled included oxazoles, thiazoles, substituted pyrazoles, pyridines and pyrazine. The chlorides included quinolines, benzothiazole and pyridyl substrates. All the couplings were achieved in good to excellent yields. Whilst the reaction was successful, the catalyst used is potentially very expensive (PAd-DalPhos is £284 per 250 mg, with the corresponding nickel catalyst reaching £465 per 250 mg) to use on a large scale. The catalyst loading, as is ours, is also quite high, adding to the cost and reducing atom economy, particularly with such bulky ligands.

As shown, there can be a number of challenges to overcome when attempting to cross-couple heterocyclic substrates. Often, catalyst loadings will need to be elevated to adjust for reduced reactivity or inhibitory side reactions and harsher conditions may need to be used. Moreover, there are a variety of ligands which need to be used, meaning a lack of general applicability is present in these methods.

What *is* known about these couplings is that oxidative addition can be much faster when coupling certain heterocycles, particularly ortho-halopyridines. This effect has been reported with palladium based catalysts.[7] It was found that in all cases using the three common halides (Cl, Br, I), oxidative addition to the *ortho*-pyridyl analogue was much faster than the aryl halides (**Scheme 5.5**).

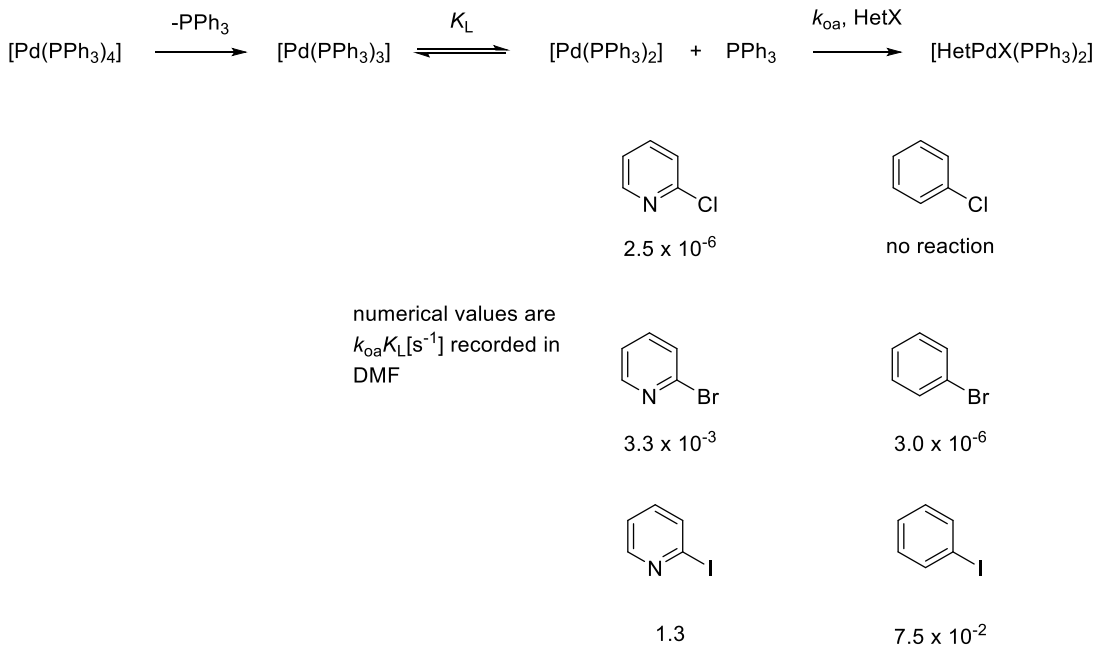

Scheme 5.5 Relative oxidative addition rates of heterocycles to $[Pd(PPh_3)_2]$

The rates follow the expected trend (for both analogues I > Br > Cl), but in all cases the heterocyclic substrate undergoes oxidative addition much more readily. Since nickel is, in general, much more nucleophilic and, hence, better suited to oxidative addition, the same trend would be expected.

Introduction

Transition metal-catalysed cross-coupling is one of the most widely used reactions in modern synthetic chemistry.[1–8] The formation of carbon-carbon and carbon-nitrogen bonds is a key step in the synthesis of many pharmaceuticals and agrochemicals.[9–15] The advancement of research in this area is therefore of high importance in both academic and industrial contexts. The Suzuki-Miyaura cross-coupling reaction is one of the most common methods of carbon-carbon bond formation, using a palladium catalyst, aryl or alkyl halide and a boronic acid coupling partner. More recently, the shift from palladium to nickel catalysts has become an area of growing interest, owing largely to the higher nucleophilicity of nickel, allowing it to cross couple generally less reactive electrophiles. Another important area of Suzuki coupling is developing conditions and catalysts that are able to efficiently cross-couple heterocyclic electrophiles, as these scaffolds are present in a large number of agrochemical products.[16–19] In previous work, we were able to demonstrate the remarkable selectivity and reactivity of our chosen bidentate phosphine based nickel catalysts in simple biaryl cross-couplings (**Scheme 1**). During this current work, this same catalyst was applied to Suzuki-Miyaura cross-coupling reactions involving nitrogen-containing heterocycles that are often seen in agrochemical structures, such as pyridines and quinolines. As before, the focus was on using heteroaryl chlorides due to their wide commercial availability and applicability, as well as nickel catalysts being more reactive for aryl chloride cross-coupling than palladium catalysts (**Scheme 1**).[20]

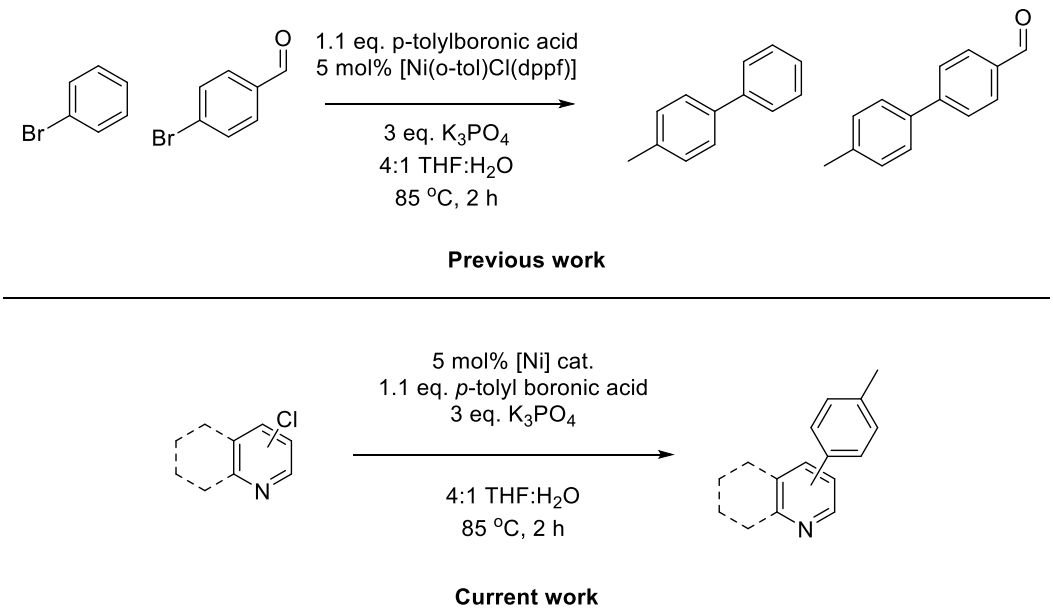

Scheme 1 Previous Suzuki selectivity work and this heterocyclic work

Results & Discussion

Our previous work describes the use of Design of Experiments to attain a set of optimised conditions for the cross-coupling of aryl substrates using our nickel precatalyst, [Ni(dppf)(*o*-tolyl)Cl] and it was these same conditions that were used for this work. Initially, *N*-containing heterocycles (pyridines and quinolines) were chosen and a variety of heteroaryl chlorides were used in the optimised cross coupling conditions (**Scheme 2**).

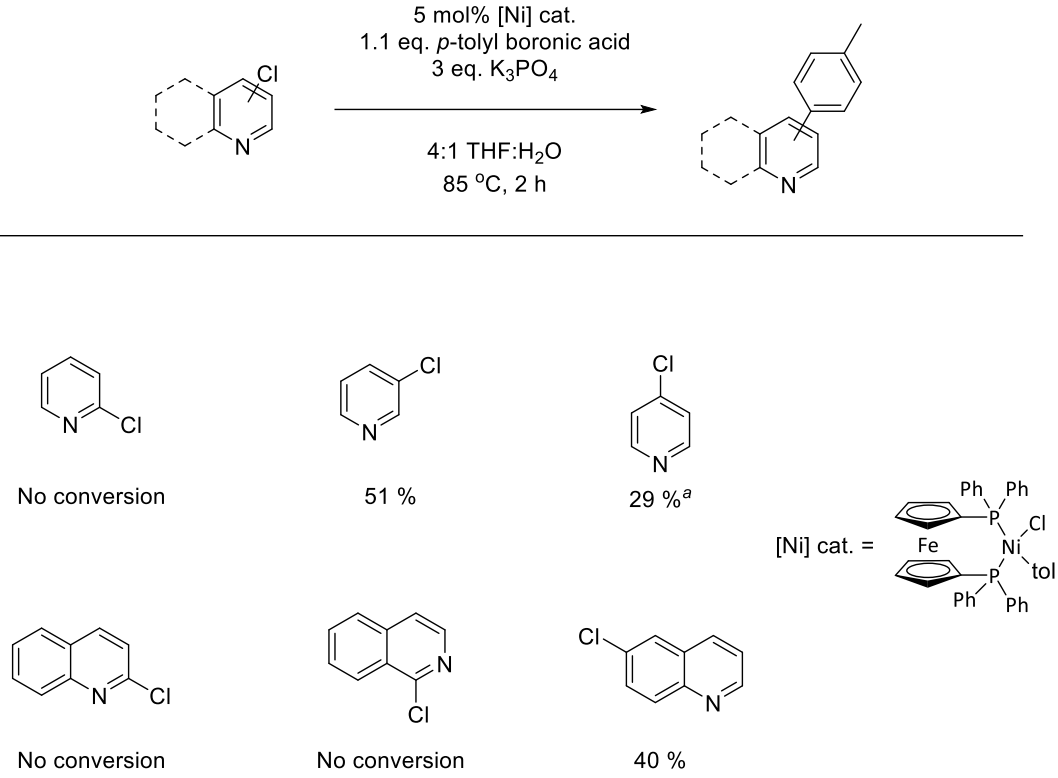

Conversions based on calibrated GC-FID, average of two runs
a: 4 eq. of base used as starting material comes as HCl salt

Scheme 2 Nickel catalysed Suzuki cross-couplings of *N*-heterocycles using optimised conditions

Pleasingly, the conversions for substrates that did react (3 & 4-chloropyridine and 6-chloroquinoline) were significant. However, as can be seen from this screen, there is no conversion of substrate where the chlorine is *ortho* to the nitrogen. This is true even when the chlorine is in an electronically different environment (compare 1-chloroisoquinoline with 2-chloroquinoline). This came as a surprise since it is known in the literature that oxidative addition to α-halo pyridines is faster that to the analogous halobenzenes for $[Pd(PPh_3)_4]$.[#] It was predicted that nickel would also exhibit this enhanced oxidative addition and, therefore, these substrates would be the best performers in this reaction. The GC-FID traces for these reactions showed no other side-product that was hindering product formation. Upon using the analogous palladium catalyst that had been used previously, $[Pd(dppf)Cl_2]$, we found that it

was (perhaps not unsurprisingly) ineffective at coupling these heteroaryl chlorides. There is precedent in the literature for this, as [Pd(PEPPSI)(Ipr)] is often used in heterocyclic cross-coupling.

The trend observed when using the nickel catalyst was not apparent when using palladium. There was no appreciable difference in conversion between the 2-, 3-, and 4-chloropyridines, as well as between 6-chloroquinoline, 2-chloroquinoline, and 1-chloroisoquinoline. To observe any potential inhibitory complexes that had formed during the reaction, $^{31}P\{^{1}H\}$ NMR spectroscopic analysis was carried out on the 2-chloropyridine reaction mixture. None of the signals associated with the pre-catalyst were present (doublets at 11 and 29 ppm). However, singlets were observed at -17 and 22 ppm. The larger of the two signals (-17 ppm) can be attributed to free ligand (dppf) from comparison with an authentic sample. The new peak does not relate to any other complexes that we had seen either in previous couplings or in the synthesis of the pre-catalyst itself. In an attempt to isolate this compound and analyse it further, a route to synthesise it independently of other coupling reactants was designed (**Scheme 3**).

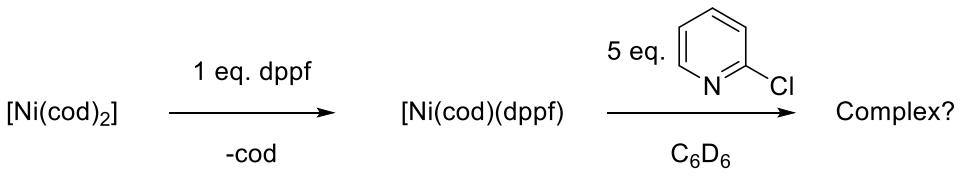

Scheme 3 Potential route to unknown complex

Initially this was done on a small scale in an NMR tube. Upon the addition of 2-chloropyridine, the solution changed colour from dark orange (the colour of [Ni(cod)(dppf)]) to a deep red. This solution was analysed *via* $^{31}P\{^{1}H\}$ NMR spectroscopy and, pleasingly, the only signal observed was a singlet at 22 ppm. We were confident that this was the same complex that was being formed during the coupling reactions. We were surprised to find crystals had formed in the NMR tube and were able to obtain a crystal structure (**Figure 1**).

Figure 1 Crystal structure of complex formed from [Ni(cod)(dppf)] and 2-chloropyridine

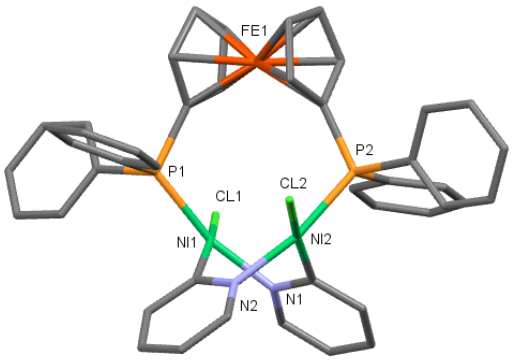

The crystal structure shows a bridged dimeric nickel complex, where the nickel centres have oxidatively added into the C-Cl bonds of the pyridines and are also coordinated to the nitrogen of the pyridine opposite. Notably, there is only one dppf ligand attached, bridging both nickel centres. This is consistent with the free dppf peak observed in the $^{31}P\{^{1}H\}$ NMR spectrum of the cross-coupling reaction mixtures. This procedure was repeated on a larger scale in order to obtain enough material to carry out further reactions. Crystals were again obtained and confirmed to be the same structure *via* single crystal X-ray diffraction analysis. Both the solid and leftover solution were analysed *via* $^{31}P\{H\}$ NMR spectroscopy to confirm that the solid was producing the singlet at 22 ppm and this was the case. The solution gave no signal in the $^{31}P\{^{1}H\}$ NMR spectrum. At this point it was believed that the formation of this complex prevented the Suzuki-Miyaura cross-coupling reactions from occurring. To test this hypothesis, the dimer was used as a catalyst in Suzuki-Miyaura cross-couplings, as well as attempting to transmetalate the dimer with the boronic acid (**Scheme 4**).

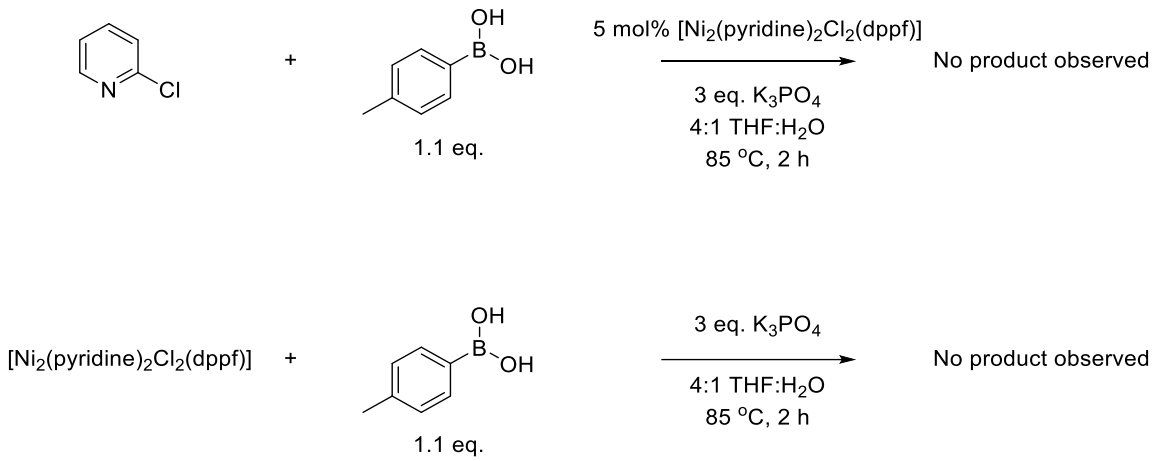

Scheme 4 Use of nickel dimer complex as a Suzuki catalyst

In both cases, no product was observed, which suggests that this complex is not catalytically active. The next step was to attempt the synthesis of the analogous quinoline dimeric complexes to confirm that this is a general complex that can be formed when attempting the coupling of 2-halopyridyl/quinolyl substrates (**Scheme 5**).

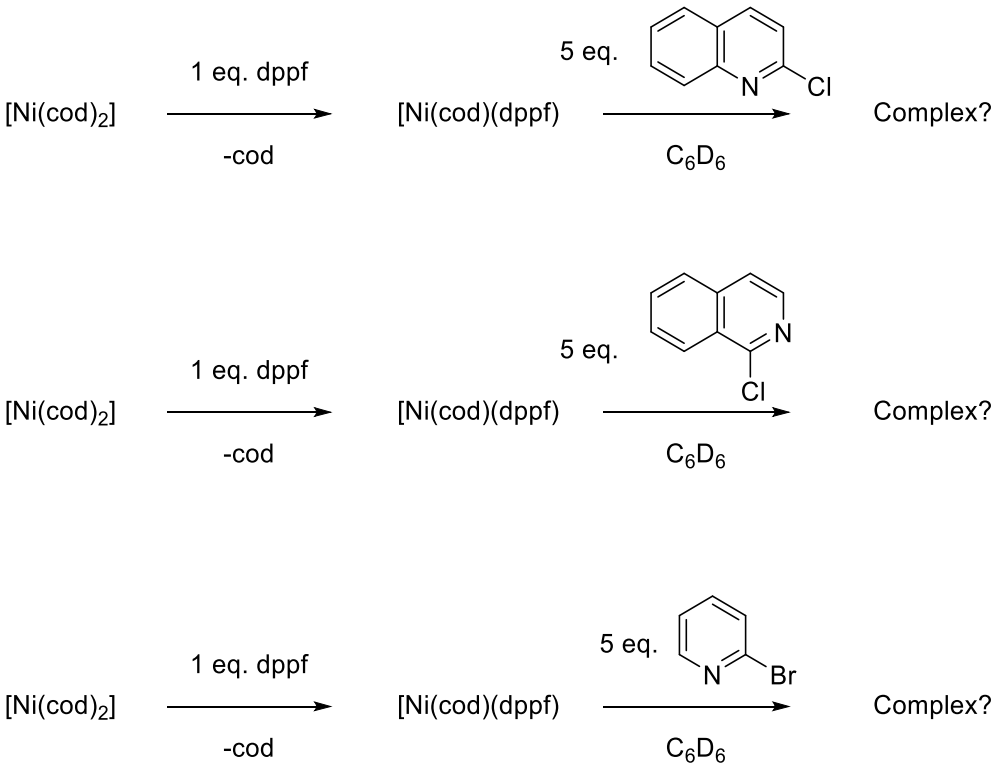

Scheme 5 Analogous complex formation with $^{31}P\{^{1}H\}$ NMR spectra

These reactions produced solids of similar colour and the NMR signals are present in the same region of the $^{31}P\{^{1}H\}$ NMR spectrum. Crystal structures of one of these analogues were obtained and these were characterised using multinuclear NMR spectroscopy (**Figure 4**).

Figure 4 Crystal structure of $[Ni_2Br_2(pyridine)_2(dppf)]$

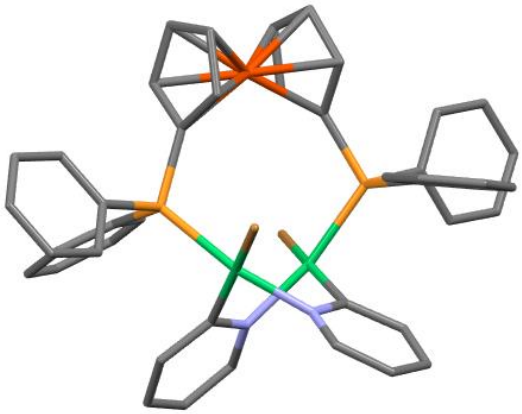

The quinoline complexes appeared to form much faster than those derived from pyridine, as the colour change was observed as the addition of the heterocycle was completed.

We have established that these complexes inhibit Suzuki-Miyaura cross-coupling reactions of pyridines/quinolines with the halogen adjacent to a heteroatom. Oxidative addition of palladium(0) to these heteroarenes, as we know, is very fast, although no data has been obtained yet for nickel. This could suggest that it is the transmetalation with the boronic acids that is slower than the formation of these dimers. This would also suggest that the dimer formation is either non-reversible, or that at least the equilibrium lies almost entirely on the dimer formation side. If the transmetalation reagent was more nucleophilic, then, it may be possible to achieve coupling conversion. To this end, we attempted Kumada couplings, which employ Grignard reagent coupling partners that generally transmetalate much more readily than boronic acids. We elected to try the initial set of heteroaryl chlorides as substrates for Kumada reactions, as well as attempting to use the 2-chloropyridine dimer as a Kumada catalyst, and attempting to use a Grignard reagent to transmetalate the dimer (**Scheme 6**).

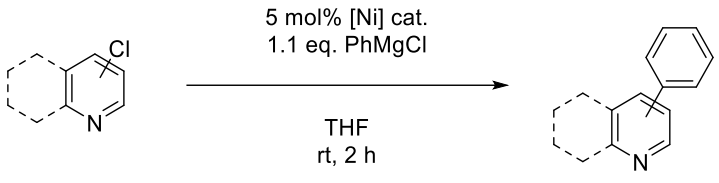

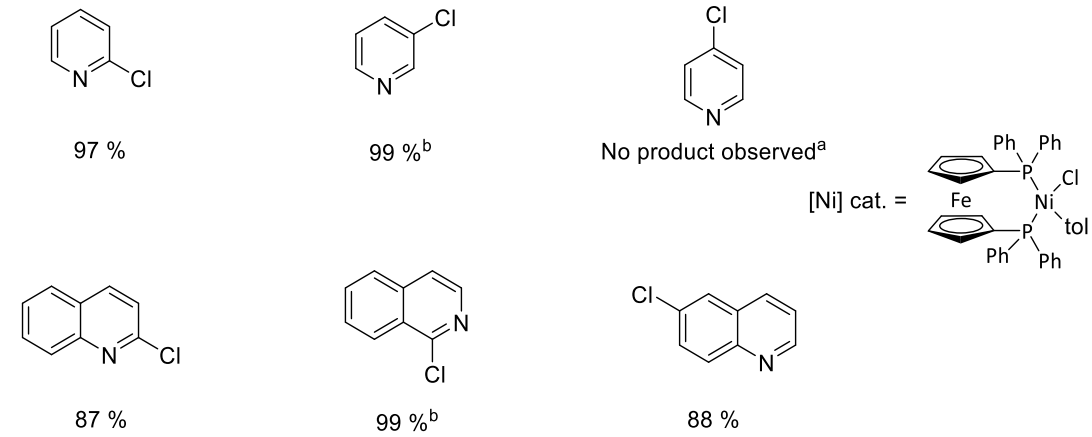

Conversions based on calibrated GC-FID, average of two runs
a: 2.1 eq. of Grignard used as starting material comes as HCl salt
b: Quantitative conversion

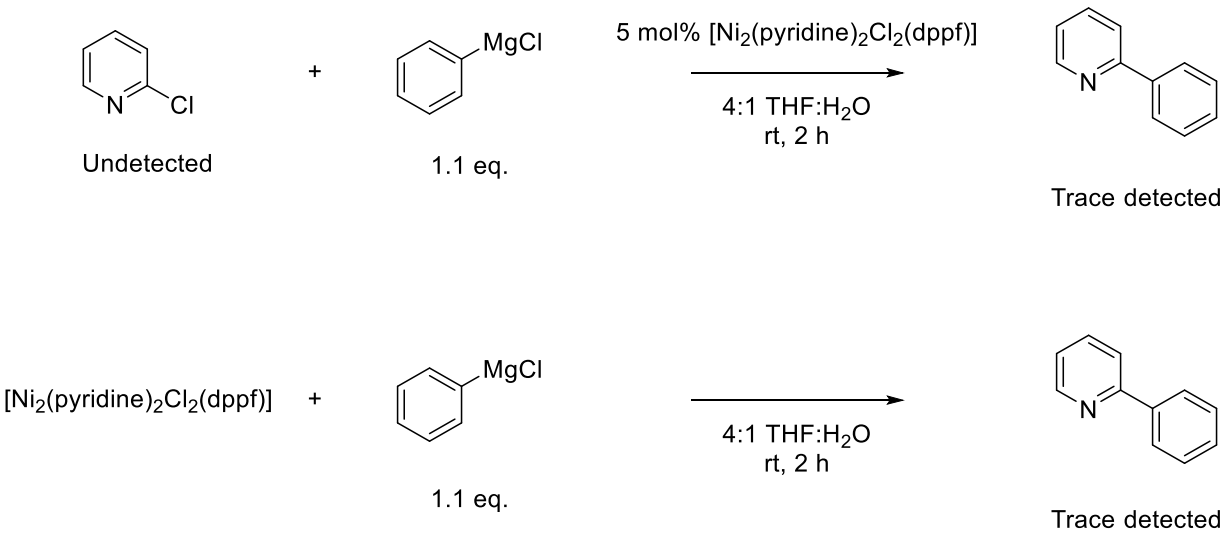

Scheme 6 Kumada couplings of initial chlorides and use of dimer as Kumada catalyst

As shown, the Kumada couplings of the original chlorides achieved excellent conversions, even in the cases where the chlorine is adjacent to the nitrogen (4-chloro pyridine is an outlier, potentially due to the salt not being soluble in THF). Coupled product was also observed in the case where the dimer was used as a catalyst to couple 2-chloropyridine with phenylmagnesium chloride. These results suggest two possibilities:

- the Grignard reagent is fast enough to transmetalate the oxidative addition intermediate before the dimer is able to form (as the 2-chloropyridine does couple under Kumada conditions using the dppf pre-catalyst)
- the Grignard reagent is a strong enough transmetalating agent that it is able to break the dimer apart and transmetalate to give the pre-reductive elimination intermediate (as reacting stoichiometric dimer with Grignard gives Kumada coupling product)

Conclusions

In this work, it was elucidated why some Suzuki-Miyaura cross-coupling reactions with *ortho*-haloheteroarenes using bidentate phosphine nickel catalysts can sometimes be challenging. Oxidative addition is sufficiently fast that this step can proceed rapidly, as seen from the accompanying rapid colour changes when synthesising the complexes. The result, however, is a catalytically inactive dimeric complex which completely inhibits Suzuki-Miyaura cross-coupling reactions. The exact mechanism for the formation of this is still unknown, particularly as to how one dppf ligand is removed from the final product. The formation of this dimer is faster than transmetalation with our chosen boronic acid, but using Grignard reagents, Kumada couplings are possible. The Grignard reagents are also capable of breaking the dimer and transmetalating to achieve coupled Kumada product. Further investigations into the occurrence and role(s) of such complexes are ongoing in our laboratories.

References

1 K. W. Quasdorf, X. Tian and N. K. Garg, *J. Am. Chem. Soc.*, 2008, **130**, 14422–14423.

2 K. W. Quasdorf, A. Antoft-Finch, P. Liu, A. L. Silberstein, A. Komaromi, T. Blackburn, S. D. Ramgren, K. N. Houk, V. Snieckus and N. K. Garg, *J. Am. Chem. Soc.*, 2011, **133**, 6352–6363.

3 L. Hie, J. J. Chang and N. K. Garg, *J. Chem. Educ.*, 2015, **92**, 571–574.

4 L. Hie, S. D. Ramgren, T. Mesganaw and N. K. Garg, *Org. Lett.*, 2012, **14**, 4182–4185.

5 A. Suzuki, *J. Organomet. Chem.*, 1999, **576**, 147–168.

6 N. Miyaura and A. Suzuki, *Chem. Rev.*, 1995, **95**, 2457–2483.

7 A. J. J. Lennox and G. C. Lloyd-Jones, *Chem. Soc. Rev.*, 2014, **43**, 412–443.

8 C. Pan, M. Liu, L. Zhang, H. Wu, J. Ding and J. Cheng, *Catal. Commun.*, 2008, **9**, 508–510.

9 F. Inoue, M. Kashihara, M. R. Yadav and Y. Nakao, *Angew. Chemie Int. Ed.*, 2017, **56**, 13307–13309.

10 S. D. Ramgren, A. L. Silberstein, Y. Yang and N. K. Garg, *Angew. Chemie Int. Ed.*, 2011, **50**, 2171–2173.

11 M. J. Buskes and M.-J. Blanco, *Molecules*, 2020, **25**, 3493.

12 A. O. King and N. Yasuda, 2017, 205–245.

13 A. F. P. Biajoli, C. S. Schwalm, J. Limberger, T. S. Claudino and A. L. Monteiro, *J. Braz. Chem. Soc.*, , DOI:10.5935/0103-5053.20140255.

14 P. Devendar, R.-Y. Qu, W.-M. Kang, B. He and G.-F. Yang, *J. Agric. Food Chem.*, 2018, **66**, 8914–8934.

15 C. Torborg and M. Beller, *Adv. Synth. Catal.*, 2009, **351**, 3027–3043.

16 C. Lamberth, *Pest Manag. Sci.*, 2013, **69**, 1106–1114.

17 C. Lamberth, *J. Sulfur Chem.*, 2004, **25**, 39–62.

18 E. A. Al-Harbi, *Agric. Res. Technol. Open Access J.*, , DOI:10.19080/ARTOAJ.2018.16.555986.

19 Y. Ogawa, E. Tokunaga, O. Kobayashi, K. Hirai and N. Shibata, *iScience*, 2020, **23**, 101467.

20 A. K. Cooper, D. K. Leonard, S. Bajo, P. M. Burton and D. J. Nelson, *Chem. Sci.*, 2020, **11**, 1905–1911.

5.4 Extended Discussion

This piece of work served as a satisfactory continuation of the work discussed in previous chapters. It was possible to use the existing optimised conditions and apply them to substrates which are known to occasionally pose problems in coupling and achieve reasonable conversions. During this study, other examples of these nickel dimer complexes were found in the literature, though they were never used for catalysis. One of the first examples was reported by Pringle *et al*.[8] They were able to synthesise $[Ni(PPh_3)_4]$ from $[Ni(cod)_2]$ and subsequently displace two of the phosphine ligands using 2,5-dibromopyridine (**Scheme 5.6**).

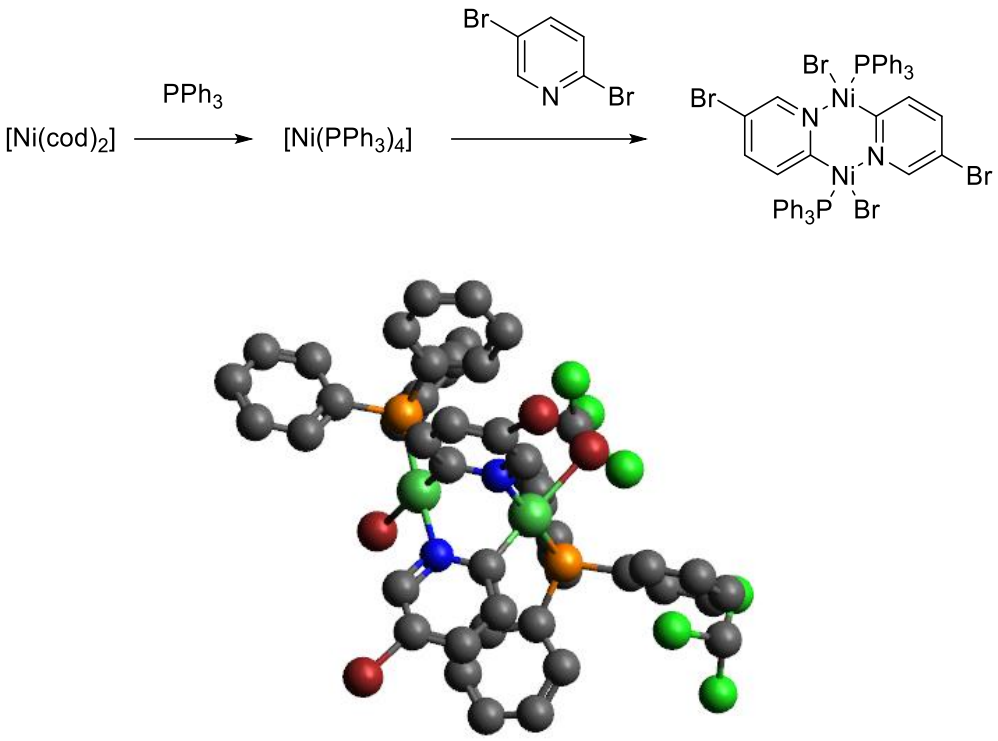

Scheme 5.6 Synthesis of 2,5-dibromopyridine nickel dimer and crystal structure

The crystal structure given for this complex is similar to the structure reported here, suggesting a trend in these kind of complexes, where the central metallocycle follows a boat structure. Analogous palladium dimers were also reported although, when using platinum only the monomeric species was isolated. The nickel dimers were used to investigate electrochemical reduction and synthesis of polypyridines. An analogous chloride complex was also reported by a separate group.[9] The synthesis in this case involved a zinc catalysed reduction of

$[NiCl_2(PPh_3)_2]$ with AIBN to form the dimer, eliminating the need for a glovebox, as there is no air sensitive $[Ni(cod)_2]$ (**Scheme 5.7**). Monomeric complexes were also isolated, using both monodentate and bidentate phosphine ligands. It was shown that addition of PEt_3 to the dimer gave the monomeric complex, whereas addition of dcpe had no effect (**Scheme 5.7**).

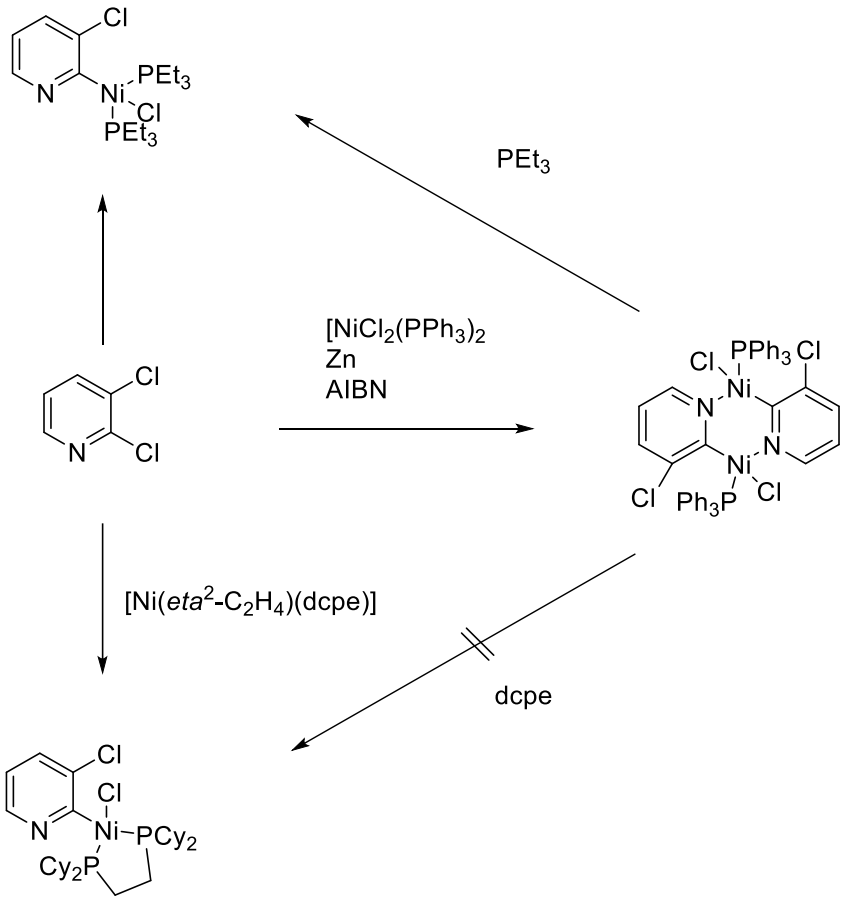

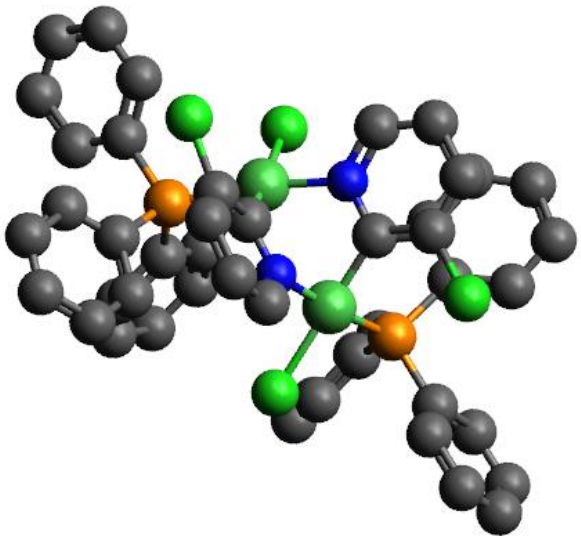

Scheme 5.7 Synthesis of monomeric and dimeric complexes and crystal structure of dimer

This group speculates that the mechanism of formation of these complexes involves prior coordination to the nitrogen atom in the pyridine. Treating the dcpe monomeric complex with 1 % Na-Hg amalgam appeared to produce a 2,3-pyridyne complex, but this compound was highly sensitive. A further example was reported by Perutz *et al*.[10] Preparation of this dimer involved treating the pre-dimeric oxidative addition complex with a solution of HBF_4 in diethyl ether (**Scheme 5.8**).

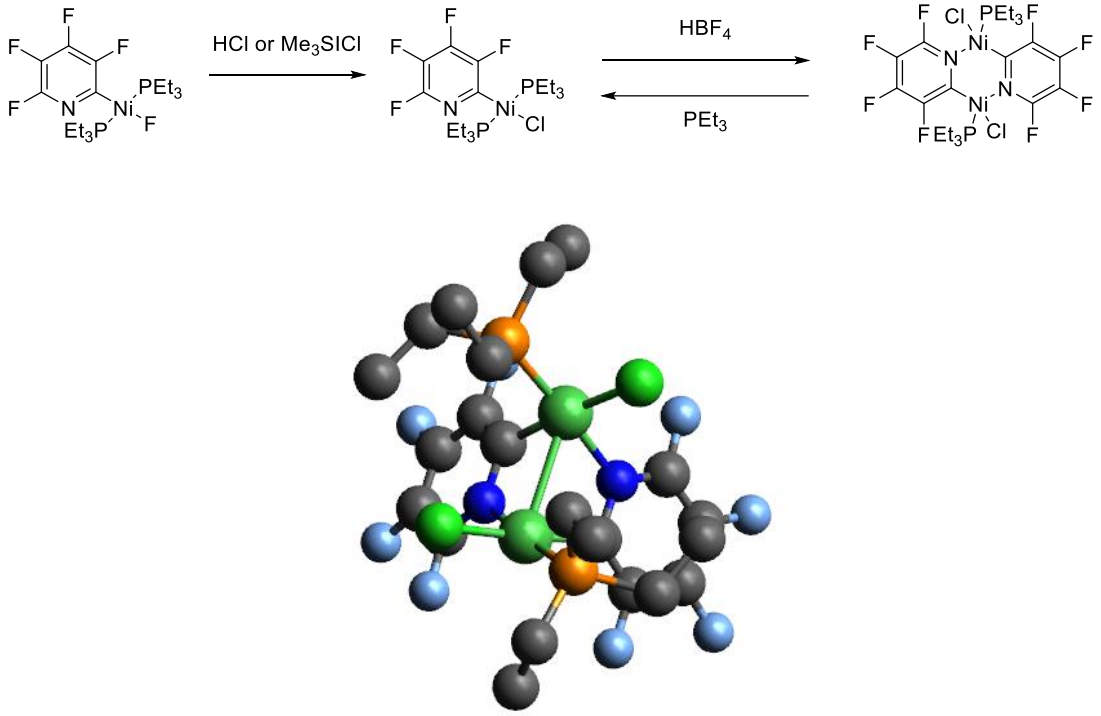

Scheme 5.8 Synthesis of fluorinated-pyridine dimer and crystal structure

Addition of excess phosphine ligand regenerated the initial monomeric complex. The group postulates that this dimeric compound could be a potential starting point for the synthesis of reactive monomeric tetrafluoropyridyl nickel derivatives bearing only one phosphine.

5.5 References

1 C. Lamberth and J. Dinges, in *Bioactive Heterocyclic Compound Classes*, Wiley-VCH Verlag GmbH & Co. KGaA, Weinheim, Germany, 2012, pp. 1–20.

2 T. Koyanagi and T. Haga, 1995, pp. 15–24.

3 K. E. Pallett, S. M. Cramp, J. P. Little, P. Veerasekaran, A. J. Crudace and A. E. Slater, *Pest Manag. Sci.*, 2001, **57**, 133–142.

4 M. A. Düfert, K. L. Billingsley and S. L. Buchwald, *J. Am. Chem. Soc.*, 2013, **135**, 12877–12885.

5 E. J. Tollefson, L. E. Hanna and E. R. Jarvo, *Acc. Chem. Res.*, 2015, **48**, 2344–2353.

6 J. S. K. Clark, M. J. Ferguson, R. McDonald and M. Stradiotto, *Angew. Chemie Int. Ed.*, 2019, **58**, 6391–6395.

7 B. U. W. Maes, S. Verbeeck, T. Verhelst, A. Ekomié, N. von Wolff, G. Lefèvre, E. A. Mitchell and A. Jutand, *Chem. - A Eur. J.*, 2015, **21**, 7858–7865.

8 N. W. Alcock, P. N. Bartlett, V. M. Eastwick-Field, G. A. Pike and P. G. Pringle, *J. Mater. Chem.*, 1991, **1**, 569–576.

9 M. A. Bennett, D. C. R. Hockless and E. Wenger, *Polyhedron*, 1995, **14**, 2637–2645.

10 S. J. Archibald, T. Braun, J. A. Gaunt, J. E. Hobson and R. N. Perutz, *J. Chem. Soc. Dalt. Trans.*, 2000, 2013–2018.

Chapter 6: Conclusions & Future Work

Over the course of this project, some important aspects of nickel catalyst reactivity in Suzuki-Miyaura cross-coupling have been uncovered. Examples of common functional groups overriding the expected (based upon oxidative addition rates) reactivity of aryl halides with nickel catalysts using η^2-coordination (**Scheme 6.1**) were shown.

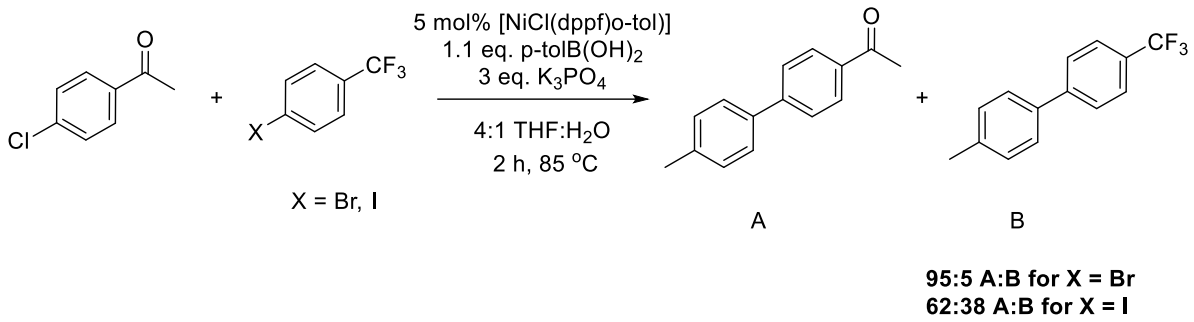

Scheme 6.1 Competition reactions showing preferential conversion of aryl chloride containing a coordinating group over aryl bromide and iodide

This effect was shown to be powerful enough for an aryl chloride to react preferentially to an aryl iodide in the same reaction mixture, with very similar electronic groups (in terms of electron withdrawing strength). Tentative quantification of this effect for a variety of electron withdrawing and donating groups was achieved, allowing a relative ranking of the strengths of coordinating groups to be proposed. This effect could find use in the synthesis of complex structures, as it may be possible to selectively and sequentially couple different sites on the same molecule in a one-pot procedure (**Scheme 6.2**).

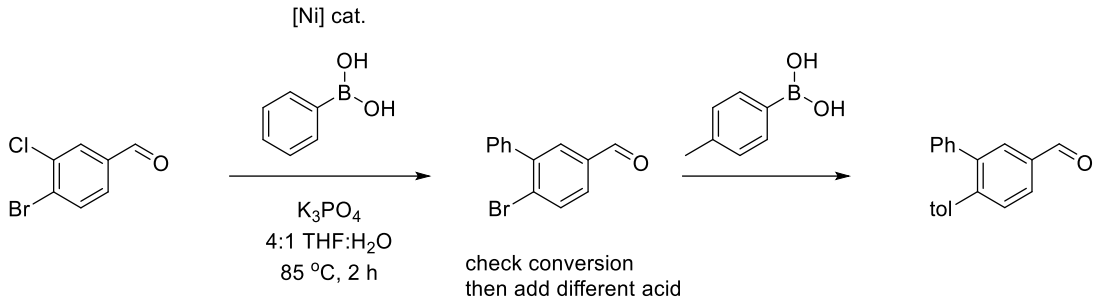

Scheme 6.2 Potential sequential synthesis using different boronic acids and exploiting coordination effect

Unfortunately, during these studies, this effect was not implemented particularly successfully (the chalcone examples gave overall low conversion, leading to relatively inconclusive results) but this may be possible in future with more time.

One of the major positive results was that the effect is much more pronounced with nickel catalysts than palladium catalysts. This was expected, as palladium is known to have a much higher functional group tolerance than nickel (owing to its lower reactivity for oxidative addition). Indeed, during the robustness screen work, it was found that palladium was essentially unaffected by additives with coordinating groups, whereas nickel catalysed reactions were, in some cases (where coordinating groups were strongest i.e. aldehydes) completely shut down. Additionally, palladium did not exhibit the same selectivity as nickel in the competition reactions, owing potentially to the same reasons. This work then serves as a useful addition to the scientific community in the area of transition metal catalysed cross-coupling, as it highlights the ability of nickel to cross couple challenging substrates if there is the possibility of installing a suitable coordinating group. This is important as there is still a vast amount of work being caried out in the academic setting to bring nickel catalysts to the forefront of cross-coupling chemistry and see it being used in more industrial scenarios.
Whilst the robustness screening work presented here covers a large variety of important functional groups (amines, ethers, imines, carbonyls, sulfides, sulfoxides, sulfones, alkenes, alkynes, amides, esters and nitriles), it would be desirable in the future to further investigate heterocyclic additives (**Scheme 6.3**).

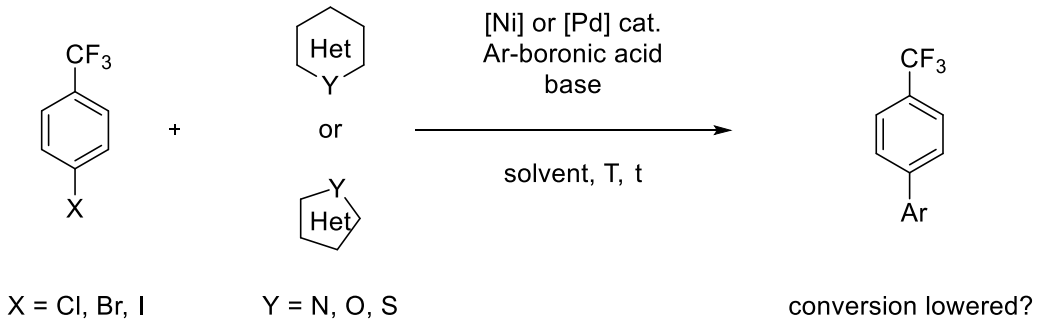

Scheme 6.3 General robustness screen with heterocyclic additives

This could potentially be particularly interesting and elucidating when using 5-membered nitrogen heterocycles, as often these nitrogen atoms appear to be similar to imine systems, which were observed to heavily inhibit coupling. Upon using pyridyl and quinolyl halides (shown in Chapter 5), there seemed to be no great positive coordinating effect, but this would benefit from further investigation, with competition reactions similar to those presented above.

The mechanistic work that was carried out (almost entirely at Syngenta in Jealott's Hill) did help to elucidate some of the initial kinetic aspects of the coupling reactions. While it was unfortunate that the exact optimised conditions were not used (lowered catalyst loading from 5 to 2 mol%, lowered temperature from 85 to 65 ^{o}C), it is not unreasonable to assume that the reactions would behave similarly to our conditions. What was observed was very rapid initial conversion for two of the coordinating groups (C(O)H and CN). Unfortunately, overall, the reactions were very difficult to reliably reproduce using the calorimeter and it could be possible that some of the traces for the lower strength coordinating substrates are inaccurate, as low conversion was reached in many cases. Given more time, it would be possible to test more reaction conditions and possibly find conditions that are similar enough to the optimised procedure but that give reliable conversion. A reliable seal on the vials would also help as the suspected issue appeared to arise during injection of the boronic acid to activate the catalyst. As can be seen from the combined conversion and heat flow vs. time graph presented in Chapter 4, it is possible that a degree of catalyst decomposition takes place, which would only be exacerbated by improper sealing of vials allowing air into the reaction. It was not possible to gain any deep kinetic understanding of the reaction (which is typically very difficult for multi-step mechanisms), such as reaction order in either of the substrates or in catalyst. The attempts to deduce the order in catalyst did not yield conclusive results, instead giving the possibility that the catalyst order could be a fractional order between 0 and 1. As noted, the technique used relies on catalyst concentration remaining constant throughout the reaction, which is almost certainly not the case. Again, more time would allow further probing of this, using higher catalyst loadings to mitigate catalyst decomposition effects as well as providing higher data density. It would also be important to carry out reactions with a coordinating product already present, in case there is any inhibition taking place (**Scheme 6.4**).

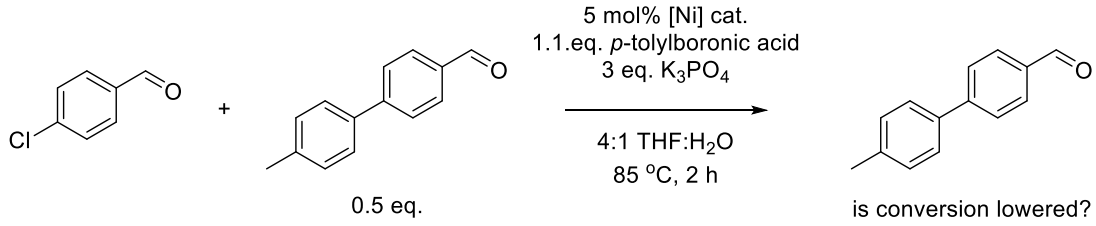

Scheme 6.4 Product inhibition study

This could be done for many of the coordinating substrates investigated in this work, furtheringknowledge of the mechanism of these couplings.

The heterocyclic work presented here is perhaps the piece which opens the most avenues for exploration. Due to the initial observation of the dimer formation, much of the time devoted to this work was spent synthesising and characterising this dimer and its analogues. Whilst good conversions were obtained for a selection of the simple nitrogen-containing heterocyclic chlorides, investigation into a wider variety of heterocycles (much like the robustness screen) would be prudent. This would also elucidate whether heterocycles that inhibit the reaction as additives actually perform better when in competition reactions. Furthermore, it would be interesting to investigate whether coordinating functional groups promote the coupling of these substrates and if they inhibit them as additives (**Scheme 6.5**).

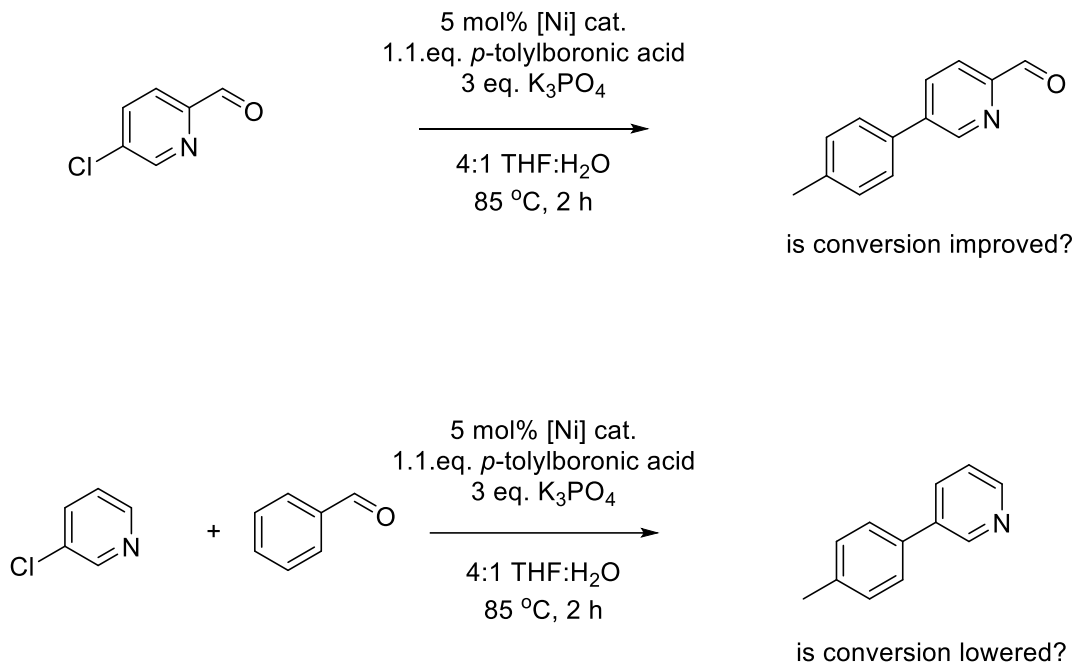

Scheme 6.5 Potential coordination and inhibition study of heterocyclic couplings

Further investigation into the dimeric complexes would also be beneficial, for instance, determining whether these complexes form using our other phosphine-based nickel catalysts (where ligand = PCy_3, PPh_3, dppe) or if these catalysts allow for Suzuki coupling. As shown, the Kumada couplings of the *ortho*-haloheteroarenes were successful, indicating a potentially rate-limiting transmetalation step. To probe this further, Suzuki coupling using more nucleophilic boronic acids could be carried out (**Scheme 6.6**).

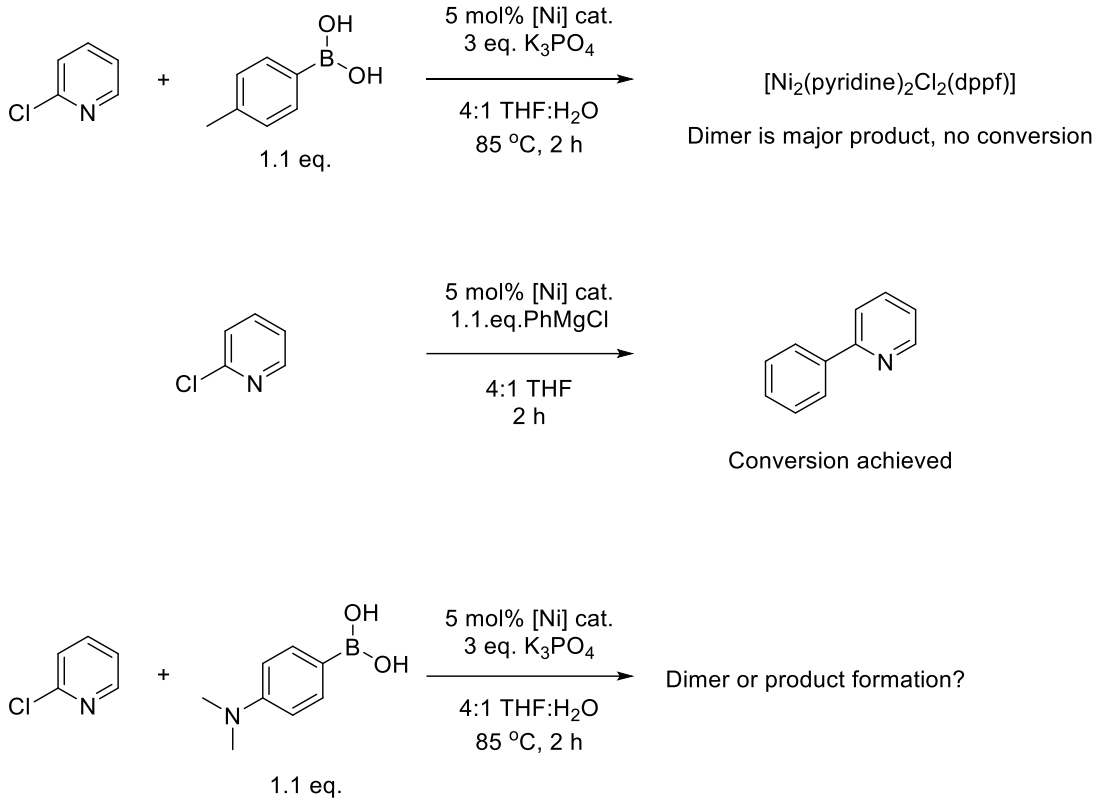

Scheme 6.6 Future boronic acid Suzuki coupling building upon transmetalation rate investigation

If these boronic acids are able to convert these electrophiles, then transmetalation is likely to be rate-limiting.

Overall, the work presented here has made a significant contribution to the scientific community, as evidenced by the publication of two (potentially three) manuscripts (one of which has been cited 6 times), but, as shown, there are plenty of avenues to explore to build upon these findings.

7 Experimental

GENERAL EXPERIMENTAL DETAILS

General. The manipulations of air-sensitive nickel complexes and the execution of cross-coupling reactions were carried out under an atmosphere of argon or nitrogen using Schlenk techniques or an argon-filled Innovative Technology PureLab HE glovebox.

Reagents and Solvents. Most aryl halides were obtained from commercial sources and used as supplied. The syntheses of **22-Br** and **23-Br** are detailed subsequently. Complexes **1**, **7**, **20**, and **21** were prepared using literature methods.[1, 2] Anhydrous toluene and THF were obtained from an Innovative Technology PureSolv apparatus; regular Karl-Fisher analyses ensured that water content was always below 10 ppm. Anhydrous benzene-d_6 was obtained by drying over 4 Å molecular sieves that had been activated by heating under high vacuum. Distilled water was degassed by sparging with argon or nitrogen before use. Potassium phosphate was obtained commercially and dried overnight under vacuum at 50 °C before use and stored in a desiccator.

Analyses. NMR spectra were obtained using a Bruker AV3-400 instrument with a QNP probe or a liquid nitrogen Prodigy cryoprobe. Kinetic experiments were executed using a Bruker AVII-600 instrument equipped with a BBO-*z*-ATMA probe. ^{1}H NMR spectra are referenced to residual protonated solvent,[3] ^{13}C{^{1}H} NMR spectra are referenced to solvent signals,[3] ^{19}F NMR spectra are externally referenced to $CFCl_3$, and ^{31}P and ^{31}P{^{1}H} NMR spectra are externally referenced to H_3PO_4. GC-MS analyses were carried out using an Agilent 7890A gas chromatograph fitted with a RESTEK RXi-5Sil column (30 m x 0.32 mm I.D. x 0.25 µm) and an Agilent 5975C MSD running in EI mode. GC-FID analyses were carried out using an Agilent 7890A gas chromatograph fitted with an Agilent HP5 column (30 m x 0.25 mm I.D. x 0.25 µm).

DATA FOR CHAPTER 2

SYNTHESIS OF ORGANIC COMPOUNDS

General Procedure A. To a microwave vial equipped with a stirrer bar, 4-tolylboronic acid (1.1 eq.), [$PdCl_2$(dppf)] (1 – 5 mol%), K_3PO_4 (3 eq.) and, if solid, aryl halide (1 mmol, 1 eq.) were added. The vial was capped and purged/backfilled with N_2. Anhydrous toluene (2 mL) was added *via* oven-dried glass syringe. If the aryl halide was a liquid, it was added here. H_2O (10 eq.) was then added. The reaction was stirred for 2 hours at 85 °C. The reaction was then cooled to room temperature. The mixture was filtered through celite and analysed *via* GC-FID. The reaction was then analysed *via* TLC. The mixture was evaporated to dryness *in vacuo* and purified *via* flash column chromatography to furnish the product as a white solid.

4-methyl-4'-(trifluoromethyl)-1,1'-biphenyl

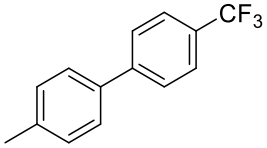

Synthesised according to the General Procedure A using 4-bromobenzotrifluoride (140 µL, 225.0 mg, 1 mmol), 4-tolylboronic acid (149.7 mg, 1.1 mmol), [$PdCl_2$(dppf)] (36.5 mg, 5 mol %) and K_3PO_4 (634.2 mg, 3 mmol) in 2 mL toluene. The desired product was purified *via* flash column chromatography (eluting with hexane) to yield a white solid (163.7 mg, 69%).
^{1}H NMR (400 MHz, $CDCl_3$): δ_H 7.70 (s, 4H, 4 x ArH), 7.53 (d, 2H, 2 x ArH, *J* = 8.3 Hz), 7.31 (d, 2H, 2 x ArH, *J* = 7.9 Hz), 2.44 (s, 3H, CH_3). **^{13}C{^{1}H} NMR** (101 MHz, $CDCl_3$): δ_C 144.2, 137.7, 136.4, 129.2 (2C), 128.5 (q, $^2J_{C-F}$ = 32.5 Hz), 126.7 (2C), 126.6 (2C), 125.2 (q, 2C, $^3J_{C-F}$ = 3.7 Hz), 123.9 (q, $^1J_{C-F}$ = 271.9 Hz), 20.6. **^{19}F NMR** (376 MHz, $CDCl_3$): δ_F -62.4 (s, 3F, CF_3). **m/z** (GCMS EI): 236.1 (M^+). NMR data are consistent with the literature.[4]

methyl 4'-methyl-[1,1'-biphenyl]-4-carboxylate

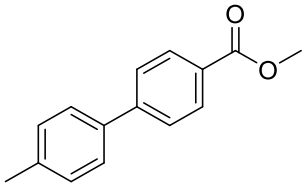

Synthesised according to the General Procedure A using methyl 4-bromobenzoate (214.6 mg, 1 mmol), 4-tolylboronic acid (150.1 mg, 1.1 mmol), [$PdCl_2$(dppf)] (36.4 mg, 5 mol %) and K_3PO_4 (634.0 mg, 3 mmol) in 2 mL toluene. The desired product was purified *via* flash column chromatography (eluting with 0 – 5 % EtOAc in hexane) to yield a white solid (209.1 mg, 92%).
^{1}H NMR (400 MHz, $CDCl_3$): δ_H 8.11 (d, 2H, 2 x ArH, *J* = 8.6 Hz), 7.67 (d, 2H, 2 x ArH, *J* = 8.5 Hz), 7.55 (d, 2H, 2 x ArH, *J* = 8.1 Hz), 7.31 (s, 2H, 2 x ArH), 3.96 (s, 3H, CO_2CH_3), 2.43 (s, 3H, CH_3). **^{13}C{^{1}H} NMR** (101 MHz, $CDCl_3$): δ_C 166.6, 145.1, 137.6, 136.6, 129.6 (2C), 129.2 (2C), 128.1, 126.6 (2C), 126.3 (2C), 51.6, 20.7. $\boldsymbol{\nu}_{\mathbf{max}}$ (neat): 3024, 2943, 2845, 1701, 1597, 1491 cm^{-1}. **m/z** (GC-MS EI) m/z: 226.1 (M^+). NMR data are consistent with the literature.[5]

_N,N,_4'-trimethyl-[1,1'-biphenyl]-4-amine

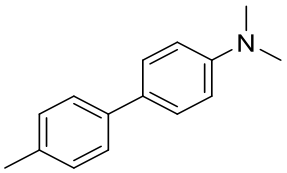

Synthesised according to the General Procedure A using 4-bromo-*N,N*-dimethylaniline (200.9 mg, 1 mmol), 4-tolylboronic acid (149.6 mg, 1.1 mmol), [$PdCl_2$(dppf)] (36.5 mg, 5 mol %) and K_3PO_4 (634.4 mg, 3 mmol) in 2 mL toluene. The desired product was purified *via* flash column chromatography (eluting with 0 – 10 % EtOAc in hexane) to yield a white solid (174.8 mg, 83 %).

^{1}H NMR (400 MHz, $CDCl_3$): δ_H 7.52 – 7.46 (m, 4H, 4 x ArH, *J* = 22.1 Hz), 7.23 (d, 2H, 2 x ArH, *J* = 8.0 Hz), 6.83 (d, 2H, 2 x ArH, *J* = 8.9 Hz), 3.02 (s, 6H, $N(CH_3)_2$), 2.40 (s, 3H, CH_3). **^{13}C{^{1}H} NMR** (101 MHz, $CDCl_3$): δ_C 149.3, 137.9, 135.1, 128.9 (2C), 127.0 (2C), 125.7 (2C), 112.4 (2C), 40.2 (2C), 20.5. **m/z** (GCMS EI): 211.1 (M^+). NMR data are consistent with the literature.[6]

4-methoxy-4'-methyl-1,1'-biphenyl

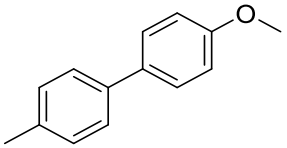

Synthesised according to the General Procedure A using 4-bromoanisole (125 µL, 186.8 mg, 1 mmol), 4-tolylboronic acid (149.3 mg, 1.1 mmol), [$PdCl_2$(dppf)] (36.7 mg, 5 mol %) and K_3PO_4 (634.4 mg, 3 mmol) in 2 mL toluene. The desired product was purified *via* flash column chromatography (eluting with 0 – 10 % EtOAc in hexane) to yield a white solid (99.6 mg, 50 %).

^{1}H NMR (400 MHz, $CDCl_3$): δ_H 7.53 (d, 2H, 2 x ArH, *J* = 9.0 Hz), 7.47 (d, 2H, 2 x ArH, *J* = 8.3 Hz), 7.25 (d, 2H, 2 x ArH, *J* = 7.8 Hz), 6.99 (d, 2H, 2 x ArH, *J* = 8.8 Hz), 3.88 (s, 3H, OCH_3), 2.41 (s, 3H, CH_3). **^{13}C{^{1}H} NMR** (101 MHz, $CDCl_3$): δ 158.4, 137.5, 135.9, 133.3, 128.9 (2C), 127.5 (2C), 126.1 (2C), 113.7 (2C), 54.9, 20.5. **m/z** (GCMS EI): 198.1 (M^+). NMR data are consistent with the literature.[4]

4'-methyl-[1,1'-biphenyl]-4-carbaldehyde

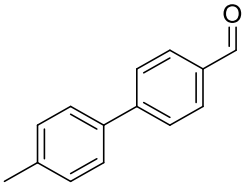

Synthesised according to the General Procedure A using 4-bromobenzaldehyde (186.2 mg, 1 mmol), 4-tolylboronic acid (150.1 mg, 1.1 mmol), [$PdCl_2$(dppf)] (37.0 mg, 5 mol %) and K_3PO_4 (634.4 mg, 3 mmol) in 2 mL toluene. The desired product was purified *via* flash column chromatography (eluting with 0 – 5 % EtOAc in hexane) to yield a white solid (115.2 mg, 59 %).

^{1}H NMR (400 MHz, $CDCl_3$): δ_H 10.08 (s, 1H, C(O)H), 7.96 (d, 2H, 2 x ArH, *J* = 8.6 Hz), 7.77 (d, 2H, 2 x ArH, *J* = 8.3 Hz), 7.57 (d, 2H, 2 x ArH, *J* = 8.1 Hz), 7.32 (d, 2H, 2 x ArH, *J* = 7.9 Hz), 2.45 (s, 3H, CH_3). **^{13}C{^{1}H} NMR** (101 MHz, $CDCl_3$): δ_C 191.4, 146.7, 138.0, 136.3, 134.5, 129.8 (2C),

129.3 (2C), 126.9 (2C), 126.7 (2C), 20.7. ν_{max} (neat): 3022, 2845, 1694, 1597, 1493 cm^{-1}. **m/z** (GCMS EI): 196.1 (M^+). NMR data are consistent with the literature.[7]

1-(4'-methyl-[1,1'-biphenyl]-4-yl)ethan-1-one

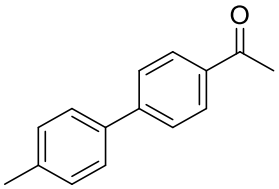

Synthesised according to the General Procedure A using 4'-bromoacetophenone (201.4 mg, 1 mmol), 4-tolylboronic acid (150.2 mg, 1.1 mmol), [$PdCl_2$(dppf)] (36.4 mg, 5 mol %) and K_3PO_4 (634.7 mg, 3 mmol) in 2 mL toluene. The desired product was purified *via* flash column chromatography (eluting with 0 – 5 % EtOAc in hexane) to yield a white solid (160.8 mg, 77 %).

^{1}H NMR (400 MHz, $CDCl_3$): δ_H 8.05 (d, 2H, 2 x ArH, *J* = 8.7 Hz), 7.70 (d, 2H, 2 x ArH, *J* = 8.7 Hz), 7.56 (d, 2H, 2 x ArH, *J* = 8.2 Hz), 7.31 (d, 2H, 2 x ArH, *J* = 8.2 Hz), 2.66 (s, 3H, $C(O)CH_3$), 2.44 (s, 3H, CH_3). **^{13}C{^{1}H} NMR** (101 MHz, $CDCl_3$): δ_C 197.3, 145.3, 137.8, 136.5, 135.1, 129.2 (2C), 128.4 (2C), 126.6 (2C), 126.5 (2C), 26.1, 20.7. ν_{max} (neat): 3026, 2928, 1674, 1597, 1522, 1491, 1420 cm^{-1}. **m/z** (GCMS EI): 210.1 (M^+). NMR data are consistent with the literature.[7]

(4'-methyl-[1,1'-biphenyl]-4-yl)(phenyl)methanone

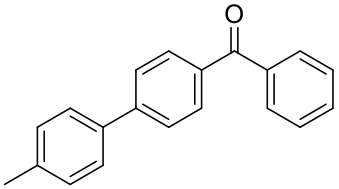

Synthesised according to the General Procedure A using 4-bromobenzophenone (261.1 mg, 1 mmol), 4-tolylboronic acid (150.3 mg, 1.1 mmol), [$PdCl_2$(dppf)] (36.7 mg, 5 mol %) and K_3PO_4 (634.9 mg, 3 mmol) in 2 mL toluene. The desired product was purified *via* flash column chromatography (eluting with 0 – 5 % EtOAc in hexane) to yield a white solid (136.3 mg, 50 %).

^{1}H NMR (400 MHz, $CDCl_3$): δ_H 7.91 (d, 2H, 2 x ArH, *J* = 8.5 Hz), 7.86 (d, 2H, 2 x ArH, *J* = 7.1 Hz), 7.72 (d, 2H, 2 x ArH, *J* = 8.6 Hz), 7.63 (t, 1H, 1 x ArH, *J* = 7.3 Hz), 7.58 (d, 2H, 2 x ArH, *J* = 8.3 Hz), 7.53 (t, 2H, 2 x ArH, *J* = 7.8 Hz), 7.32 (d, 2H, 2 x ArH, *J* = 8.1 Hz), 2.45 (s, 3H, CH_3). **^{13}C{^{1}H} NMR** (101 MHz, $CDCl_3$): δ_C 195.9, 144.7, 137.7, 137.4, 136.6, 135.5, 131.8, 130.2 (2C), 129.5 (2C), 129.2 (2C), 127.8 (2C), 126.6 (2C), 126.2 (2C), 20.7. ν_{max} (neat): 3022, 2911, 2853, 1643, 1595, 1528, 1491, 1443 cm^{-1}. **m/z** (GCMS EI): 272.1 (M^+). NMR data are consistent with the literature.[8]

4-fluoro-4'-methyl-1,1'-biphenyl

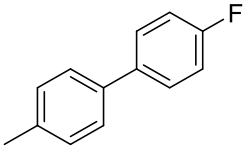

Synthesised according to the General Procedure A using 4-bromofluorobenzene (110 µL, 175.2 mg 1 mmol), 4-tolylboronic acid (135.6 mg, 1 mmol), [$PdCl_2$(dppf)] (7.5 mg, 1 mol %)

and K_3PO_4 (633.3 mg, 3 mmol) in 2 mL toluene. The desired product was purified *via* flash column chromatography (eluting with hexane) to yield a white solid (160.1 mg, 86 %).
^{1}H NMR (400 MHz, $CDCl_3$): δ_H 7.57 – 7.53 (dd, 2H, 2 x ArH, $^3J_{H-H}$ = 8.8 Hz, $^4J_{H-F}$ = 5.3 Hz), 7.46 (d, 2H, 2 x ArH, *J* = 8.1 Hz), 7.27 (d, 2H, 2 x ArH, *J* = 8.0 Hz), 7.13 (t, 2H, 2 x ArH, *J* = 8.8 Hz), 2.42 (s, 3H, CH_3). **^{13}C{^{1}H} NMR** (101 MHz, $CDCl_3$): δ_C 161.8 (d, $^1J_{C-F}$ = 245.6 Hz), 136.9, 136.8 (d, $^4J_{C-F}$ = 3.3 Hz), 136.5, 129.0 (2C), 128.0 (d, 2C, $^3J_{C-F}$ = 7.7 Hz), 126.4 (2C), 115.1 (d, 2C, $^2J_{C-F}$ = 21.2 Hz), 20.6. **^{19}F NMR** (376 MHz, $CDCl_3$): δ_F -116.3 (tt, 1F, 1 x ArF, $^3J_{F-H}$ = 8.7 Hz, $^4J_{F-H}$ = 5.3 Hz). **^{19}F{^{1}H} NMR** (376 MHz, $CDCl_3$): δ_F -116.3 (s, 1F, 1 x ArF). **m/z** (GCMS EI): 186.1 (M^+). NMR data are consistent with the literature.[4]

4-(difluoromethoxy)-4'-methyl-1,1'-biphenyl

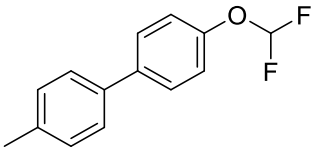

Synthesised according to the General Procedure A using 1-bromo-4-(difluoromethoxy)benzene (137 µL, 223.4 mg, 1 mmol), 4-tolylboronic acid (135.4 mg, 1 mmol), [$PdCl_2$(dppf)] (6.8 mg, 1 mol %) and K_3PO_4 (637.5 mg, 3 mmol) in 2 mL toluene. The desired product was purified *via* flash column chromatography (eluting with hexane) to yield a white solid (182.7 mg, 78 %).
^{1}H NMR (400 MHz, $CDCl_3$): δ_H 7.58 (d, 2H, 2 x ArH, *J* = 8.8 Hz), 7.48 (d, 2H, 2 x ArH, *J* = 8.2 Hz), 7.28 (d, 2H, 2 x ArH, *J* = 8.0 Hz), 7.20 (d, 2H, 2 x ArH, *J* = 8.5 Hz), 6.56 (t, 1H, CF_2H, *J* = 74.2 Hz), 2.42 (s, 3H, CH_3). **^{13}C{^{1}H} NMR** (101 MHz, $CDCl_3$): δ_C 149.9, 138.1, 136.8, 136.7, 129.1 (2C), 127.8 (2C), 126.4 (2C), 119.3 (2C), 115.5 (t, $^1J_{C-F}$ = 259.7 Hz), 20.6. **^{19}F NMR** (376 MHz, $CDCl_3$): δ_F -80.6 (d, 2F, CHF_2, *J* = 73.8 Hz). **m/z** (GCMS EI): 234.1 (M^+).

4-methyl-4'-(trifluoromethoxy)-1,1'-biphenyl

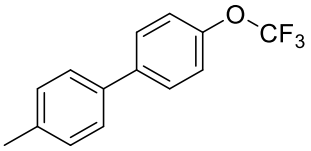

Synthesised according to the General Procedure A using 1-bromo-4-(trifluoromethoxy)benzene (149 µL, 241.7 mg, 1 mmol), 4-tolylboronic acid (136.7 mg, 1 mmol), [$PdCl_2$(dppf)] (7.1 mg, 1 mol %) and K_3PO_4 (641.9 mg, 3 mmol) in 2 mL toluene. The desired product was purified *via* flash column chromatography (eluting with hexane) to yield a white solid (180.1 mg, 71 %).
^{1}H NMR (400 MHz, $CDCl_3$): δ_H 7.60 (d, 2H, 2 x ArH, *J* = 8.2 Hz), 7.48 (d, 2H, 2 x ArH, *J* = 8.2 Hz), 2.42 (s, 3H, CH_3). **^{13}C{^{1}H} NMR** (101 MHz, $CDCl_3$): δ_C 148.0, 139.4, 137.0, 136.5, 129.1 (2C), 127.7 (2C), 126.4 (2C), 120.7 (2C), 119.6 (q, $^1J_{C-F}$ = 256.9 Hz), 20.6. **^{19}F NMR** (376 MHz, $CDCl_3$): δ_F -57.8 (s, 3F, OCF_3). **m/z** (GCMS EI): 252.1 (M^+). NMR data are consistent with the literature.[9]

4'-methyl-4-ispropyl-1,1'-biphenyl

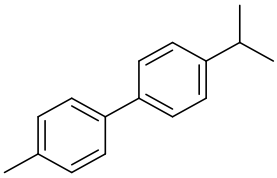

Synthesised according to the General Procedure A using 1-bromo-4-isopropylbenzene (155 µL, 199.3 mg, 1 mmol), 4-tolylboronic acid (135.7 mg, 1 mmol), [$PdCl_2$(dppf)] (7.3 mg, 1 mol %) and K_3PO_4 (633.3 mg, 3 mmol) in 2 mL toluene. The desired product was purified *via* flash column chromatography (eluting with hexane) to yield a white solid (155.0 mg, 74 %).
^{1}H NMR (400 MHz, $CDCl_3$): δ_H 7.55 – 7.50 (m, 4H, 4 x ArH, *J* = 20.4 Hz), 7.31 (d, 2H, 2 x ArH, *J* = 7.9 Hz), 7.26 (d, 2H, 2 x ArH, *J* = 7.9 Hz), 2.97 (h, 1H, $C(CH_3)_2H$, *J* = 7.1 Hz), 2.41 (s, 3H, CH_3), 1.31 (d, 6H, $(CH_3)_2$, *J* = 6.9 Hz). **^{13}C{^{1}H} NMR** (101 MHz, $CDCl_3$): δ_C 147.2, 138.2, 137.8, 136.2, 128.9 (2C), 126.4 (2C), 126.4 (2C), 126.3 (2C), 33.3, 23.5 (2C), 20.6. **m/z** (GCMS EI): 210.1 (M^+). NMR data are consistent with the literature.[10]

N,N-diethyl-4'-methyl-[1,1'-biphenyl]-4-amine

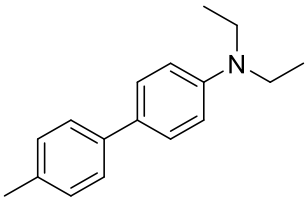

Synthesised according to the General Procedure A using 4-bromo-N,N-diethylaniline (228.2 mg, 1 mmol), 4-tolylboronic acid (135.5 mg, 1 mmol), [$PdCl_2$(dppf)] (7.2 mg, 1 mol %) and K_3PO_4 (635.3 mg, 3 mmol) in 2 mL toluene. The desired product was purified *via* flash column chromatography (eluting with 0 – 5 % EtOAc in hexane) to yield a white solid (214.6 mg, 90 %).
^{1}H NMR (400 MHz, $CDCl_3$): δ_H 7.51 – 7.47 (m, 4H, 4 x ArH, *J* = 14.1 Hz), 7.23 (d, 2H, 2 x ArH, *J* = 8.0 Hz), 6.78 (d, 2H, 2 x ArH, *J* = 8.5 Hz), 3.43 (q, 4H, $(CH_2CH_3)_2$, *J* = 7.1 Hz), 2.41 (s, 3H, CH_3), 1.23 (t, 6H, $(CH_2CH_3)_2$, *J* = 7.1 Hz). **^{13}C{^{1}H} NMR** (101 MHz, $CDCl_3$): δ_C 146.5, 138.0, 134.9, 128.9 (2C), 127.7, 127.3 (2C), 125.6 (2C), 111.5 (2C), 43.9 (2C), 20.6, 12.2 (2C). **m/z** (GCMS EI): 239.4 (M^+).

2,2,2-trifluoro-1-(4'-methyl-[1,1'-biphenyl]-4-yl)ethan-1-one

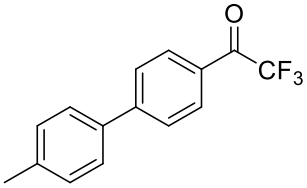

Synthesised according to the General Procedure A using 1-(4-bromophenyl)-2,2,2-trifluoroethan-1-one (253.0 mg, 1 mmol), 4-tolylboronic acid (134.8 mg, 1 mmol), [$PdCl_2$(dppf)] (7.1 mg, 1 mol %) and K_3PO_4 (638.2 mg, 3 mmol) in 2 mL toluene. The desired product was purified *via* flash column chromatography (eluting with 0 – 5 % EtOAc in hexane) to yield a white solid (178.6 mg, 68 %).
^{1}H NMR (400 MHz, $CDCl_3$): δ_H 8.17 (d, 2H, 2 x ArH, *J* = 7.6 Hz), 7.79 (d, 2H, 2 x ArH, *J* = 8.7 Hz), 7.59 (d, 2H, 2 x ArH, *J* = 8.2 Hz), 7.34 (d, 2H, 2 x ArH, *J* = 8.0 Hz), 2.46 (s, 3H, CH_3). **^{13}C{^{1}H} NMR** (101 MHz, $CDCl_3$): δ_C 179.6 (q, $^2J_{C\text{-}F}$ = 34.5 Hz), 147.7, 138.6, 135.7, 130.3 (2C), 129.4 (2C),

127.8 (2C), 126.8, 126.7 (2C), 116.4 (q, $^{1}J_{C\text{-}F}$ = 291.1 Hz), 20.7. **^{19}F NMR** (376 MHz, $CDCl_3$): δ_F -71.3 (s, 3F, CF_3). **m/z** (GCMS EI): 264.3 (M^+). NMR data are consistent with the literature.[11]

4'-methyl-N-phenyl-[1,1'-biphenyl]-4-amine

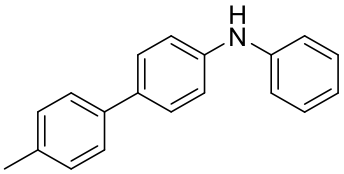

Synthesised according to the General Procedure A using 4-bromo-N-phenylaniline (248.1 mg, 1 mmol), 4-tolylboronic acid (135.5 mg, 1 mmol), [$PdCl_2$(dppf)] (7.4 mg, 1 mol %) and K_3PO_4 (637.4 mg, 3 mmol) in 2 mL toluene. The desired product was purified *via* flash column chromatography (eluting with 0 – 5 % EtOAc in hexane) to yield a white solid (216.0 mg, 83 %).

^{1}H NMR (400 MHz, $CDCl_3$): δ_H 7.52 (t, 5H, 5 x ArH, *J* = 8.4 Hz), 7.32 (t, 3H, 3 x ArH, *J* = 6.9 Hz), 7.26 (d, 3H, 3 x ArH, *J* = 7.7 Hz), 7.17 (bs, 4H, 4 x ArH), 6.99 (bs, 1H, 1 x ArH), 2.42 (s, 3H, CH_3). **^{13}C{^{1}H} NMR** (101 MHz, $CDCl_3$): δ_C 142.5, 141.7, 137.5, 135.8 (2C), 133.4, 129.0 (2C), 128.9 (2C), 127.3 (2C), 125.9 (2C), 120.7 (2C), 117.5 (2C), 20.6 . **m/z** (GCMS EI): 259.4 (M^+).

4-methyl-4'-(methylsulfonyl)-1,1'-biphenyl

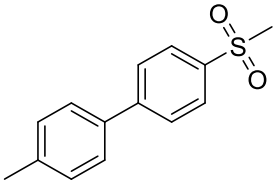

Synthesised according to the General Procedure A using 1-bromo-4-(methylsulfonyl)benzene (235.4 mg, 1 mmol), 4-tolylboronic acid (135.2 mg, 1 mmol), [$PdCl_2$(dppf)] (7.0 mg, 1 mol %) and K_3PO_4 (635.4 mg, 3 mmol) in 2 mL toluene. The desired product was purified *via* flash column chromatography (eluting with 0 – 10 % EtOAc in hexane) to yield a white solid (174.1 mg, 71 %).

^{1}H NMR (400 MHz, $CDCl_3$): δ_H 8.02 (d, 2H, 2 x ArH, *J* = 7.8 Hz), 7.79 (d, 2H, 2 x ArH, *J* = 7.4 Hz), 7.55 (d, 2H, 2 x ArH, *J* = 7.4 Hz), 7.33 (d, 2H, 2 x ArH, *J* = 7.8 Hz), 3.12 (s, SO_2CH_3), 2.46 (s, 3H, CH_3). **^{13}C{^{1}H} NMR** (101 MHz, $CDCl_3$): δ_C 146.2, 138.3 (2C), 135.7, 129.3 (2C), 127.4 (2C), 127.2 (2C), 126.7 (2C), 44.2, 20.7. **m/z** (GCMS EI): 246.3 (M^+). NMR data are consistent with the literature.[12]

3-methoxy-4'-methyl-1,1'-biphenyl

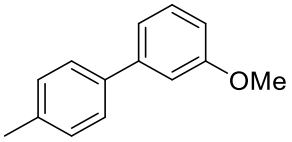

Synthesised according to the General Procedure A using 3-bromoanisole (180 µL, 266 mg, 1.4 mmol), 4-tolylboronic acid (247.0 mg, 1.8 mmol), [$PdCl_2$(dppf)] (41.9 mg, 4.4 mol%), and K_3PO_4 (902.0 mg, 4.2 mmol) in 5 mL toluene. The desired product was purified *via* flash column chromatography (eluting with hexane) to yield a pale oil (120.5 mg, 43%).

^{1}H NMR (400 MHz, $CDCl_3$): δ_H 7.58 (d, 2H, *J* = 8.1 Hz, Ar CH), 7.43 (t, 1H, *J* = 8.1 Hz, Ar CH), 7.33 (d, 2H, *J* = 7.9 Hz, Ar CH), 7.26 (dt, 1H, *J* = 7.9, 1.4 Hz, Ar CH), 7.22 (t, 1H, *J* = 2.2 Hz, Ar CH), 6.97 (ddd, 1H, *J* = 8.3, 2.5, 0.7 Hz, Ar CH), 3.93 (s, 3H, OMe), 2.48 (s, 3H, Me). **^{13}C{^{1}H}**

NMR (101 MHz, $CDCl_3$): δ_C 160.1, 142.8, 138.3, 137.3, 129.8, 129.6, 127.1, 119.6, 112.8, 112.5, 55.4, 21.2. **m/z** (GCMS EI): 198.2 (M^+). NMR data are consistent with the literature.[13]

4-methyl-3-(trifluoromethyl)-1,1'-biphenyl

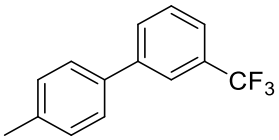

Synthesised according to the General Procedure A using 3-bromobenzotrifluoride (180 µL, 290 mg, 1.3 mmol), 4-tolylboronic acid (206.1 mg, 1.5 mmol), [$PdCl_2$(dppf)] (40.1 mg, 4.2 mol%), and K_3PO_4 (808.9 mg, 3.8 mmol) in 5 mL toluene. The desired product was purified *via* flash column chromatography (eluting with hexane) to yield a colourless oil that solidified upon drying under high vacuum (252.8 mg, 83%).
^{1}H NMR (400 MHz, $CDCl_3$): δ_H 7.90 (s, 1H, Ar CH), 7.81 (d, 1H, *J* = 7.7 Hz, Ar CH), 7.68 – 7.53 (m, 4H, Ar CH), 7.34 (d, 2H, *J* = 8.1 Hz, Ar CH), 2.48 (s, 3H, Me). **^{13}C{^{1}H} NMR** (101 MHz, $CDCl_3$): δ_C 142.1, 138.1, 137.0, 131.3 (q, *J* = 33.0 Hz), 130.8, 130.3, 129.9, 192.3, 127.1, 124.4 (q, *J* = 272.0 Hz), 123.8 (q, *J* = 3.8 Hz), 21.2. **m/z** (GCMS EI): 236.1 (M^+). NMR data are consistent with the literature.[6]

1-(4'-methyl-[1,1'-biphenyl]-3-yl)ethan-1-one

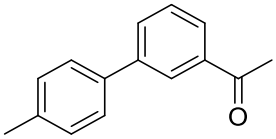

Synthesised according to the General Procedure A using 3'-bromoacetophenone (170 µL, 256 mg, 1.3 mmol), 4-tolylboronic acid (175.7 mg, 1.3 mmol), [$PdCl_2$(dppf)] (42.0 mg, 4.4 mol%), and K_3PO_4 (902.0 mg, 4.2 mmol) in 5 mL toluene. The desired product was purified *via* flash column chromatography (eluting with 0 – 2% Et_2O in hexane) to yield an oil that solidified upon drying under high vacuum (172.4 mg, 64%).
^{1}H NMR (400 MHz, $CDCl_3$): δ_H 8.20 (t, 1H, *J* = 1.7 Hz, Ar CH), 7.94 (dt, 1H, *J* = 7.7, 1.2 Hz, Ar CH), 7.82 – 7.78 (m, 1H, Ar CH), 7.59 – 7.53 (m, 3H, Ar CH), 7.31 (d, 2H, *J* = 8.2 Hz, Ar CH), 2.68 (s, 3H, COMe), 2.44 (s, 3H, Me). **^{13}C{^{1}H} NMR** (101 MHz, $CDCl_3$): δ_C 198.2, 141.7, 137.8, 137.7, 137.4, 131.6, 129.8, 129.1, 127.1, 127.0, 126.8, 26.8, 21.2. **m/z** (GCMS EI): 210.1 (M^+). NMR data are consistent with the literature.[14]

4'-methyl-[1,1'-biphenyl]-4-carbonitrile

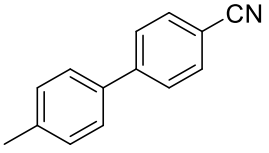

Synthesised according to General Procedure A using 4-bromobenzonitrile (182.0 mg, 1 mmol), 4-tolylboronic acid (148.4 mg, 1.1 mmol), [$PdCl_2$(dppf)] (7.2 mg, 1 mol%) and K_3PO_4 (634.2 mg, 3 mmol) in 2 mL PhMe. The desired product was purified *via* flash column chromatography (eluting with 5 % EtOAc in hexane) to yield a white solid (148.5 mg, 77 %). %). **^{1}H NMR** (400 MHz, $CDCl_3$): δ_H 7.73 (d, 2H, 2 x ArH, *J* = 8.3 Hz), 7.69 (d, 2H, 2 x ArH, *J* = 8.3

Hz), 7.52 (d, 2H, 2 x ArH, *J* = 8.0 Hz), 7.32 (d, 2H,2 x ArH, *J* = 8.2 Hz), 2.45 (s, 3H, CH_3). **$^{13}C\{^1H\}$ NMR** (101 MHz, $CDCl_3$): δ_C 145.1, 138.3, 135.8, 132.1 (2C), 129.4 (2C), 127.0 (2C), 126.6 (2C), 118.5, 110.1, 20.7. **m/z** (GCMS EI): 193.1 (M^+). NMR data are consistent with the literature.[2]

4-methyl-4'-(phenylethynyl)-1,1'-biphenyl

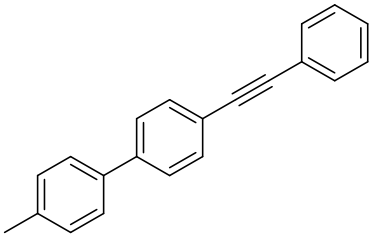

Synthesised according to General Procedure A using 1-bromo-4-(phenylethynyl)benzene (257.4 mg, 1 mmol), 4-tolylboronic acid (149.3 mg, 1.1 mmol), [$PdCl_2$(dppf)] (7.4 mg, 1 mol%) and K_3PO_4 (638.1mg, 3 mmol) in 2 mL PhMe. The desired product was purified *via* passing the mixture through a silica pad to yield a white solid (141.2 mg, 53 %). **^1H NMR** (400 MHz, $CDCl_3$): δ_H 7.65 – 7.58 (m, 6H, 6 x ArH, *J* = 25.1 Hz), 7.56 (d, 2H, 2 x ArH, *J* = 8.1 Hz), 7.42 – 7.37 (m, 3H, 3 x ArH, *J* = 21.1 Hz), 7.30 (d, 2H, 2 x ArH, *J* = 7.8 Hz), 2.44 (s, 3H, CH_3). **$^{13}C\{^1H\}$ NMR** (101 MHz, $CDCl_3$): δ_C 140.4, 137.0, 137.0, 131.5 (2C), 131.1 (2C), 129.1 (2C), 127.9 (2C), 127.7, 126.4 (2C), 126.3 (2C), 122.9, 121.4, 89.5, 88.9, 20.6. **m/z** (GCMS EI): 268.1 (M^+). NMR data are consistent with the literature.[3]

General Procedure B: Synthesis of Chalcone Derivatives

Chalcone. In a round bottom flask equipped with a stirrer bar, aldehyde (1 eq.) and ketone (1 eq.) were dissolved in EtOH (14 mL) or a mixture of EtOH (25 mL) and THF (25 mL). Once dissolved, 10 % w/v solution of NaOH (6 mL) was added. The mixture was stirred for 5-15 minutes at room temperature and the resulting chalcone was filtered and washed with EtOH (3 x 5 mL) to give a white or off-white solid. GC-MS was carried out to check conversion and crude material was carried through to the next step.

Allylic Alcohol. In a round bottom flask equipped with a stirrer bar, chalcone (1 eq.) and $CeCl_3.7H_2O$ (1 eq.) were dissolved in MeOH (10 mL) and THF (50 mL). Once dissolved, the mixture was cooled to 0 ^oC with an ice bath. $NaBH_4$ (1.5 eq.) was slowly added in portions. Once all of the $NaBH_4$ was added, the mixture was warmed to room temperature and stirred for 15 minutes. The reaction was neutralised to pH 7 with 1 M HCl and distilled water (100 mL) was added. The mixture was extracted 3 times with Et_2O (3 x 50 mL). The combined organic phases were dried over $MgSO_4$, which was filtered and the Et_2O removed under vacuum to furnish the allylic alcohol as a white oil. NMR was carried out to check conversion and crude material was carried through to the next step.

Rearrangement to Saturated Chalcone. In a microwave vial equipped with a stirrer bar, allylic alcohol (1 eq.), [IrCl(IPr)(COD)] (0.1 mol%) and KOH (10 mol%) were dissolved (KOH suspended) in THF (2 – 4 mL). The reaction was heated in a Biotage Initiator Microwave Synthesiser at 150 ^oC for 2 – 4 hours. The resulting mixture was filtered through celite and the solvent removed under reduced pressure.^1H NMR was carried out to check conversion. The desired compound was either: purified *via* flash column chromatography, eluting with

hexane to yield a white or off-white solid; or recrystallised from hot hexane and filtered to yield a white or off-white solid.

1,3-bis(4-chlorophenyl)propan-1-one

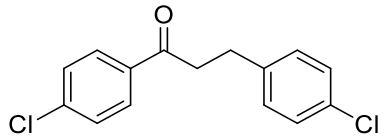

Chalcone. Using 4'-chloroacetophenone (1.1162 g, 1.20 mL, 7.22 mmol) and 4-chlorobenzaldehyde (1.0141 g, 7.22 mmol) to give an off-white solid (1.9724 g, 99 %).
Allylic Alcohol. Using chalcone (1.9724 g, 7.12 mmol), $CeCl_3 7.H_2O$ (2.6516 g, 7.12 mmol) and $NaBH_4$ (0.40410 g, 10.68 mmol) to yield a white oil (0.5384 g, 27 %).
Saturated Chalcone. Using allylic alcohol (0.5384 g, 1.93 mmol), [IrCl(IPr)(COD)] (0.0014 g, 0.1 mol%) and KOH (0.0081 g, 10 mol%). The product was purified *via* flash column chromatography, eluting with hexane to yield a white solid (286.3 mg, 53 %).
^{1}H NMR (400 MHz, $CDCl_3$): δ_H 7.89 (d, 2H, 2 x ArH, *J* = 8.0 Hz), 7.44 (d, 2H, 2 x ArH, *J* = 8.0 Hz), 7.27 (d, 2H, 2 x ArH, *J* = 8.0 Hz), 7.18 (d, 2H, 2 x ArH, *J* = 8.4 Hz), 3.25 (t, 2H, CH_2, *J* = 7.5 Hz), 3.04 (t, 2H, CH_2, *J* = 7.5 Hz). **^{13}C{^{1}H} NMR** (101 MHz, $CDCl_3$): δ_C 197.1, 139.1, 139.0, 134.6, 131.5, 129.3 (2C), 128.9 (2C), 128.5 (2C), 128.1 (2C), 39.6, 28.8. **m/z** (GCMS EI): 278.0 (M^+). NMR data are consistent with the literature.[15]

1-([1,1'-biphenyl]-4-yl)-3-(4-chlorophenyl)propan-1-one

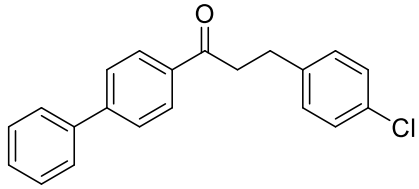

Chalcone. Using 1-([1,1'-biphenyl]-4-yl)ethan-1-one (1.2324 g, 6.27 mmol) and 4-chlorobenzaldehyde (0.8814 g, 6.27 mmol) to give an off-white solid (1.9347 g, 97 %).
Allylic Alcohol. Using chalcone (1.9347 g, 6.07 mmol), $CeCl_3 7.H_2O$ (2.2805 g, 6.07 mmol) and $NaBH_4$ (0.4731 g, 9.11 mmol) to yield a white oil (0.7032 g, 36 %).
Saturated Chalcone. Using allylic alcohol (0.7032 g, 2.19 mmol), [IrCl(IPr)(COD)] (0.0014 g, 0.1 mol%) and KOH (0.0089 g, 10 mol%). The product was purified *via* recrystallisation from hexane to yield a white solid (469.9 mg, 67 %).
^{1}H NMR (400 MHz, $CDCl_3$): δ_H 8.06 (d, 2H, 2 x ArH, *J* = 8.0 Hz), 7.71 (d, 2H, 2 x ArH, *J* = 8.0 Hz), 7.65 (d, 2H, 2 x ArH, *J* = 7.2 Hz), 7.50 (t, 2H, 2 x ArH, *J* = 8.0 Hz), 7.43 (t, 1H, 1 x ArH, *J* = 8.0 Hz), 7.30 (d, 2H, 2 x ArH, *J* = 8.0 Hz), 7.23 (d, 2H, 2 x ArH, *J* = 8.0 Hz), 3.34 (t, 2H, CH_2, *J* = 7.4 Hz), 3.10 (t, 2H, CH_2, *J* = 7.8 Hz). **^{13}C{^{1}H} NMR** (101 MHz, $CDCl_3$): δ_C 197.9, 145.4, 139.3, 139.3, 135.0, 131.4, 129.3 (2C), 128.5 (2C), 128.1 (4C), 127.8 (2C), 126.8 (3C), 39.7, 29.0. **m/z** (GCMS EI): 320.1 (M^+). NMR data are consistent with the literature.

1,3-di([1,1'-biphenyl]-4-yl)propan-1-one

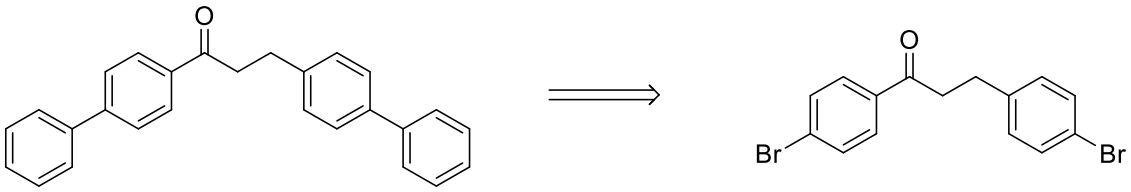

Chalcone (dibromo). Using 4'-bromoacetophenone (1.092 g, 5.46 mmol) and 4-bromobenzaldehyde (1.017 g, 5.46 mmol) to give an off-white solid (1.7970 g, 90 %).
Allylic Alcohol (dibromo). Using chalcone (1.7970 g, 4.88 mmol), $CeCl_3 7.H_2O$ (1.8192 g, 4.88 mmol) and $NaBH_4$ (0.3773 g, 7.98 mmol) to yield a white oil (1.1037 g, 61 %).
Saturated Chalcone (dibromo). Using allylic alcohol (1.1037 g, 3.00 mmol), [IrCl(IPr)(COD)] (0.0022 g, 0.1 mol%) and KOH (0.0126 g, 10 mol%). The product was purified *via* recrystallisation from hexane to yield a white solid (734.3 mg, 67 %).
Saturated Chalcone (diphenyl). Using dibromo saturated chalcone (734.3 mg, 2.00 mmol), phenyl boronic acid (487.7 mg, 4.00 mmol), [$PdCl_2$(dppf)] (14.9 mg, 1 mol%) and K_3PO_4 (1.3013 g, 6.00 mmol) in 4 mL 4:1 THF:H_2O. The desired product was purified *via* flash column chromatography, eluting with hexane to give a white solid (502.9 mg, 69 %). **^{1}H NMR** (400 MHz, $CDCl_3$): δ_H 8.09 (d, 2H, 2 x ArH, *J* = 8.5 Hz), 7.72 (d, 2H, 2 x ArH, *J* = 8.5 Hz), 7.66 (d, 2H, 2 x ArH, *J* = 7.4 Hz), .61 (d, 2H, 2 x ArH, *J* = 7.4 Hz), 7.58 (d, 2H, 2 x ArH, *J* = 8.1 Hz), 7.52 – 7.43 (m, 5H, 5 x ArH, *J* = 35.9 Hz), 7.39 – 7.37 (m, 3H, 3 x ArH, *J* = 8.1 Hz), 3.41 (t, 2H, CH_2, *J* = 8.0 Hz), 3.18 (t, 2H, CH_2, *J* = 7.6 Hz). **^{13}C{^{1}H} NMR** (101 MHz, $CDCl_3$): δ_C 198.3, 145.3, 140.5, 139.9, 139.4, 138.7, 135.1, 128.5 (2C), 128.4 (2C), 128.3 (2C), 128.2 (2C), 127.7 (2C), 126.8 (4C), 126.6 (2C), 126.5 (2C), 39.9, 29.3. **m/z** (GCMS EI): 362.2 (M^+).

DATA FOR CHAPTER 2

GC-FID CALIBRATION

The GC-FID apparatus was calibrated for each analyte using a series of standards, accurately prepared, containing varying ratios of internal standard and analyte. In each case, a plot of the relative peak areas *versus* the molar ratio gave a straight line, and the slope of this line was used as the response factor.

Substrate	Internal Standard	Response Factor
4-methyl-1,1'-biphenyl	n-dodecane	0.9947
4,4'-dimethyl-1,1'-biphenyl	n-dodecane	0.9516
4-methyl-4'-(trifluoromethyl)-1,1'-biphenyl	n-dodecane	1.0982
methyl 4'-methyl-[1,1'-biphenyl]-4-carboxylate	n-dodecane	0.7552
N,N,4'-trimethyl-[1,1'-biphenyl]-4-amine	n-dodecane	0.2497
4-methoxy-4'-methyl-1,1'-biphenyl	n-dodecane	0.8421
1-(4'-methyl-[1,1'-biphenyl]-4-yl)ethan-1-one	n-dodecane	0.7493
(4'-methyl-[1,1'-biphenyl]-4-yl)(phenyl)methanone	n-dodecane	1.1964
4'-methyl-[1,1'-biphenyl]-4-carbaldehyde	n-dodecane	0.7491
4-fluoro-4'-methyl-1,1'-biphenyl	n-dodecane	0.9598
4-(difluoromethoxy)-4'-methyl-1,1'-biphenyl	n-dodecane	1.1663
4-methyl-4'-(trifluoromethoxy)-1,1'-biphenyl	n-dodecane	1.1355
4'-methyl-4-ispropyl-1,1'-biphenyl	n-dodecane	1.0987
4'-methyl-N-phenyl-[1,1'-biphenyl]-4-amine	n-dodecane	0.7828
N,N-diethyl-4'-methyl-[1,1'-biphenyl]-4-amine	n-dodecane	0.8638
2,2,2-trifluoro-1-(4'-methyl-[1,1'-biphenyl]-4-yl)ethan-1-one	n-dodecane	1.0027
4-methyl-4'-(methylsulfonyl)-1,1'-biphenyl	n-dodecane	0.7081
3-methoxy-4'-methyl-1,1'-biphenyl	n-dodecane	0.9447
4-methyl-3-(trifluoromethyl)-1,1'-biphenyl	n-dodecane	1.0034
1-(4'-methyl-[1,1'-biphenyl]-3-yl)ethan-1-one	n-dodecane	0.9589

DATA FROM COMPETITIVE CROSS-COUPLING REACTIONS

Competition Reactions Between Substituted Aryl Bromides and Bromobenzene

Competition reactions carried out between PhBr (1 equiv.) and substrates of the form XC_6H_4Br (1 equiv.). Solid components (catalyst **7**, K_3PO_4, solid substrates) were loaded into a microwave tube equipped with a stir bar, sealed with a septum-fitted crimp-cap, and evacuated and backfilled with Ar or N_2 several times. Liquid reagents (PhBr and the other substrate, if liquid) and the solvent were added *via* syringe through the septum. The reactions were heated and stirred for 2 h, cooled to room temperature, and an accurately-known mass of *n*-dodecane was added. A sample of the solution was diluted in chloroform for analysis by GC-FID.

Reactions in Toluene Solution[a]					
Substrate X =	**Product from PhBr**	**Product from XC_6H_4Br**	**Total conversion**	**Selectivity**	**σ (X)**
p-NMe_2	59	38	97	-0.23	-0.83
p-NEt_2	60	54	114	-0.05	-0.72
p-NHPh	44	45	99	0.01	-0.56
p-OMe	57	42	99	-0.15	-0.27
p-*i*-Pr	63	33	96	-0.32	-0.15
p-OCF_2H	52	37	89	-0.18	0.18
p-OCF_3	54	40	94	-0.16	0.35
p-CO_2Me	37	76	113	0.35	0.45
p-CF_3	62	48	110	-0.13	0.54
p-SO_2Me	22	78	100	0.56	0.72
p-CHO	8	96	104	0.85	0.42
p-C(O)Ph	11	75	86	0.75	0.43
p-C(O)Me	15	95	110	0.74	0.50
p-$C(O)CF_3$	5	72	77	0.88	0.80
m-CF_3	28	55	83	0.33	0.43
m-OMe	40	31	71	-0.12	0.12
m-Ac	8	78	86	0.81	0.38
Reactions in THF/Water Solution[a] [16]					
Substrate X =	**Product from PhBr**	**Product from *p*-XC_6H_4Br**	**Total conversion**	**Selectivity**	**σ_p (X)**
NMe_2	37	58	95	0.22	-0.83
NEt_2	43	20	63	-0.37	-0.72
NHPh	42	24	66	-0.28	-0.56
OMe	38	23	61	-0.25	-0.27
i-Pr	38	16	54	-0.40	-0.15
OCF_2H	52	32	84	-0.24	0.18
OCF_3	50	28	78	-0.33	0.35
CO_2Me	32	38	70	0.09	0.45
CF_3	38	35	73	-0.05	0.54
SO_2Me	40	30	70	-0.15	0.72
CHO	0	108	108	1.00	0.42
C(O)Ph	6	58	64	0.83	0.43
C(O)Me	5	95	100	0.91	0.50
$C(O)CF_3$	*N/A – ketone undergoes hydration*				

a – all values quoted as an average of two replicate reactions

Competition Reactions Between Substituted Aryl Bromides and Bromobenzene with Alternative Catalysts

Values quoted in the manuscript are the average of four replicates

Ligand	Product from *p*-$F_3CC_6H_4Br$	Product from *p*-$OHCC_6H_4Br$	Total Conversion
dppe	0	48	48
	0	47	47
	0	55	55
	0	57	57
Xantphos	0	14	14
	0	13	13
	0	8	8
	0	8	8

Competition Reactions with Boronic Acids

Reaction of 1 equiv. *p*-bromotoluene with 1 equiv. of each of two boronic acids. Yields of each product determined by calibrated GC-FID analysis. Results are quoted as the average of two replicates.

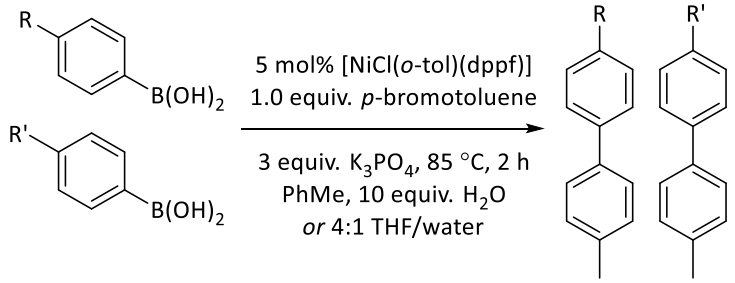

Solvent	R	Yield of Product	R	Yield of Product
THF/water	H	21(1)%	Ac	24(1)%
THF/water	CF_3	16(1)%	Ac	21(1)%
THF/water	H	20(3)%	CF_3	17(2)%
PhMe	H	26(1)%	Ac	7(2)%
PhMe	CF_3	41(3)%	Ac	17(1)%
PhMe	H	33(1)%	CF_3	26(1)%

Competition Reactions Between Different Substituted Aryl Bromides

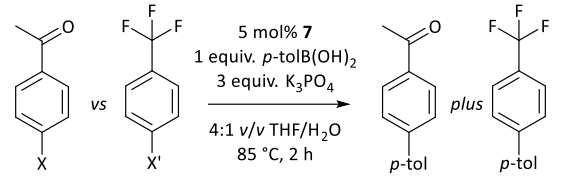

X = Br	X' = Br	91(12)%	:	3%
X = Br	X' = I	71(4)%	:	34(4)%
X = Cl	X' = Cl	104(1)%	:	3(1)%
X = Cl	X' = Br	100(1)%	:	5%
X = Cl	X' = I	62(3)%	:	38(2)%

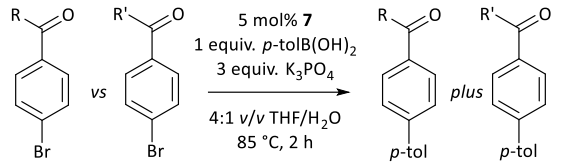

R = Me	R = H	1%	:	80(2)%
R = Me	R = Ph	65(4)%	:	32(1)%
R = H	R = Ph	96(1)%	:	5%
			:	
			:	

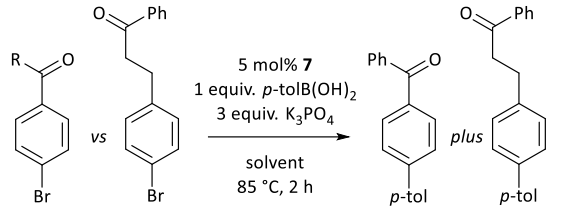

4-Br (R = Ph)	**22-Br**	20%	:	<1%
3-Br (R = H)	**22-Br**	71(6)%	:	<1%

Intramolecular Competition Reactions

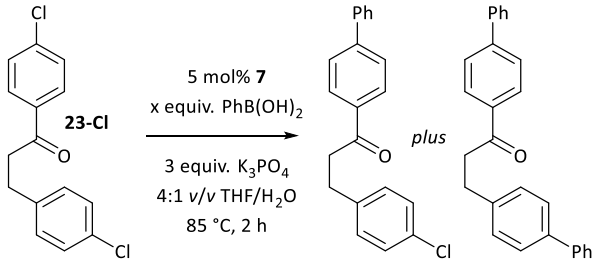

x = 2	20 ± 3%	7 ± 2%
x = 1	14 ± 2%	2 ± 1%
x = 0.5	12 ± 1%	1 ± 1%

DESIGN OF EXPERIMENTS DATA FOR REACTION OPTIMISATION

For each reaction, solid components were loaded into a microwave tube equipped with a stir bar, sealed with a septum-fitted crimp-cap, and evacuated and backfilled with argon or nitrogen several times. The liquid reagents and the reaction solvent were added *via* syringe through the septum. The reactions were then heated, with stirring, for 18 h. After this time, the reaction was cooled to room temperature, and an accurately-known mass of dodecane or tetradecane was added. A sample of the solution was then diluted in chloroform for analysis by GC-FID. The DoE study was initially conducted using the dppe ligand, but comparable results are obtained using dppf under the same conditions. All other work was conducted with dppf as the model nickel(0) complex for kinetic studies and ligand binding studies used a dppf ligand.

Initial Screen

Run	T (°C)	Cat. Loading (mol%)	Boronic Acid equiv.	Base equiv.	Water equiv.	Conversion (%)
1	30	10	1	1	0	0
2	110	1	1	1	0	62
3	110	10	2	1	0	96
4	110	1	2	1	20	0
5	30	1	1	5	0	2
6	110	10	1	5	0	69
7	110	1	2	5	0	80
8	110	10	1	1	20	75
9	30	1	2	5	20	20
10	70	5.5	1.5	3	10	>99
11	30	10	1	5	20	0
12	110	1	1	5	20	78
13	70	5.5	1.5	3	10	>99
14	30	1	1	1	20	5
15	30	10	2	5	0	18
16	30	1	2	1	0	0
17	70	5.5	1.5	3	10	>99
18	30	10	2	1	20	15
19	70	5.5	1.5	3	10	>99
20	110	10	2	5	20	97

Data were analysed using DesignExpert 8. From this, it was deduced that the catalyst loading had a positive effect on conversion, though it was not as significant as the temperature effect. Overall, this initial screen gave positive results, since the centre points appeared to proceed to full conversion. In order to further probe the reaction conditions, and potentially reduce factors such as catalyst loading, the experiment design was augmented to narrow in on optimised conditions.

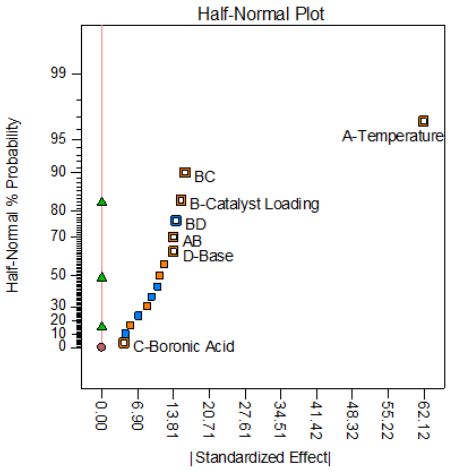

Half-normal plot

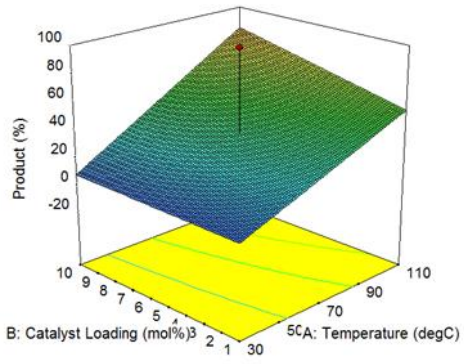

3D response surface

Second Screen

Run	T (°C)	Cat. Loading (mol%)	Boronic Acid eq.	Base eq.	Water eq.	Conversion (%)
21	70	1	1.5	3	10	0
22	70	5.5	1.5	5	10	91
23	70	5.5	1.5	3	0	90
24	70	5.5	1.5	1	10	21
25	110	5.5	1.5	3	10	97
26	70	5.5	1	3	10	81
27	70	5.5	1.5	3	10	98
28	70	5.5	1.5	3	10	97
29	70	5.5	1.5	3	20	58
30	30	5.5	1.5	3	10	0
31	70	5.5	2	3	10	70
32	70	10	1.5	3	10	91

Using these data, the software suggested that the optimum conditions were: 5 mol % catalyst loading; 1.1 equivalents of boronic acid; temperature of 85 °C; 3 equivalents of base; 10 equivalents of water. These conditions were used in triplicate to verify that the reaction was reproducible and tested also on a non-carbonyl substrate.

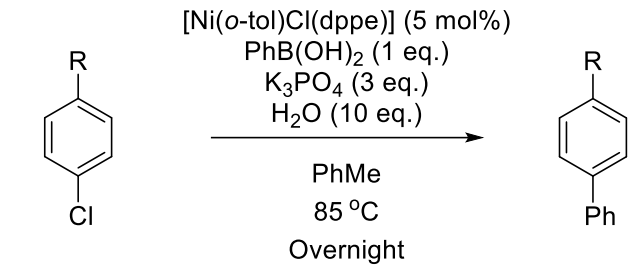

R = COMe, CF_3

Substrate	Conversion (%)
4'chloroacetophenone	92
4'chloroacetophenone	95
4'chloroacetophenone	>99
4-chlorobenzotrifluoride	91

A small time study was conducted, using these optimised conditions, in an effort to reduce the reaction time.

Substrate	Reaction Time (h)	Conversion (%)
4'-chloroacetophenone	2	99*
4'chloroacetophenone	4	99*
4'chloroacetophenone	6	99*
4'chloroacetophenone	8	99*

DATA FOR CHAPTER 3

DATA FROM ROBUSTNESS SCREENING REACTIONS

A microwave tube equipped with a stir bar was charged with **7** (5 mol%), K_3PO_4 (3 equiv.), *p*-tolB$(OH)_2$ (1.1 equiv.) and the additive (if solid). The tube was sealed with a crimp cap and evacuated and backfilled with nitrogen or argon. 4-(Trifluoromethyl)bromobenzene was added *via* syringe (0.25 mmol, 1 equiv.), followed by the additive (if liquid), anhydrous toluene (1 mL), and degassed distilled water (10 equiv.). The reaction was heated to 85 °C with stirring for 2 h. Upon cooling, the tube was opened, a known mass of tetradecane or dodecane was added, and the mixture was stirred briefly. A sample was withdrawn, diluted with chloroform, and analysed by GC-FID.

Additive	**Conversion (%)**			**Additive Remaining (%)**	
	Replicate 1	**Replicate 2**	**Average**	**Replicate 1**	**Replicate 2**
None	88	93	88	N/A	N/A
Phenyl acetate	75	81	78	60	82
Methyl benzoate	87	89	88	91	98
Benzamide	86	87	86	0 [a]	0 [a]
Benzophenone	33	43	38	100	100
Benzaldehyde	11	13	12	98	100
2,2,2-Trifluoroacetophenone	1	1	1	85 [b]	88 [b]
Acetophenone	73	83	78	92	95
Diphenylamine	72	81	77	100	100
Anisole	82	84	83	100	100
N,*N*-Dimethylaniline	81	90	86	97	100
Methyl phenyl sulfone	85	88	87	7	8

a) Analysis of a control reaction without a nickel catalyst also shows no recovery of the additive.
b) This additive undergoes hydration in the presence of water.

Experiments with Different Catalysts

Ligand	**Conversion (%)**			
	No additive		**1 equiv. PhCHO**	
dppe	53	62	10	0
Xantphos	66	79	16	27

Experiment with the Cross-Coupling of 4-Cl

Reaction conducted between **4-Cl** (1 equiv.) and *p*-tolylboronic acid (1.1 equiv.) in the presence of benzaldehyde (1 equiv.) using 5 mol% **7**, 3 equiv. K_3PO_4, and 10 equiv. water in toluene.

Conversion (two replicates): 100% 100%

EQUILIBRIUM CONSTANTS FOR THE BINDING OF ALDEHYDES AND KETONES TO NICKEL(0)

Equilibrium constant determination

$$K_{eq} = \frac{[Ni-L][COD]}{[L][Ni-COD]} = \frac{[Ni-L]([Ni-COD]_0 - [Ni-COD])}{([L]_0 - [Ni-L])[Ni-COD]}$$

L is the aldehyde or ketone, Ni-COD = [Ni(COD)(dppf)], and Ni-L = [Ni(L)(dppf)], with concentrations determined from ^{31}P NMR analyses. A plot of [Ni-L]·([Ni-COD]$_0$ – [Ni-COD]) *versus* ([L]$_0$ – [Ni-L])·[Ni-COD] should yield a straight line of gradient K_{eq}.

Acetophenone

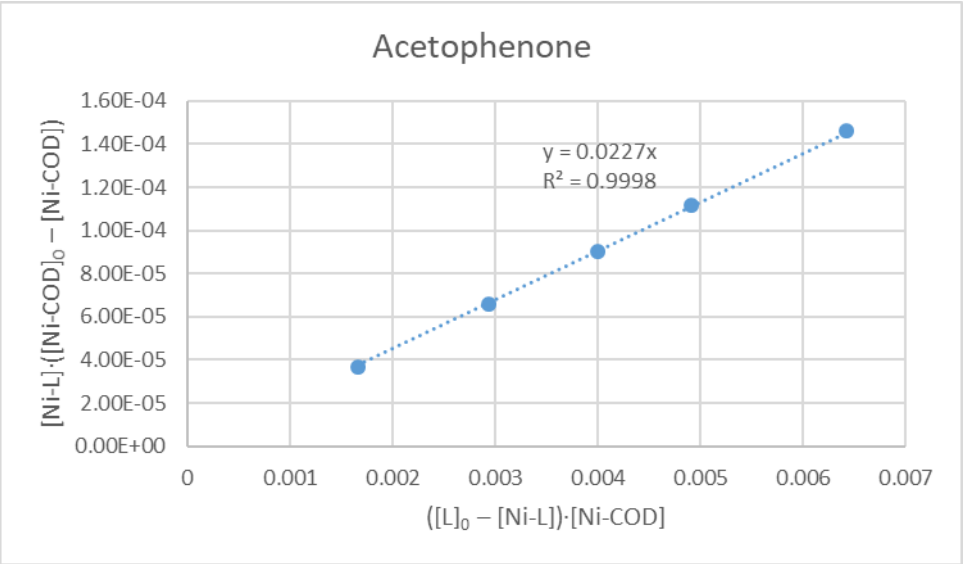

Benzaldehyde

The addition of 1 equiv. benzaldehyde to [Ni(COD)(dppf)] led to complete formation of [Ni(η^2-OHCPh)(dppf)] and so K_{eq} is estimated at > 20.

Benzophenone

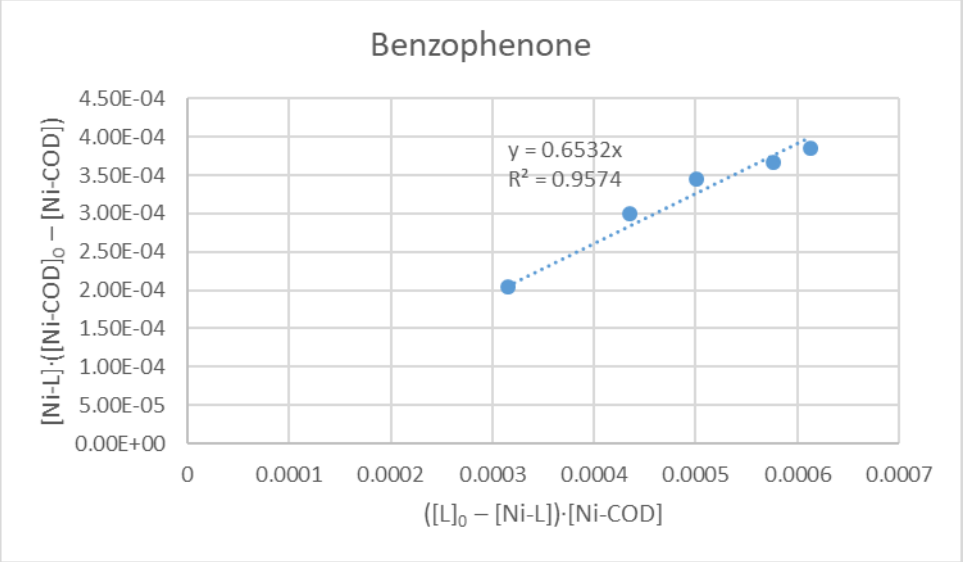

KINETIC DATA FOR OXIDATIVE ADDITION TO NICKEL(0)

Kinetic data were obtained in the same manner as that used for our previous paper.[17] Liquid substrates were added neat to a septum-fitted NMR tube containing a solution of [Ni(COD)(dppf)] (**1**) in benzene-d_6 that had been equilibrated at 20 °C. For solid substrates, a solution of [Ni(COD)(dppf)] in benzene-d_6, equilibrated at 20 °C, was added to the solid substrate. ^{31}P NMR spectra were acquired at intervals, with a long D1 (25 seconds) and without ^{1}H decoupling. All kinetic data showed pseudo-first order behaviour in [Ni(COD)(dppf)] and so plots of ln(**1**) *versus* time yielded k_{obs}. Each experiment was performed in duplicate and so rate constants are quoted as the average of these two replicates. Data for **5-Cl**, **5-Br**, **5-I**, and **6-Cl** can be found in our previous manuscript.

Substrate	k_{obs} (rep. 1)	k_{obs} (rep. 2)	k_{obs} (mean)
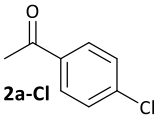 **2a-Cl**	2.20 x 10^{-4} s^{-1}	2.87 x 10^{-4} s^{-1}	2.5(3) x 10^{-4} s^{-1}
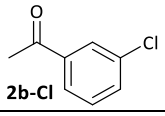 **2b-Cl**	3.89 x 10^{-4} s^{-1}	4.50 x 10^{-4} s^{-1}	4.2(3) x 10^{-4} s^{-1}
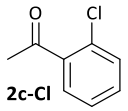 **2c-Cl**	3.25 x 10^{-4} s^{-1}	2.79 x 10^{-4} s^{-1}	3.0(2) x 10^{-4} s^{-1}
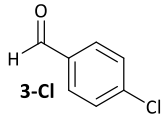 **3-Cl**	1.40 x 10^{-4} s^{-1}	1.42 x 10^{-4} s^{-1}	1.41(1) x 10^{-4} s^{-1}
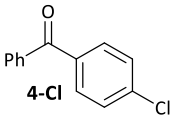 **4-Cl**	9.41 x 10^{-5} s^{-1}	9.06 x 10^{-5} s^{-1}	9.2(2) x 10^{-5} s^{-1}

Kinetic data (integral *versus* time and ln(integral) *versus* time) follow on the subsequent pages. A stack plot is provided for the reaction of **3-Cl** in which signals consistent with an η^2(CO) are observed to appear.

2a-Cl

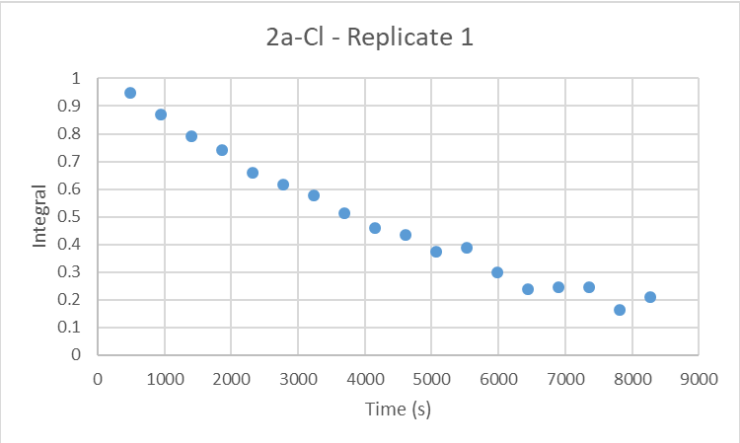
2a-Cl - Replicate 1
Integral
Time (s)
1
0.9
0.8
0.7
0.6
0.5
0.4
0.3
0.2
0.1
0
0
1000
2000
3000
4000
5000
6000
7000
8000
9000

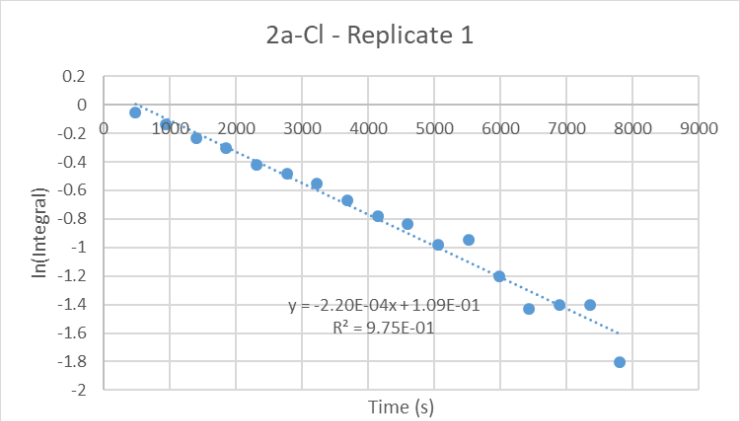
2a-Cl - Replicate 1
ln(Integral)
Time (s)
y = -2.20E-04x + 1.09E-01
R² = 9.75E-01
0.2
0
-0.2
-0.4
-0.6
-0.8
-1
-1.2
-1.4
-1.6
-1.8
-2
0
1000
2000
3000
4000
5000
6000
7000
8000
9000

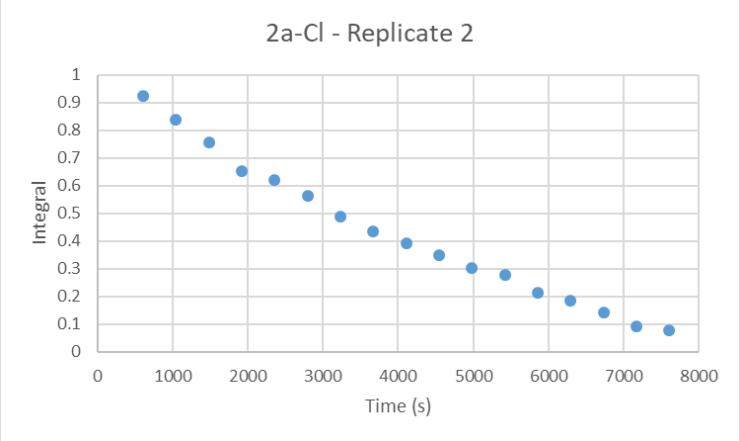
2a-Cl - Replicate 2
Integral
Time (s)
1
0.9
0.8
0.7
0.6
0.5
0.4
0.3
0.2
0.1
0
0
1000
2000
3000
4000
5000
6000
7000
8000

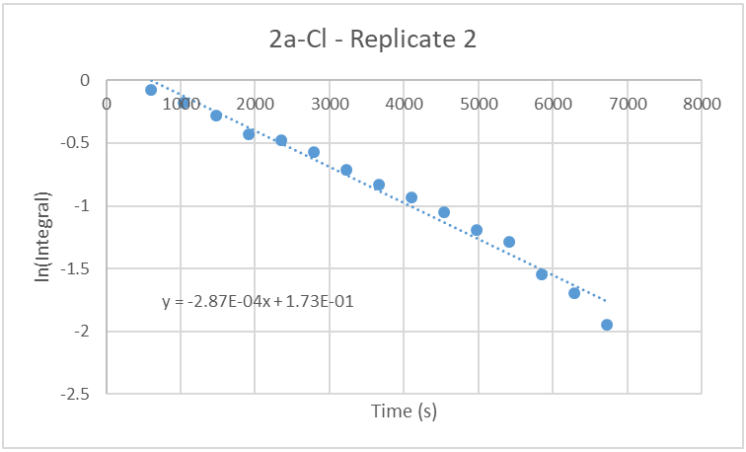
2a-Cl - Replicate 2
0
-0.5
-1
-1.5
-2
-2.5
0
1000
2000
3000
4000
5000
6000
7000
8000
ln(Integral)
Time (s)
y = -2.87E-04x + 1.73E-01

2b-Cl

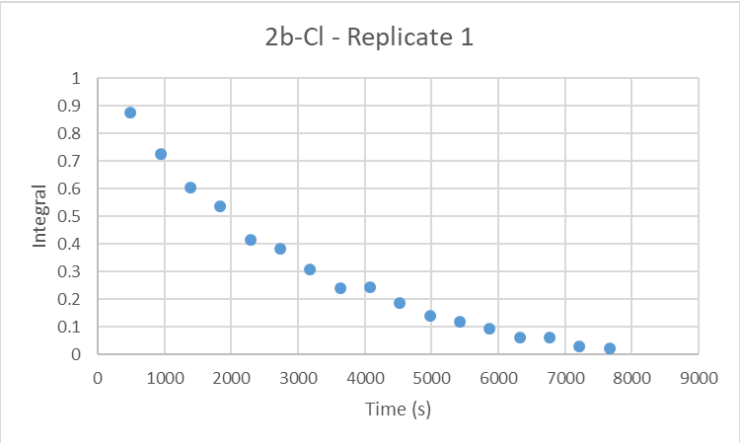
2b-Cl - Replicate 1
Integral
Time (s)
1
0.9
0.8
0.7
0.6
0.5
0.4
0.3
0.2
0.1
0
0
1000
2000
3000
4000
5000
6000
7000
8000
9000

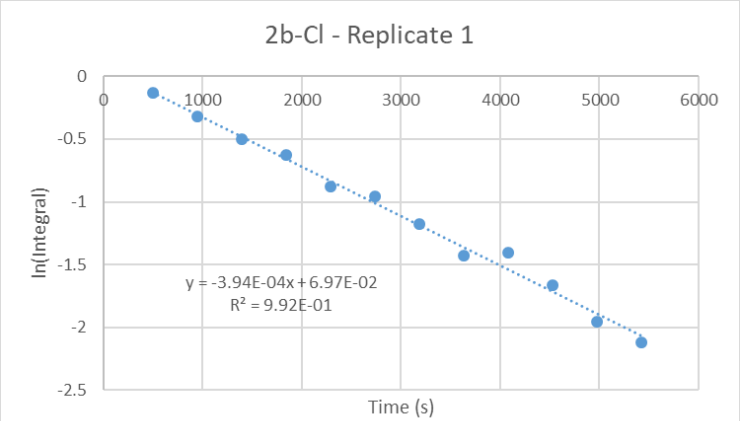
2b-Cl - Replicate 1
ln(Integral)
Time (s)
y = -3.94E-04x + 6.97E-02
R² = 9.92E-01
0
-0.5
-1
-1.5
-2
-2.5
0
1000
2000
3000
4000
5000
6000

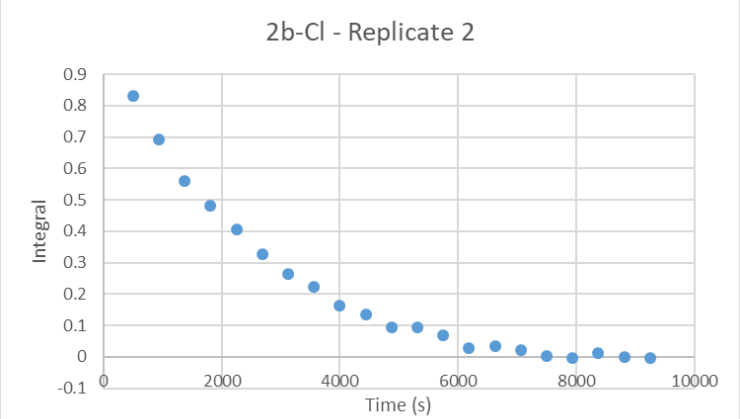
2b-Cl - Replicate 2
Integral
Time (s)
0.9
0.8
0.7
0.6
0.5
0.4
0.3
0.2
0.1
0
-0.1
0
2000
4000
6000
8000
10000

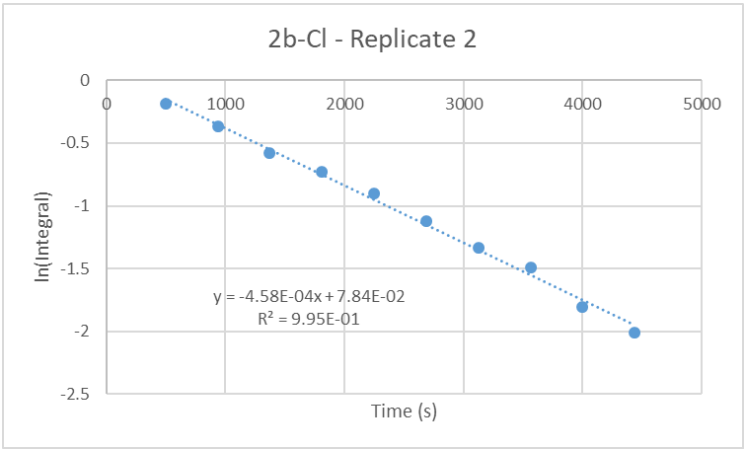
2b-Cl - Replicate 2
0
-0.5
-1
-1.5
-2
-2.5
0
1000
2000
3000
4000
5000
ln(Integral)
Time (s)
y = -4.58E-04x + 7.84E-02
R² = 9.95E-01

2c-Cl

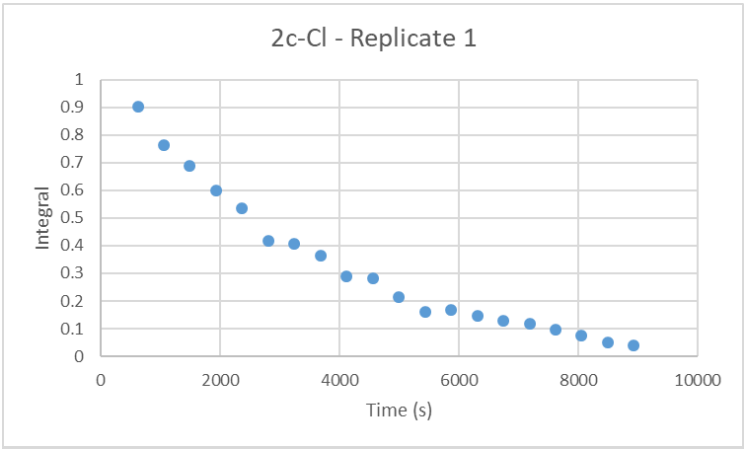
2c-Cl - Replicate 1
Integral
Time (s)
0
0.1
0.2
0.3
0.4
0.5
0.6
0.7
0.8
0.9
1
0
2000
4000
6000
8000
10000

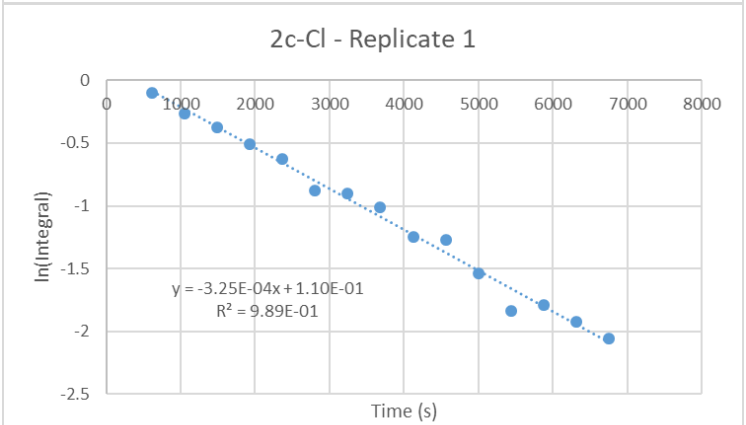
2c-Cl - Replicate 1
ln(Integral)
Time (s)
y = -3.25E-04x + 1.10E-01
R² = 9.89E-01
0
-0.5
-1
-1.5
-2
-2.5
0
1000
2000
3000
4000
5000
6000
7000
8000

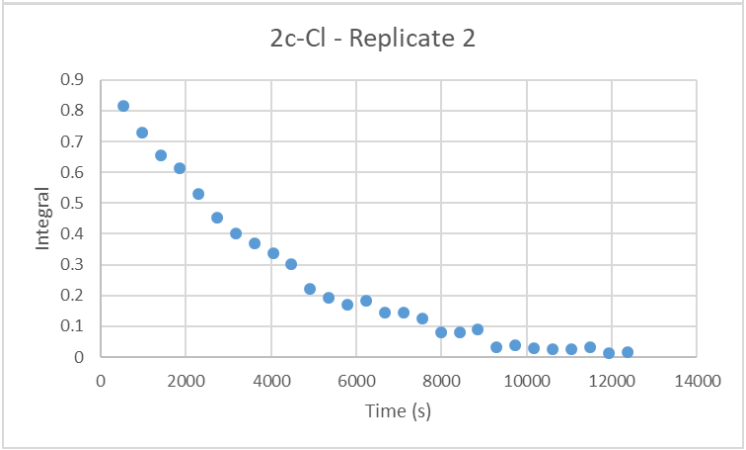
2c-Cl - Replicate 2
Integral
Time (s)
0
0.1
0.2
0.3
0.4
0.5
0.6
0.7
0.8
0.9
0
2000
4000
6000
8000
10000
12000
14000

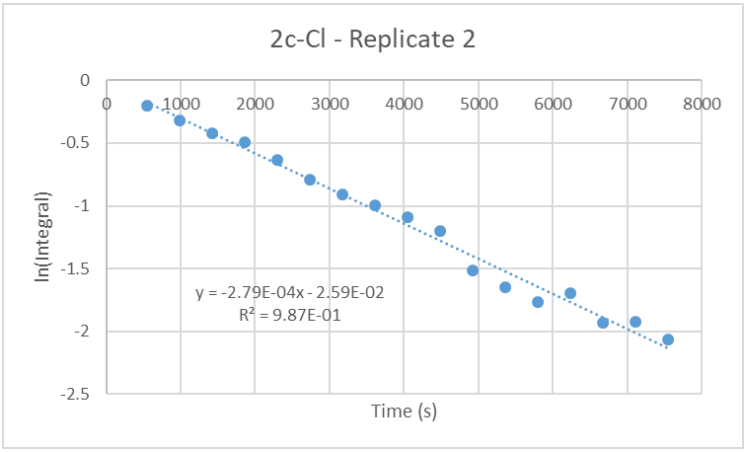
2c-Cl - Replicate 2
0
-0.5
-1
-1.5
-2
-2.5
0
1000
2000
3000
4000
5000
6000
7000
8000
ln(Integral)
Time (s)
y = -2.79E-04x - 2.59E-02
R² = 9.87E-01

3-Cl

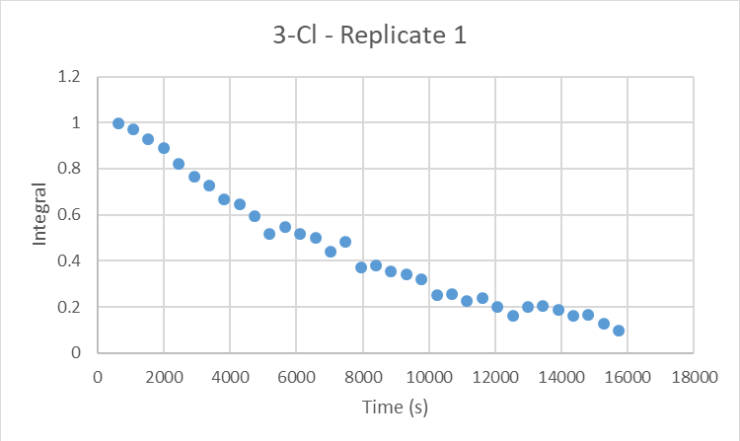
3-Cl - Replicate 1
Integral
Time (s)
0
0.2
0.4
0.6
0.8
1
1.2
0
2000
4000
6000
8000
10000
12000
14000
16000
18000

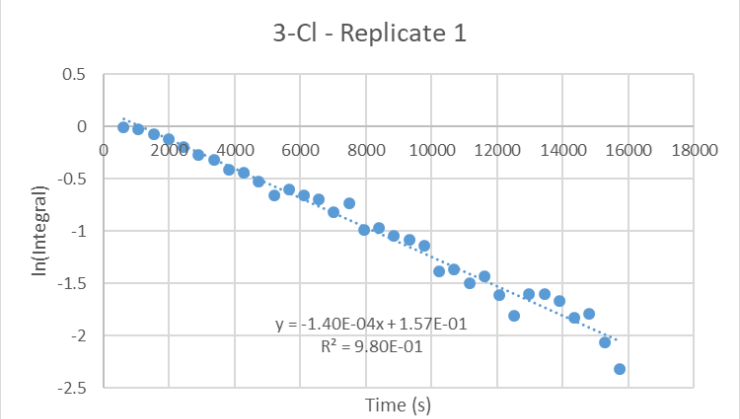
3-Cl - Replicate 1
ln(Integral)
Time (s)
y = -1.40E-04x + 1.57E-01
R² = 9.80E-01
0.5
0
-0.5
-1
-1.5
-2
-2.5
0
2000
4000
6000
8000
10000
12000
14000
16000
18000

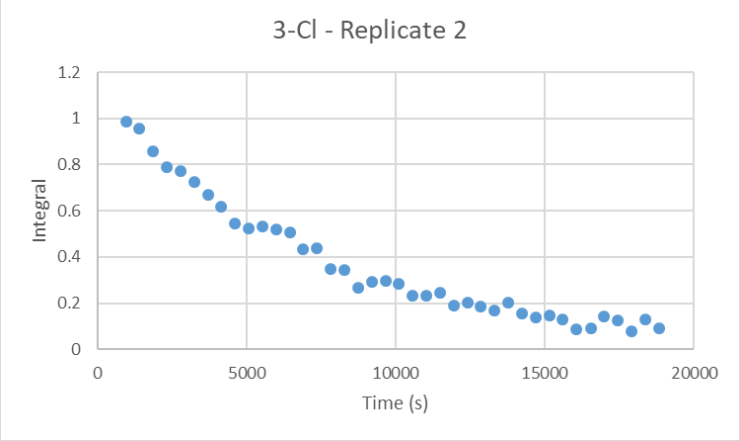
3-Cl - Replicate 2
Integral
Time (s)
0
0.2
0.4
0.6
0.8
1
1.2
0
5000
10000
15000
20000

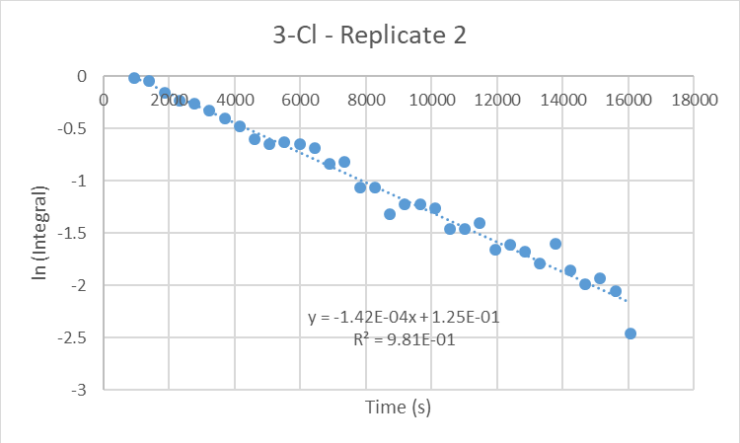

Stack plot for reaction of 1 with 3-Cl (20 equiv.) followed by ^{31}P NMR Spectroscopy (no decoupling) (243 MHz, C_6D_6) at 20 °C.

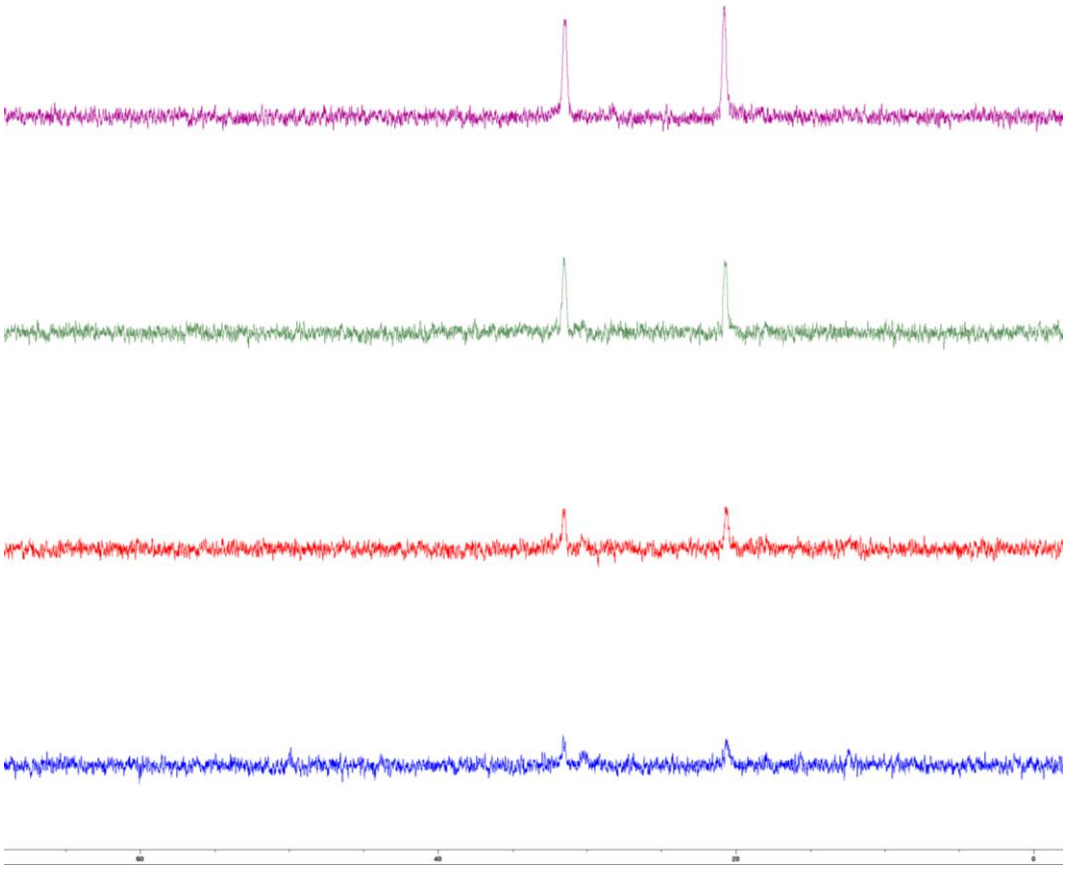

Sample of 1 plus 3-Cl analysed by $^{31}P\{^1H\}$ NMR Spectroscopy (162 MHz, C_6D_6) after 5 min.

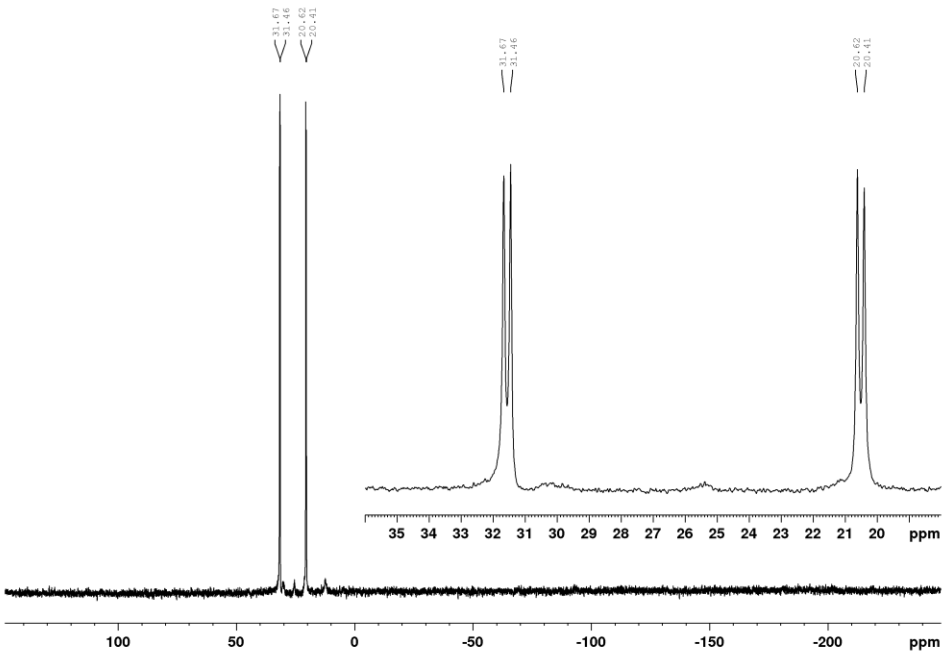
31.67
31.46
20.62
20.41
31.67
31.46
20.62
20.41
35 34 33 32 31 30 29 28 27 26 25 24 23 22 21 20 ppm
100 50 0 -50 -100 -150 -200 ppm

4-Cl

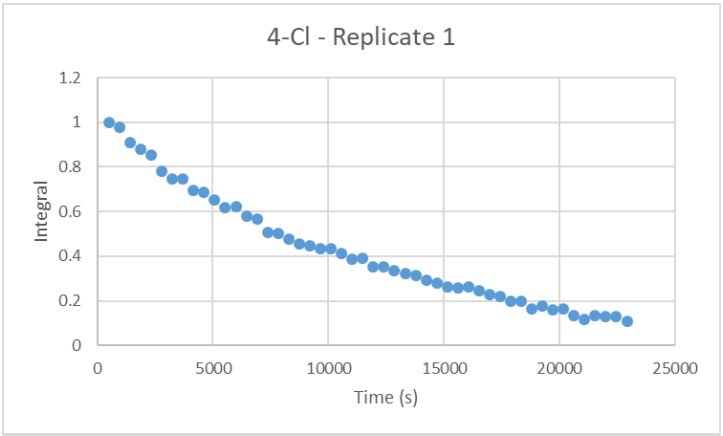
4-Cl - Replicate 1
Integral
Time (s)
0
0.2
0.4
0.6
0.8
1
1.2
0
5000
10000
15000
20000
25000

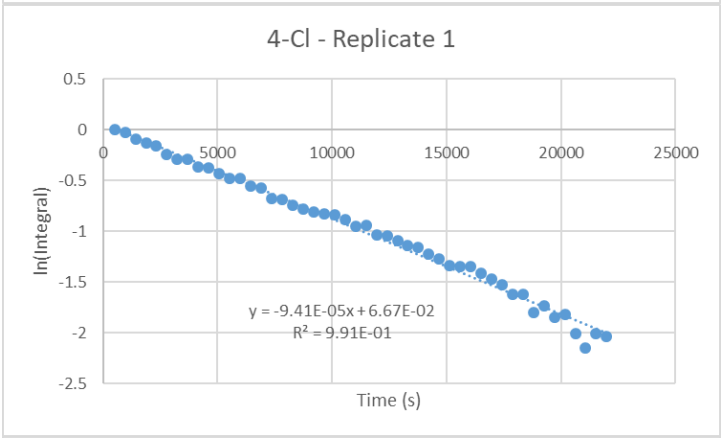
4-Cl - Replicate 1
ln(Integral)
Time (s)
y = -9.41E-05x + 6.67E-02
R² = 9.91E-01
0.5
0
-0.5
-1
-1.5
-2
-2.5
0
5000
10000
15000
20000
25000

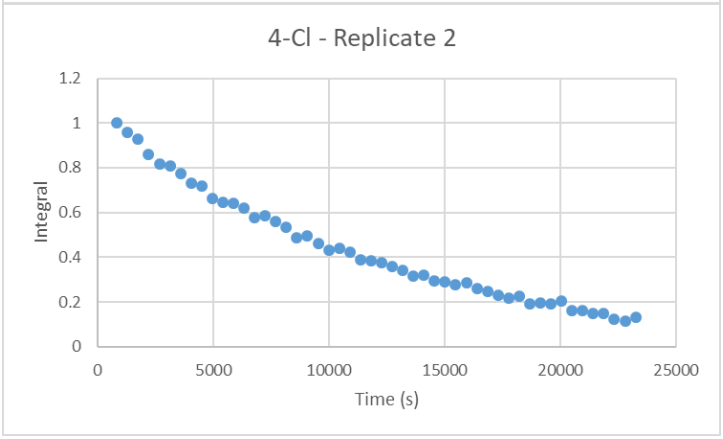
4-Cl - Replicate 2
Integral
Time (s)
0
0.2
0.4
0.6
0.8
1
1.2
0
5000
10000
15000
20000
25000

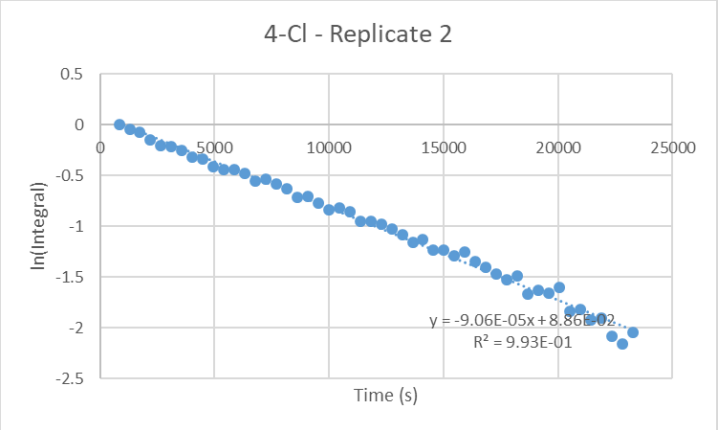

REFERENCES

1. G. Yin, I. Kalvet, U. Englert and F. Schoenebeck, *J. Am. Chem. Soc.*, 2015, **137**, 4164-4172.
2. E. A. Standley, S. J. Smith, P. Müller and T. F. Jamison, *Organometallics*, 2014, **33**, 2012-2018.
3. G. R. Fulmer, A. J. M. Miller, N. H. Sherden, H. E. Gottlieb, A. Nudelman, B. M. Stoltz, J. E. Bercaw and K. I. Goldberg, *Organometallics*, 2010, **29**, 2176-2179.
4. C. Fricke, G. J. Sherborne, I. Funes-Ardoiz, E. Senol, S. Guven and F. Schoenebeck, *Angew. Chem. Int. Ed.*, 2019, **58**, 17788-17795.
5. F. Kloss, T. Neuwirth, V. G. Haensch and C. Hertweck, *Angew. Chem. Int. Ed.*, 2018, **57**, 14476-14481.
6. R. Ambre, H. Yang, W.-C. Chen, G. P. A. Yap, T. Jurca and T.-G. Ong, *Eur. J. Inorg. Chem.*, 2019, **2019**, 3511-3517.
7. S. Kamio, I. Kageyuki, I. Osaka and H. Yoshida, *Chem. Commun.*, 2019, **55**, 2624-2627.
8. F. Serpier, F. Pan, W. S. Ham, J. Jacq, C. Genicot and T. Ritter, *Angew. Chem. Int. Ed.*, 2018, **57**, 10697-10701.
9. K. L. Wilson, J. Murray, C. Jamieson and A. J. B. Watson, *Synlett*, 2018, **29**, 650-654.
10. T. Yamada, K. Saito and T. Akiyama, *Adv. Synth. Catal.*, 2016, **358**, 62-66.
11. M. Bandini, R. Sinisi and A. Umani-Ronchi, *Chem. Commun.*, 2008, DOI: 10.1039/B807640E, 4360-4362.
12. J. Tang, A. Biafora and L. J. Goossen, *Angew. Chem. Int. Ed.*, 2015, **54**, 13130-13133.
13. Z. Luo, L. Xiong, T. Liu, Y. Zhang, S. Lu, Y. Chen, W. Guo, Y. Zhu and Z. Zeng, *J. Org. Chem.*, 2019, **84**, 10559-10568.
14. J. W. Fyfe, N. J. Fazakerley and A. J. Watson, *Angew Chem Int Ed Engl*, 2017, **56**, 1249-1253.
15. Z.-Q. Zhu, J.-S. He, H.-J. Wang and Z.-Z. Huang, *J. Org. Chem.*, 2015, **80**, 9354-9359.
16. A. K. Cooper, P. M. Burton and D. J. Nelson, *Synthesis*, 2020, DOI: 10.1055/s-0039-1690045.
17. S. Bajo, G. Laidlaw, A. R. Kennedy, S. Sproules and D. J. Nelson, *Organometallics*, 2017, **36**, 1662-1672.
18. S. Grimme, J. Antony, S. Ehrlich and H. Krieg, *J. Chem. Phys.*, 2010, **132**, 154104-154119.
19. U. Ryde, R. A. Mata and S. Grimme, *Dalton Trans.*, 2011, **40**, 11176-11183.
20. N. Fey, B. M. Ridgway, J. Jover, C. L. McMullin and J. N. Harvey, *Dalton Trans.*, 2011, **40**, 11184-11191.

21. A. V. Marenich, C. J. Cramer and D. G. Truhlar, *J. Phys. Chem. B*, 2009, **113**, 6378-6396.
22. P. J. Hay and W. R. Wadt, *J. Chem. Phys.*, 1985, **82**, 299-310.
23. W. R. Wadt and P. J. Hay, *J. Chem. Phys.*, 1985, **82**, 284-298.
24. P. J. Hay and W. R. Wadt, *J. Chem. Phys.*, 1985, **82**, 270-283.
25. C. E. Check, T. O. Faust, J. M. Bailey, B. J. Wright, T. M. Gilbert and L. S. Sunderlin, *J. Phys. Chem. A*, 2001, **105**, 8111-8116.

EQUILIBRIUM CONSTANTS FOR THE BINDING OF ALDEHYDES, KETONES, NITRILES, ALKENES & ALKYNES TO NICKEL(0)

Equilibrium constant determination

$$K_{eq} = \frac{[Ni-L][COD]}{[L][Ni-COD]} = \frac{[Ni-L]([Ni-COD]_0 - [Ni-COD])}{([L]_0 - [Ni-L])[Ni-COD]}$$

L is the aldehyde or ketone, Ni-COD = [Ni(COD)(dppf)], and Ni-L = [Ni(L)(dppf)], with concentrations determined from ^{31}P NMR analyses. A plot of [Ni-L]·([Ni-COD]$_0$ – [Ni-COD]) *versus* ([L]$_0$ – [Ni-L])·[Ni-COD] should yield a straight line of gradient K_{eq}.

Acetophenone

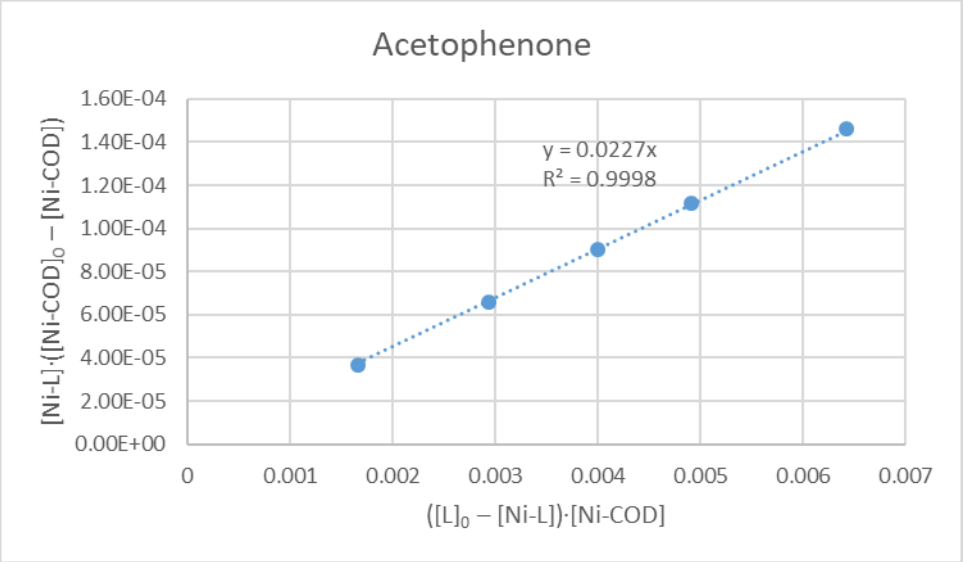

Benzaldehyde

The addition of 1 equiv. benzaldehyde to [Ni(COD)(dppf)] led to complete formation of [Ni(η^2-OHCPh)(dppf)] and so K_{eq} is estimated at > 20.

Benzophenone

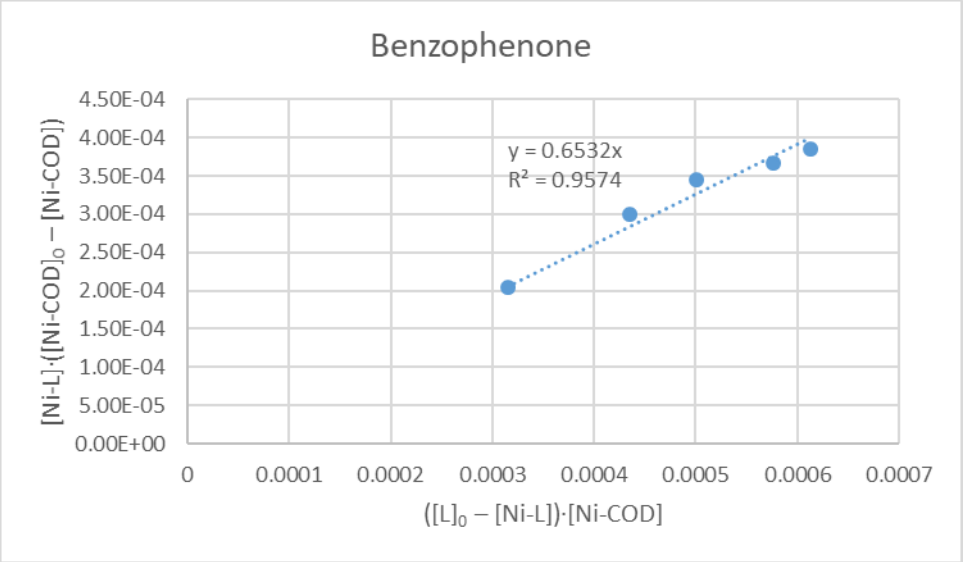

Benzonitrile

Styrene

The addition of 1 equiv. styrene to [Ni(COD)(dppf)] led to complete formation of [Ni(η^2-CH_2CHPh)(dppf)] and so K_{eq} is estimated at > 20.

Diphenylacetylene

The addition of 1 equiv. diphenylacetylene to [Ni(COD)(dppf)] led to complete formation of [Ni(η^2-PhC_2Ph)(dppf)] and so K_{eq} is estimated at > 20.

DATA FOR CHAPTER 4

CALORIMETRY RAW DATA CURVES

Each coupling was carried out in duplicate and the heat flow data taken directly from the instrument. Shown are the raw heat flow *versus* time curves which have been truncated to show the reaction period.

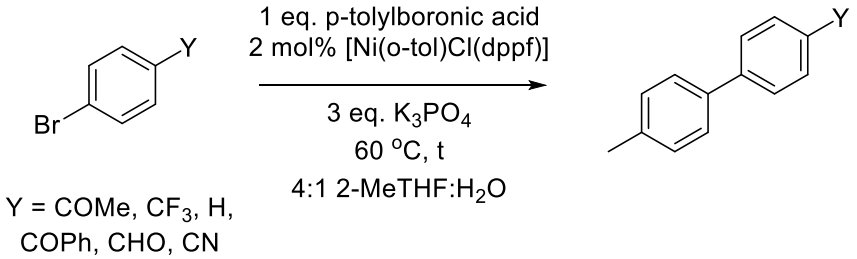

Bromobenzene

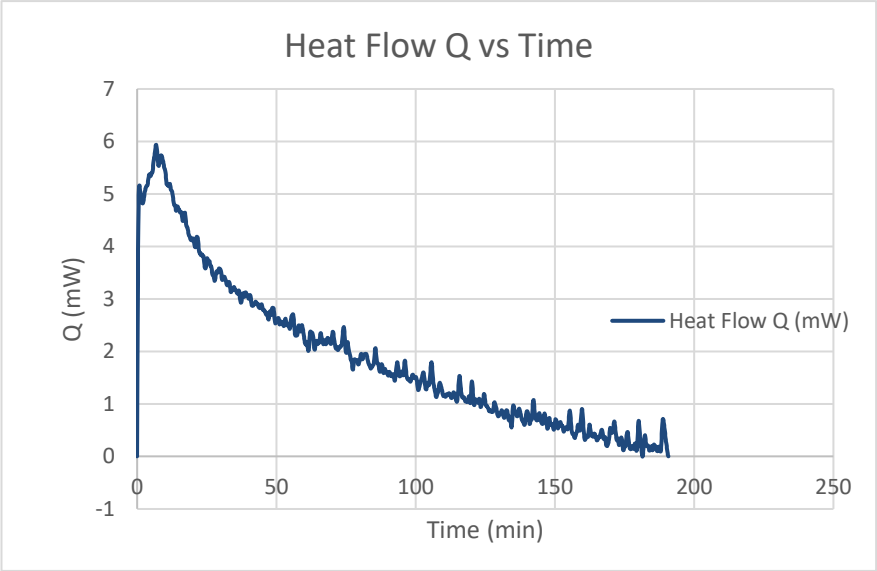

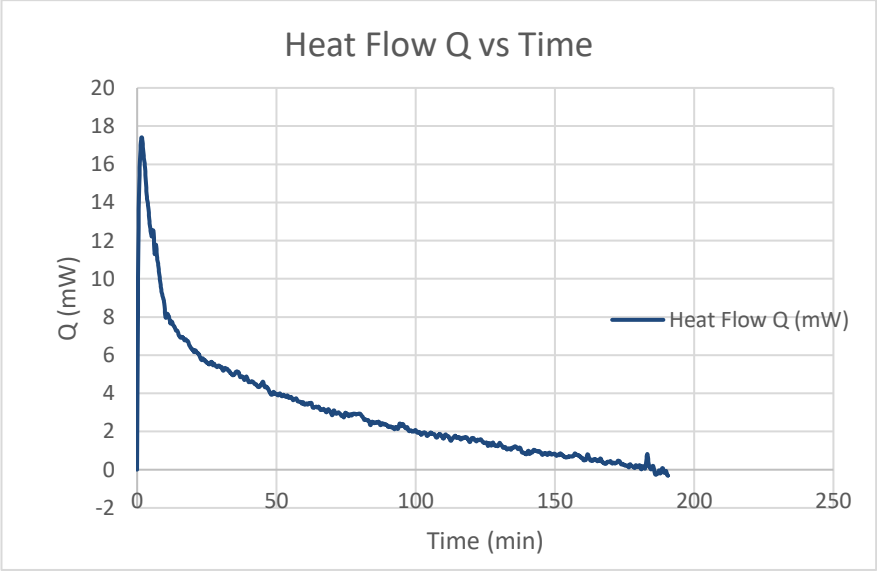

4’-bromoacetophenone

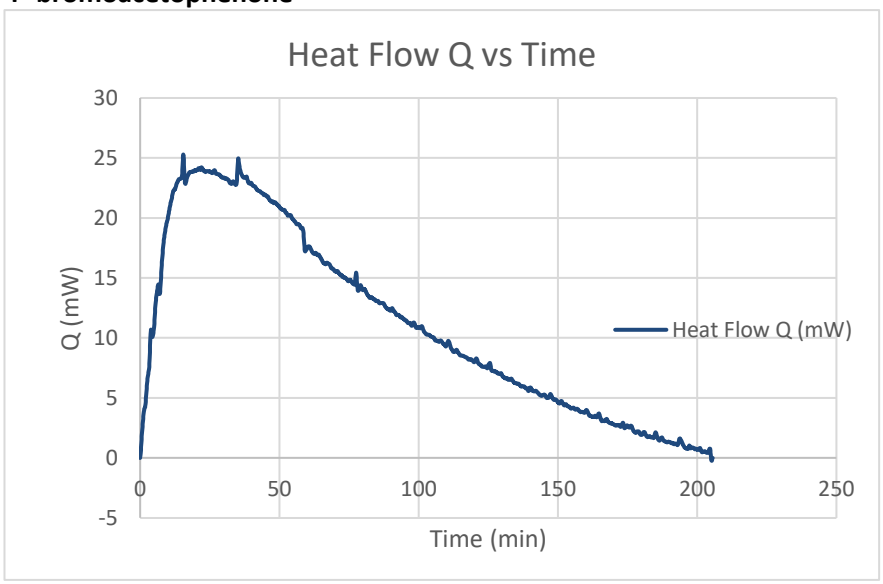

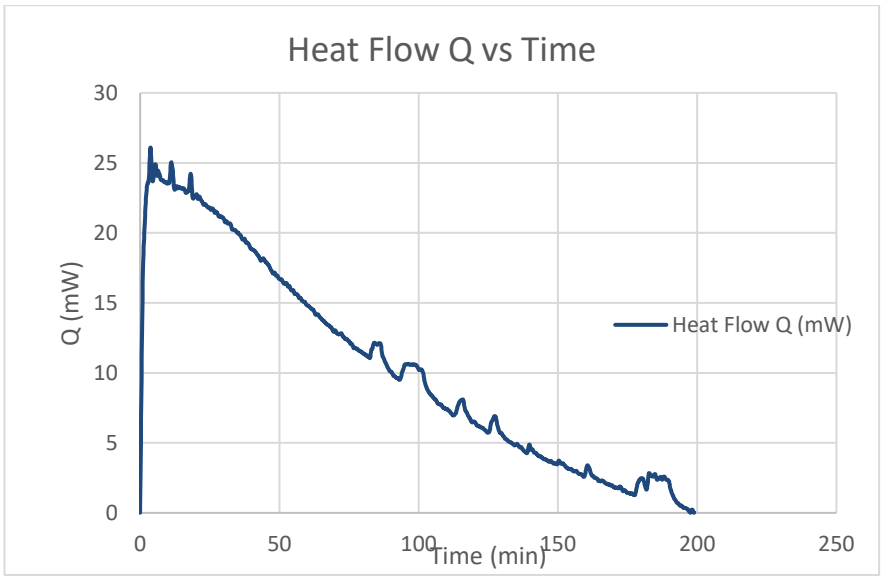

4-bromobenzaldehyde

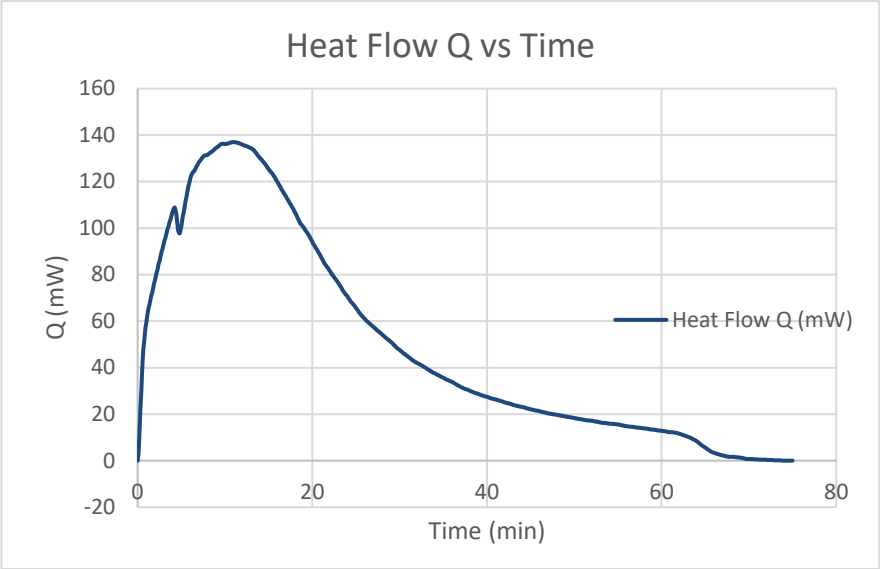

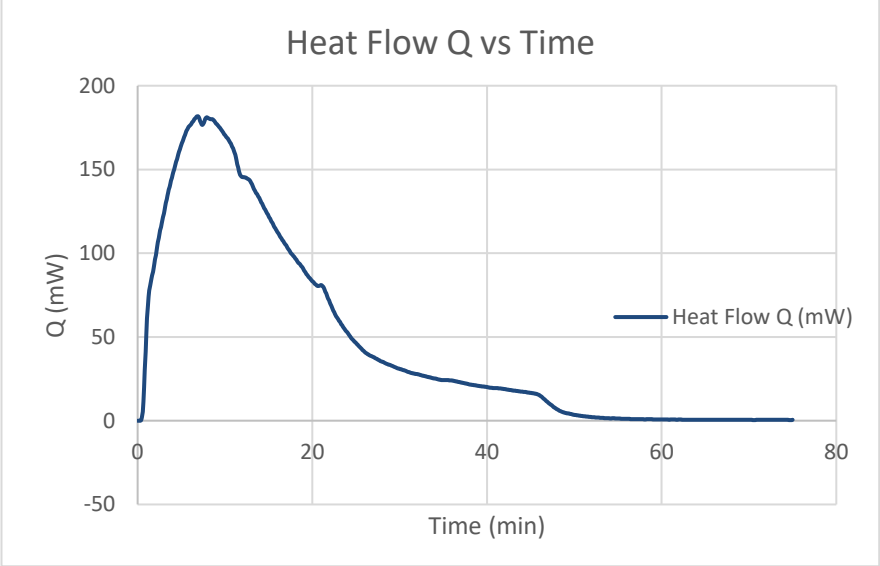

4-bromobenzophenone

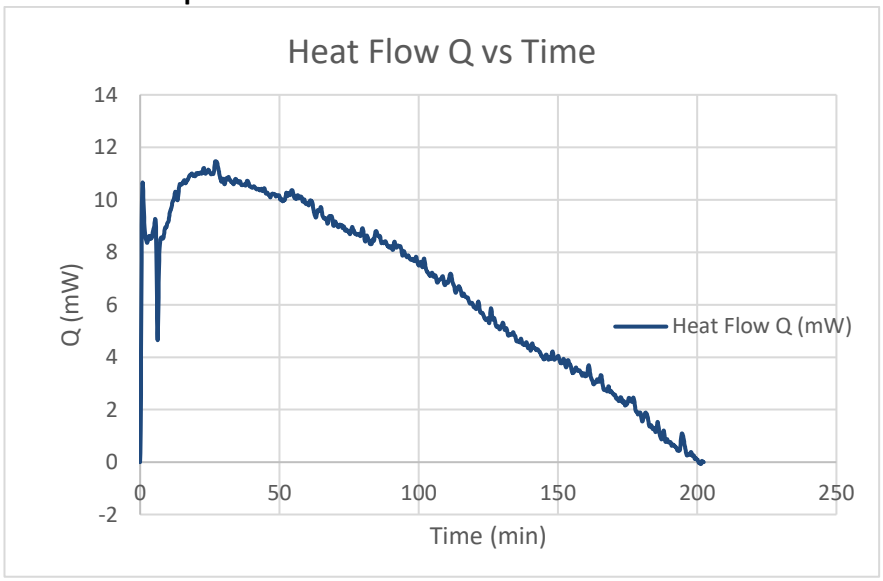

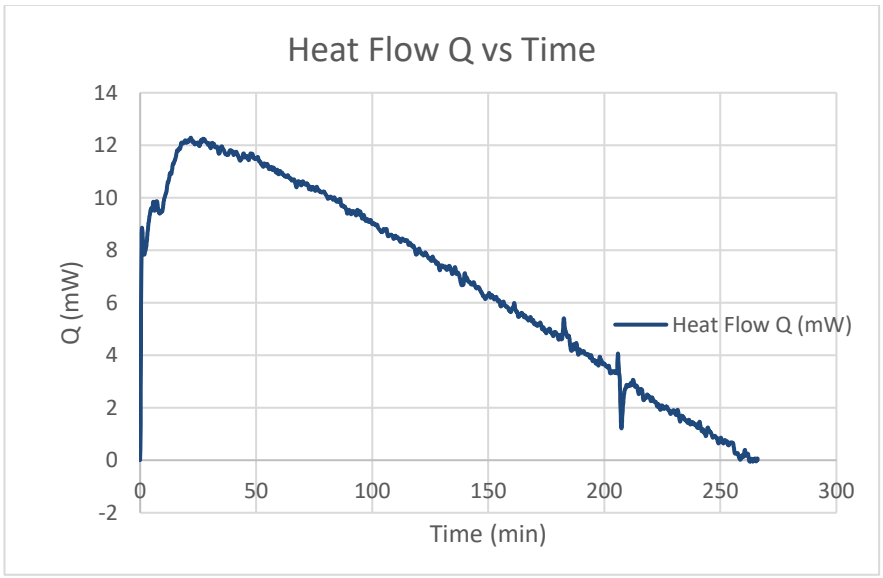

4-bromobenzotrifluoride

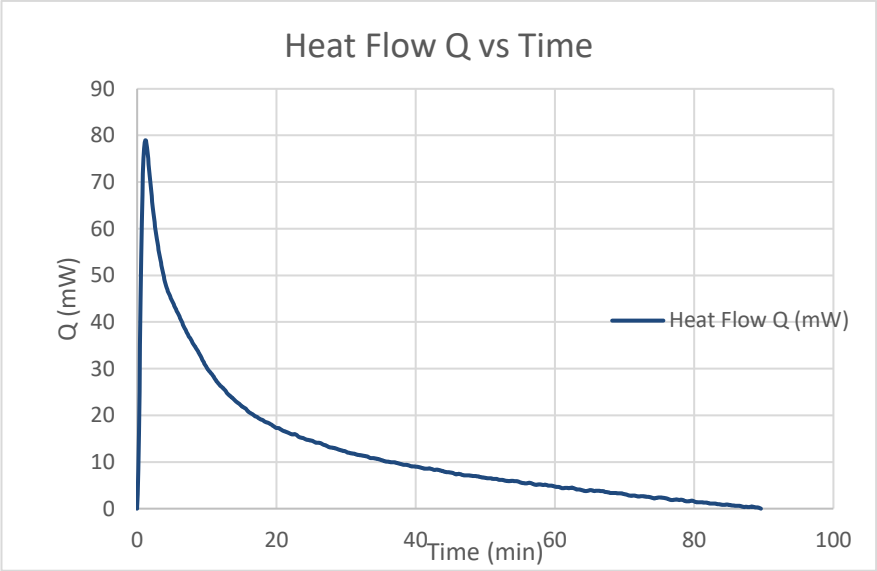

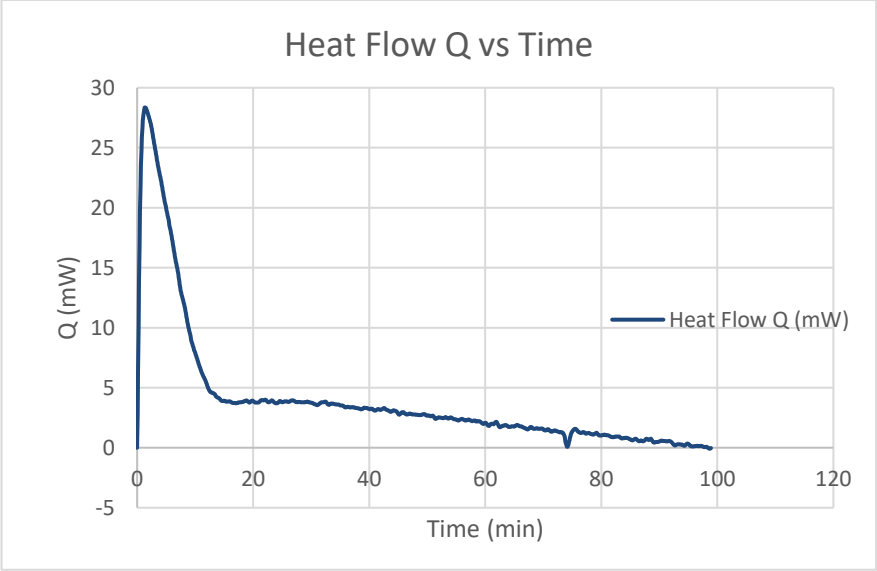

4-bromoanisole

GC-FID analysis of these couplings showed no conversion, which gave no heat flow curve.

4-bromobenzonitrile

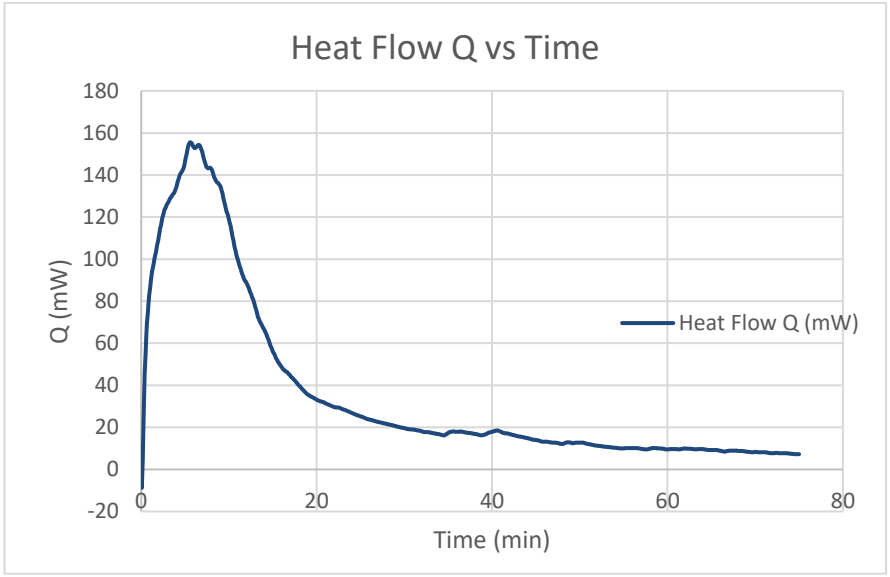

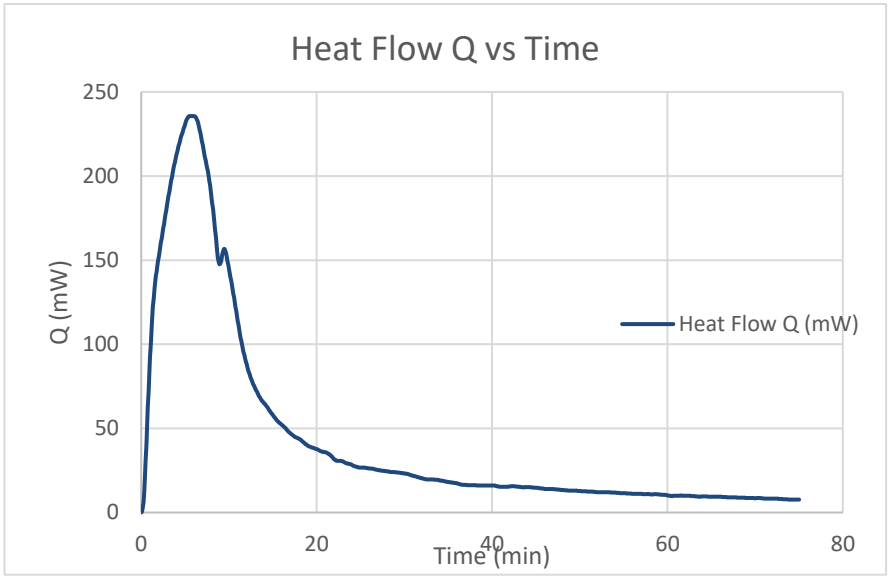

4-bromobenzaldehyde with 2.1 equiv. boronic acid

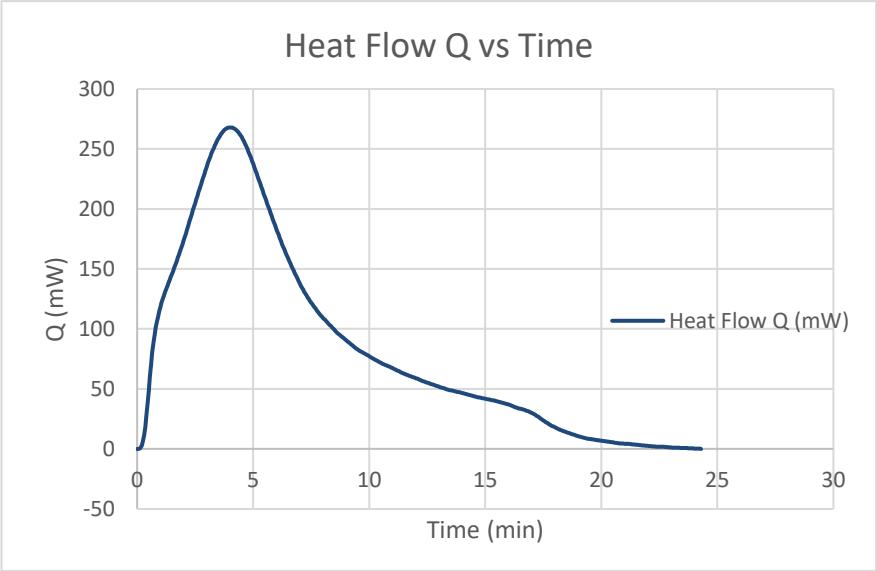

4-bromobenzaldehyde added in 0.25 mmol doses

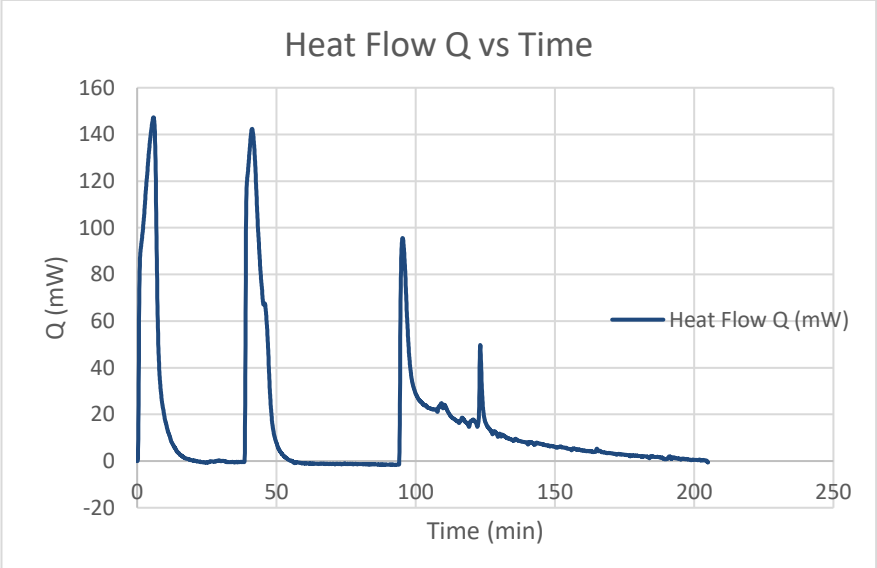

4-bromobenzaldehyde with 1 mol% catalyst

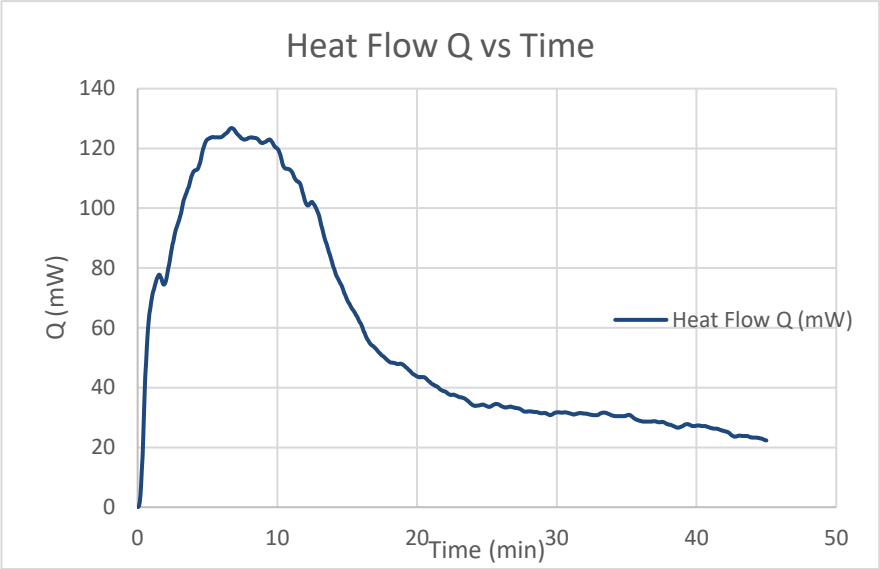

4-bromobenzaldehyde with 0.5 mol% catalyst

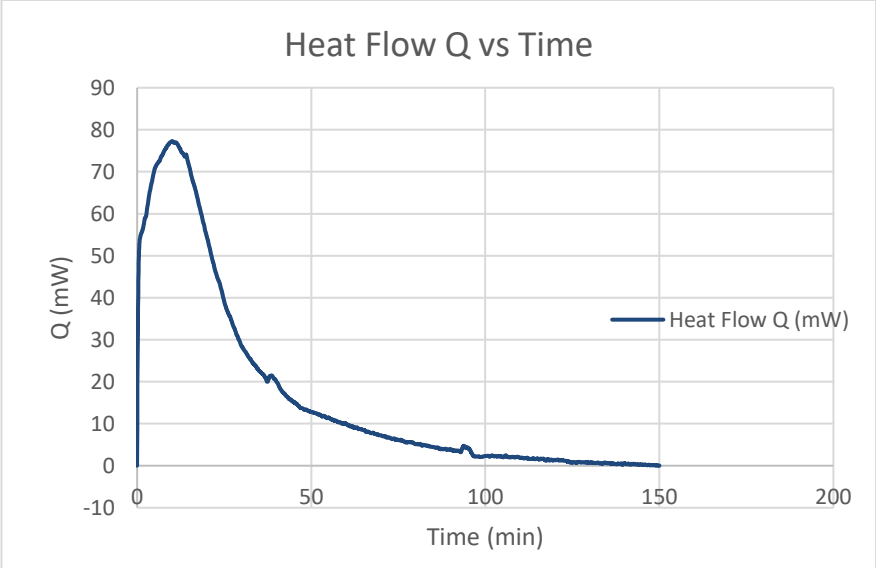

CALORIMETRY RAW FRACTIONAL CONVERSION CURVES

Each coupling was carried out in duplicate and final conversion was determined *via* calibrated GC-FID. The heat flow values (Q) were converted to heat flow per unit time values (Q') using the following equation:

$$Q' = Q\ at\ t_n * (t_n - t_{n-1})$$

These values were then converted to integral heat flow (Q_I):

$$Q_I = Q_I\ at\ t_n + Q' at\ t_{n+1}$$

Fractional conversion values (F) at each time point were obtained using the following equation:

$$F = \left(\frac{Q_I}{Total\ Q}\right) * Final\ conversion$$

Fractional conversion curves were obtained by plotting F *versus* time.

Bromobenzene

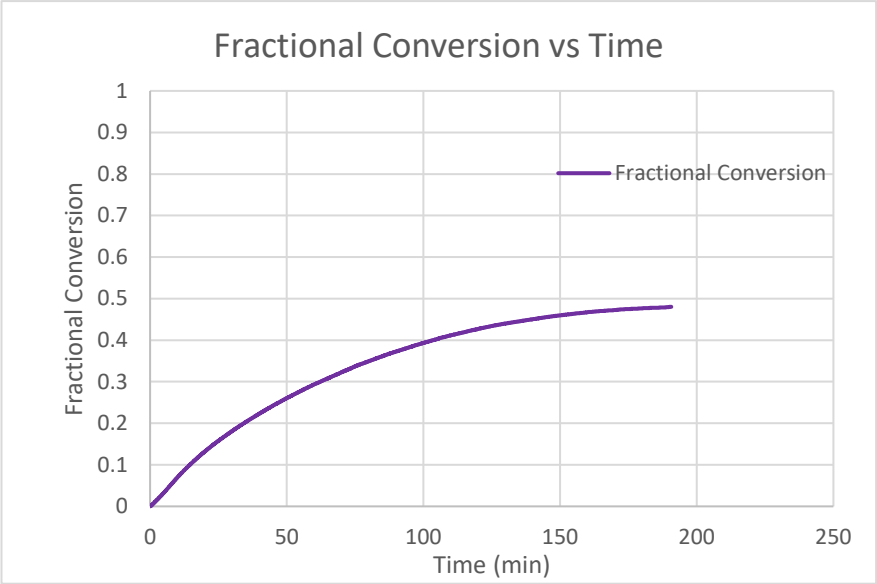

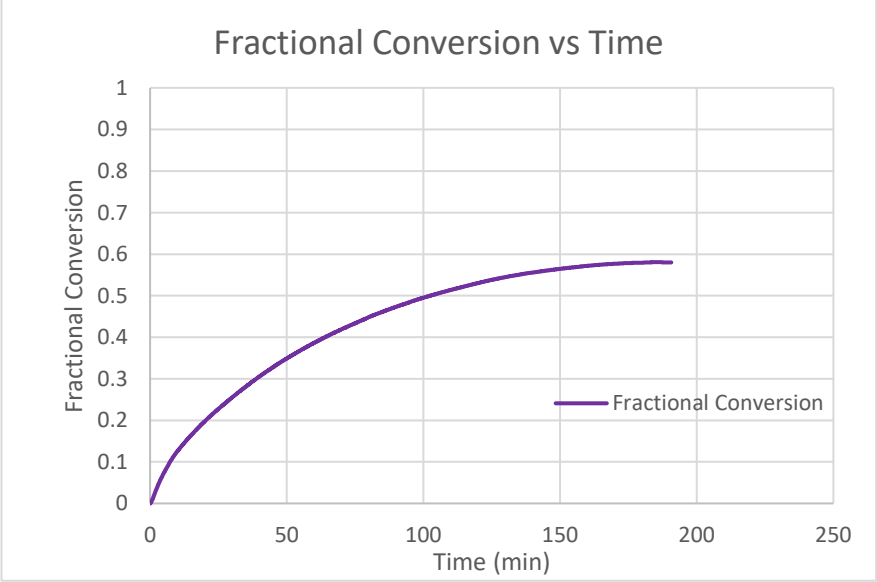

4’-bromoacetophenone

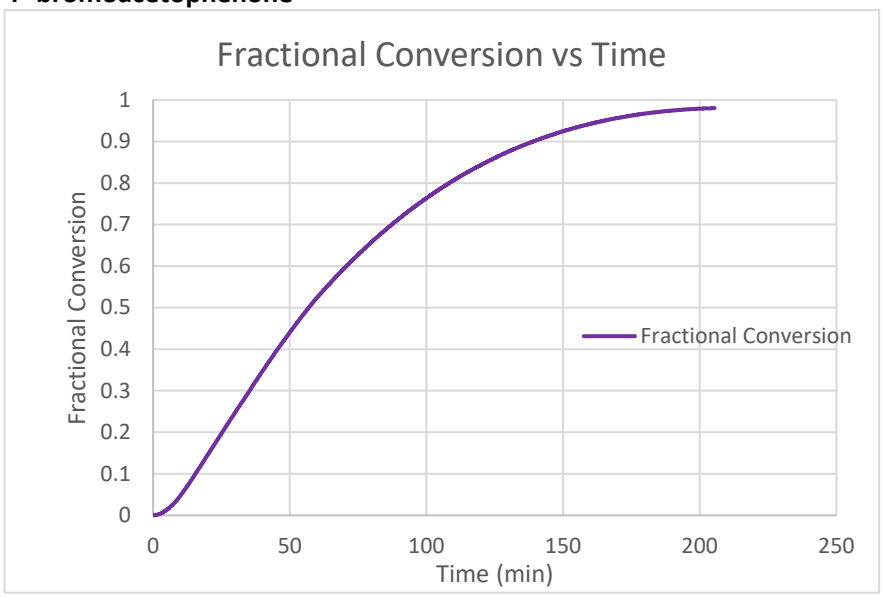

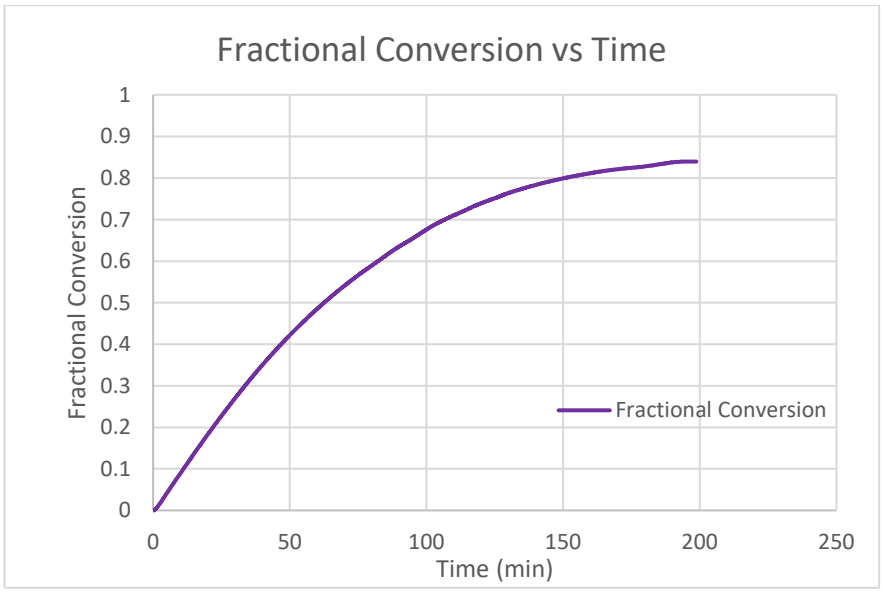

4-bromobenzaldehyde

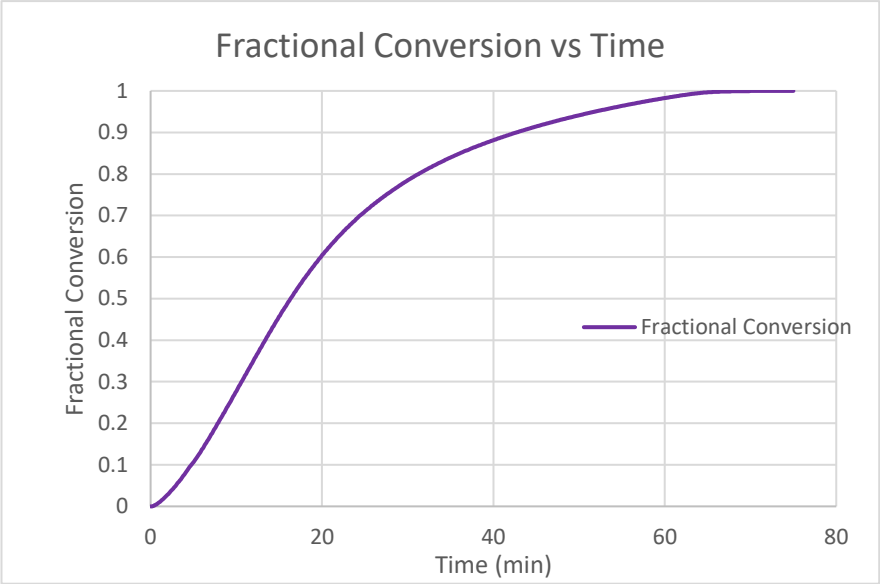

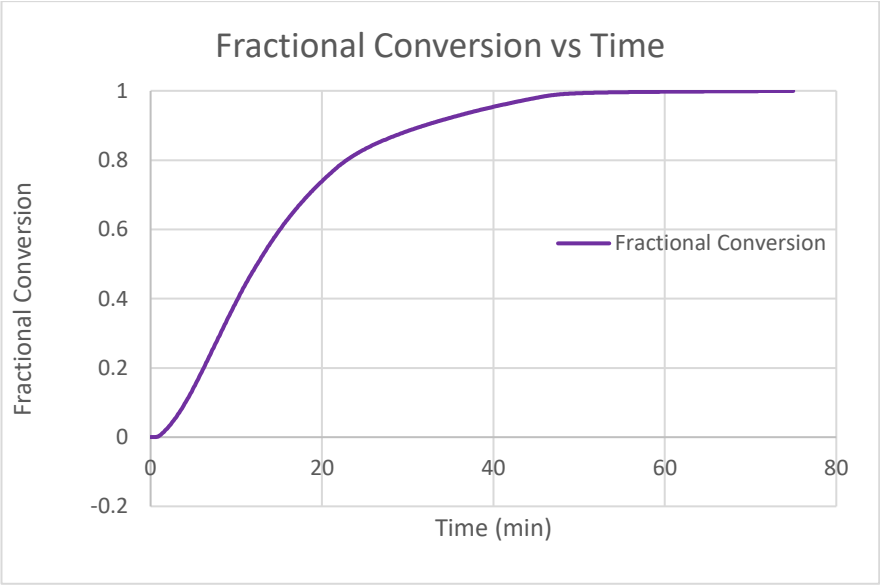

4-bromobenzophenone

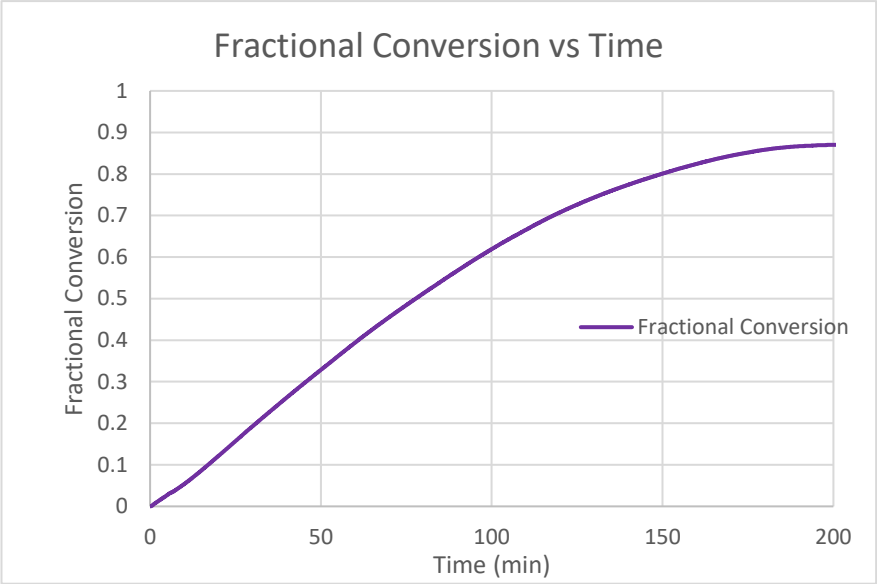

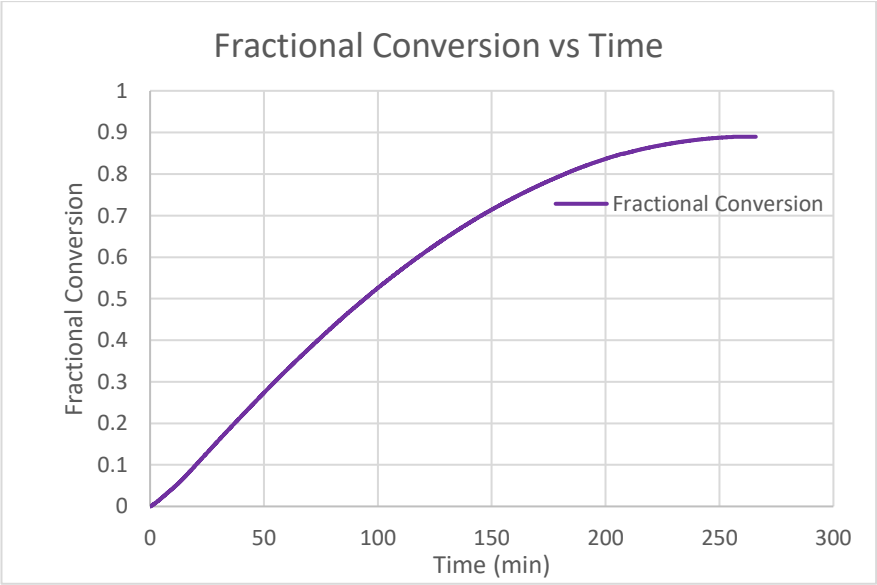

4-bromobenzotrifluoride

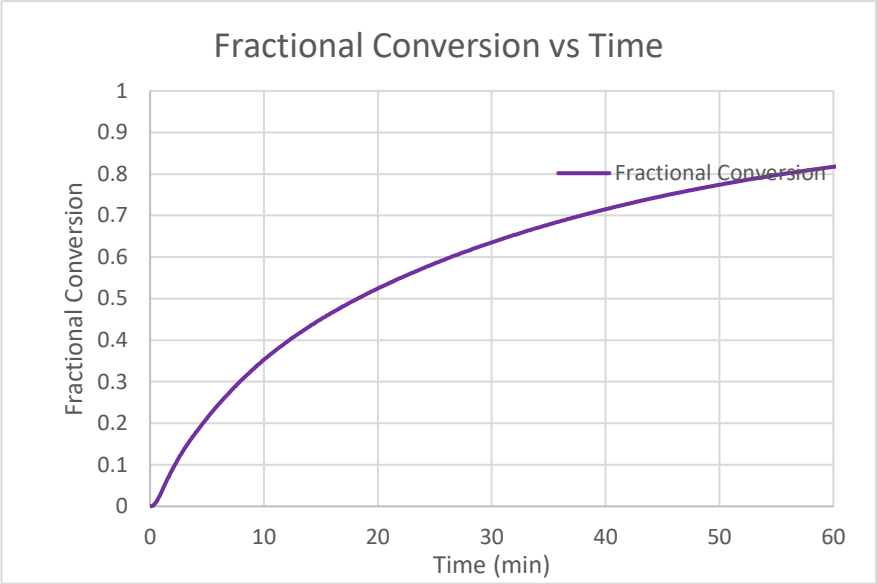

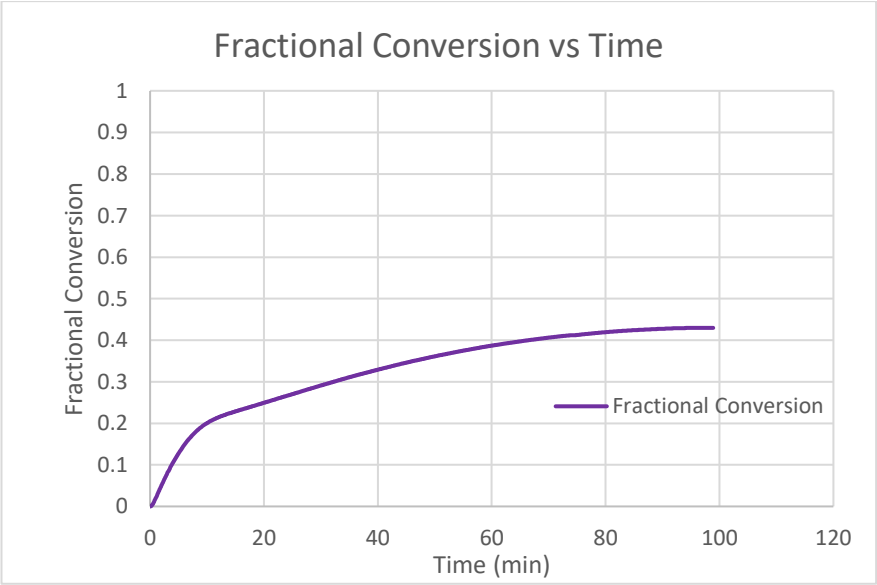

4-bromoanisole

GC-FID analysis of these couplings showed no conversion, which gave no heat flow curve.

4-bromobenzonitrile

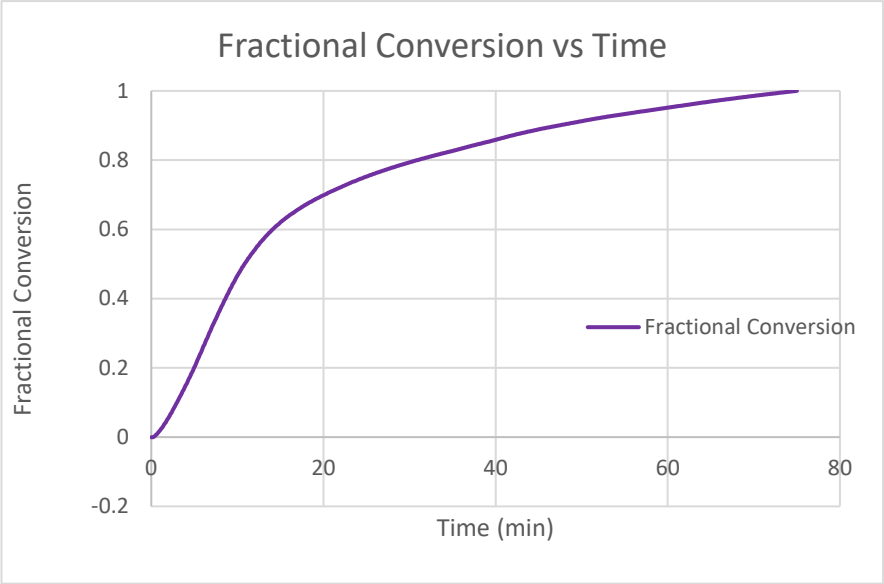

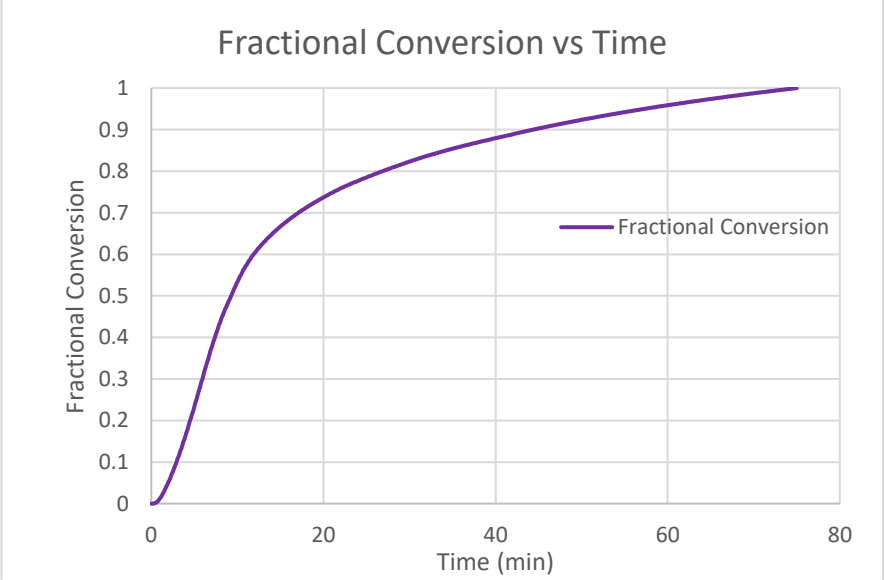

4-bromobenzaldehyde with 2.1 equiv. boronic acid

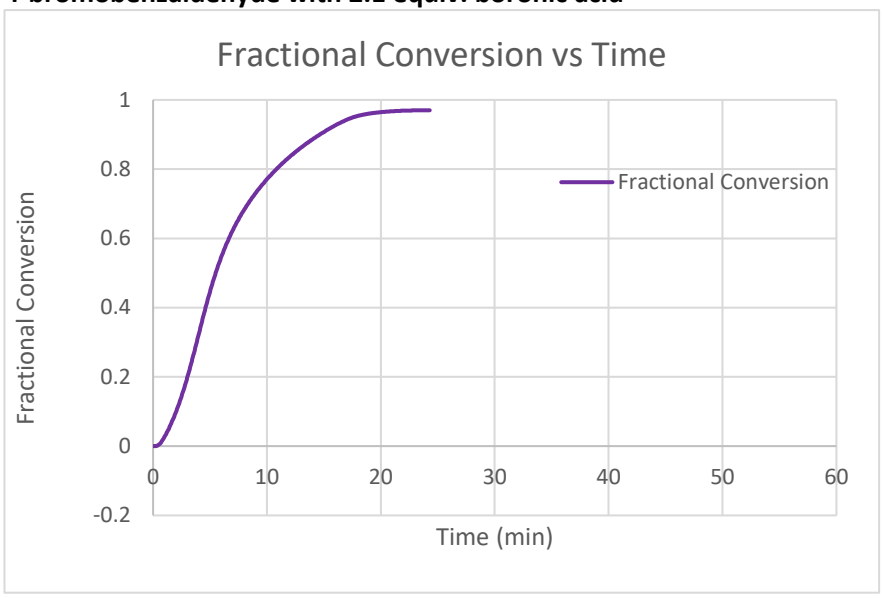

4-bromobenzaldehyde added in 0.25 mmol doses

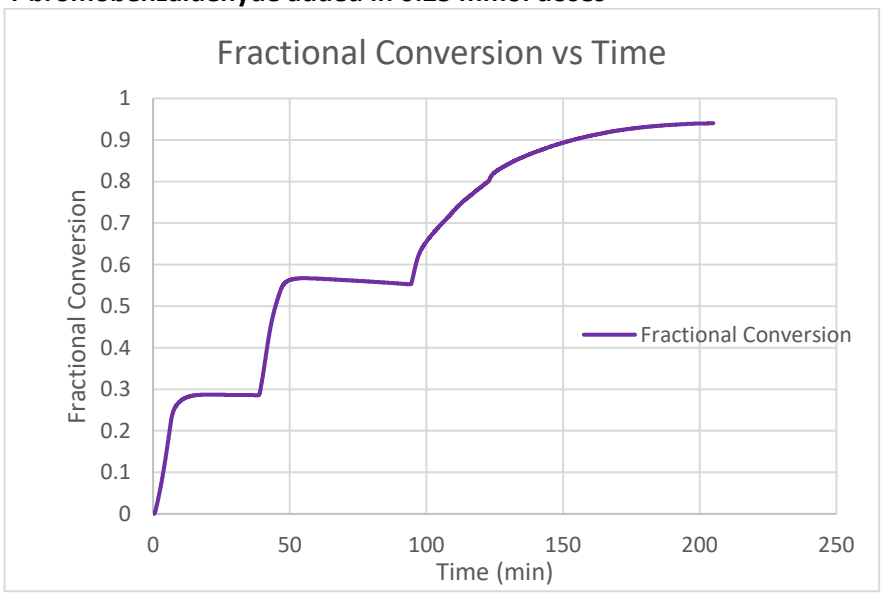

4-bromobenzaldehyde with 1 mol% catalyst

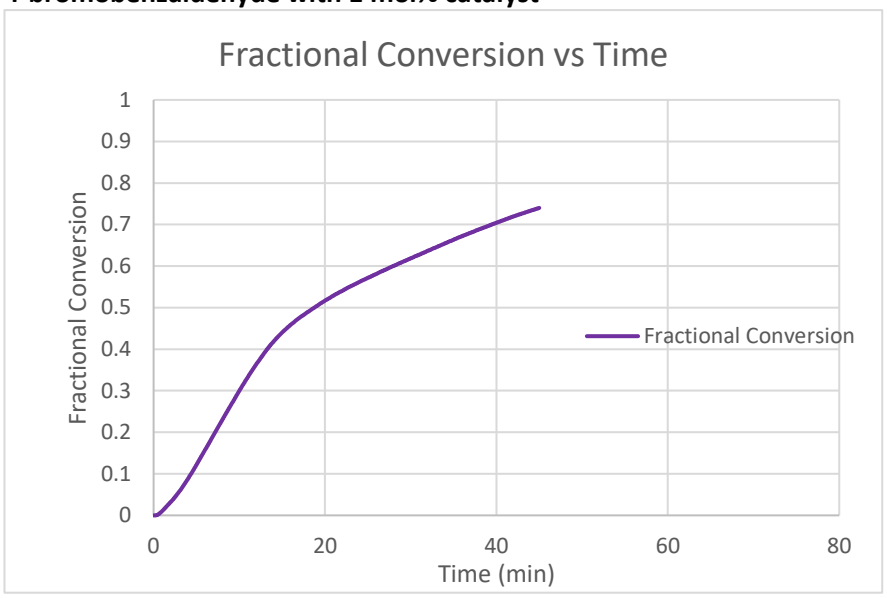

4-bromobenzaldehyde with 0.5 mol% catalyst

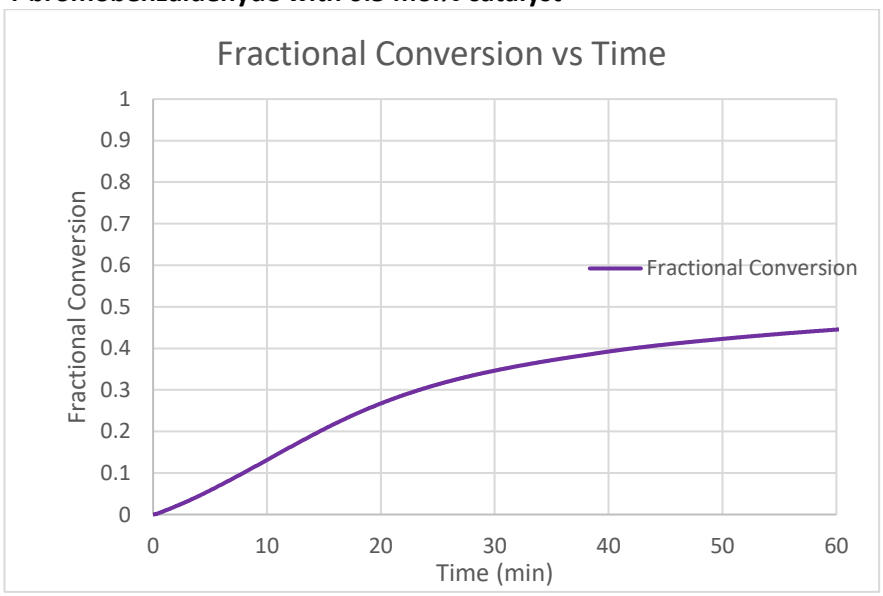

DATA FOR CHAPTER 5

SYNTHESIS OF NICKEL DIMER COMPLEXES

General Procedure C. To a Schlenk flask equipped with a stirrer bar was added [Ni(cod)$_2$] and dppf (1 equiv.) in an argon-filled glovebox. Anhydrous toluene was added and the mixture was stirred at room temperature for 2 hours. After 2 hours, aryl halide (5 equiv.) was added and the resulting mixture was stirred at room temperature overnight. The resulting solid was filtered *via* gravity to yield a dark red/rust-coloured powder.

[Ni$_2$Cl$_2$(pyridine)$_2$(dppf)]

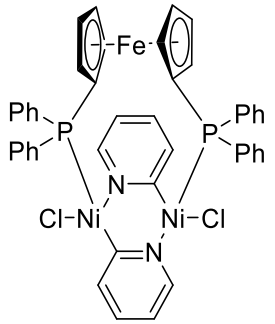

Synthesised according to General Procedure C using [Ni(cod)$_2$] (100.1 mg, 0.363 mmol, 1 equiv.), dppf (201.7 mg, 0.363 mmol, 1 equiv.) and 2-chloropyridine (0.171 mL, 1.815 mmol, 5 equiv.) in 2 mL of PhMe. The mixture was filtered to give a dark red powder (147 mg, 45 %). **^{1}H NMR** (400 MHz, $CDCl_3$): δ_H 8.42 (s, 2H, 2 x ArH), 7.83 – 7.70 (m, 8H, 8 x ArH, *J* = 51.1 Hz), 7.53 (s, 5H, 5 x ArH), 7.41 – 7.39 (m, 3H, 3 x ArH, *J* = 7.5 Hz), 7.08 – 7.04 (m, 6 H, 6 x ArH, *J* = 22.6 Hz), 6.50 (s, 2H, 2 x ArH), 6.33 (s, 2H, 2 x ArH), 6.05 (s, 2H, 2 x ferrocene H), 4.65 (s, 2H, 2 x ferrocene H), 4.46 (s, 2H, 2 x ferrocene H), 3.88 (s, 2H, 2 x ferrocene H). **^{31}P{^{1}H} NMR** (162 MHz, $CDCl_3$): δ_P 21.6 2P.

[Ni$_2$Br$_2$(pyridine)$_2$(dppf)]

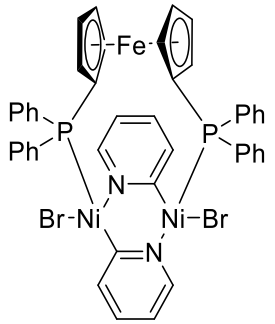

Synthesised according to General Procedure C using [Ni(cod)$_2$] (101.3 mg, 0.363 mmol, 1 equiv.), dppf (201.1 mg, 0.363 mmol, 1 equiv.) and 2-bromopyridine (0.174 mL, 1.815 mmol, 5 equiv.) in 2 mL of PhMe. The mixture was filtered to give a rust brown/red powder (98.1, 27 %). **^{1}H NMR** (400 MHz, $CDCl_3$): δ_H 8.62 (s, 2H, 2 x ArH), 7.74 (s, 8H, 8 x ArH), 7.52 (s, 6H, 6 x ArH), 7.45 – 7.43 (d, 2H, 2 x ArH, *J* = 8.0 Hz), 7.08 (s, 6H, 6 x ArH), 6.52 (s, 2H, 2 x ArH), 6.30

(s, 2H, 2 x ArH), 6.14 (s, 2H, 2 x ferrocene H), 4.69 (s, 2H, 2 x ferrocene H), 4.49 (s, 2H, 2 x ferrocene H), 3.90 (s, 2H, 2 x ferrocene H). **$^{31}P\{^{1}H\}$ NMR** (162 MHz, $CDCl_3$): δ_P 22.5 2P.

[Ni_2Cl_2(quinoline)$_2$(dppf)]

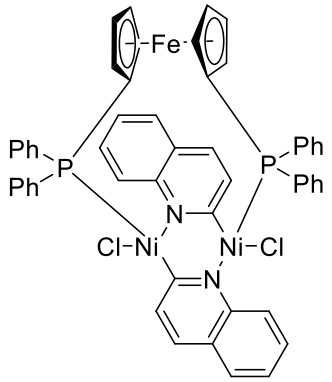

Synthesised according to General Procedure C using [Ni(cod)$_2$] (102.3 mg, 0.363 mmol, 1 equiv.), dppf (202.4 mg, 0.363 mmol, 1 equiv.) and 2-chloroquinoline (297.1 mg, 1.815 mmol, 5 equiv.) in 2 mL of PhMe. The mixture was filtered to give a dark red powder (75.1 mg, 21 %). **^{1}H NMR** (400 MHz, $CDCl_3$): δ_H 9.14 – 9.12 (d, 2H, 2 x ArH, *J* = 8.6 Hz), 8.13 (s, 3H, 3 x ArH), 7.84 (s, 3H, 3 x ArH), 7.61 (s, 11H, 11 x ArH), 7.20 – 7.18 (m, 4H, 4 x ArH, *J* = 7.7 Hz), 7.01 – 6.99 (m, 2H, 2 x ArH, *J* = 7.8 Hz), 6.92 – 6.90 (m, 6H, 6 x ArH, *J* = 23.5 Hz), 6.19 (s, 2H, 2 x ferrocene H), 4.63 (s, 2H, 2 x ferrocene H), 4.42 (s, 2H, 2 x ferrocene H), 3.93 (s, 2H, 2 x ferrocene H). **$^{31}P\{^{1}H\}$ NMR** (162 MHz, $CDCl_3$): δ_P 22.6 2P.

[Ni_2Cl_2(isoquinoline)$_2$(dppf)]

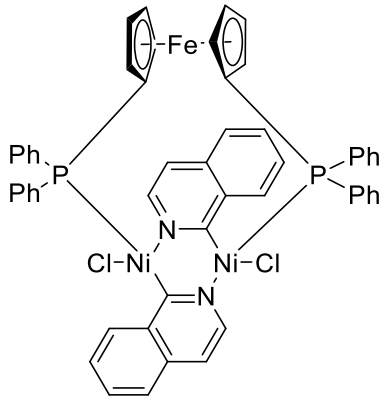

Synthesised according to General Procedure C using [Ni(cod)$_2$] (100.6 mg, 0.363 mmol, 1 equiv.), dppf (201.2 mg, 0.363 mmol, 1 equiv.) and 1-chloroisoquinoline (297.4 mg, 1.815 mmol, 5 equiv.) in 2 mL of PhMe. The mixture was filtered to give a dark red powder (21 mg, 6 %). **^{1}H NMR** (400 MHz, $CDCl_3$): δ_H 10.21 – 10.19 (d, 2H, 2 x ArH, *J* = 8.1 Hz), 8.37 – 8.34 (dd, 2H, 2 x ArH, $^{3}J_{HH}$ = 6.5 Hz, $^{4}J_{HH}$ = 2.3 Hz), 8.11 – 8.07 (m, 4H, 4 x ArH, *J* = 17.3 Hz), 7.48 – 7.45 (m, 10H, 10 x ArH, *J* = 19.8 Hz), 7.34 (t, 2H, 2 x ArH, *J* = 7.6 Hz), 7.21 – 7.18 (m, 2H, 2 x ArH, *J* = 9.9 Hz), 7.16 – 7.14 (m, 2H, 2 x ArH, *J* = 7.3 Hz), 6.84 (t, 2H, 2 x ArH, *J* = 8.0 Hz), 6.72 (t, 4H,

4 x ArH, *J* = 8.0 Hz), 6.57 (d, 2H, 2 x ArH, *J* = 8.0 Hz), 6.10 (s, 2H, 2 x ferrocene H), 4.58 (s, 2H, 2 x ferrocene H), 4.42 (s, 2H, 2 x ferrocene H), 4.24 (s, 2H, 2 x ferrocene H). **$^{31}P\{^{1}H\}$ NMR** (162 MHz, $CDCl_3$): δ_P 18.2 2P.

REFERENCES

1 N. A. Weires, E. L. Baker and N. K. Garg, *Nat. Chem.*, 2015, **8**, 75–79.

2 D.-G. Yu, M. Yu, B.-T. Guan, B.-J. Li, Y. Zheng, Z.-H. Wu and Z.-J. Shi, *Org. Lett.*, 2009, **11**, 3374–3377.

3 D.-S. Kim and J. Ham, *Org. Lett.*, 2010, **12**, 1092–1095.